Low temperature pyrolysis of waste fractions in a spout-fluid bed reactor

LOW TEMPERATURE PYROLYSIS OF WASTE FRACTIONS IN A SPOUT-FLUID BED REACTOR

C.P.M. VAN GINNEKEN

DISSERTATIE DRUKKERIJ
wibro
HELMOND
TELEFOON 04920-23981

LOW TEMPERATURE PYROLYSIS OF WASTE FRACTIONS IN A SPOUT-FLUID BED REACTOR

LOW TEMPERATURE PYROLYSIS OF WASTE FRACTIONS IN A SPOUT-FLUID BED REACTOR

PROEFSCHRIFT

TER VERKRIJGING VAN DE GRAAD VAN DOCTOR IN DE TECHNISCHE WETENSCHAPPEN AAN DE TECHNISCHE HOGESCHOOL EINDHOVEN, OP GEZAG VAN DE RECTOR MAGNIFICUS, PROF. DR. S. T. M. ACKERMANS, VOOR EEN COMMISSIE AANGEWEZEN DOOR HET COLLEGE VAN DEKANEN IN HET OPENBAAR TE VERDEDIGEN OP VRIJDAG 10 SEPTEMBER 1982 TE 16.00 UUR

DOOR

CORNELIS PETRUS MARIA VAN GINNEKEN

GEBOREN TE ROOSENDAAL EN NISPEN

DIT PROEFSCHRIFT IS GOEDGEKEURD DOOR
DE PROMOTOREN:

PROF. IR. M. TELS

PROF. DR. IR. W.P.M. VAN SWAAIJ

Dankwoord

Het in dit proefschrift beschreven onderzoek is verricht in de vakgroep Fysische Technologie.
Mijn dank gaat uit naar allen die aan het onderzoek en de totstandkoming van dit proefschrift hebben bijgedragen.

Het Ministerie van Volksgezondheid en Milieuhygiëne heeft het onderzoek financieel ondersteund. Het Instituut voor Afvalstoffenonderzoek was door haar aangewezen als advies lichaam. Aan de leden van de Begeleidingscommissie is mijn dank verschuldigd voor hun inspanningen en vruchtbare discussies.

De pyrolyse pilot plant is voor een groot deel gebouwd door Henk de Goeij en Piet van Eeten aan de hand van tekeningen die door Karel Janssen vervaardigd zijn. Technische bijstand werd van tijd tot tijd verleend door andere leden van de technische staf. Naar hen allen gaat mijn dank uit voor het goede werk dat zij verricht hebben evenals naar de Centrale Technische Dienst die een aantal vitale onderdelen met zorg heeft vervaardigd. Henk van Kessel heeft het grootste deel van de electrotechnische werkzaamheden verricht. Ook hem ben ik zeer erkentelijk.
Veel dank ben ik verschuldigd aan Chris Luyk die gedurende 4 jaren als technicus/operator heeft meegewerkt aan het pyrolyse onderzoek. Zijn taak omvatte onder meer de afronding van de bouw van de installatie, het aanbrengen van verbeteringen en het bedrijfsklaar maken, opstarten en bedrijven van de pilot plant. Daarnaast heeft hij bij de voorbereiding van de proeven en bij analyses assistentie verleend.
Van groot belang is het werk geweest van de studenten die op dit onderzoek zijn afgestudeerd. Zij hebben zowel experimenteel als theoretisch een wezenlijke bijdrage geleverd aan het onderzoek dat in dit proefschrift beschreven wordt. Mijn erkentelijkheid gaat dan ook uit naar Jan Henselmans, Wim Kox, Jan Notermans, Gerben Mooiweer, Jean Cuijpers, Henk van der Horst, Bram Keijzers, Jean Claessens, Leo Derks, Sjef Voncken en Ruud Beerkens.

Ook aan de studenten die hebben meegewerkt aan het college procesont-

wikkeling dat gewijd was aan de technisch-economische evaluatie van het pyrolyse proces ben ik dank verschuldigd. Thijs Senden, Bob Hoedt en Marius Vorstman ben ik erkentelijk voor hun bijdrage aan dit college procesontwikkeling. Met Marius Vorstman heb ik vele vruchtbare gesprekken gevoerd met name over verbeteringen in de pyrolyse installatie.

Dank ben ik verschuldigd aan Willem Schoeber die de eerste aanzet heeft gegeven tot de mathematische modellering en aan Adri van den Oever die geassisteerd heeft bij de analyse van de waterige fractie.

De medewerking van de vakgroepen Organische Chemie (element analyses), Instrumentele Analyse (analyses op chloorhoudende organische verbindingen) en Anorganische Chemie (wier thermobalans gebruikt is in het thermoanalytisch onderzoek) is door mij zeer op prijs gesteld.

Ik wil Mieke Barts en Anniek van Bemmelen bedanken die het proefschrift met grote zorg getypt hebben.

Tenslotte wil ik iedereen uit mijn naaste omgeving, met name Marianne, bedanken voor hun morele steun.

CONTENTS

Summary

Pyrolysis is a method to process wastes while recovering fuels. Pyrolysis is the thermal decomposition of organic materials in the absence of air or with just enough air to generate the required heat. The pyrolysis of the organic fraction of domestic waste which was emphasized in the present investigation yields the below products:

1. a low to medium calorific value gas that contains CO, CO_2, H_2 and lower hydrocarbons.
2. a tar fraction.
3. a char.
4. a contaminated water fraction.

The three products mentioned first can be used as fuels that are easier to handle than the starting material (domestic waste).

The present study was directed towards low temperature pyrolysis (up to about 600^{o}C) in a spout-fluid bed reactor. The spout-fluid bed reactor is a combination of a fluidised bed and a spouted bed. This results in the following characteristics: good local solid phase mixing, good overall circulation, good heat transfer characteristics and the possibility to introduce the feed into the reactor through pneumatic transport by the spout gas. The relatively high gas flow rates that may be applied in the bed make this type of reactor particularly suitable for low temperature pyrolysis. Components that are gaseous at reaction temperature, such as the tar, are quickly removed from the reactor. Cracking reactions may be prevented in this way as much as possible. Tar yields can therefore be relatively high. The tar is considered to be a more attractive fuel than the char or the low calorific value gas. The tar can easily be stored and transported in tank cars (if necessary after dilution with water). The material is easy to burn. The tar may be used as a Diesel oil substitute after dilution with water.

The influences of various reaction conditions on the pyrolysis of shredded thin cardboard have been investigated in introductory experiments in a pilot plant unit fitted with a spout-fluid bed reactor (maximum capacity 10 kg/hr). Shredded thin cardboard was selected as a model substitute for the organic fractions of domestic waste because of the resemblances in chemical composition and flow characteristics.

Both shredded thin cardboard and shredded domestic waste show poor flow characteristics.

The influences of reaction temperature (in the range of 440-600^{o}C), of the humidity of the feed, the particle size of the feed, the solid feed rate and the total gas flow rate in the reactor have been investigated. The reaction temperature was found to have a considerable influence on the pyrolysis process. Increasing reaction temperature led to increasing gas yield and decreasing char production. The tar yield showed a maximum at a reaction temperature of about 500-525^{o}C. Increasing reaction temperature also led to increasing heats of combustion of the gas and the char produced.

Pyrolysis experiments on organic fractions from shredded domestic waste (RDF: refuse derived fuel) were carried out after these introductory experiments. The aim of the experiments on RDF was to verify the results obtained in the pyrolysis experiments on cardboard and - more importantly - to investigate the properties of the pyrolysis products and the environmental impact of the process. The organic fractions were separated from shredded domestic waste by means of handpicking (removal of large pieces of glass and cans), air classification and sieving.

The trends in the product distribution as a function of reaction temperature were roughly the same as those that were observed in the pyrolysis experiments on cardboard. However, tar yield is much lower and char yield higher in RDF pyrolysis than the corresponding yields that were found in the pyrolysis experiments on shredded thin cardboard. It is felt that these phenomena may be ascribed to catalytic influences of certain inorganic compounds present in the domestic waste on some of the reactions that take place during the pyrolysis process.

The study of the environmental impact of the pyrolysis process led to the following results:

- the char ash contains heavy metals. However, the heavy metals contents of the char ash are low so that the char ash is not a chemical waste according to Dutch law.
- the organic contaminents of the water phase are bio-degradable. No chlorine containing organic compounds could be traced in the water phase.

- the pyrolysis gas contains HCl mainly as a result of the presence of PVC in the RDF fractions. No definite answer can be given yet to the question whether chlorine containing organic compounds are present in the gas.

The fundamentals of the pyrolysis of cellulosic materials have been investigated. Models were derived to describe the pyrolysis behavior of this type of materials. The models were based on the below reaction scheme of cellulose pyrolysis. The scheme is a drastic simplification of the complex series of parallel and consecutive reactions that take place during cellulose pyrolysis.

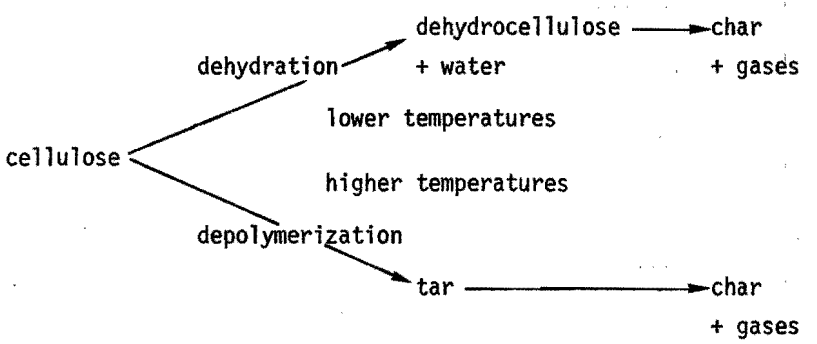

The physical transport processes that take place during the pyrolysis process were also simplified in the models.
The reaction kinetic data that were required in the models were determined by means of thermoanalytical experiments.
The models provide a good insight in what the limiting factors in the pyrolysis process are. The models do not yield accurate predictions of experimental product distributions. This is not surprising in view of the simplifications that have been introduced in the models with respect to reaction mechanism and physical processes.

An economic evaluation of the low temperature pyrolysis process in a spout-fluid bed reactor was carried out for a combined material recovery and pyrolysis plant with a capacity of 100,000 tons of domestic waste per year. It was concluded from this evaluation that the pyrolysis process leads to costs per ton of domestic waste that are comparable to or higher than those of conventional incineration of domestic waste, depending on the process scheme of the plant and on the way in which it is operated.

Samenvatting

Pyrolyse is een methode om afvalstoffen te verwerken met terugwinning van energie in de vorm van brandstoffen. Pyrolyse is de thermische ontleding van organisch materiaal onder uitsluiting van of met ondermaat lucht. De pyrolyse van de organische fractie van huishoudelijk afval waarop in dit onderzoek de nadruk heeft gelegen levert de volgende produkten op:

1. een laag tot middel calorisch gas bestaande uit CO, CO_2, H_2 en lagere koolwaterstoffen.
2. een teer fractie.
3. een houtskoolachtige vaste fractie.
4. een verontreinigde water fractie.

De drie eerstgenoemde produkten kunnen worden gebruikt als brandstoffen, die gemakkelijker hanteerbaar zijn dan het uitgangsmateriaal (huishoudelijk afval).

Het onderzoek heeft zich met name gericht op de lage temperatuur pyrolyse (tot ongeveer 600°C) in een spout-fluid bed reactor. De spout-fluid bed reactor is een combinatie van een gefluïdiseerd bed en een spouted bed. Dit resulteert in de volgende eigenschappen:goede lokale vaste stof menging, goede overall circulatie, goede warmte overdrachtseigenschappen en de mogelijkheid om de voeding via het spoutgas in de reactor te brengen. De relatief hoge gassnelheden, die in de reactor mogelijk zijn, maken dit type reactor bijzonder geschikt voor het lage temperatuur pyrolyse proces. Componenten die bij de reactietemperatuur gasvormig zijn (zoals de teer) worden dan snel uit de reactor gespoeld zodat kraakreacties zoveel mogelijk voorkomen kunnen worden. Hierdoor kan de teer produktie relatief hoog zijn. De teer wordt gezien als een aantrekkelijker brandstof dan de houtskool of het laag calorisch gas. Teer kan gemakkelijk opgeslagen en in tankwagens getransporteerd worden (eventueel na verdunning met water) en is gemakkelijk te verbranden. De teer kan wellicht ook worden gebruikt als Dieselolie substituut na verdunning met water.

In inleidende pyrolyse experimenten in een pilot installatie met een spout-fluid bed reactor (maximale capaciteit 10 kg/hr) is de invloed onderzocht van diverse reactiecondities op de pyrolyse van papiersnippers. Papiersnippers werden gekozen als modelstof voor de organische fractie van huisvuil wegens de overeenkomsten in chemische

samenstelling en stromingseigenschappen. Zowel papiersnippers als verkleind huisvuil zijn slecht stromende materialen. Gekeken is naar de invloed van de pyrolyse temperatuur (in de range 440-600^{o}C), het vochtgehalte van de voeding, de deeltjesgrootte van de voeding, het voedingsdebiet en de gassnelheid in de reactor.
Met name de pyrolyse temperatuur bleek van grote invloed te zijn op het pyrolyse proces. Hogere temperaturen leidden tot toename van de gasproduktie en afnemende houtskool opbrengst. De teer opbrengst vertoonde een maximum bij een pyrolyse temperatuur van ca. 500-525^{o}C. Toenemende pyrolyse temperatuur leidde verder tot een toename in de verbrandingswaarden van het gas en de houtskool.
Na deze inleidende experimenten werden pyrolyse proeven uitgevoerd met als voeding organische fracties van verkleind huisvuil (RDF: refuse derived fuel). Deze experimenten waren bedoeld ter verificatie van de resultaten behaald met pyrolyse van papier maar vooral ook ter bestudering van de eigenschappen van de pyrolyse produkten en de milieuconsequenties van het proces. De organische fracties werden uit verkleind huisvuil bereid door middel van "handpicking" (verwijdering van grote stukken glas en blik), windziften en zeven.
De trends in de produkten verdeling als functie van de pyrolyse temperatuur waren globaal dezelfde als die, welke gevonden waren bij de pyrolyse van papiersnippers. De teer opbrengst was echter veel lager en de opbrengst aan houtskool hoger in geval van de pyrolyse van RDF dan de overeenkomstige opbrengsten, die gevonden waren bij de pyrolyse van papier. Dit wordt toegeschreven aan katalytische invloeden van bepaalde anorganische bestanddelen van het huisvuil op bepaalde reacties die zich tijdens het pyrolyse proces afspelen.
Het onderzoek naar de milieuconsequenties van het pyrolyse proces leverde de volgende resultaten op:

- de as aanwezig in de houtskool bevat weliswaar zware metalen, maar niet in zulke grote hoeveelheden, dat de as een chemisch afval is in de zin van de Nederlandse wet.
- de organische verontreinigingen in de water fractie zijn biologisch afbreekbaar. Er werden geen chloorhoudende organische stoffen aangetroffen in de water fractie.
- het pyrolyse gas bevat HCl voornamelijk als gevolg van de aanwezigheid van PVC in de RDF fracties. Over de mogelijke aanwezig-

heid van chloorhoudende organische verbindingen in het gas kon nog geen definitieve uitspraak worden gedaan.

Er is fundamenteel onderzoek verricht naar de pyrolyse van cellulose-achtige materialen. Modellen zijn opgesteld ter beschrijving van het pyrolyse gedrag van dergelijke materialen gebaseerd op het onderstaande reactieschema, dat een sterke vereenvoudiging inhoudt van het complex van parallelle en opeenvolgende reacties, die zich tijdens de pyrolyse van cellulose afspelen.

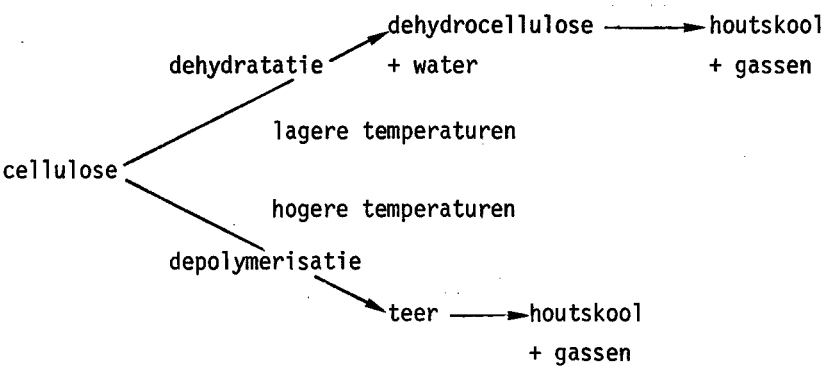

Ook de fysische transport- en overdrachtsprocessen tijdens de pyrolyse werden vereenvoudigd ingevoerd in de modellen.
Met behulp van thermoanalytische methoden werden de reactie kinetische gegevens bepaald, die nodig waren in de modellen.
De modellen verschaffen een goed inzicht in wat de factoren zijn, die het verloop van het pyrolyse proces bepalen. Het blijkt echter niet goed mogelijk om met behulp van de modellen nauwkeurige voorspellingen te geven van experimentele produkten verdelingen. Dit is ook niet verwonderlijk gezien de vereenvoudigingen die in de modellen zijn ingevoerd, zowel in het reactie mechanisme als in de fysische processen.

Een economische evaluatie van het lage temperatuur pyrolyse proces in een spout-fluid bed reactor is uitgevoerd voor een gecombineerde huisvuilscheiding en pyrolyse fabriek met een capaciteit van 100.000 ton huishoudelijk afval per jaar. Uit de evaluatie blijkt dat het pyrolyse proces leidt tot een verwerkingsprijs per ton huisvuil die vergelijkbaar of hoger is dan die voor de conventionele verbranding van huisvuil, afhankelijk van de uitvoering van het proces.

1. INTRODUCTION

This thesis reports a study which is part of a more general research effort aimed at the disposal or the processing of wastes. This research effort is primarily directed towards domestic waste, but other types of waste have not been forgotten.

The disposal of domestic waste has become an increasingly difficult and costly problem. There are several reasons for this, including:

a. Land available for landfill is rapidly becoming scarce. This is true throughout continental Western Europe and especially so in the western provinces of the Netherlands (North and South Holland and parts of Utrecht) where the development of new landfill sites has become all but impossible. This fact and the regionalisation policy recently adopted in the Netherlands, which stipulates that each region must in principle take care of the waste generated there, has led to a waste disposal situation that is rapidly becoming very difficult.
   In addition, the urbanization of the population causes substantially more refuse per unit area to be generated in areas where land availability for landfill is diminishing. Even if land for landfill is still available in less densely populated areas, sites will have to be kept in reserve to service the cities. It is to be noted in this respect that deposition is still the basis of all treatment of municipal wastes: all of the modern treatment methods leave some residue that must be disposed of by landfill. It seems highly important that this residue should have as small a volume as is possible.

b. Over the last decades the quantities of municipal solid wastes produced per unit time have been increasing. This has been due to both increases in the per capita generation of wastes and to population growth. However, population growth has recently diminished in the Netherlands and in several other countries in Western Europe. The economic crisis that now exists in most western nations may put a -possibly temporary- end to the increase of the per capita generation of domestic waste as consumption growth may stagnate. In the Netherlands, for instance, the years 1980 and 1981 showed a minor decrease in the quantity of waste generated per capita. This had not happened for some decades.

Some data on the production of domestic wastes in the Netherlands are shown below [1.1].

year	domestic waste	(bulky waste)	in kg/capita, year
1979	300	40	
1980	295	40	
1981	290	40	

c. The inhabitants of cities and villages have shown increasing reluctance to accept landfill sites on their territories.

It is obvious from the above that there is a problem. To judge the extent of the problem and to find indications of how it might be solved some data on the composition of domestic wastes are now presented. For the Netherlands these figures were in 1978 [1.2]:
Mean composition of the domestic waste (including bulky waste) in weight percentages on wet basis 'as received':

paper, cardboard	22%
glass	12%
iron	3%
plastics	6%
wood	1%
vegetables, garden waste, etc.	48%
bread	2%
animal waste	1%
textiles, rags	2%
carpets, leather	1%
rubbers	1%
stones	1%

The figures given here are mean values of percentages that can vary enormously. The composition is highly dependent of the time and the place of collection of the waste. It is clear that there is a number of components in the waste that are potentially valuable. Iron, glass, paper, cardboard and plastics are often felt to be materials that can be recycled more or less directly. Glass is economicly less attractive to recuperate it from domestic waste. Separate collection of glass (which is being done in large parts of Holland) may be a better alternative. But then there is still a lot of waste left that cannot be recycled directly: vegetables and garden waste, wood, textiles,

rags. These account for more than 50% or, if paper and plastics are included, over 80% of the total amount of domestic waste.
The fraction of the domestic waste that cannot be recycled directly must be removed from the cycle of raw materials or must be converted into new products or energy. The following processes are often used to dispose of waste materials:
-controlled landfill
-incineration without energy recovery.
Conversion of (organic) waste into chemicals or energy can be done by a number of processes including:
-biological conversion: composting, fermentation (into forage, chemicals or fuel)
-chemical conversion : 1. thermal conversion: degasification (pyrolysis)
2. other chemical conversions: hydrolysis, gasification, partial oxidation, incineration with heat recovery.

All these processes have been considered for the treatment of the organic fraction of domestic waste. The choice between the various processes is an economic and political one. As a result of varying circumstances one cannot claim that one of the processes is the best one and the only one suitable under all conditions. All of the processes have application possibilities or will have so in future.

Since the first energy crisis in the early seventies there has been an increasing interest in alternative energy sources. It was soon recognised that the organic fraction of domestic waste is such a source. Waste treatment processes providing means for energy recovery, either directly (steam, heat, electricity) or indirectly (fuels) aroused the growing interest of investigators and environmental authorities. Of these processes only the chemical conversion methods will be discussed here. (Hydrolysis of waste components to produce methanol and/or ethanol is not discussed here either. Investigations into these conversions have not yielded very encouraging results so far).

1.1 Nature of incineration, pyrolysis and gasification

Discussing the incineration process will be of help in introducing the pyrolysis. For this reason, a short description of this established method of waste treatment is presented here. Four different stages can be distinguished in the combustion of humid organic material [1.3]:

1. Drying of the material: moisture is evaporated.
2. Degasification or pyrolysis: volatile components are distilled off to produce char, condensible and non-condensible gases. The inflamable gases burn outside the boundaries of the solid waste particle.
3. Gasification: reactions of oxygen and steam with the char that yield hydrogen and carbon monoxide which burn.
4. Combustion of the char to produce CO_2 and H_2O.

A number of terms have been introduced in the above description: pyrolysis, degasification and gasification. In literature these and other terms (like carbonization, swelling, partial oxidation, destructive distillation, coking) are used to describe different kinds of processes in which (organic) material is decomposed by the action of heat but where one cannot speak of complete combustion. In chemical literature the terms pyrolysis (degasification) and gasification are used for two different, well defined processes. When these same process names are used in literature on waste disposal their significance is often somewhat different from the definitions used in chemistry. Fortunately, many investigators in the field of waste treatment nowadays define the terms they use when referring to thermochemical processes. Speaking of pyrolysis they all use in one way or the other the expression: thermal decomposition of organic material in the absence of air. But most of the authors give additional information as is shown in the following three examples:

"Pyrolysis is the decomposition of organic materials by the action of heat in which process big molecules are cleaved into smaller and more simple ones. In the technical terminology the process is called degasification if it is carried out in absence of air and gasification when the char and water are converted into carbon oxides and hydrogen by introducing understechiometric amounts of air." [1.4].

"Pyrolysis is the thermal decomposition of organic material resulting in the formation of condensible and non-condensible gases and solid carbonaceous residues. The process is called degasification when the decomposition is achieved by the action of heat only and it is called gasification when in the process a reactive gas is introduced (like oxygen, air, steam, carbon dioxide, hydrogen) to convert the carbonising residues into additional gaseous products." [1.5]
"Pyrolysis: the chemical decomposition of a substance by the action of heat in an inert or self-generated atmosphere. Gasification: pyrolysis process in which the carbonised residue is converted into combustible gas by partial combustion with air, oxygen, steam or any of their mixtures as a reactant." [1.6]
From the above it is clear that the term pyrolysis is used to describe a general thermochemical decomposition process whereas the use of the terms degasification and gasification is limited to thermochemical processes under specific conditions. In chemical literature pyrolysis and degasification are synonymous and stand for the thermal decomposition of organic material in absence of oxygen or other externally supplied reactants.
In this thesis the term pyrolysis will refer to strict degasification processes and to other thermochemical processes in which (f.i. through partial combustion) organic substances are converted into condensible and non-condensible gases and carbonaceous residue. The term gasification is used to indicate thermochemical processes in which organic substances are converted into combustible gases with the aid of gasification agents: air, oxygen, CO_2, steam, H_2 or mixtures of them. The organic carbon thus may be converted to gases via the following equilibrium reactions [1.7]:

$C + O_2 \rightleftarrows CO_2$
$C + CO_2 \rightleftarrows 2CO$
$C + H_2O \rightleftarrows CO + H_2$
$C + 2H_2 \rightleftarrows CH_4$

Some differences in the reaction conditions of pyrolysis on the one hand and gasification on the other hand are:
-In general the reaction temperature is (much) lower for pyrolysis processes than it is in the gasification of waste materials.
-In pyrolysis processes air may be introduced for partial combustion

of part of the feed, thus generating the heat required for the drying and pyrolysis of the waste. In gasification processes not only air but oxygen and/or steam may be used to convert the organic solid or liquid waste into gas.
In practice, however, it is difficult to draw a sharp line between both processes: pyrolysis gradually passes into gasification at higher temperatures as water is one of the pyrolysis products and the feedstock often contains substantial amounts of water.

As mentioned before, the thermochemical conversion methods discussed here owe part of their charm to the fact that fuels or energy are produced. In incineration processes the energy is gained as hot water, steam and/or electricity. This is achieved by installing heat exchangers in the combustion furnaces. Water is passed through the heat exchangers to give hot water (f.i. for district heating) or steam. If electricity is the desired product the steam is fed to (a) turbo-generator(s).
In pyrolysis and gasification processes fuels are produced. The products of the pyrolysis of domestic waste are a combustible gas, a tar, a char and a water fraction. Except for the last all can be used as a fuel. Gasification of wastes gives a gas with a low to medium heating value.
It is emphasized that, however nice the recovery of energy from domestic wastes may be, the primary objective of the thermochemical processes remains of course the reduction of the volume of the waste. This may be demonstrated by the fact that only about 1 percent of the energy requirement of the Netherlands could be met by the energy released if all domestic waste generated in the Netherlands would be incinerated. Only the ashes would have to be disposed of in that case which means that a considerable volume reduction of the waste would be accomplished.

1.2 Reasons for pyrolysis

Pyrolysis is a means to produce fuels from organic wastes. Domestic waste (at least the organic part of it) can be combusted directly. The question therefore arises what the use of pyrolysing can be. Why try to prepare fuels from wastes by pyrolysis or gasification when

the organic part of domestic waste is a fuel in itself?
A number of reasons are given in literature but only a few of the claims stated there have already been proved correct. The validity of most of the other claims is still in doubt. A comparison between incineration and pyrolysis will first be made. After that the relative uses of pyrolysis and gasification will be discussed.
Advantages of the pyrolysis process above the direct combustion or incineration of domestic waste are [1.6, 1.8, 1.9]:

a. There is less gas to be cleaned in the case of pyrolysis.
   The gases produced (product gas or off gas) have to be cleaned in pyrolysis as well as in direct combustion of domestic waste. These gases contain hazardous components like HCl (in part from PVC), SO_2 and particulate matter that may contain heavy metals compounds. A surplus of air must be used for the combustion of domestic waste. However, no air is introduced in the pyrolysis process or only just enough air to generate the heat (by partial combustion) that is needed to sustain the process. In this way the volume of air required for the combustion of one kg of waste may be seven times or more the volume needed to pyrolyse the same kg. The cost of gas cleaning is therefore much higher in case of the incineration of domestic waste than for the pyrolysis of the same amount of waste. On the other hand the fuels produced in pyrolysis (char, oil/tar, gas) are still to be used in combustion processes. It is not quite clear if or how much cleaning is required for the off gases from the combustion of the fuels. However, the combustion of the fuels requires (far) less excess air than the direct combustion of domestic waste [1.6]. If cleaning is indeed required for the flue gases from the combustion of the fuels produced through pyrolysis the amount of gas that has to be cleaned is less than in case of direct combustion of domestic waste.
b. Pyrolysis is more flexible than incineration.
   The steam generated in the incineration process of course cannot be stored. Steam must be used at once and more or less on the spot to generate electricity. The domestic waste is difficult to handle and not very suited for application as a fuel that can be used to generate a large amount of steam in a short period of time. Consequently, the electricity generated by means of incineration of

domestic waste cannot be supplied specifically in peak hours when the (provincial) electricity supply works need the extra energy. The fuels obtained in the pyrolysis process, on the other hand, can be stored, transported and used where and whenever one so desires. Pyrolysis of domestic waste provides a flexibility that is lacking in the incineration process.

c. Energy losses in the pyrolysis process may be less than in the direct combustion of domestic waste:
As stated above the volume of gas produced in the pyrolysis process is (much) less than in the combustion process. Consequently, the heat losses during the cleaning of the gas and in the stack are lower in case of pyrolysis. Besides, the cleaning of the gas requires less energy as a result of the smaller volume.

d. Investment and operating costs may be lower for pyrolysis than for incineration:
The investment and operating costs for pyrolysis furnaces may be lower than for competitive combustion furnaces due to a number of aspects summarized in table 1.1. Practical data are scarce, however, and the validity of this arqument is still to be proved.

e. Pyrolysis processes can handle high heating value wastes:
Wastes that have a high heating value (like plastics, rubber, paints) cannot be handled easily in normal type combustion furnaces as temperatures would rise too high. (Unless they are mixed with low heating value wastes of course). It is claimed, on the other hand, that pyrolysis of these wastes could result in fuels having relatively high caloric values. The caloric value of the gas obtained in pyrolysis of plastics may be up to 45000 kJ/m^3 [1.10].

f. Recovery of specific components is easier:
The domestic waste contains specific components (metal, glass) which can be recovered more easily or completely after a controlled thermal treatment than after high temperature combustion.

g. In pyrolysis processes less chlorine and sulphur containing compounds will be released:
Due to the (much) lower temperature in the pyrolysis processes the decomposition of substantial quantities of inorganic constituents in the waste such as ashes, salts, etc. is prevented. As a result HCl, other chlorine and sulphur containing compounds will be

released during pyrolysis mostly by the decomposition of some organic components which contain chlorine and sulphur. Consequently, the rate at which these compounds are released during pyrolysis is much lower than during incineration.

Table 1.1 Some aspects of pyrolysis and combustion furnaces that could be of interest for the relative investment and operating costs

Aspects	Pyrolysis	Combustion
Atmosphere	reducing	oxidizing, sometimes alternately reducing and oxidizing
Temperature	mostly lower	especially local high temperatures are possible (on grate)
Construction	in most cases only few moving parts	mostly mechanically moved grates
Corrosion during heat recovery	small in case of pure pyrolysis (gas cleaning before energy recovery)	deposition of fly ash; corrosion of the tubes of steam boiler (gas cleaning after energy recovery)

So far, only the advantages of pyrolysis have been summed up. The incineration of domestic waste does of course have certain advantages over pyrolysis and gasification. First of all, incineration of domestic waste is a reliable method to dispose this waste and the technique of waste incineration has been amply proven. Furthermore, the incineration residue is sterile while waste water, that may be generated when the slag is quenched in water, can easily be purified.

A comparison of gasification and incineration would mostly result in a repetition of the arguments in favor of pyrolysis that have been discussed above. There are, however, some important differences between pyrolysis and gasification as table 1.2 demonstrates.

Table 1.2 Comparison of gasification and pyrolysis of domestic waste [1.8]

Advantages of gasification	Advantages of pyrolysis
a. less or no contaminated water	a.-
b. no char, nearly no tar (the process is cleaner, there are fewer difficulties with respect to tar condensation	b. char and tar (the process is more flexible, results in more condensed storage of fuels)
c. -	c. lower temperature (no need for fire proof lining of reactor, no problems with molten slag)

A further disadvantage of gasification is the difficulty of marketing the relatively low heating value gas. This difficulty is being encountered in some countries [1.11].

The supposed advantages of gasification and pyrolysis make it worthwhile to investigate these processes as an alternative to the incineration of domestic waste. This thesis answers some of the questions that have arisen with respect to the application of pyrolysis to domestic waste disposal.

1.3 History of pyrolysis

Pyrolysis is an ancient art: the prebiblical Egyptians already pyrolysed wood to obtain charcoal, fluid wood tar and pyroligneous acids useful for embalming. In feudal England the art of making charcoal through pyrolysis (in a closed vessel from which oxygen had been removed) was a jealously guarded secret that was passed down from

father to son through generations [1.12].
For centuries the destructive distillation (pyrolysis) of wood was the major source of charcoal, acetic acid, methanol and acetone until synthetic processes became more economical during and following World War I. Another pyrolysis process known of old is the production of coke and city gas from coal.
The thermal cracking of naphta has been practised for decades now in oil refineries to produce ethylene, propylene, butadiene and aromatics (sometimes in catalytic rather than thermal processes).
Only the last decade has pyrolysis been investigated and used as a new method for solid waste treatment.
The pyrolysis of domestic wastes is a process comparable to the destructive distillation of wood and the production of coke and city gas from coal. This is not surprising as domestic wastes contain many cellulosic materials while wood consists predominantly of cellulose and coal is a product of a very slow carbonization of wood and similar materials. The products of the three processes are given in table 1.3.

Table 1.3 Products of thermal decomposition of wood, the organic part of domestic waste and coal

Products	destructive distillation of wood	pyrolysis of domestic waste	coking of coal
gaseous	CO_2, H_2 light hydrocarbons	CO, CO_2, H_2, light hydrocarbons	CO, H_2, light hydrocarbons
watery fraction	'wood spirit', a solution of methanol, acetic acid, acetone	watery solution of numerous organic components	watery solution
liquid organic fraction	terpentine, wood tar	tar	coal tar
solid product	charcoal, alkaline products[1]	charcoal	coke

1) used for soap making

Typical yields from the destructive distillation of wood are [1.13]:

gas	14.2 - 16.8 wt.%
methanol	1.6 - 2.1 wt.%
acetic acid	3.6 - 7.7 wt.%
tar	12.3 - 16.2 wt.%
charcoal	31.0 - 36.5 wt.%

Mean values for yields from the production of coke from coal (high temperature coking of coal) are (in wt.%) [1.14]:

coke	70%
gas	15%
tar	4%
crude light oil	1%
breeze	6%

It is not possible to give typical yields for the pyrolysis of domestic waste because of the use of very different types of reactors and widely diverging conditions for the pyrolysis process, and, of course, because of the strongly varying composition of domestic waste. In the next paragraphs details will be given regarding the types of reactors used in solid waste pyrolysis processes. Attention will be paid to some of the existing commercial pyrolysis systems.

1.4 Reactors used in solid waste pyrolysis systems

Before discussing the different types of pyrolysis furnaces it may be useful to formulate some general demands the pyrolysis reactor will have to meet:

- -solid materials must be transported into, through and out of the reactor
- -gaseous reaction products must be removed from the apparatus
- -heat must be supplied to the solid material for drying, for bringing the solid to reaction temperature and to compensate for possible endothermicity of the reaction.

With these requirements in mind the various reactors that are used can be classified in two different ways: according to the way the solids are transported into and through the reactor, and according to the way heat is supplied to the solids.

Firstly the classification of the reactors based on the transport of

the solids into and through the reactor (with some examples):

a. moving bed (shaft furnaces)
b. bed in which the particles move under the influence of mechanical forces (rotary kiln, moving grate)
c. bed in which the particles move under the influence of fluid flow (fluid bed, spouted bed, entrained bed)
d. suspension reactors (molten salt reactor)

Going from type a. to d. particle size of the domestic waste decreases, the heat transfer rate increases while residence time in and volume of the apparatus decreases, energy costs for transport through the apparatus increase and the apparatus will become more complex. It is hard to predict in what way these factors influence the process economy.

The second way of classifying pyrolysis furnaces is on base of the way heat is supplied to the solids:

a. indirect heat transfer through the reactor wall or pipes in the bed
b. direct heat transfer that results from introducing heated (inert) material into the bed (circulation of heated sand or hot gases)
c. heat supply by means of exothermic chemical reactions (partial combustion of the feed or pyrolysis products).

The two ways of classifying the reactors are not independent. When the transport of the solids in the reactor is fast the heat transfer to the solids must be very good to make sure that the solids reach the reaction temperature. On the other hand, when the solids are moving slowly through the reactor no fast heat transfer to the solids is required.

The types of pyrolysis reactors used most often will be discussed in this paragraph and some of the existing pyrolysis systems fitted with one of these types of reactors will be reviewed in §1.5. Although this includes the most important combinations of solids transport and forms of heat supply, more combinations exist or existed. There is almost no combination of way of solids transport and way of heat supply that is not being investigated or practised in the field of waste pyrolysis as is demonstrated by the matrix[1)] below:

way of heat supply to the solids / way of packing and transport of solids in the reactor	indirect heat transfer (via pipes, reactor wall)	direct heat transfer without chemical reaction (hot gases, sand)	direct heat transfer with chemical reaction (partial oxidation)
moving bed (shaft furnace)	Destrugas (§1.5)	Warren Springs [1.15]	Andco Torrax 2) [1.16]
bed motion by mechanical forces (rotary kiln)	Babcock-Krauss-Maffei (§1.5)		Monsanto Langard [1.17]
bed motion by fluid (fluid bed, spout-fluid bed, entrained bed)	present research	Ebara (§1.5)	Occidental Oil Cy. (§1.5) Hitachi (§1.5)

1) An example is given for each combination that is being investigated or practised. A literature reference is given for the systems that will not be discussed in §1.5.

2) Gasification process.

This might indicate that not all fundamental aspects of the pyrolysis process are already known and that a good deal of trial and error is still going on. This is held to justify the inclusion in this thesis of sections (chapters 2 and 7) that deal with the fundamentals of pyrolysis.

The types of pyrolysis reactors used most often are:
1. Vertical shaft furnaces.
2. Rotary kiln.

3. Fluid bed reactor.
4. Entrained bed reactor.

Characteristics and (dis)advantages of these different types of reactors will be discussed briefly [1.5, 1.6, 1.8, 1.18]:

1. Vertical shaft furnace

This type of reactor is seldom used for pure degasification processes as heat transfer from the heated furnace wall to the solids is very poor. It is used more often for gasification processes where air or oxygen is introduced in the reactor. As a result of the poor heat transfer the residence time of the solid material in the reactor must be in the order of many hours and yields of gas and char are high. An advantage is that little or no shredding of the feedstock is required. Disadvantages are: low capacity on basis of reactor volume and long lasting start-up and shut-down procedures.

2. Rotary kiln

This reactor type is used most often for low temperature pyrolysis processes (450 - 600^{o}C). Residence time for the material, that has only to be shredded roughly, is about half an hour. Advantages are those that result from low temperature operation, viz. the easy recovery of non-oxidized metal and glass from the residue, little chemical corrosion of reactor wall and low energy losses. A disadvantage is the poor contact between gases and solids so addition of lime or other additives to the bed is not very effective. In addition, it is said that the reactor wall may be damaged as a result of the large axial mixing that leads to hot particles getting into contact with cold parts of the reactor wall and cold waste particles getting into contact with hot parts of the reactor wall.

3. Fluid bed

Fluid bed pyrolysis reactors are operated in a wide temperature range (400 - 900^{o}C). When production of tar is desired reaction temperatures are about 450 - 550^{o}C, when gas is desired the reactor is operated at temperatures from 650 to 900^{o}C. (The influence of pyrolysis temperature and residence time on the product distribution will be discussed in Chapter 2.) Short residence times (in the order of minutes) make high tar yields possible. In fluid beds the temperature is homogeneous

and can be kept constant easily due to the very good heat transfer in the solid phase of a fluid bed and the fact that the inert bed material acts as a thermal flywheel. The impact of variations in feedrate or composition is therefore rather small. The removal of hazardous compounds through injecting additives that will react with these compounds into the bed may be very effective. Disadvantages of fluid bed pyrolysis reactors are: a considerable size reduction of feedstock is required, ashes must be removed from the bed and dust loadings of the product gas may be high. The removal of ashes is not a very great disadvantage as it can easily be accomplished by means of a standpipe.

4. Entrained bed

In an entrained bed reactor residence time is very small resulting in high yields of tar and oil. Its capacity per unit of reactor volume is high. The extensive pretreatment of the feed is a disadvantage: presorting and strong size reduction are required to produce the light, fluffy material that is used as feedstock.

1.5 Some existing domestic waste pyrolysis systems

Once again, the discussion will be limited to pyrolysis systems so that well-known gasification processes like Andco-Torrax will either be left out or mentioned only briefly. An example of all types of reactors listed in paragraph 1.4 will be discussed. For shaft furnaces this is the Destrugas system [1.4, 1.15, 1.19, 1.20, 1.21, 1.22]. In the mid-sixties Destrugas developed the idea of using old coke-ovens as units for the thermal processing of domestic wastes. The Destrugas process is a high temperature pyrolysis (900 - 1000^{o}C) of domestic wastes in an externally heated shaft furnace. A charging system is placed on top of the furnace. This also serves as a gas lock. The water present in the waste is vaporized in the upper part of the shaft. Then in the middle part of the shaft the organic substances are decomposed into gas and tar while in the lower part the tar is being cracked to give gases. The high caloric gases that are generated are extracted from the bottom part of the shaft and sent to the gas refining system. Thus the pyrolysis gases move co-currently with the waste downwards through the reactor. Char is removed from the bottom part of the furnace at an adjustable rate. Residence time of the waste in the reactor is about 20 hours. The domestic waste used

as feedstock is shredded to pieces smaller than 10 cm (mostly < 5 cm). Part of the product gas is burnt to heat the furnace walls. Product distribution: mean values for the pyrolysis of domestic waste containing ca. 35 wt.% moisture (calculated from [1.4]):

Gas	36 wt.%	
Residue	28 wt.%	(inclusive of 2 wt.% iron)
Tar	4 wt.%	
Water	32 wt.%	

No plants have been in continuous operation so far but pilot and demonstration plants have been constructed (table 1.4).

Table 1.4 Pilot and demonstration plants according to the Destrugas system

Place	Capacity (t/day)	Period of testing
Kolding	18	1967 [1.15]
Kalundborg	5	1970 [1.4, 1.15, 1.19, 1.20]
Technical University of Berlin	0.24	1977/79 [1.21]
Hitachi City	4	1976 [1.22]

Examples of rotary kiln processes are numerous. The best known process for thermochemical decomposition of domestic waste that applies a rotary kiln used to be the Monsanto-Langard process [1.17, 1.23]. This is a gasification process that has been operated on a large scale in U.S.A. and Japan. However, the 900 t/day plant constructed at Baltimore (MD) has been a complete failure and Monsanto has left the domestic waste treatment business [1.18].
Rotary kiln processes that will be discussed in more detail are the Babcock-Krauss-Maffei and Kiener processes.

The Babcock-Krauss-Maffei (Pyrocal) process [1.9, 1.18, 1.24, 1.25]

This process has been developed from a 5-10 kg/hr laboratory plant (1976) via a 500 kg/hr pilot plant (1977) to a 2x3 t/hr plant that is to be erected in 1982 [1.9]. The description of the process that

follows now is based on the 500 kg/hr pilot plant that has been operated for more than 2500 hours with domestic waste and sewage sludge as feedstock. The pyrolysis reactor consists of a rotary kiln that is heated indirectly. For start-up the rotary kiln is heated with natural gases, during normal operation the kiln is heated by burning part of the cleaned low temperature pyrolysis gas. The heating chamber is divided into 6 heating zones which can be heated independently. This construction makes it possible to follow the heat requirements for drying and decomposition reactions that differ along the rotary kiln. Pyrolysis is effected at low temperatures of 400 - 550°C, depending on feedstock. Residence times of the solid particles are normally half an hour to one hour. The low temperature charcoal is discharged through a gastight sluices system. Glass and metals can be separated from the residue to some extent by screening. The pyrolysis gas that has been generated is cleaned in three stages: 1. dedusting of the gas in heated cyclones, 2. thermal cracking of the gas at 1000°C so tar constituents will be cracked to give low molecular gas and char, and 3. cooling of the gas and cleaning in a scrubber and washing tower. Part of the gas is used for heating the rotary kiln and thermal cracker. Composition of the recovered gas (mean values [1.24]):

H_2	15 - 25 vol.%
CO	8 - 15 vol.%
CO_2	5 - 12 vol.%
N_2	45 - 55 vol.%
Hydrocarbons	3 - 8 vol.%

The product distribution (for pyrolysis of wood having a moisture content of 65 wt.%) at 550°C is [1.25]:

low temperature carbonization coke: 25 wt.% (of moisture and ashfree feed)

low temperature carbonization gas	: 30 wt.%
condensate	: 20 wt.%
water	: 20 wt.%

Kiener pyrolysis system [1.26, 1.27]

As the Babcock-Krauss-Maffei process the Kiener pyrolysis system is a low temperature (450 - 500°C) pyrolysis process in an indirectly heat-

ed rotary kiln. The heat required is obtained from the exhaust gases of a gas motor (see below). Pyrolysis takes place in an air free atmosphere in a reducing zone. Pyrolysis gases flow from the rotary kiln into a gas cracker where at the same time just enough air is injected so that the pyrolysis gas reaches a temperature of 1100 - 1200°C by partial combustion. Long chain molecules and aromatic compounds are cracked. After washing and cooling the clean gas is fed to the above gas motor. The gas motor is used to drive an electricity generator.
Exhaust gases from the motor are used to heat the rotary kiln.
A second variant of the Kiener process exists in which the rotary kiln pyrolysis is followed by a two stage condensation giving a high boiling oil and a low boiling, waterrich oil [1.28].

Two different systems that belong to the fluid bed pyrolysis processes will be discussed: the partial oxidation of shredded domestic waste in a fluid bed (Hitachi) and the pyrolysis of fractions of shredded domestic waste in a two bed pyrolysis system (Ebara, Tsukishima Kikai).

The Hitachi process [1.18, 1.29] is a low temperature pyrolysis process where shredded domestic waste is treated in a fluid sand bed. The feedstock is fed to the fluidised bed by a screw-feeder and is decomposed in the reactor into gases and char. The heat required is provided by partial oxidation of the feedstock and pyrolysis products through introducing air into the reactor. Char floating on top of the sand bed is discharged from the bed through an overflow pipe. The hot gases flow from the top of the reactor into a couple of cyclones to separate fine char particles. From there the gases flow through a dual-stage scrubber unit, where the gas is cooled down to obtain a high calorific "plastic oil" (about 35 MJ/kg) and a "cellulosic oil" that condenses together with the water. Pilot plant capacity was 100 - 150 kg/hr. Pyrolysis temperature is in the range 450 - 550°C.
Typical product distribution [1.29]:

gas	30 wt.%
water	37 wt.%
char	13 wt.%
oil	17 wt.% (12 wt.% plastic oil)
incombustible	3 wt.%

Of the different two bed pyrolysis systems only the Ebara system will be discussed. In the Ebara two bed pyrolysis system [1.30, 1.31] sand is circulated between the fluid bed pyrolysis reactor, where the endothermic degasification reactions take place, and a second fluid bed (regenerator) where exothermic combustion of the char takes place. Sand acts as heat carrier. A high calorific gas can be produced as a result of the strict separation of the pyrolysis and combustion processes. Cleaning of the gas is carried out in cyclones and scrubbers. The fluidisation gas used in the pyrolysis reactor is recirculated product gas. Feedstock is an organic fraction of domestic waste. Pilot plants with a capacity of up to 200 kg/hr have been operated and a plant with a capacity of 30 t/day is being tested on the Yokohama demonstration site [1.31]. Reaction temperature is in the range 700 - 900°C and the main product is gas (lower heating value about 20 MJ/m^3). Small amounts of char and tar only are produced.

The last pyrolysis system that will be discussed is the entrained bed pyrolysis process of Occidental Oil Cy. [1.23, 1.32]. This process was developed by the Garrett Research and Development Company and involves the rapid heating of finely shredded organic waste in the absence of air using a proprietary heat exchange system. The dry, finely divided feed that is claimed to be essentially free of inorganics is introduced into an empty tubular reactor by being entrained by recycle gas and is mixed with recirculated, glowing carbon particles at temperatures of about 750°C. As result of the turbulent mixing the temperature drops to about 450 - 510°C. Degasification takes place within a few seconds so that the gaseous products formed are not exposed to high temperatures long enough to permit thermal degradation. This flash pyrolysis technique was developed to maximize liquid fuel yields. A 4 t/day pilot installation was operated in La Verne (Cal.) for years. A 180 t/day pilot installation was constructed in El Cajon (Cal.) but has proved to be incapable of properly producing the pyrolysis feedstock. The idea was abandoned after very few unsuccessful test runs. More details on in- and output of the pyrolysis unit are: feedstock: organic fraction of domestic waste, dried (<5% water) and shredded (<0.4 mm). Typical product distribution:

gas	27 wt.%
water	13 wt.%
oil/tar	40 wt.%
char	20 wt.%

1.6 Low temperature pyrolysis in a spout-fluid bed

In recent years a trend towards pyrolysing at lower temperatures appears to have developed (Babcock-Krauss-Maffei, Kiener, Tech-Air [1.33]). This tendency seems to have been prompted by difficulties encountered in marketing in some countries the relatively low heating value gas that results from gasification. The expectation that the formation of thermodynamically stable, chlorine containing organic hazardous contaminants might be more easily avoided at lower reaction temperatures appears to be a second consideration.
Some interest now exists in the possibility of using the tar obtained in low temperature pyrolysis as a Diesel oil substitute after dilution with water. If the manufacturer so desires the tar can also be cracked in a secondary reactor to produce more gas (Babcock-Krauss-Maffei).

This thesis discusses the application of a spout-fluid bed reactor to low temperature pyrolysis of organic waste fractions. The spout-fluid bed reactor was selected because it emphasizes a distinctive feature of low temperature pyrolysis in that it tends to produce relatively large amounts of tar. This type of reactor was first proposed by Chatterjee [1.34]. The scheme of figure 1.1 explains the principles of its operation by comparing it to the well-known fluid bed and spouted bed reactors. Domestic waste may be fluidised in a sand bed in all three apparatuses shown in figure 1.1. This is advantageous in that these types of reactors show relatively good mixing characteristics in the solid phase. The author believes that the mixing in the solid phase may be better in a spout-fluid bed than in either a fluid bed or spouted bed on the basis of the following observations: shredded domestic waste suspended in a fluid sand bed shows a considerable tendency to segregate so that the upper parts of the bed contain more waste material than the lower ones. In spouted sand beds to which domestic waste has been added zones containing higher than average

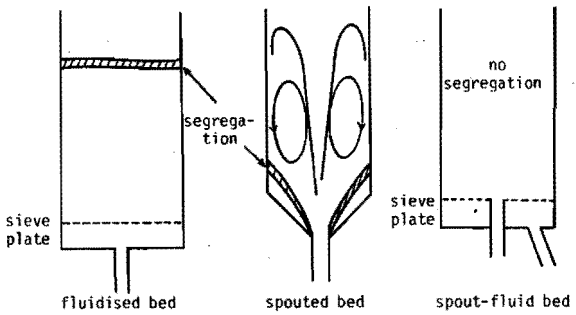

Fig.1.1 Fluidised, spouted and spout-fluid bed

concentrations of organic wastes were often found to occur near the walls in the conical part of the apparatus (fig.1.1). Solid phase mixing apparently is not very intense in that section. The spout-fluid bed reactor was found to feature very good solid phase mixing behavior so that segregation can be avoided.

Two important aspects of the intensive solid phase mixing of the spout-fluid bed reactors are: a. It is possible to keep a material like domestic waste (which cannot be fluidised itself) well distributed in the bed without risk of sticking and obstruction by segregation, in spite of relatively high tar production in the bed (see below); b. The reactor shows excellent heat transfer characteristics. Good heat transfer is important in pyrolysis as the domestic waste must be brought to reaction temperature and the water in it must be evaporated.

The spout-fluid bed reactor is very flexible because the flow of the gas through the sieve plate (fluidisation gas) and that through the spout (spout gas) can both be varied at will over considerable ranges. It is thus quite easy to operate the reactor by appropriate choices of the fluidisation and spout gas rates in one of several flow regimes where no continuous gas spout exists between the upper end of the spout pipe and the top of the bed. The gas near the axis of the reactor then rises through the apparatus in large but separate bubbles. The amount of organic material that is blown out of the reactor without having had sufficient residence time in it to react can thus be reduced to a minimum.

A distinctive characteristic of the spout-fluid bed reactor is the relatively large gas flow rate through the apparatus. This gas flow quickly removes gaseous reaction products from the bed. The residence time of gaseous reaction products such as tar constituents in the high temperature zone will therefore be relatively short. Secondary cracking of these tar constituents will thus be comparatively slight so that tar yields will be relatively high.
An advantage of both spouted and spout-fluid bed reactors is that the shredded domestic waste may be introduced into the reactor through the spout pipe. The organic material is entrained by the spout gas and is thus moved to the reactor through pneumatic transport. This obviates the need for complicated feed systems.
All in all there appeared to be sufficient reason to apply the spout-fluid bed reactor to low temperature pyrolysis. The results obtained will be shown in the next sections.

Literature

1.1 Personal communication, Institute for Waste Disposal (IVA) (April 1982)
1.2 SVA report 3000/175, Amersfoort, The Netherlands (1979)
1.3 R.Rasch, Aufbereitungstechnik 3, pp 138 (1977)
1.4 O.Tabasaran, Müll und Abfall 5, pp 127 (1975)
1.5 A.Buekens, Müll und Abfall 12, pp 353 (1978)
1.6 J.Schoeters, Proceedings of the 2nd International Symposium Material and Energy from Refuse (Ed.A.Buekens), pp 89 (October 1981)
1.7 W.P.M. van Swaaij, Resources and Conservation, vol.7, pp.337 (1981)
1.8 C.P.M.van Ginneken, M.Tels, Postgraduate Course "Gezondheidstechniek", on disposal and recycling of wastes. Delft (1980)
1.9 R.Schmidt, Proceedings of the 2nd International Symposium M.E.R. pp 9.67 (October 1981)
1.10 W.Kaminsky, H.Sinn, J.Janning, Chem.Ing.Technik, vol.51, no.5, p.419 (1979)
1.11 C.P.M. van Ginneken, M.Tels, Proceedings of the 2nd International Symposium M.E.R., pp 9.41 (October 1981)
1.12 J.E.Liebeskind, Chemtech 9, pp 537 (1973)

1.13 H.C.Brocksiepe et al., Chemische Technologie, Band III, pp 417, Karl Hanser Verlag, München (1971)
1.14 P.J.Wilson, J.H.Wells, Coals, coke and coal chemicals, Chemical Engineering Series, McGraw-Hill Book Cy. Inc. (1950)
1.15 E.Douglas, M.Webb, G.R.Daborn, The pyrolysis of waste and product assessment, Symposium on the treatment and recycling of solid wastes, Manchester (January 11, 1974)
1.16 C.Melan, Müll und Abfall 12, pp 371 (1978)
1.17 A.J.Helmstetter, D.B.Sussman, A technical and economic evaluation of the Baltimore Langard Demonstration, U.S.Environmental Protection Agency (1978)
1.18 A.Buekens, Müll und Abfall 6, pp 184 (1980)
1.19 O.Tabasan, Umwelt 2, pp 81 (1976)
1.20 K.H.Rymsa, Müll und Abfall 12, pp 377 (1978)
1.21 J.M.Segebrecht, Trans.Recycling Berlin '79, vol.1, pp 615 (1979)
1.22 N.Shikata, M.Wakabayashi, Trans.Recycling Berlin '79, vol.1, pp 634 (1979)
1.23 S.J.Levy, Waste Age, pp 14 (October 1974)
1.24 R.Schmidt, Müll und Abfall 12, pp 375 (1978)
1.25 R.Schmidt, Trans.Recycling Berlin '79, vol.1, pp 646 (1979)
1.26 S.Lenz, Trans.Recycling Berlin '79, vol.1, pp 640 (1979)
1.27 S.Lenz, Müll und Abfall 12, pp 371 (1978)
1.28 O.Tabasaran, Müll und Abfall 10, pp 293 (1977)
1.29 K.Shimada, S.Nogita, M.Ishida, et al., Proceedings 2nd International Symposium M.E.R., pp 9.1 (October 1981)
1.30 M.Andoh, Y. Ishii, Y.Hirayama, K.Ito, Trans.Recycling Berlin '79, vol.1, pp 575 (1979)
1.31 S.Gotoh, Proceedings 2nd International Symposium M.E.R., pp 37 (October 1981)
1.32 G.M.Mallan, C.S.Finney, AIChE Symposium Series, vol.69, no.133, pp 56 (1973)
1.33 M.D.Bowen, E.D.Smyly, ACS Symposium Series, no.76, pp 94 (1978)
1.34 A.Chatterjee, Ind.Eng.Chem.Process Design Development, vol.9, no.2, pp 340 (1970)

2. FUNDAMENTAL ASPECTS OF PYROLYSIS

Abstract

It is felt to be useful to investigate the fundamentals of pyrolysis because there seems to be a lack of insight in what the factors are that limit the rate of conversion.

The fundamentals of pyrolysis are discussed on the basis of the findings and theories on the pyrolysis of cellulose rather than on the basis of the pyrolysis of domestic waste. The composition of the organic fraction of domestic waste varies strongly. This causes domestic waste to be unattractive for use in fundamental research.

The pyrolysis of cellulose is discussed on the basis of the chemical reactions and physical transport processes that take place during the pyrolysis process.

The mechanism of the chemical reactions may be divided into three stages:

1. reactions without loss in weight (recristallization, primary depolymerization).
2. primary decomposition reactions (dehydration and anhydro-sugar formation)
3. secondary decomposition reactions that yield a wide variety of pyrolysis products.

The rate limiting physical transport processes in pyrolysis are generally confined to heat transport. Mass transport is not assumed to be a limiting factor because of the high porosity of cellulose. The following heat transport processes must in principle be taken into account:

1. heat transfer to the particles by radiation and convection.
2. heat transport inside the particle by conduction through solids and convection of gases.

Models for cellulose pyrolysis that have been found in literature and that are based on the above chemical and physical processes are surveyed. Simplified reaction models were used in all models to approximate the complex series of parallel and consecutive reactions that take place in cellulose pyrolysis. All models provided no more than a description of the pyrolysis of a single particle.

We decided on the basis of this survey to derive models for the pyrolysis of one cellulose particle in which both multiple reactions and

heat transport through conduction and convection are taken into account. The cellulose particle is represented in these models by an infinite cellulose slab of finite thickness in which heat is transported by both conduction and gas convection while mass is transported by gas convection only. The simplified reaction scheme applied in our models is given below.

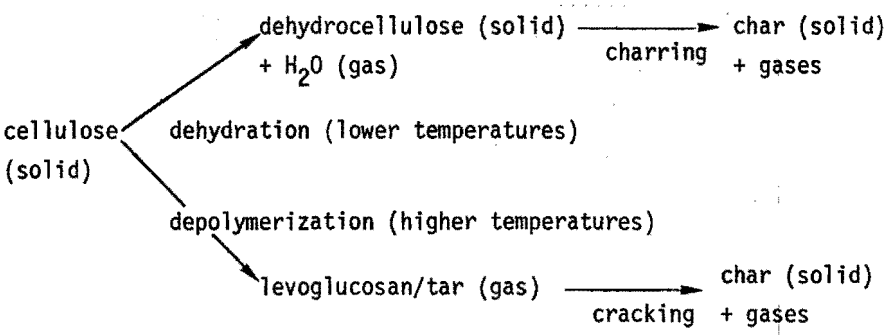

The levoglucosan/tar will in practice partly evaporate and partly decompose into char and gases. Two models are derived that represent two extreme situations:

1. the tar evaporates without being decomposed
2. the tar remains in the particle and is there subjected to cracking reactions.

A third model was developed in which the conversion rate is limited by the rates of the chemical reactions only.

A literature review of reaction kinetic parameters for cellulose pyrolysis revealed widely varying kinetic data. It was decided therefore to determine experimentally the reaction kinetic data (activation energy, frequency factor and gas yield factor) for each of the above four model reactions. This was done by means of thermoanalytical methods (thermogravimetry and differential thermal analysis).

The models derived will be applied to calculate product distributions and reaction times for the pyrolysis of cellulose using the kinetic data obtained by the thermoanalytical experiments (see Chapter 7). The results obtained from the models will be compared to experimental results.

2.1 Introduction

The fundamentals of pyrolysis will be discussed in this chapter. It is felt to be necessary to do so for a number of reasons. Some of these reasons originate from waste pyrolysis practice and some arise from the point of view of the present research.
In paragraph 1.5 a survey was given of existing pyrolysis systems. This survey shows that a wide variety of reactors is used in the pyrolysis systems. The reactors used vary from a shaft furnace with indirect heat transfer and long residence times of solid particles to an entrained bed with direct heat transfer and very short residence time. All intermediate combinations of ways the heat is transferred to the waste and of residence time are applied in practice or have been considered (see matrix in §1.5). This seems to indicate a lack of insight into what is going on in the reactor. Insufficient information is available about the fundamentals of the pyrolysis conversion. It is not known what the factors that limit the rate of this conversion are. This seems to be confirmed by the problems that have sometimes been encountered in the scale-up of pyrolysis units.
Another reason for investigating the fundamental aspects of the pyrolysis conversions is the expectation that a better understanding of it may be of assistance in improving process control.

The fundamentals of pyrolysis will be discussed on the basis of the findings and theories on the pyrolysis of cellulose rather than the pyrolysis of domestic waste. It was mentioned above that the composition of the organic fraction from domestic waste varies enormously. This makes that fraction unattractive for use in fundamental research. A better defined model material has for this reason been used in this investigation. As the chemical composition of the organic fraction from domestic waste shows a good resemblance to that of cellulose (see §4.2.1) many investigators in the field of the pyrolysis of domestic waste have chosen cellulose for their fundamental studies of the pyrolysis conversion.
A further advantage may be that the pyrolysis of cellulosic materials has already been studied by many investigators and much is known already about the mechanism. Investigations on the pyrolysis of wood for making methanol, acetic acid, wood preservatives etc. from it

began as early as the second half of the 19th century. This type of investigation did, however, end with the advent of the Fischer-Tropsch process on the one hand and access to cheap petroleum on the other. There has been a short revival of the research for energy and chemicals from sources other than petroleum in the Second World War, but these investigations were mostly directed towards the gasification of wood and the direct (Bergius) coal hydrogenation in Germany and the Fischer-Tropsch process (methanol manufacture) in South Africa. The growing share of cellulose derived fibers in the textile industry also stimulated the investigation of structure, properties and combustion characteristics (textile flame proofing) of cellulose. The research efforts in the field of the reduction of inflammability (fire resistance) of wood -an important construction material- by the addition of inorganic salts can also be included in the investigations of the pyrolysis of cellulose and related compounds.
It was decided for these reasons to select cellulose as a model material for studying the fundamental aspects of the pyrolysis process.

2.2 Cellulose pyrolysis

2.2.1 Cellulose

Cellulose is a polymer that is present in nature in large amounts. This natural or native cellulose can be produced by mechanical separation from cotton, jute, hemp and flax. Wood contains about 40% cellulose that can be separated from lignin and hemicellulose by treating it with alkaline. The primary chemical structure of cellulose is that of a linear polymer of glucopyranose units which is described more accurately as poly-(β-1,4-glucopyranose) (fig.2.1).

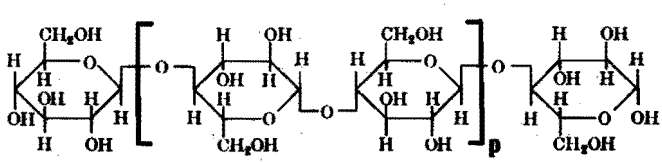

Fig.2.1 Cellulose

Other carbohydrates inclusive of branched chain carbohydrates may

occur to a very minor extent in natural cellulose. Celluloses obtained from cotton and wood are 100% respectively 99% pure. The elemental formula of cellulose, $C_{6p}\ H_{10p+1}\ O_{5p+1}$, approaches $(C_6H_{10}O_5)p$ for large values of p(the degree of polymerization). The limit of the molecular weight thus is 162.14xp.
The degree of polymerization of cellulose varies widely according to source and method of isolation. Natural (native) cellulose may have a degree of polymerization between 3500 and 10,000 [2.1] while cellulose isolated from wood has a degree of polymerization of 800 - 3000. (Chemical methods of isolation and purification are attended with depolymerization of cellulose.)

Cellulose occurs in various crystalline modifications which vary slightly in dimensions and angles of the unit cell. The exact position of the hydrogen bonds in the individual modifications is not known. The glucopyranoses in cellulose are arranged in the chain form with all the OH and CH_2OH groups arranged equatorially (fig. 2.2).

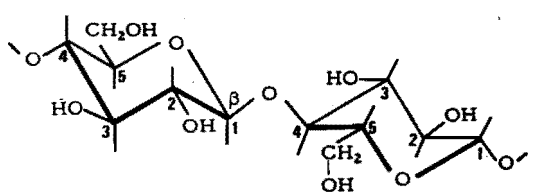

Fig.2.2 Arrangement of glucopyranoses in cellulose

An intramolecular hydrogen bond exists between O at C-3 and O at C-5. In addition, seven intermolecular hydrogen bonds are possible which result in bundles of cellulose chains situated side by side. The bundles are tangled to a rope-like structure (micells) that are grouped to form fibrils. If the fibrils are ideally packed they are called crystallites. The crystalline regions are surrounded by semi-crystalline and amorphous regions, the so-called LOR's (less ordered regions). The various methods used for determining the crystallinity of cellulose, a concept that is ill-defined in literature, give different values (table 2.1 [2.2]).

Cellulose can be classified on the basis of its crystallinity or on the basis of the treatments it has been subjected to. The types of

cellulose are [2.2]:

cellulose I (= native cellulose): most crystalline modification

cellulose II (= hydrated cellulose, regenerated cellulose): less crystalline modification. Obtained by dissolving and reprecipitating cellulose I.

cellulose III (= ammoniacal cellulose): amorphous. Obtained by treating cellulose I or II with liquid ammonia (-50°C) or ethylamine anhydride.

cellulose IV (= high temperature cellulose): amorphous. Obtained by heating cellulose III in glycerine to 290°C.

Other terms such as α, β and γ-cellulose are used in the wood pulp industry to indicate celluloses that have been subjected to different chemical treatments.

Table 2.1 Crystallinities of cellulose

Material	Percentage crystallinity determined by				
	Acid hydrolysis ($HCl+FeCl_3$)	X-ray scattering	density	Deuterium exchange	formylation
Ramie	95	70	60	-	-
Cotton	82-87	70	60	60	72
Cotton, mercerized under stress	78	-	-	-	-
Cotton, mercerized unstressed	68	-	-	-	48
Wood pulp	-	65	65	45-50	53-65
Viscose fiber	68	40	40	32	-

2.2.2 Fundamentals of pyrolysis

Understanding the pyrolysis process of a solid requires knowledge of the physical and chemical phenomena that occur. Models to predict or describe the thermal decomposition behavior of a solid must incorporate these phenomena or at least those that are rate-limiting.
Both a phenomenological description of the pyrolysis process and mathematical models of the pyrolysis of cellulose will be discussed in this paragraph and in the ones that follow. Physical and chemical parameters required in mathematical modelling will be discussed also.

A phenomenological description of the pyrolysis process is given on the basis of figure 2.3 [2.3]. Figure 2.3 represents the zone of a space-time map of an externally heated particle that is being subjected to pyrolysis. The heat flux can be either radiative or convective. In time period I the temperature in the solid gradually increases by pure transient conduction. Some of the heat that flows into the particle will be used to evaporate the free water present which leaves the solid. When the surface layer becomes hot enough pyrolysis starts (II) and volatiles are formed. Char is left when the reaction is completed. As more heat is supplied the pyrolysing layer moves deeper into the wood leaving char behind it. The rate at which the pyrolysis layer moves through the solid depends on the heat effects of the chemical reactions and the net heat transfer through the char layer and pyrolysing zone. The volatiles formed in the pyrolysis layer flow through the char matrix to the surface of the sample. The temperature of the char is higher than that of the volatiles (in case that no exothermic reactions occur). Heat will therefore be transferred from the char to the volatiles. Eventually heavy pyrolysis gases might be thermally cracked into lighter gases in the char layer. When the char front reaches the plane of symmetry of the sample the pyrolysis process ends.

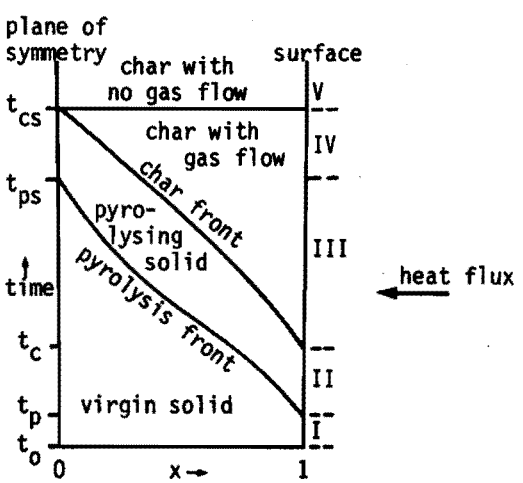

Fig.2.3 A qualitative diagram showing the zones of a space-time map in a pyrolysing solid.

It should be kept in mind that the exact nature of the char, that is the solid end product of the pyrolysis reactions, depends on the temperature of the reactor contents and possibly to some extent on the residence time in the reactor of the particle in question. The solid end product of a pyrolysis carried out at a certain reactor temperature might pyrolyse further and might again produce pyrolysis gases when it is subjected to a higher temperature in a subsequent experiment. This point will be discussed in more detail below.
It is obvious from the above considerations that for a model to predict or describe thermal decomposition processes in solid materials the effects of chemical reactions as well as of physical transport processes must be taken into account as long as it is not clear which elements determine the conversion rate.

2.2.2.1 Chemical reactions in cellulose pyrolysis

The pyrolysis of cellulose proceeds through a complex series of cocurrent and consecutive chemical reactions in the solid as well as in the gaseous phase. The mechanism of the chemical reactions may be divided into three stages:

1. reactions without loss in weight: recrystallization of cellulose and primary depolymerization reactions
2. primary decomposition reactions: dehydration reactions and anhydrosugar formation reactions
3. secondary decomposition reactions which proceed according to largely unknown reaction mechanisms and that yield a wide variety of pyrolysis products.

ad 1. Mild heating of cellulose to temperatures of about 150 - 250°C results in primary depolymerization of cellulose. The initial degree of polymerization that is highly dependent on the type of cellulose will decrease to a value of 200 - 400. Results obtained by a number of authors who used a wide variety of cellulose samples agree with this conclusion [2.4, 2.5, 2.6, 2.7, 2.8]. The decrease in degree of polymerization will be continued during the early stage of weight loss.
ad 2. Primary decomposition occurs through dehydration reactions and reactions in which anhydrosugars are formed (depolymerization). The dehydration reaction is a cross-linking reaction in which OH-groups

of adjacent cellulose chains form a cellulose ether. Cross-linking by ester bridge formation between cellulose chains is a dehydration reaction that requires the presence of a carboxyl group. A carboxyl group may be present in oxidized cellulose. Alternatively, an acidic degradation product of cellulose may link two chains. Cross-linking of cellulose by ester formation between chains is presented in figure 2.4.

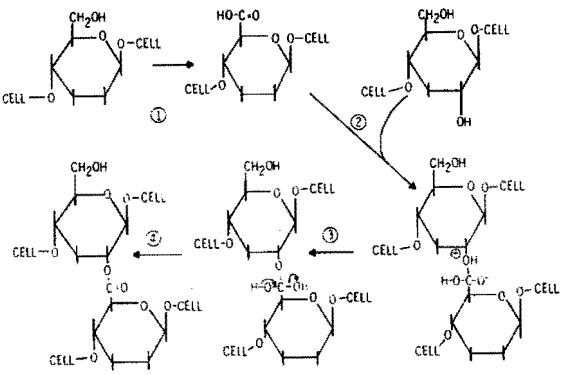

Fig.2.4 Cross-linking of cellulose by ester formation between chains.

The depolymerization of cellulose occurs through cleavage of the β 4-1 glucoside bonding giving 1-2 and 1-4 anhydrosugars that subsequently rearrange to levoglucosan (1,6-anhydro-β-D-glycopyranose (fig. 2.5)) that is more stable. Although levoglucosan is undoubtedly an important product there may be other depolymerization products that are far less stable and that consequently decompose much faster.

ad 3. The "dehydrocellulose" formed in the cross-linking dehydration reaction is assumed to decompose into char and light gases (charring reaction). Aromatization reactions play a role in the decomposition of "dehydrocellulose". These aromatization reactions finally lead to a graphite structure. The char will therefore contain aromatic structures such as f.i. benzene and diphenyl [2.9].

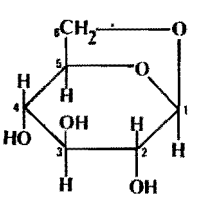

Fig.2.5 Levoglucosan

The depolymerization products (mainly levoglucosan) are also subjected to further degradation reactions. Thermal decomposition of levoglucosan yields the same decomposition products as thermal decomposition of cellulose [2.10, 2.11, 2.12, 2.13]. It is, however, not clear whether these products that are identified in cellulose pyrolysis are indeed the result of degradation of levoglucosan or whether they are formed via an other mechanism.
Levoglucosenone (fig. 2.6) is a product that has been identified in the tar from cellulose pyrolysis as well as in the products of the thermal decomposition of levoglucosan. Levoglucosenone polymerizes rapidly even at room temperature. Its polymerization competes with its further degradation to simpler structures. Whatever the route of secundary decomposition may be (via levoglucosan and/or levoglucosenone), it has been observed that these secundary decomposition reactions result in the formation of low molecuar weight products and char.

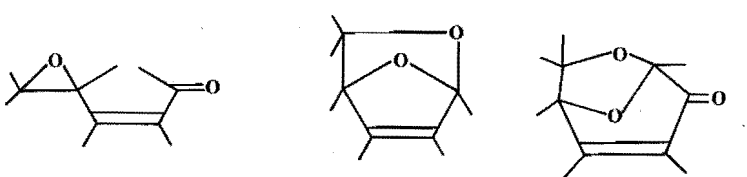

Fig.2.6 Structures proposed for levoglucosenone

The above three stages of the cellulose pyrolysis mechanism may be influenced by the chemical structure of the cellulose sample involved (apart from physical parameters that will be discussed later). The crystallinity of cellulose is one of the properties that may influence the pyrolysis. In experiments using cellulose with different percentages of crystallinity it was demonstrated that the dehydration reaction followed by the charring reaction is predominant in the L.O.R.'s (less ordered regions) [2.4]. The presence of inorganic substances (ash content) in cellulose exerts a major effect on the course of its thermal degradation [2.14, 2.15, 2.16, 2.17, 2.18, 2.19]. A dramatical raise of levoglucosan yield that occurred when inorganic comtaminants were removed from the cellulose before dry distilling it was observed as early as 1924 [2.20]. An increasing ash content of the cellulose results in an increase of char yield [2.18].It is generally assumed

that inorganic salts act catalytically on the dehydration reaction and consequently give rise to higher char yields.

2.2.2.2 Physical transport processes in pyrolysis

Mass transfer is not assumed to be a limiting factor in the models on the pyrolysis of cellulosic materials proposed in the literature so far. The gas permeability of the virgin solid material is assumed to be high enough so that mass transfer cannot limit the conversion rate. The resistance against the flow of pyrolysis gases must be even less in a solid in which a pyrolysis region moves inward leaving char behind as is normally the case. The volatiles can flow out of the solid particle through a relatively open char matrix.
Heat transfer to and heat transport inside the pyrolysing cellulose particle may be limiting factors in the pyrolysis process. These processes determine the heating rate of the cellulose inside a particle. Consequently the heating rate must be an important factor in the pyrolysis conversion. At low heating rates pyrolysis takes place at low temperature. In the low temperature range the dehydration reactions followed by charring reactions may be predominant so more char and less tar will be produced. The following heat transport processes must in principle be taken into account:

- Heat transfer to the particle by radiation and convection
- Heat transport inside the particle by conduction through solids and convection of gases.

Heat transfer by radiation, which undoubtedly also takes place within a pyrolysing particle, will be neglected in the present treatment in order not to complicate the model too much.

2.3 Modelling of cellulose pyrolysis

2.3.1 Simplified reaction models

It was mentioned in § 2.2.2.1 that the pyrolysis of cellulose proceeds through a complex series of competitive and consecutive chemical reactions. It was stated that 3 different stages can be distinguished. Some or all of these stages can be recognized in all simplified reaction schemes proposed in literature for cellulose pyrolysis.

Kilzer and Broido[2.17] considered the experimental work on the thermal analysis of cellulose that had then been presented in literature. They concluded that the pyrolysis of cellulose must be described by at least two competing (endothermic) reactions and a consecutive exothermic reaction. The reaction scheme these authors used is shown in fig. 2.7. Shafizadeh [2.21] proposed a reaction scheme in which the tar forming reaction is followed by a decomposition reaction for the tar (fig.2.8). In recent articles [2.22] Shafizadeh postulated a three-reaction model for pyrolysis at reduced pressure. In this model it is assumed that an initation reaction leads to formation of an active cellulose which subsequently decomposes by two competitive first-order reactions, one yielding volatiles (tar) and the other one char and a gaseous fraction (fig. 2.9).

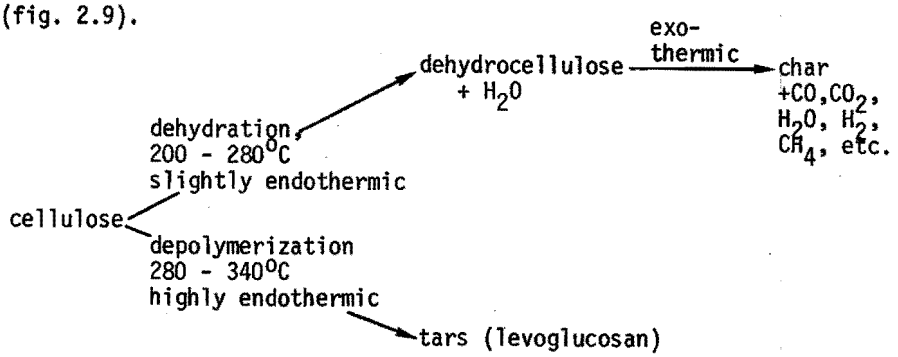

Fig.2.7 Reaction mechanism after Kilzer and Broido [2.17]

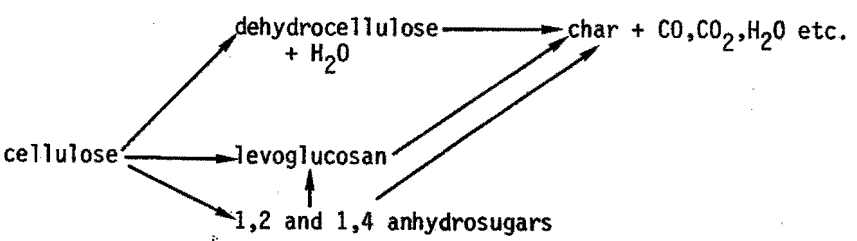

Fig.2.8 Reaction scheme proposed by Shafizadeh [2.21]

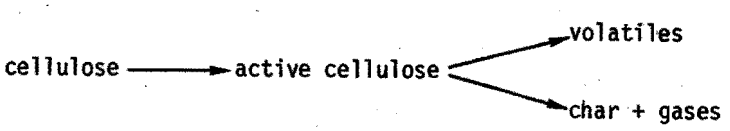

Fig.2.9 Reaction scheme proposed by Shafizadeh [2.22]

Broido and Weinstein[2.23] proposed a reaction scheme based on the scheme of Kilzer and Broido (see above) that has been extended to include a precursor reaction for cellulose and further degradation of the char.
In most kinetic models, however, the pyrolysis of cellulosic materials is assumed to proceed according to a single "overall" reaction, that in most cases is a first order Arrhenius type reaction. It will be clear that it may be possible in this way to describe the weight loss of cellulose during pyrolysis and the rate of this process but that it is virtually impossible to predict the yields of the various products.

2.3.2 Survey of models describing the pyrolysis of cellulosic materials

No resistance to mass transport is assumed to exist in the models discussed below. The first mathematical model used to describe the pyrolysis of cellulosic materials is that of Bramford et al. [2.24]. This model describes the pyrolysis of a wood slab heated on both faces. A number of simplifying assumptions were made:

1. No heat transfer between the solid and gas phase within the wood slab.
2. Constant values of specific heat, density, thermal conductivity and kinetic parameters.
3. The thermal decomposition is represented by a single exothermic reaction of the first order.

The model these authors obtained reads:

$$\rho.Cp\ \frac{\partial T}{\partial t} = \lambda.\frac{\partial^2 T}{\partial x^2} + \Delta H.r$$

in which ρ,Cp and λ are the density, specific heat and thermal conductivity respectively and the reaction rate:

$$r = -\frac{\partial W}{\partial t} = k_o.W.\exp(-E/RT)$$

where ΔH = heat of reaction, W = the weight of the sample. For a slab of wood of thickness 2ℓ heated on both faces the initial and boundary conditions were written as:

$T = T_0$ at $t = 0$ and $0 < x < 2\ell$

W = constant at $t = 0$ and $0 < x < 2\ell$

$$-\lambda.\frac{\partial T}{\partial x} = H(T_0) \quad \text{at } t > 0 \text{ and } x = 0,\ x = \ell$$

where T_0 is the surface temperature of the wood. $H(T_0)$ is an empirical function of surface temperature that expresses the rate of heat transfer to the wood slab.

Rittmann [2.25] was the first investigator to include variation in physical and thermal properties and multiple decomposition reactions into the heat transfer problem. Rittmann proposed that the thermal conductivity λ of a pyrolysing solid can be described as a function of density ρ:

$$\lambda = \lambda_0.\rho/\rho_0$$

where λ_0 = thermal conductivity of virgin solid (J/m.sec.^oC) and
ρ_0 = density of virgin solid (kg/m^3).
Rittmann employed the reaction scheme for the pyrolysis of cellulose proposed by Kilzer and Broido (see § 2.3.1). The symbols are given in fig. 2.10.
Both the effect of bulk flow through the char matrix that causes con-

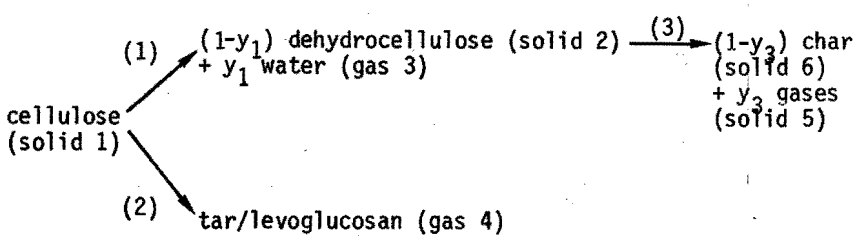

y_1, y_3: gas yield factors (fractional gas yield per unit of mass of solid converted)

Fig.2.10 Reactions in the slab (Rittman [2.25])

vective heat transfer and the change in specific heat due to pyrolysis were neglected. The following equation was derived:

$$Cp(\rho_1+\rho_2+\rho_3).\frac{\partial T}{\partial t} = \frac{\lambda_o}{\rho_o}.\rho.\frac{\partial^2 T}{\partial x^2} + \frac{\lambda_o}{\rho_o}.\frac{\partial \rho}{\partial x}.\frac{\partial T}{\partial x} + k_1\rho_1\Delta H_1 +$$

$$k_2\rho_1\Delta H_2 + k_3\rho_2\Delta H_3$$

Or: accumulation = conduction + reactions.

The rate of change of each solid species is given by:

$$-\frac{\partial \rho_1}{\partial t} = k_1\rho_1 + k_2\rho_1 \qquad \text{with } \rho_1 = \rho_o \text{ at } t=0$$

$$-\frac{\partial \rho_2}{\partial t} = k_3\rho_2 - (1-y_1)k_1\rho_1 \qquad \text{with } \rho_2 = 0 \text{ at } t=0$$

$$\frac{\partial \rho_3}{\partial t} = (1-y_3)k_3\rho_2 \qquad \text{with } \rho_2 = 0 \text{ at } t=0$$

A model in which internal convection is taken into account was developed by Kung [2.26]. He did, however, use a single Arrhenius type of reaction in his model. Kungs model leads to the following equation:

$$\frac{\partial}{\partial t}(\rho_s h_s) = \frac{\partial}{\partial x}(\lambda.\frac{\partial T}{\partial x}) + \frac{\partial}{\partial x}(m_g h_g) + r.\Delta H$$

in which: h = enthalpy
ρ = density
λ = thermal conductivity of pyrolysing solid
m = mass flux of gas through char matrix
r = reaction rate
ΔH = heat of reaction
subscripts s = solid
g = gas

Initial and boundary conditions:

at t=0 $T = T_\infty$ (ambient temperature)
$\rho = \rho_o$ (density of virgin solid)
$m_g = 0$

at x=0 (at surface): $\lambda \frac{\partial T}{\partial x} = -q$ (heat flux received by the exposed surface).

at $x=\ell$ (plane of symmetry): $\frac{\partial T}{\partial x} = 0, m_g = 0$.

Some of Kungs conclusions were: a thermally thin slab pyrolyses with approximately uniform temperature; the pyrolysis rate being sensitive to the heat effect of reaction but not to char conductivity.

Rittmann nor Kung have compared their models to experimental results.

Maa [2.3] applied the unreacted shrinking core model to the pyrolysis of solid cylinders. Fig. 2.11 describes a partially pyrolysed cylinder. The central core region from r=0 to $r=r_c$ is unreacted solid. This is surrounded by a solid layer of pyrolysed material between $r=r_c$ and r=R, that is composed of ash and char resulting from the pyrolysis. The pyrolysis takes place at a surface of radius r_c. The char in the char layer is assumed to be inert. The unreacted core temperature T_c is assumed to be independent of position. It is pointed out that Maa's assumption of a flat temperature profile in the unreacted core which is equal to the temperature of the reaction front T_c seems illogical. In such a situation there would be no reason why the unreacted core should not react. The gas and char are assumed to be in thermal equilibrium. The partial differential equation that represents the heat transfer in the char layer is given as:

$$\rho . C_p . \frac{\partial T}{\partial t} = \frac{1}{r} . \frac{\partial}{\partial r} . (\lambda . r . \frac{\partial T}{\partial r}) + y . C_{pg} . (\rho_{core} . \frac{\partial r_c}{\partial t}) . \frac{r_c}{r} . \frac{\partial T}{\partial r}$$

for $r_c \leq r \leq R$

where ρ = density of char
λ = effective thermal conductivity
C_p = specific heat of char
C_{pg} = specific heat of pyrolysis gas
y = fractional gas yield per mass unit converted solid.

The second term on the righthand side corresponds to the heat that is removed from the particle by the bulk flow of the pyrolysis gas.
Initial and boundary conditions:

at t=0 for $0 \leq r \leq R$ $\quad T = T_o$

at t=t for r = R $\quad \lambda . \frac{\partial T}{\partial r} = h_{eff} (T_\infty - T_s) + \sigma(e_\infty T_\infty^4 - e_s . T_s^4)$

and $T = T_s$

for $r = r_c$ $\quad T = T_c$

and $2.\pi.r_c.\lambda . \frac{\partial T}{\partial r} = - \rho_{core} . \frac{dr_c}{dt} .2.\pi r_c.\Delta H +$

$\rho_{core}\ C_{pcore} . \pi . r_c^2 . \frac{\partial T_c}{\partial t}$

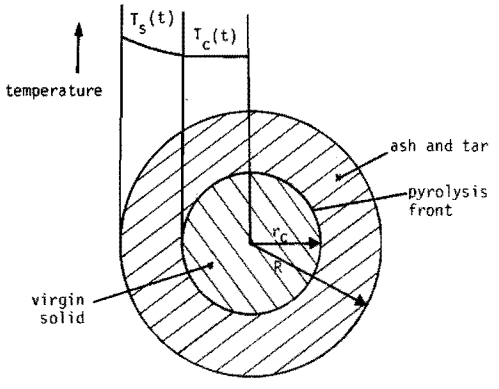

Fig.2.11 Partially pyrolysed cylinder (Maa [2.3])

The pyrolysis reaction that is assumed to occur at the surface of the unreacted core is taken to be proportional to the area of the surface at which the reaction occurs.
From a solid balance over the unreacted core:

$$- \rho_{core} . 2\pi r_c . \frac{dr_c}{dt} = k_p . 2\pi r_c . \rho_{core}$$

the shrinking core rate is obtained as $\frac{dr_c}{dt} = k_p$. The reaction rate constant k_p is assumed to vary with temperature by:

$k_p = k_{po} . \exp(-E/RT)$, where: k_p = reaction rate constant
k_{po} = frequency factor
E = activation energy for pyrolysis.

Maa concluded from his calculations that the pyrolysis process at specific activation energy and frequency factor is controlled by the

chemical reaction for small particles whereas for large particles the process is heat transfer controlled.
In the case of the unreacted core shrinking model the time for complete conversion goes to zero for small particles. A homogeneous pyrolysis reaction model would on the contrary predict a limit value of the reaction time when no heat transfer limitation exists. This limit is determined by the rate of chemical reaction. It might be concluded from these considerations that the unreacted core shrinking model is not valid for small particle sizes.

2.3.3 Derivation of the present pyrolysis models

The models are derived (just like the models discussed above) for the pyrolysis of one particle.
The results obtained with the models will be compared to experimental results obtained by pyrolysis of cellulosic materials in the spout-fluid bed reactor (see Chapter 7). Macro kinetic aspects that may play a role in the pyrolysis of cellulosic materials in a reactor are neglected in the models.
It is assumed that the conversion time of one particle is short compared to the minimum residence time of the particle in the reactor so that residence time and residence time spreading of the particles in the reactor do not play a role in the pyrolysis process. It is on the basis of this assumption that the models are confined to the pyrolysis of one particle. The validity of this assumption will be discussed later on on the basis of experimental results (Chapter 7).

2.3.3.1 Introduction

It was decided to combine the previous models into a model in which multiple decomposition reactions (Rittmann) as well as heat transfer due to convection inside the pyrolysing solid (Kung, Maa) were taken into account. A number of simplifying assumptions had to be made. Most of these assumptions had been included implicitly in the models discussed above.
As in the models discussed the mass transport is considered not to be a limiting factor on account of the high porosity and low mechanical strength of the pyrolysing material. Other simplifying assumptions are [2.27]:

1. An organic particle from domestic waste can be represented by an infinite, flat cellulose slab of finite thickness in which heat and mass transport proceed in the direction perpendicular to the slab surface only. A cellulose particle conceived in this way resembles many domestic waste components, f.i. newsprint.
2. The particle contains no liquid phase. The water and tar that are produced during pyrolysis are taken to be completely vaporized at reaction temperature.
3. Heat transport through conduction within the particle occurs in the solid phase only.
4. Heat transport due to radiation within the particle has been neglected.
5. The gas phase is ideally mixed in the direction perpendicular to its direction of motion.That is, no radial concentration gradients exist.

The heat and mass flow scheme of the pyrolysis that results from assumptions 1. through 5 above is illustrated by figs. 2.12A and 2.12B.

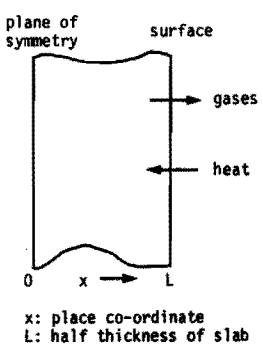

Fig.2.12A Pyrolysing cellulose slab. Heat and mass transport only perpendicular to slab surfaces.

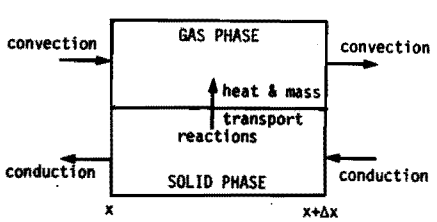

Fig.2.12B Volume element of pyrolysing cellulose particle.

6. Thermal equilibrium between gas and solid phase exists at any point within the particle.
7. Within any volume element of the particle the mass concentration of the gases is negligible in comparison to that of the solids.
8. No reaction occurs either between gaseous components or between gaseous compounds and the solid phase.
9. Cellulose and solid pyrolysis products are assumed to have the same specific heats. All pyrolysis gases are assumed to have the same specific heat. All specific heats are assumed to be independent of temperature.
10. Cellulose and solid pyrolysis products are assumed to have the same thermal conductivity which is held to be independent of temperature.
11. Energy effects connected with pressure, mechanical and viscous forces and/or gravity have been neglected.
12. No resistance to mass transport is assumed to exist within the slab.
13. The particle is taken to be isotropic.
14. The system is held to be isobaric.
15. The gas phase is assumed to move in plug flow within the particle.
16. All chemical reactions are assumed to be first order in the component that is being converted.

2.3.3.2 General model with tar evaporation *)

This model is based on the reaction scheme proposed by Kilzer and Broido [2.17] for cellulose pyrolysis (see § 2.3.1, fig. 2.7). The following symbols are used (fig. 2.13).

Fig. 2.13

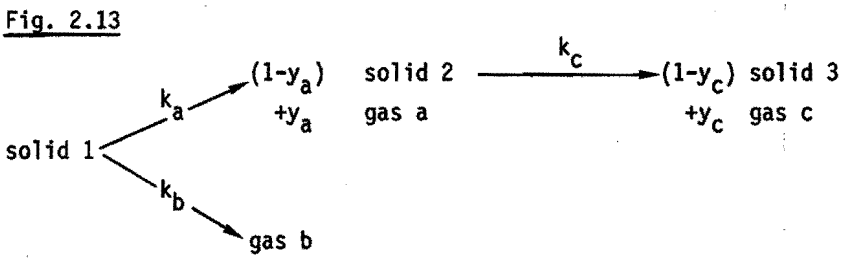

*) The term "tar evaporation" is strictly speaking not correct as it does not refer to the evaporation of a liquid but rather to the transport of gaseous tar from a particle to the bulk gas. We have retained the term "tar evaporation", however, because it is generally used in the literature on cellulose pyrolysis.

where k_a, k_b, k_c = reaction rate constants (sec^{-1})
y_a, y_c = stoechiometric coefficients expressed on weight basis (= fractional gas yield per unit mass of solid material converted).

All reactions were assumed to be first order in the component that is being converted. The reaction rate equations therefore are:

$$\frac{\partial \rho_1}{\partial t} = - k_a \rho_1 - k_b \rho_1 \qquad (2.1)$$

$$\frac{\partial \rho_2}{\partial t} = (1-y_a)\rho_1 - k_c \rho_2 \qquad (2.2)$$

$$\frac{\partial \rho_3}{\partial t} = (1-y_c) k_c \rho_2 \qquad (2.3)$$

where: ρ = mass concentration (kg/m^3)
t = time (sec)
subscripts refer to numbers of components in the above reaction scheme (fig. 2.13).

The energy balance over a volume element of a particle reads [2.28]:

$$\frac{\partial}{\partial t} (\rho \hat{H}) = - (\nabla . \rho . \hat{H} . v) - (\nabla . q_c) \qquad (2.4)$$

where: $\hat{H}$ = enthalpy per unit mass (J/kg)
v = gas velocity within particle (m/sec)
q_c = heat flux by conduction ($J/m^2.sec$)

The one-dimensional form of eq. (2.4) reads:

$$\frac{\partial}{\partial t}(\rho . \hat{H}) = - \frac{\partial}{\partial x} (\rho . v . \hat{H}) - \frac{\partial}{\partial x} (q_c) \qquad (2.5)$$

which may be transformed by a simple substitution that results from assumptions 9 and 14 into:

$$\rho . Cp . \frac{\partial T}{\partial t} = -\rho \; v . Cp \frac{\partial T}{\partial x} - \frac{\partial}{\partial x} . q_c - \hat{H} . \frac{\partial \rho}{\partial t} - \hat{H} . \frac{\partial}{\partial x} (\rho . v .) \qquad (2.6)$$

Eq. (2.6) is now written for a multicomponent system:

$$\sum_i\{\rho_i.Cp_i.\frac{\partial T_i}{\partial t}\} = -\sum_i\{\rho_i.v_i.Cp_i.\frac{\partial T_i}{\partial x}\} - \frac{\partial}{\partial x}\{q_c\} - \sum_i\{\hat{H}_i.\frac{\partial \rho_i}{\partial t}\} - \sum_i\{\hat{H}_i.\frac{\partial}{\partial x}(\rho_i.v_i)\} \quad (2.7)$$

A	B	C	D	E
accumulation due to temperature change	convection (temperature effect)	conduction	accumulation due to concentration changes	effect of net mass convection

Eq. (2.7) is still generally valid for a one-dimensional system. The following simplifications are now introduced on the basis of the above simplifying assumptions:

$T_i = T$ for i = solids 1,2,3 and gases a,b,c (ass.6)

$\rho_{ga,gb,gc} \ll \rho_{1,2,3}$ (ass.7)

$\lambda_1 = \lambda_2 = \lambda_3 = \lambda = \lambda_{eff}.(1-\varepsilon)$ (ass.10)

$\lambda_{ga,gb,gc} \ll \lambda$ (ass.3)

$$\frac{\partial \rho_{ga}}{\partial t} = \frac{\partial \rho_{gb}}{\partial t} = \frac{\partial \rho_{gc}}{\partial t} = 0 \quad \text{(ass.14)}$$

where: λ = thermal conductivity of solid materials (J/sec.m.^oC)
ε = porosity of solid phase
λ_{eff} = effective thermal conductivity of particle
subscripts 1,2,3 refer to solids nos. 1,2,3 resp.
subscripts ga,gb,gc refer to gases a,b,c resp.

These simplifications are now applied to terms A through E of eq. (2.7):

Term A: $$\sum_i\{\rho_i.Cp_i.\frac{\partial T_i}{\partial t}\} = (\rho_1 Cp_1 + \rho_2 Cp_2 + \rho_3 Cp_3).\frac{\partial T}{\partial t} \quad (2.8)$$

Term B: A mass balance over the gas phase of a volume element located between distances x and x+dx from the centre of the particle gives (cf reaction scheme):

$$\frac{\partial}{\partial x}(\rho_{ga}\, v_{ga}) = k_a \rho_1 y_a \quad (2.9a)$$

$$\frac{\partial}{\partial x}(\rho_{gb}\, v_{gb}) = k_b \rho_1 \qquad (2.9b)$$

$$\frac{\partial}{\partial x}(\rho_{gc}\, v_{gc}) = k_c \rho_2 y_c \qquad (2.9c)$$

All pyrolysis gases evolved in the volume elements located between the particle centre (x=0) and a point located at a distance x from the particle centre must pass through the above volume element located between distances x and x+dx from the particle centre. Thus:

$$-\sum_i \{\rho_i . v_i . Cp_i . \frac{\partial T_i}{\partial x}\} = -\left[\int_0^x (k_a \rho_1 y_a Cp_{ga} + k_b \rho_1 Cp_{gb} + k_c \rho_2 y_c Cp_{gc})dx\right] . \frac{\partial T}{\partial x} \qquad (2.9)$$

Term C: $$-\frac{\partial}{\partial x}\{q_c\} = \frac{\partial}{\partial x}\{\lambda_{eff} . \frac{\partial T}{\partial x}\} \qquad (2.10)$$

Term D: $$-\sum_i \{\hat{H}_i . \frac{\partial \rho_i}{\partial t}\} \doteq -\left[\hat{H}_1 \frac{\partial \rho_1}{\partial t} + \hat{H}_2 \frac{\partial \rho_2}{\partial t} + \hat{H}_3 \frac{\partial \rho_3}{\partial t}\right] \qquad (2.11a)$$

and with eqs. (2.1), (2.2) and (2.3) one obtains:

$$-\sum_i \{\hat{H}_i . \frac{\partial \rho_i}{\partial t}\} = \hat{H}_1 k_a \rho_1 + \hat{H}_1 k_b \rho_1 - \hat{H}_2 (1-y_a) k_a \rho_1 + \hat{H}_2 k_c \rho_2 - \hat{H}_3 (1-y_c) k_c \rho_2 \qquad (2.11)$$

Term E: From term E of eq. (2.7) and eqs. (2.9a),(2.9b) and (2.9c) one obtains:

$$-\sum_i \{\hat{H}_i . \frac{\partial}{\partial x}(\rho_i . v_i)\} = -(\hat{H}_{ga}\, y_a\, k_a \rho_1 + \hat{H}_{gb}\, k_b \rho_1 + \hat{H}_{gc}\, y_c\, k_c \rho_2) \qquad (2.12)$$

Term D and E: adding eq. (2.11) to eq. (2.12) leads to:

$$-\sum_i \{\hat{H}_i . \frac{\partial \rho_i}{\partial t}\} - \sum_i \{\hat{H}_i . \frac{\partial}{\partial x}(\rho_i . v_i)\} = k_a \rho_1 (\hat{H}_1 - y_a \hat{H}_{ga} - (1-y_a)\hat{H}_2) + k_b \rho_1 (\hat{H}_1 - \hat{H}_{gb}) + k_c \rho_2 (\hat{H}_2 - y_c \hat{H}_{gc} - (1-y_c)\hat{H}_3) \qquad (2.13)$$

The heats of reaction per unit mass of converted solid component are now introduced:

$$\Delta\hat{H}_a = y_a\hat{H}_{ga} + (1-y_a)\hat{H}_2 - \hat{H}_1 \qquad (2.14a)$$

$$\Delta\hat{H}_b = \hat{H}_{gb} - \hat{H}_1 \qquad (2.14b)$$

$$\Delta\hat{H}_c = y_c\,\hat{H}_{gc} + (1-y_c)\hat{H}_3 - \hat{H}_2 \qquad (2.14c)$$

Substitution in eq. (2.13) leads to:

$$-\Sigma_i\{\hat{H}_i\cdot\frac{\partial\rho_i}{\partial t}\} - \Sigma_i\{\hat{H}_i\cdot\frac{\partial}{\partial x}(\rho_i\cdot v_i)\} = -k_a\rho_1\Delta\hat{H}_a - k_b\rho_1\Delta\hat{H}_b - k_c\rho_2\Delta\hat{H}_c \qquad (2.15)$$

Differential equation: Substitution of eqs. (2.8), (2.9), (2.10) and (2.15) into eq. (2.7) yields:

$$(\rho_1 Cp_1+\rho_2 Cp_2+\rho_3 Cp_3)\cdot\frac{\partial T}{\partial t} = -\left[\int_0^x (k_a\rho_1 y_a Cp_{ga}+k_b\rho_1 Cp_{gb}+k_c\rho_2 y_c Cp_{gc})dx\right]\cdot\frac{\partial T}{\partial x} +$$

$$+ \frac{\partial}{\partial x}(\lambda_{eff}\cdot\frac{\partial T}{\partial x}) - k_a\rho_1\Delta\hat{H}_a - k_b\rho_1\Delta\hat{H}_b - k_c\rho_2\Delta\hat{H}_c \qquad (2.16)$$

Initial and boundary conditions:
When the particle is isothermal before it is introduced into the reaction zone the initial condition is:

$$T = T_0 \text{ for } t=0 \text{ and } 0 \le x \le L \qquad (2.17)$$

For reasons of symmetry:

$$\frac{\partial T}{\partial x} = 0 \text{ for } t>0 \text{ and } x=0 \text{ (cf. fig.2.12)} \qquad (2.18)$$

Depending on the reaction conditions a number of different versions of the second boundary condition may be adopted that correspond to different predominant mechanisms of heat transfer between the bulk of the reaction zone ($x=\infty$) and the particle surface ($x=L$). The versions that were applied in this investigation are:

a. radiation with large $(T_\infty - T_{x=L})$: $\lambda(\frac{\partial T}{\partial x})\Big|_{x=L}$ = constant for $t>0$ and $x=L$ (2.19a)

b. convective heat transfer predominates:

$$\lambda\left(\frac{\partial T}{\partial x}\right)\Big|_{x=L} = \alpha(T_\infty - T_{x=L}) \text{ for } t>0 \text{ and } x=L \qquad (2.19b)$$

c. heat transfer limited by heat conduction within the particle:

$$T_{x=L} = T_\infty \text{ for } t>0 \text{ and } x=L \qquad (2.19c)$$

2.3.3.3 General model without tar evaporation

The below general model has been developed to be used together with the reaction scheme of Kilzer and Broido extended to include a cracking reaction for the tar (fig. 2.14). The products

Fig. 2.14

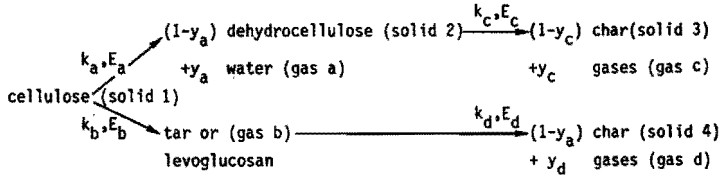

of this tar cracking reaction are char and gases. Fig. 2.14 also indicates the symbols that have been used. The simplifying assumptions given in § 2.3.3.1 apply to this model also. The only assumptions that have been modified are those that involve the behavior of levoglucosan (= tar). It is now assumed that the tar (which is a gaseous product at reaction temperature)remains at the place in the pyrolysing cellulose slab where it is formed and that the tar vapors are not removed from the slab by convection. This means that the tar is held to behave like a solid pyrolysis product in some respects: the tar does not contribute to heat or mass transport by means of convection. In other respects, however, the tar is considered as a gaseous pyrolysis product: its mass concentration is neglected in comparison to that of the solids and the tar is held not to contribute to heat transprt through the slab by conduction.

It will be clear that the general model with tar evaporation and the general model without tar evaporation are two extreme situations and that the truth must lie in between. Gas b which is tar that is held to consist of levoglucosan will partly escape from the slab without being cracked and partly remain in the pyrolysing cellulose slab where it decomposes into char and gases. It would therefore be more correct

to introduce an effective transport rate coefficient for gas b into the model. The models derived in § 2.3.3.2 and in this paragraph (see below) describe the limiting situations where levoglucosan either evaporates completely without further reaction (general model with tar evaporation) or remains in the particle and there is subjected to cracking reactions (general model without tar evaporation).
It was decided, however, not to introduce such an effective transport rate coefficient for gas b into the model as it would increase the number of unknowns. It would be almost impossible to obtain reliable data for such a transport rate coefficient. The transport rate coefficient would depend on f.i. the temperature and the porosity at any place within the particle which changes with time.
The possibility that the tar might be cracked in the bulk has been disregarded to keep the model as simple as possible.

The derivation of the general model without tar evaporation is analogous to that of the general model with tar evaporation (§ 2.3.3.2). The chemical reaction rate equations are:

$$\frac{\partial \rho_1}{\partial t} = - k_a \rho_1 - k_b \rho_1 \qquad (2.20)$$

$$\frac{\partial \rho_2}{\partial t} = (1-y_c) k_a \rho_1 - k_c \rho_2 \qquad (2.21)$$

$$\frac{\partial \rho_{gb}}{\partial t} = k_b \rho_1 - k_d \rho_{gb} \qquad (2.22)$$

$$\frac{\partial \rho_3}{\partial t} = (1-y_c) k_c \rho_2 \qquad (2.23)$$

$$\frac{\partial \rho_4}{\partial t} = (1-y_d) k_d \rho_{gb} \qquad (2.24)$$

Initial conditions:

$$\text{for } t=0 \quad \rho_1 = \rho_{1,0},\ \rho_2 = \rho_3 = \rho_4 = \rho_{gb} = 0 \qquad (2.25)$$

The one-dimensional energy balance over a volume element of a particle that has been derived for a multicomponent system in § 2.3.3.2 and that is represented by eq. (2.7) is valid here also:

$$\underset{i}{\Sigma}\{\rho_i.Cp_i.\frac{\partial T_i}{\partial t}\} = -\underset{i}{\Sigma}\{\rho_i.v_i.Cp_i.\frac{\partial T_i}{\partial x}\} - \frac{\partial}{\partial x}\{q_c\} - \underset{i}{\Sigma}\{\hat{H}_i.\frac{\partial \rho_i}{\partial t}\} - \underset{i}{\Sigma}\{\hat{H}_i.\frac{\partial}{\partial x}(\rho_i.v_i)\}$$

A B C D E

(2.26)

The following simplifications are now introduced on the basis of the simplifying assumptions (§ 2.3.3.1) and the above remarks on gas b:

$T_i = T$ i = solids 1,2,3,4 and gases a,b,c,d (ass. 6)

$\rho_{ga'gc'gd} << \rho_{1,2,3,4}$ (ass. 7)

$\rho_{gb} << \rho_{1,2,3,4}$, but must be taken into account in cases where reaction d is considered:

$\lambda_1 = \lambda_2 = \lambda_3 = \lambda_4 = \lambda = \lambda_{eff}(1-\varepsilon)$ (ass.10)

$\lambda_{ga,gb,gc,gd} << \lambda$ (ass. 3)

$\frac{\partial \rho_{ga}}{\partial t} = \frac{\partial \rho_{gc}}{\partial t} = \frac{\partial \rho_{gd}}{\partial t} = 0$ (ass. 14)

These simplifications are now applied to terms A through E of eq. (2.26) = eq. (2.7)

Term A: $\underset{i}{\Sigma}\{\rho_i.Cp_i.\frac{\partial T_i}{\partial t}\} = \rho_1 Cp_1 + \rho_2 Cp_2 + \rho_3 Cp_3 + \rho_4 Cp_4$ (2.27)

Term B: $-\underset{i}{\Sigma}\{\rho_i.v_i.Cp_i.\frac{\partial T_i}{\partial x}\} = -\left|\int_0^x (k_a \rho_1 y_a Cp_{ga} + k_c \rho_2 y_c Cp_{gc} + k_d \rho_{gb} y_d Cp_{gd})dx\right| . \frac{\partial T}{\partial x}$ (2.28)

Term C: $-\frac{\partial}{\partial x}\{q_c\} = \frac{\partial}{\partial x}\{\lambda_{eff}.\frac{\partial T}{\partial x}\}$ (2.29)

Term D: $-\underset{i}{\Sigma}\{\hat{H}_i.\frac{\partial \rho_i}{\partial t}\} = -\left\{\hat{H}_1 \frac{\partial \rho_1}{\partial t} + \hat{H}_2 \frac{\partial \rho_2}{\partial t} + \hat{H}_{gb} \frac{\partial \rho_{gb}}{\partial t} + \hat{H}_3 \frac{\partial \rho_3}{\partial t} + \hat{H}_4 \frac{\partial \rho_4}{\partial t}\right\}$ (2.30)

and with eqs. (2.20) through (2.24) one obtains:

$$-\sum_i\{\hat{H}_i\cdot\frac{\partial\rho_i}{\partial t}\} = \hat{H}_1k_a\rho_1+\hat{H}_1k_b\rho_1-\hat{H}_2(1-y_a)k_a\rho_1+\hat{H}_2k_c\rho_2-\hat{H}_{gb}k_b\rho_1+\hat{H}_{gb}k_d\rho_{gb}$$

$$-\hat{H}_3(1-y_c)k_c\rho_2 - (1-y_d)k_d\rho_{gb} \qquad (2.31)$$

Term E:

$$-\sum_i\{\hat{H}_i\cdot\frac{\partial}{\partial x}(\rho_i\cdot v_i)\} = -(\hat{H}_{ga}y_ak_a\rho_1 + \hat{H}_{gc}y_ck_c\rho_2 + \hat{H}_{gd}y_dk_d\rho_{gb}) \qquad (2.32)$$

Term D and E: adding eq. (2.32) to eq. (2.31) leads to:

$$-\sum_i\{\hat{H}_i\cdot\frac{\partial\rho_i}{\partial t}\} -\sum_i\{\hat{H}_i\cdot\frac{\partial}{\partial x}(\rho_i\cdot v_i)\}= k_a\rho_1(\hat{H}_1-y_a\hat{H}_{ga}-(1-y_a)\hat{H}_2)+k_b\rho_1(\hat{H}_1-\hat{H}_{gb}) +$$

$$+ k_c\rho_2(\hat{H}_2-y_c\hat{H}_{gc}-(1-y_c)\hat{H}_3) + k_d\rho_{gb}(\hat{H}_{gb}-y_d\hat{H}_{gd}-(1-y_d)\hat{H}_4). \qquad (2.33)$$

The heats of reaction per unit mass of converted solid component and tar are now introduced:

$$\Delta\hat{H}_a = y_a\hat{H}_{ga}+(1-y_a)\hat{H}_2-\hat{H}_1 \qquad (2.34a)$$

$$\Delta\hat{H}_b = \hat{H}_{gb}-\hat{H}_1 \qquad (2.34b)$$

$$\Delta\hat{H}_c = y_c\hat{H}_{gc}+(1-y_c)\hat{H}_3-\hat{H}_2 \qquad (2.34c)$$

$$\Delta\hat{H}_d = y_d\hat{H}_{gd}+(1-y_d)\hat{H}_4-\hat{H}_{gb} \qquad (2.34d)$$

Substitution in eq. (2.33) leads to:

$$-\sum_i\{\hat{H}_i\cdot\frac{\partial\rho_i}{\partial t}\} -\sum_i\{\hat{H}_i\cdot\frac{\partial}{\partial x}(\rho_i\cdot v_i)\} = -k_a\rho_1\Delta\hat{H}_a-k_b\rho_1\Delta\hat{H}_b-k_c\rho_2\Delta\hat{H}_c-k_d\rho_{gb}\Delta\hat{H}_d \qquad (2.35)$$

Differential equation. Substitution of eqs. (2.27),(2.28), (2.29) and (2.35) into eq. (2.26) yields:

$$(\rho_1Cp_1+\rho_2Cp_2+\rho_3Cp_3+\rho_4Cp_4)\cdot\frac{\partial T}{\partial t} = -\left|\int_0^x(k_a\rho_1y_aCp_{ga}+k_c\rho_2y_cCp_{gc}+k_dy_d\rho_{gb}Cp_{gd})dx\cdot\right|\cdot\frac{\partial T}{\partial x} +$$

$$+\frac{\partial}{\partial x}(\lambda_{eff}\cdot\frac{\partial T}{\partial x})-k_a\rho_1\Delta\hat{H}_a-k_b\rho_1\Delta\hat{H}_b-k_c\rho_2\Delta\hat{H}_c-k_d\rho_{gb}\Delta\hat{H}_d \qquad (2.36)$$

Initial and boundary conditions: eqs. (2.17) through (2.19c) (see § 2.3.3.2).

2.3.3.4 Lumped parameter model [2.29]

In the preceding paragraphs the temperature history of each place inside the pyrolysing particle was calculated from the differential equations that describe the heat transport (eqs. (2.16) and (2.36)).

To solve a non-linear second order partial differential equation like this complicated numerical calculations must be made.
It is, however, possible to simplify the calculations by considering the particle to be composed of inert material. This can, of course, be done only in calculations that involve nothing but the temperature history of a place within the particle.
It is assumed that all places inside the pyrolysing particle pass through the same temperature history except that the time at which some place will reach some temperature is different for different places inside the particle. In addition, the residence time of the particle in the reaction zone is assumed to be long enough for the conversion to be almost complete at every place inside the particle. The calculation of the initial product distribution can be simplified as result of the above assumptions. The reason is that it suffices to calculate the temperature history as a function of time only while temperature history no longer has to be computed as a function of place. This mean local temperature history is approximated with the aid of a single parameter β. The value of β is determined by the material properties of the pyrolysing solid as well as by the process conditions (boundary conditions). All relevant quantities that influence the temperature history in the pyrolysing particle are summarized in the value of β. The parameter is therefore named "lumped" parameter and the model: lumped parameter model. Introduction of the lumped parameter model enables us to derive a good description of the conversion process without making the calculations very complicated. The results obtained by the use of the lumped parameter model will be compared to that of the general model to find out whether the error introduced by this simplifications is substantial. The lumped parameter model is developed in this paragraph for the case of convective heat transfer to the slab being pyrolysed. The heat flux from the ambient medium with temperature

T_∞ to the pyrolysing cellulose is then given by:

$$\phi = \alpha(T_\infty - T_{x=L}) \qquad (2.37)$$

where ϕ = heat flux ($J/m^2.sec$)

α = effective heat transfer coefficient ($J/m^2.sec.^oC$).

We will discuss the case where α is constant. As the thermal conductivity has been assumed to be constant too, the Biot number will be constant for a fixed half thickness of slab L:

$$Bi = \frac{\alpha.L}{\lambda} = \text{constant} \qquad (2.38)$$

According to Luikov [2.30] the temperature history at place x of a particle consisting of an inert material is then given by:

$$\frac{T(x,F_o)-T_o}{T_\infty - T_o} = 1 - \sum_{n=1}^{\infty} \frac{2 \sin \mu_n}{\mu_n + \sin\mu_n.\cos\mu_n} . \cos(\mu_n.\frac{x}{L}).\exp(-\mu_n^2.F_o) \qquad (2.39)$$

$$\text{cotan } \mu = \mu/Bi \qquad (2.40)$$

in which $T(x,F_o)$ = temperature on place x of the particle at time F_o

T_o = initial temperature

T_∞ = temperature of ambient medium

F_o = Fourier time = $\frac{\lambda.t}{\rho.Cp.L^2}$

μ_n = solution of the characteristic equation (2.40) lying between $(n-1).\pi$ and $n.\pi$.

The temperature history may be approximated for sufficiently large values of F_o by equation (2.39) from which all terms except the first one have been omitted:

$$\frac{T(x,F_o)-T_o}{T_\infty - T_o} = 1 - \frac{2 \sin \mu_1}{\mu_1 + \sin\mu_1.\cos\mu_1} . \cos(\mu_1.\frac{x}{L}).\exp.(-\mu_1^2.F_o) \qquad (2.41)$$

Introduce:

$$f(x) = \frac{2 \sin \mu_1}{\mu_1 + \sin\mu_1.\cos\mu_1} . \cos(\mu_1.\frac{x}{L}) \qquad (2.42)$$

and substitute f(x) in eq. (2.41):

$$\frac{T(x,F_o) - T_o}{T_\infty - T_o} = 1 - f(x).\exp.(-\mu_1^2.F_o) \qquad (2.43)$$

Rearrangement gives:

$$\frac{T(x,F_o)-T_o}{T_\infty-T_o} = 1 - \exp\left\{-\mu_1^2.[F_o - \frac{1}{\mu_1^2}\ln\{f(x)\}]\right\} \qquad (2.44)$$

Introduce:

$$\Delta F_o(x) = \frac{1}{\mu_1^2}\ln\{f(x)\} \qquad (2.45)$$

Substitution in eq. (2.44) gives:

$$\frac{T(x,T_o)-T_o}{T_\infty-T_o} = 1 - \exp\{ - \mu_1^2.[F_o\Delta F_o(x)]\} \qquad (2.46)$$

It follows from eq. (2.46) that every place x inside the particle passes through a temperature history that is delayed by time $\Delta F_o(x)$ with respect to another place. For reasons of simplicity the product distribution is calculated at the hypothetical place x_1 for which $\Delta F_o(x_1) = 0$ is valid. Eq. (2.46) then passes into:

$$\frac{T(x_1,F_o)-T_o}{T_\infty- T_o} = 1 - \exp(-\mu_1^2.F_o) \qquad (2.47)$$

It is assumed that the distribution of the pyrolysis products obtained is independent of place so the place x_1 is irrelevant. This may be expressed by: $T(x_1,F_o)=T(F_o)$. Eq. (2.47) becomes:

$$\frac{T(F_o)-T_o}{T_\infty- T_o} = 1 - \exp.(-\mu_1^2.F_o) \qquad (2.48)$$

It is now postulated that the mean local temperature history inside the particle is described by:

$$\frac{T(t)-T_o}{T_\infty-T_o} = 1 - \exp(-\beta.t) \qquad (2.49)$$

It is seen through combining eqs. (2.48) and (2.49) that the lumped parameter β can be estimated from:

$$\beta = \frac{\mu_1^2.F_o}{t} = \frac{\mu_1^2}{L^2} \cdot \frac{\lambda}{\rho.C_p} \qquad (2.50)$$

With the aid of the temperature history given by eq. (2.49) the product distribution now can be calculated from the equations that describe the chemical conversions (eqs. (2.1) through (2.3) with the initial condition: for t=0 $\rho_1=\rho_{1,0}, \rho_2=\rho_3=0$ (General model with tar evaporation).

2.3.3.5 Reaction limited conversion rate model [2.27]

In this model it is assumed that the conversion rate is limited by the rates of the reactions only: the heat transport is supposed to be fast with respect to the chemical reactions. In that case it is no longer necessary to include equations describing the heat transport in the model and it suffices to solve the reaction rate equations. The model is developed in this paragraph for the reaction scheme given in fig. 2.15 which is the Kilzer en Broido scheme extended to include a cracking reaction of the tar. Fig. 2.15 also indicates the symbols that have been used.

Fig. 2.15

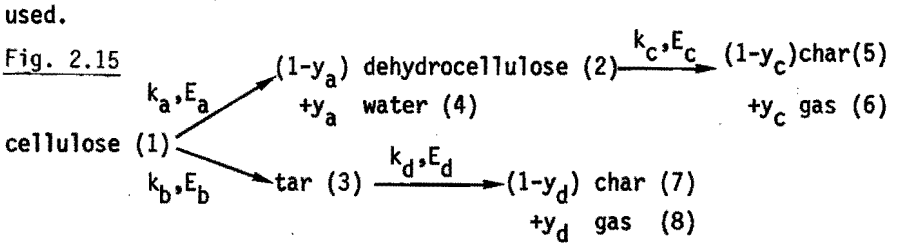

All reactions are again assumed to be first order in the component that is being converted so that the reaction rate equations are:

$$\frac{d\rho_1}{dt} = -(k_a+k_b)\rho_1 \qquad (2.51)$$

$$\frac{d\rho_2}{dt} = (1-y_a)k_a\rho_1 - k_c\rho_2 \qquad (2.52)$$

$$\frac{d\rho_3}{dt} = k_b\rho_1 - k_d\rho_3 \qquad (2.53)$$

$$\frac{d\rho_4}{dt} = y_a k_a \rho_1 \qquad (2.54)$$

$$\frac{d\rho_5}{dt} = (1-y_c)k_c\rho_2 \qquad (2.55)$$

$$\frac{d\rho_6}{dt} = y_c k_c \rho_2 \qquad (2.56)$$

$$\frac{d\rho_7}{dt} = (1-y_d)k_d\rho_3 \qquad (2.57)$$

$$\frac{d\rho_8}{dt} = y_d k_d \rho_3 \qquad (2.58)$$

with $k_i = k_{i,o}.\exp(-E_i/RT)$ (2.59)

where E = activation energy (J/mole)

$k_{i,o}$ = frequency factor (sec^{-1})

i = 1 through 8

subscripts refer to the components indicated in the above reaction scheme.

Time is eliminated by dividing eqs. (2.52) through (2.58) by eq. (2.51). The resulting equations are integrated with the initial conditions:

$\rho_1 = \rho_{1,0}$ and $\rho_j = 0$ (j=2 through 8) for t=0 (2.60)

The results are:

$$\frac{\rho_2}{\rho_{1,0}} = \frac{\alpha}{\beta-1}.\left(\frac{\rho_1}{\rho_{1,0}}\right).\left[1 - \left(\frac{\rho_1}{\rho_{1,0}}\right)^{\beta-1}\right] \qquad (2.61)$$

$$\frac{\rho_3}{\rho_{1,0}} = \frac{B}{A-1} \cdot \left(\frac{\rho_1}{\rho_{1,0}}\right) \cdot \left[1 - \left(\frac{\rho_1}{\rho_{1,0}}\right)^{A-1}\right] \qquad (2.62)$$

$$\frac{\rho_4}{\rho_{1,0}} = \frac{y_a.k_a}{k_a+k_b} \cdot \left[1 - \frac{\rho_1}{\rho_{1,0}}\right] \qquad (2.63)$$

$$\frac{\rho_5}{\rho_{1,0}} = C.\left(\frac{\rho_1}{\rho_{1,0}}\right).\left[\frac{1}{\beta}.\left(\frac{\rho_1}{\rho_{1,0}}\right)^{\beta-1} - 1\right] + \frac{C}{\beta}.(\beta-1) \qquad (2.64)$$

$$\frac{\rho_6}{\rho_{1,0}} = D.\left(\frac{\rho_1}{\rho_{1,0}}\right).\left[\frac{1}{\beta}.\left(\frac{\rho_1}{\rho_{1,0}}\right)^{\beta-1} - 1\right] + \frac{D}{\beta}(\beta-1) \qquad (2.65)$$

$$\frac{\rho_7}{\rho_{1,0}} = P.\left(\frac{\rho_1}{\rho_{1,0}}\right).\left[\frac{1}{A}.\left(\frac{\rho_1}{\rho_{1,0}}\right)^{A-1} - 1\right] + \frac{P}{A}.(A-1) \qquad (2.66)$$

$$\frac{\rho_8}{\rho_{1,0}} = Q.\left(\frac{\rho_1}{\rho_{1,0}}\right).\left[\frac{1}{A}.\left(\frac{\rho_1}{\rho_{1,0}}\right)^{A-1} - 1\right] + \frac{Q}{A}.(A-1) \qquad (2.67)$$

where $\alpha = \dfrac{(1-y_a)k_a}{k_a+k_b}$ (2.68)

$\beta = \dfrac{k_c}{k_a+k_b}$ (2.69)

$A = \dfrac{k_d}{k_a+k_b}$ (2.70)

$B = \dfrac{k_b}{k_a+k_b}$ (2.71)

$C = \dfrac{(1-y_a)(1-y_c)k_a k_c}{(k_c-k_a-k_b)(k_a+k_b)}$ (2.72)

$D = \dfrac{(1-y_a)y_c k_a k_c}{(k_c-k_a-k_b)(k_a+k_b)}$ (2.73)

$P = \dfrac{(1-y_d)\ k_d.B}{(k_a+k_b)(A-1)}$ (2.74)

$Q = \dfrac{y_d k_d B}{(k_a+k_b)(A-1)}$ (2.75)

Eqs. (2.51) through (2.58) with the boundary conditions of eq. (2.60) may also be integrated towards time. One then obtains:

$$\frac{\rho_1}{\rho_{1,0}} = \exp - (k_a+k_b).\tau \qquad (2.76)$$

$$\frac{\rho_2}{\rho_{1,0}} = \frac{(1-y_a).k_a}{k_c-(k_a+k_b)} \cdot \left[\exp -(k_a+k_b)\ \tau - \exp - (k_c\ \tau)\right] \qquad (2.77)$$

$$\frac{\rho_3}{\rho_{1,0}} = \frac{k_b}{k_d-(k_a+k_b)} \cdot \left[\exp - (k_a+k_b).\tau - \exp - (k_d\,\tau)\right] \qquad (2.78)$$

$$\frac{\rho_4}{\rho_{1,0}} = \frac{y_a k_a}{k_a+k_b} \cdot \left[1 - \exp-(k_a+k_b)\tau\right] \qquad (2.79)$$

$$\frac{\rho_5}{\rho_{1,0}} = \frac{(1-y_a)(1-y_c)k_a k_c}{k_c - (k_a+k_b)} \cdot \left[\frac{1}{k_c} \exp - (k_c\tau) - \frac{1}{k_a+k_b} \exp - (k_a+k_b)\tau + R\right] \qquad (2.80)$$

$$\frac{\rho_6}{\rho_{1,0}} = \frac{(1-y_a)y_c k_a k_c}{k_c-(k_a+k_b} \cdot \left[\frac{1}{k_c} \exp - (k_c\tau). \frac{1}{k_a+k_b} \exp - (k_a+k_b)\tau + R\right] \qquad (2.81)$$

$$\frac{\rho_7}{\rho_{1,0}} = \frac{(1-y_d)k_b k_d}{k_d-(k_a+k_b)} \cdot \left[\frac{1}{k_d} \exp - (k_d\tau) - \frac{1}{k_a+k_b} . \exp - (k_a+k_b)\tau + S\right] \qquad (2.82)$$

$$\frac{\rho_8}{\rho_{1,0}} = \frac{y_d k_b k_d}{k_d-(k_a+k_b)} \cdot \left[\frac{1}{k_d} \exp - (k_d\tau) - \frac{1}{k_a+k_b} \exp - (k_a+k_b)\tau + S\right] \qquad (2.83)$$

where τ = chemical reaction time (sec)

$$R = \frac{k_c-(k_a+k_b)}{k_c(k_a+k_b)} \qquad (2.84)$$

$$S = \frac{k_d-(k_a+k_b)}{k_d(k_a+k_b)} \qquad (2.85)$$

2.4 Numerical solution of the general model

2.4.1 General description of methods to solve heat transfer equations

Parabolic differential equations with boundary conditions like the equations (2.16) and (2.36) can be solved numerically by dividing the time and place co-ordinate axes into discrete intervals. A rectangular grid is thus obtained (fig. 2.16).

The value of the function $T = f(x,t)$ which is defined by the differential equation (and initial and boundary conditions) is indicated with a variable V_i at any point of the grid. It is possible to derive a number of relations between these variables with the aid of the differential equation, the initial and the boundary conditions. When the number of relations is equal to the number of points of the grid the system of equations thus obtained can be solved. The values T_i calculated from this system are generally not identical to the real function values V_i.

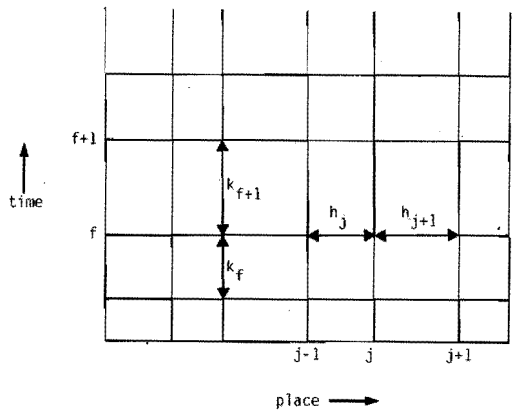

Fig.2.16 Rectangular grid obtained by dividing time and place coordinate axes into discrete intervals

The difference between both variables depends on:

- the way of transformation of the differential equation into a numerical relation (discretisation)
- the spacing of the intervals in time and place domain
- the accuracy of computing
- the numerical stability of the computing process.

2.4.2 Derivation of numerical relations from the differential equation

The parabolic partial differential equation describing the heat transport can be represented in its simplest form as:

$$\frac{\partial T}{\partial t} = \frac{\partial^2 t}{\partial x^2} \tag{2.86}$$

By applying Taylor series expansion to the left side of eq. (2.86) $\frac{\partial T}{\partial t}$ may be replaced by a difference-quotient:

$$T(t+\Delta t) = T(t) + \Delta t.\frac{\partial T}{\partial t} + \left(\frac{\Delta t}{2!}\right)^2 . \frac{\partial^2 T}{\partial t^2} + 0\ (\Delta t^3) \tag{2.87}$$

so that

$$\frac{\partial T}{\partial t} = \frac{T(t+\Delta t) - T(t)}{\Delta t} + F(\Delta t) \tag{2.88}$$

where $F(\Delta t) = -\frac{\Delta t}{2} \cdot \frac{\partial^2 T}{\partial t^2} - O(\Delta t^2)$ (2.89)

A truncation error is introduced by setting $F(\Delta t)$ equal to 0. This truncation error is a first order function of Δt. The above method is called first order discretisation. The approximation of the first derivative requires at least two points of the grid.In this case let the points of the grid be $T(x,t+\Delta t)$ and $T(x,t)$.
The Taylor series expansion is applied twice for discretisation of the right side of eq. (2.86), viz. for $T(x+\Delta x)$ and $T(x-\Delta x)$:

$$T(x+\Delta x) = T(x) + \Delta x.\frac{\partial T}{\partial x} + \frac{(\Delta x)^2}{2!}\frac{\partial^2 T}{\partial x^2} + \frac{(\Delta x)^3}{3!}\frac{\partial^3 T}{\partial x^3} + O(\Delta x^4) \quad (2.90)$$

$$T(x-\Delta x) = T(x) - \Delta x.\frac{\partial T}{\partial x} + \frac{(\Delta x)^2}{2!}\frac{\partial^2 T}{\partial x^2} - \frac{(\Delta x)^3}{3!}.\frac{\partial^3 T}{\partial x^3} + O(\Delta x^4) \quad (2.91)$$

Adding eq. (2.90) to eq. (2.91) results in the difference quotient for $\frac{\partial^2 T}{\partial x^2}$ (rest terms are omitted):

$$\frac{\partial^2 T}{\partial x^2} = \frac{T(x-\Delta x)-2T(x)+T(x+\Delta x)}{(\Delta x)^2} \quad (2.92)$$

The deduction of $\frac{\partial^2 T}{\partial x^2}$ requires at least three points of the grid, viz. $T(x-\Delta x,t)$, $T(x,t)$ and $T(x+\Delta x,t)$.
It is clear from the fact that at least 3 points of the grid are required for the discretisation with respect to place and at least 2 for the discretisation with respect to time that at least 4 points of the grid are required for the discretisation of eq. (2.86). Two discretisation schemes can be set up (fig. 2.17).

Fig. 2.17

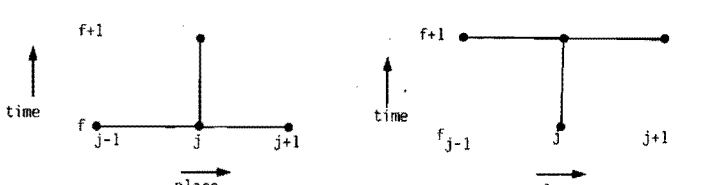

Discretisation scheme I (explicit, forward difference)

Discretisation scheme II (implicit, backward difference)

The points of the grid $T(x-\Delta x,t)$, $T(x,t)$ and $(Tx+\Delta x,t)$ are represented in scheme I by $T_{j-1,f}$, $T_{j,f}$ and $T_{j+1,f}$. The discretisation in respect to place is represented by the horizontal lines and the discretisation in respect to time by the vertical lines.
Close examination of eq. (2.86) and both discretisation schemes shows that in discretisation scheme I the first derivative towards time is equal to the second derivative towards place at the previous time level, while in scheme II the first derivative towards time equals the second derivative towards place at the next time level. An average second derivative may be used in addition to these two extreme schemes. This is accomplished by attaching a weight factor to the results of both discretisation schemes I and II. Fig. 2.18 represents the new scheme.
Fig. 2.18

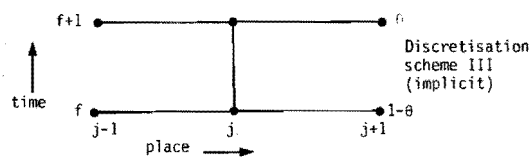

Discretisation scheme III is composed of scheme I (with a weight factor $1-\theta$) and of scheme II (with a weight factor θ). For $\theta=1/2$ we get the Crank-Nicholson scheme which has been used for the numerical computation of the heat transport equation. The Crank-Nicholson scheme consists in principle of an averaging around point of the grid $(j,f+1/2)$. The Crank-Nicholson scheme leads to a truncation error that is second order in place as well as in time [2.31].

Computational procedure: All variables at time t=0 are known from the initial conditions. The variables at the new time level can be calculated from the variables at the previous time levels by use of one of the discretisation schemes. The discretisation relations together with the two boundary conditions form a set of n equations with n unknows. This set of equations can be represented by the general form of equation (2.93):

$$\underline{\underline{A}}.\bar{T}_{f+1} = \underline{\underline{B}}.\bar{T}_{f} \qquad (2.93)$$

where $\bar{\bar{A}}$ and $\bar{\bar{B}}$: coefficient matrices

$\bar{T}_f$ and $\bar{T}_{f+1}$: vectors, having all variables at time level f, respectively f+1 as elements.

The above equation (2.93) is based on the assumption that two time levels only are involved in the discretisation.

In an implicit scheme a relation is given between variables at three successive points of the grid of the new time level. The coefficient matrix $\bar{\bar{A}}$ then generally is a tridiagonal matrix. The discretisation scheme according to Crank-Nicholson is implicit so the matrix $\bar{\bar{A}}$ in eq. (2.93) can be represented by:

$$\bar{\bar{A}} = \begin{pmatrix} a_0 & c_0 & & & & & \\ b_0 & a_1 & c_1 & & & & \\ & b_1 & a_2 & c_2 & & & \\ & & \ddots & \ddots & \ddots & & \\ & & & b_{n-2} & a_{n-1} & c_{n-1} & \\ & & & & b_{n-1} & a_n & \end{pmatrix} \qquad (2.94)$$

The vector $\bar{T}_f$ in eq. (2.93) is known. The product $\bar{\bar{B}}.\bar{T}_f$ therefore can be replaced by a vector $\bar{y}_f$:

$$\bar{\bar{A}}.\bar{T}_{f+1} = \bar{y}_f \qquad (2.95)$$

Standard procedures to solve this set of equations are available.

More details about the computing process, its stability and the discretisation of the heat transport equation, boundary conditions and reaction rate equations are given in appendix 2.1.

2.5 Data required in the models

2.5.1 Introduction

To apply all models derived in § 2.3 one must know the values of the reaction kinetic parameters (activation energy E, frequency factor k_o

and gas yield factor y) for all three or four reactions. Application of the general models and lumped parameter model required knowledge of the values of the heat transport parameters as well: f.i. heat capacity and thermal conductivity of the solids and heat capacity of the gaseous products. The values of the heat transport parameters used in the models have been taken from literature, except for the heat conductivities of cellulose (paper) and char which have been determined experimentally.

The kinetic parameters, however, (except for one or two parameters) have been determined by means of thermogravimetric and differential thermal analysis.

The thermo-analytical methods that were used to determine the kinetic parameters will be discussed briefly. The kinetic parameters given in the literature will be surveyed. The experimental determiniation of the reaction kinetic parameters which have been carried out in the course of this investigation will then be described.

2.5.2 Thermoanalytical methods used to determine reaction kinetic parameters [2.32]

Qualitative as well as quantitative investigation of the kinetics of the chemical reactions that play a role in the thermal degradation of cellulose may be carried out by means of the thermoanalytical methods such as thermogravimetry (TG), differential thermal analysis (DTA) and differential scanning calorimetry (DSC). In thermoanalysis a sample of a material may be heated according to a temperature-time program (f.i. linear temperature rise, exponential temperature rise, isothermal condition) and during the heating the changes in weight or energy may be recorded:

In TG: weight change as a function of temperature or time.

In DTA: the temperature difference between the sample and an inert material (both in the same furnace)as a function of time or temperature.

In DSC: the heat supplied to or withdrawn from reference and sample pans to keep both pans or crucibles (both in the same furnace) at the same temperature as a function of temperature.

All thermoanalytical methods require very good control and accurate measurement of the temperature in the furnace and/or sample and reference pans/crucibles.

Thermogravimetry will be discussed in more detail as quantitative data are, in most cases, "distilled" from TG curves and, in any case, thermogravimetry has been used in this study to obtain numerical information on kinetic data.

Solids (s) that undergo chemical reactions at increased temperature and thereby decompose into products that are partly gaseous (g) will lose weight during the process of heating. For instance: $A(s) \rightarrow P(s) + R(g)$. The recorded weight loss is caused by the amount of gases produced. The heating of the sample of A generally proceeds via one of the following time-temperature programs:

a. The sample is heated as fast as possible up to the desired temperature of investigation and then kept at that temperature. The change in weight of the sample is recorded as a function of the time (isothermal TG).
b. The sample is heated to produce a linear temperature rise (constant heating rate q). The change in weight of the sample is recorded as a function of the time or the temperature (dynamic TG).

Practical considerations in applying thermogravimetry

In using a thermobalance one has to take into account the various influences that may give cause to considerable errors in the results. Some of the effects that may influence the isothermal or dynamic thermogravimetric analysis are briefly discussed [2.33]:

1. Influence of buoyancy.
   An apparent weight gain usually occurs when an empty thermally inert crucible is heated.This so-called "buoyancy" effect is the result of a complex interplay of three factors: decreased buoyancy, increased convection and the effect of heat on the balance mechanism. The best method of correcting for this effect is to prepare a correction curve with an empty crucible or a crucible filled with thermally inert material up to a temperature of at least $100^{o}C$ above the working temperature, under conditions identical to those of the actual experiment.
2. Effect of container design.
   The geometry of the crucible will often greatly affect the shape of the TG curve. A crucible with a large opening promotes exchange of gases between the sample and the surrounding atmosphere.

3. Effect of sample weight.
   It is best to use as small a sample weight as possible relative to the sensitivity of the balance to minimize the temperature gradient throughout the sample.
4. Temperature measurement.
   The temperature recorded by a thermobalance is either the actual sample temperature or, more usually, the temperature at some point in the furnace near the sample.If the latter method is chosen, it must be realized that these measurements are subject to certain errors which are caused by the use of a heating program in which the furnace temperature is continually increased. A difference exists between sample temperature and measured temperature due to thermal lag. This thermal lag is significant and can amount to as much as $15^{o}C$ at a heating rate of $10^{o}C/min$(in modern thermobalances). The thermal lag is related to the mass, heat capacity, thermal conductivity and particle size of the material, to the gas flow rate in the furnace and to the heating rate.
5. Effect of heating rate.
   In temperature programmed heating of the sample the same conversion occurs at increased temperature when the heating rate is increased. The shape of a TG curve therefore depends on the heating rate. When several reactions take place in dynamic TG analysis and the reactions play a role at different temperatures the weight loss will generally take place in steps. It is advisable to choose a low heating rate in order to separate the various steps.
6. Effect of atmosphere.
   The composition of the atmosphere in the furnace may influence the thermal reactions. Good ventilation (for instance by flushing the furnace with an inert gas)may be of help in accelerating the removal of gaseous products so that they do not influence further decomposition of the sample.
7. Effect of heat of reaction.
   The heat of reaction will affect the extent to which the sample temperature precedes or succeeds the furnace temperature depending on whether the reaction is exo - or endothermic (The very existence of this temperature difference is indeed the basis of DTA). When large difference exist between furnace temperature and sample temperature the kinetic constants calculated from thermogravimetric data will

contain considerable errors.

8. Miscellaneous effects (condensation of volatile products on the cooler parts of the sample support system, sunbeams etc.).

2.5.3 Determination of kinetic data from TG curves

Two methods of investigation are used to obtain kinetic data from thermogravimetric experiments: the isothermal method and the dynamic method. The disadvantage of the isothermal method is that the constant temperature must refer to the environment and not to the sample itself. This is because almost all reactions are either endothermic or exothermic. The reacting material thus must be subject to temperature changes during the decomposition. The disadvantage of the rising temperature technique is that, unlike in many homogeneous reactions the conversion kinetics may not or not only be limited by the rates of reaction but (also) by mass and heat transport.
Most methods for obtaining kinetic parameters from TG are based on the combination of three equations:

$$\frac{d\alpha}{dt} = k.f(\alpha) \ , \ k = k_0.\exp(-E/RT) \text{ and } T = T_0 + q.t,$$

in which α = fraction decomposed
t = time
k = rate constant
E = activation energy
R = gas constant
k_0 = frequency factor
T = absolute temperature
T_0 = starting temperature for the experiment
q = heating rate.

Some of the methods that are used for obtaining kinetic data from TG experiments(isothermal or dynamic) will be discussed in the § 2.5.5 in which a description is given of our determinations of kinetic data for each of the 4 model reactions included in the reaction scheme for the pyrolysis of cellulose postulated in § 2.3.3.

2.5.4 Survey of kinetic parameters found in the literature for the pyrolysis of cellulose

Four reaction rate constants are named in the reaction scheme for the pyrolysis of cellulose postulated in § 2.3.3:

k_a, for the dehydration of cellulose giving dehydrocellulose

k_b, for the depolymerization of cellulose giving levoglucosan

k_c, for the decomposition of dehydrocellulose

k_d, for the decomposition of levoglucosan.

Once again, the reaction scheme is a simplified model of a complex series of reactions.

Many authors have investigated the thermal decomposition of cellulose. Most of them have been working under such experimental conditions that more than one reaction may occur (f.i. in a temperature range, where more than one reaction can occur). They calculated kinetic data by fitting the TG curve starting from the assumption that only one overall reaction occurs rather than a series of parallel and consecutive reactions. For this reason a wide variety of values for the activation energy and the frequency factor for this supposed overall reaction are found in literature. The values found depend on the experimental conditions these authors used as well as on the kinetic models of the decomposition that they used.

We feel that it should be possible to model the cellulose pyrolysis with a four step reaction scheme and our purpose is to determine kinetic data for each of the four model reactions (Each of the four model reactions may in fact be composed of several reactions and the kinetic data that are ascribed by us to one of the four model reactions may therefore be data that belong to a complex of reactions).

We therefore attempted to ascribe the data given in the literature to one of the four model reactions. It proved possible in some instances to ascribe an activation energy and frequency factor to one of the reaction steps in our scheme (fig. 2.14) from the experimental conditions (temperature, atmosphere, basic material).

2.5.4.1 The dehydration reaction

Only few data are available in literature that can be connected to the dehydration reaction. However, the various values for the activation

energy that have been found for cellulose pyrolysis at low temperatures (about 200°C) and little weight loss only (< 5%) show reasonable agreement.

The temperature range in which the dehydration predominates is 180° - 260°C. Initially, the dehydration is the only reaction that occurs. At somewhat higher temperature, however, the dehydration is followed by a charring reaction for the dehydrocellulose. Bolkunevich [2.34] measured an activation energy equal to 23.6 kcal/mole and a frequency factor of about $1.2*10^{9}sec^{-1}$ for what we assume to have been the dehydration. The weight loss that Bolkunevich found was less than 0.5%. Bradbury, Sakai and Shafizadeh [2.22] report an overall reaction for the decomposition of cellulose into char and gases for which an activation energy of 36.6 kcal/mole and a frequency factor of $2.8*10^{19}sec^{-1}$ are given. Arsenau [2.12] found an activation energy of 36.2 kcal/mole for the first 5 percent of weight loss at temperatures<280°C. Murphy [2.35] calculated an activation energy for the initial weight loss of 34.0 kcal/mole and a frequency factor of $2.8*10^{9}sec^{-1}$ for the thermal degradation of cellulose in the temperature range <250°C. The above values are summarized in table 2.2.

Table 2.2 Kinetic data that the present author ascribes to the dehydration reaction (reaction a).

activation energy (kcal/mole)	frequency factor (sec^{-1})	weight loss (%)	reference
23.6	$1.2*10^{9}$	0.5	[2.34]
36.6	$2.8*10^{19}$	-	[2.22]
36.2	-	5.0	[2.12]
34.0	$2.8*10^{9}$	-	[2.35]

2.5.4.2 The depolymerization reaction

Depolymerization of cellulose (giving levoglucosan) should predominate at temperatures of about 300°C(and higher) (see § 2.3.1). We ascribe kinetic data found for the pyrolysis of cellulose in this temperature range and under conditions where levoglucosan is not subject to further degradation (or where the depolymerization reaction can without difficulty be distinguished from the decomposition of levoglucosan to char

and gases) to the depolymerization reaction. The literature values for the activation energy can be divided into two groups. One group of investigators found an activation energy of about 45-50 kcal/mole, a second group found a value of about 35 kcal/mole. The findings of both groups are summarized in tables 2.3 and 2.4.

The activation energy and frequency factor that have been found by the authors quoted in tables 2.3 and 2.4 may have been influenced by:

1. thermal analysis technique (dynamic or isothermal TG, DTA).
2. method of calculating the kinetic data.
3. atmosphere: in a vacuum atmosphere the volatile pyrolysis products are quickly removed from the furnace so that further degradation of the volatiles (f.i. levoglucosan) may be avoided.
4. type of cellulose.
5. the heating rate; the period of heating before the temperature of investigation has been reached in isothermal TG is very important. Much of the cellulose may already have been decomposed into dehydrocellulose before the desired temperature had been reached when the initial heating period was long.Considerable temperature gradients may have existed in the sample and in the furnace at high heating rates in dynamic TG.

It is not quite clear what causes the great difference between the activation energy determined by group 1 and group 2. I am inclined to doubt, however, whether the kinetic data determined by isothermal TG can be ascribed to the depolymerization reaction. A large part of the cellulose probably had decomposed into dehydrocellulose before the desired temperature has been reached. If the cellulose had indeed reacted according to reaction a (dehydration of cellulose) during the heating up period the investigators of group 2 have been measuring the activation energy for the dehydration reaction rather than for the depolymerization of cellulose. Such an explanation is in fact suggested by the value of the activation energy these authors have found (about 35 kcal/mole). This value shows a remarkable resemblance to the one that other investigators have found for the dehydration reaction (see table 2.2).

Table 2.3 Kinetic data ascribed to the depolymerization of cellulose (reaction b). Group 1

reference	temperature range (^{o}C)	activation energy (kcal/mole)	frequency factor (sec^{-1})	atmosphere (-)	type of cellulose	method	heating rate (^{o}C/sec)
[2.18]	275-305	50	-	vacuum	cotton-cellulose	isothermal TG	-
[2.16]	287-357	53.51	$1.05*10^{7}$	vacuum	α-cellulose	dynamic TG/DTA [1])	0.01 - 0.05
[2.22]	259-341	47.3	-	vacuum	Whatmann cellulose powder	dynamic TG	-
[2.12]	285-320	45.4	-	N_2,1 atm.	Whatmann cellulose powder	dynamic TG	0.025
[2.36]	275-312	49.0	-	N_2,1 atm.	cotton cellulose fine	isothermal TG	-
[2.19]	310-360	53.1-55.7	-	vacuum	α-cellulose	dynamic TG	0.2

[1]) kinetic data obtained by means of the Kissinger method (see §2.5.5.3).

Tabel 2.4 Kinetic data ascribed to the depolymerization of cellulose (reaction b). Group 2.

Reference	temperature range (^{o}C)	activation energy (kcal/mole)	frequency factor (sec^{-1})	atmosphere	type of cellulose	method
[2.37]	-	34	-	vacuum	-	-
[2.38]	250-800	33.4	$6.79*10^{9}$	vacuum	Black Label filter paper	isothermal TG [1])
[2.38]	250-800	37.0	$7.67*10^{10}$	vacuum	Black Label filter paper	isothermal TG [2])
[2.39]	270-300	37.1	-	helium, 1 atm.	fine cotton-cellulose	isothermal TG

[1]) one first order reaction

[2]) depolymerization according to a series of reactions with a Gauss distribution for the activation energy.

2.5.4.3 The degradation of dehydrocellulose

Few kinetic data are available in the literature for the reaction that follows the dehydration. Broido and Weinstein [2.23] have carried out isothermal thermogravimetric experiments with high purity cellulose paper at 226°C. They obtained kinetic data from these experiments which they based on the assumption that cellulose pyrolysis proceeds according to the below reaction scheme:

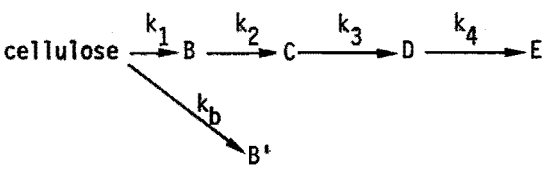

Here B is cellulose having a lower degree of polymerization than the initial material, B' is a volatile product comparable to tar (gaseous at 226°C), C is dehydrocellulose (loss of some water molecules), D is dehydrocellulose that result from further dehydration, E is char plus gases. k_1 through k_4 are reaction rate constants. Broido and Weinstein applied a reaction kinetic model based on first order reactions. Two possible solutions for reaction rate constant k_4 resulted from their calculations:

$$k_{4,1} = 8.2*10^{-7} sec^{-1} \text{ and } k_{4,2} = 1.64*10^{-6} see^{-1} \text{ (both at 226°C)}$$

No further kinetic data (activation energy, frequency factor) that could be ascribed with some certainity to the decomposition of dehydrocellulose (reaction c) could be traced in literature.

2.5.4.4 The degradation of levoglucosan

Not many quantitative data for the degradation of the tar are available in literature. The most important component present in the tar is the anhydrosugar levoglucosan ([2.12],[2.13],[2.36],[2,39],[2.40]). Langley, Drews and Barker [2.36] have carried out isothermal and dynamic TG (heating rate 20°C/min) and DSC analysis for levoglucosan in a nitrogen atmosphere. On the basis of these experiments they postulate that the thermal degradation of levoglucosan proceeds through two consecutive reactions: polycondensation of the levoglucosan (at about 270°C in dynamic TG) followed by decomposition of the polycondensation product

at temperatures above 300°C.They found an activation energy for the polycondensation of levoglucosan of 40.3 kcal/mole from isothermal TG experiments for levoglucosan in the temperature range of 210-238°C.They do not give an activation energy for the consecutive degradation of the polycondensation product.

2.5.5 Determination of reaction kinetic parameters for cellulose pyrolysis

A discussion is now presented of the methods used to interpret the data obtained in the thermoanalytical experiments that were carried out as part of the present attempt to determine kinetic parameters for the pyrolysis of cellulose. A sort description of the experiments themselves and of the results of the interpretation will be given in paragraph 2.5.6.

2.5.5.1 Assumptions made in the determination of the reaction kinetic parameters

The following assumptions were made in the investigation of the reaction kinetics of the thermal degradation of cellulose:

1. The reactions fit the four step reaction scheme as proposed in § 2.3.3.3, figs. 2.14 and 2.19.
2. All reactions are first order reactions in the compound that is being converted (as was assumed by for instance Lipska and Parker [2.41], Stamm [2.42] and Broido [2.23]).
3. The depolymerization reaction (reaction b, in which levoglucosan is formed) occurs with negligible reaction rate at temperatures below 260°C.
4. At temperatures above 300°C the depolymerization predominates and the dehydration is negligible.
5. The temperature dependence of the reaction rate constant k is given by the Arrhenius relation: $k = k_0.\exp(-E/RT)$ in which
   k_0 = frequency factor
   E = activation energy
   R = gas constant
   T = absolute temperature

The symbols used are shown in fig. 2.19.

Fig. 2.19

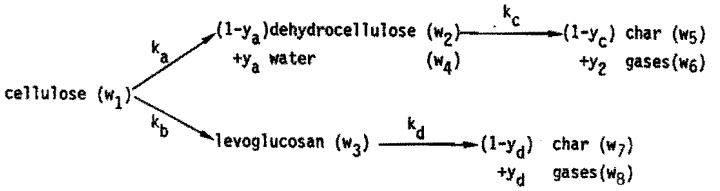

where: w_i = weight of component i (i=1 through 8).
k_j = reaction rate constant for reaction j (j=a,b,c,d)
y_j = gas yield factor for reaction j (j=a,b,c,d).

2.5.5.2 Isothermal pyrolysis of cellulose in a thermo-balance at temperatures ≤ 260°C

The following equations may be derived on the basis of the above assumptions 1,2 and 3.

$$\frac{dw_1}{dt} = k_a w_1 \qquad (2.96)$$

$$\frac{dw_2}{dt} = (1-y_a)k_a w_1 - k_c w_2 \qquad (2.97)$$

$$\frac{dw_5}{dt} = (1-y_c)k_c w_2 \qquad (2.98)$$

Initial conditions: for t=0 $w_1=w_o$ (=initial weight of cellulose sample)

$$w_2=w_5=0 \qquad (2.99)$$

The solution of the above set of equations is given by:

$$w_1 = w_o\, e^{-k_a t} \qquad (2.100)$$

$$w_2 = \frac{(1-y_a)k_a}{k_c-k_a} \cdot (e^{-k_a t} - e^{-k_c t}).w_o \qquad (2.101)$$

$$w_5 = \frac{(1-y_a)k_a(1-y_c)k_c}{k_c-k_a} \cdot \left[\frac{1}{k_c} e^{-k_c t} - \frac{1}{k_a} e^{-k_a t} + \frac{k_c-k_a}{k_a k_c}\right].w_o \qquad (2.102)$$

The total weight of the sample w_t (weight of the solids) is measured in the thermobalance as a function of the residence time t:

$$w_t = w_1 + w_2 + w_5 \qquad (2.103)$$

Substitution of eqs. (2.100), (2.101) and (2.102) into eq. (2.103) yields:

$$\frac{w_t}{w_o} = \frac{(1-y_a)k_a}{k_c-k_a} \cdot \left| \frac{k_a-k_c(1-y_c)}{k_a} \cdot e^{-k_a t} - y_c\, e^{-k_c t} \right| + (1-y_a)(1-y_c) + e^{-k_a t} \qquad (2.104)$$

$\frac{w_t}{w_o}$ is measured in a thermobalance as a function of time at constant temperature (in this case < 260°C). Determination of $\frac{w_t}{w_o}$ at different t gives sets of values of $(\frac{w_t}{w_o}, t)$ which are used as input data for a curve fitting computer program in which k_a, k_c, y_a and y_c are calculated numerically from equation (2.104). Details about the computing procedure are given in appendix 2.2. It was assumed above that the relation between reaction rate constant and absolute temperature is given by:

$k = k_o . \exp(-E/RT)$.

E_a, E_c, k_{ao} and k_{co} can be found from the determiniation of k_a and k_c at different temperatures by plotting ln k versus 1/T (slope-E/R, $\ln k_o = \ln k$ for 1/T=0).

The determination of k_a and y_a according to the above curve fitting method gave some problems while at temperatures above 230°C the heating time effect plays an important role: before the desired temperature of investigation is reached part of the cellulose probably has been converted to dehydrocellulose. This effect is nil at temperatures below 230 °C. In addition, the reaction rate constant k_c is very small in this temperature range so that the consecutive conversion of the dehydrocellulose proceeds only very slowly. It was therefore decided to determine k_a and y_a from isothermal experiments at temperatures below 230°C.

The experiments led to the conclusion that values can be found for k_a and y_a for the first 1.5-2.5 % weight loss that meet the following expression:

$$\frac{w_t}{w_o} = (1-y_a) + y_a\, e^{-k_a t} \qquad (2.105)$$

(The consecutive degradation of dehydrocellulose (reaction c) apparently does not take place at these low temperatures).

The heating time effect is less important in the determination of k_c and y_c as reaction c essentially proceeds only when a fair amount of dehydrocellulose has already been formed. The initial period of the pyrolysis of cellulose therefore has little effect on the course of reaction c. The determination of k_c and y_c at temperatures below 260°C according to the curve fitting method described above yielded better results in these experiments. Plotting of ln k_c versus 1/T gave a straight line.

2.5.5.3 Use of the Kissinger method for the determination of the kinetic parameters for the depolymerization of cellulose

The dehydration of cellulose can be neglected at pyrolysis temperatures above 300°C according to assumption 4 and to the findings of other investigators([2.12],[2.17],[2.23],[2.40]).The depolymerization and consecutive degradation of levoglucosan predominate at higher temperatures. It might therefore seem reasonable to use the same method that was described in § 2.5.5.2 (but at higher temperatures) for determining k_b and k_d. There are, however, some objections against using this method at higher pyrolysis temperatures:

1. The product formed in the depolymerization of cellulose (levoglucosan) is volatile in the relevant temperature range. Levoglucosan may evaporate from the analysis crucible without degradation.
2. The heating up period for the furnace of the thermobalance is substantial. Before the temperature of investigation has been reached a large part of the cellulose may have decomposed into dehydrocellulose. This heating up effect complicates the determination of k_b and k_d according to the above method. The method would be done as is discussed below: if there is still a considerable amount of cellulose present at the temperature of investigation (>300°C) and if it is

assumed that no substantial amount of dehydrocellulose is present, the weight loss during the isothermal determination is ascribed to the depolymerization of cellulose. And if the experiments are carried out under vacuum the levoglucosan evaporates from the furnace immediately after its formation. The following equation describes the weight loss in that case:

$$\frac{dw_1}{dt} = - k_b w_1 \qquad (2.106)$$

The problem is, however, to determine the amount of cellulose (w_1) that is still present at the time the temperature of investigation has been reached.

Such problems do not arise when the Kissinger method [2.16] is applied.

Kissinger method at linear temperature rise of a sample

A sample of cellulose is heated at linear temperature rise under vacuum. It is assumed that at temperatures above 200°C the remaining cellulose decomposes through a depolymerization reaction into gaseous levoglucosan. Relationship (2.106) may then be applied. According to assumption 5 of § 2.5.5.1 k_b is given by:

$$k_b = k_{bo}.\exp(-E_b/RT) \qquad (2.107)$$

The heating rate q (°C/sec) may be written as:

$$q = \frac{dT}{dt} \text{ or } q.dt = dT \qquad (2.108)$$

Combination of eqs. (2.106), (2.107) and (2.108) gives:

$$\frac{dw_1}{w_1} = - \frac{k_{bo}}{q} . \exp.(-E_b/RT).dT \qquad (2.109)$$

For T = 300°C (= 573°K): w_1=L (L being the amount of cellulose still present at 300°C).

The solution for eq. (2.109) with this initial condition is:

$$\ln \frac{w_1}{L} = - \frac{k_{bo}}{q} \int_{573}^{T} \exp(-E_b/RT).dT \qquad (2.110)$$

$$\text{Or: } w_1 = L.\exp\left\{ -\frac{k_{bo}}{q} \int_{573}^{T} \exp(-E_b/RT).dT \right\} \qquad (2.111)$$

Let T_{max} to be temperature at which the conversion rate (k_b,w_1) reaches its maximum for the given heating rate q. The below relations can then be derived if no other reactions then those indicated above occur:

$$\left(\frac{d^2w_1}{dT^2}\right)_{T=T_{max}} = 0 = -\frac{L}{q}.k_{bo}.\frac{E_b}{RT^2_{max}}.\exp.(-E_b/RT_{max}).\exp.\left[-\frac{k_{bo}}{q} \int_{573}^{T} \exp(-E_b/RT).dT \right] +$$

$$+ L.\frac{k^2_{bo}}{q^2}.\exp(-E_b/RT_{max}).\exp(-E_b/RT_{max}).\exp.\left[-\frac{k_{bo}}{q} \int_{573}^{T} \exp(-E_b/RT).dT \right] \qquad (2.112)$$

$$L.\frac{k_{bo}}{q}.\frac{E_b}{RT^2_{max}} = \frac{L.k^2_{bo}}{q^2}.\exp.(E/RT_{max}) \qquad (2.113)$$

$$\ln \frac{E_b.q}{RT^2_{max}.k_{bo}} = \frac{-E_b}{RT_{max}} \qquad (2.114)$$

The temperature at which the conversion rate reaches its maximum (T_{max}) corresponds to the temperature at which the weight loss (TG) or heat effect (DTA,DSC) shows a maximum.Experiments at different heating rates (q) give different values for T_{max}. Plotting $\ln \frac{q}{T^2_{max}}$ versus $\frac{1}{T_{max}}$ results in a straight line with slope $-E_b/R$. Substitution of E_b , q and T_{max} into eq. (2.114) gives k_{bo}.

2.5.5.4 Isothermal pyrolysis of levoglucosan ($200^oC < T < 250^oC$)

The depolymerization of cellulose results in the formation of levoglucosan at relatively high temperature (according to the proposed reaction scheme). The levoglucosan may either evaporate from the furnace as a vapor or it may decompose into char and gases or it may do both (see § 2.3.3.3). The reaction kinetic parameters for the decomposition of levoglucosan (reaction d) were determined by means of isothermal thermogravimetry between 200^oC and 250^oC using pure levoglucosan covered with inert aluminium oxide. It was found from DTA experiments on pure levoglucosan covered with aluminium oxide that the thermal degradation takes

place in two steps. These steps presumably are:

1. polycondensation of levoglucosan, which is accompanied by a loss of weight [2.36].
2. further carbonization of the resulting product, also accompanied by the formation of gases at temperatures above 300°C.

Fig. 2.20a represents the assumed mechanism for the pyrolysis of levoglucosan.

Fig. 2.20a 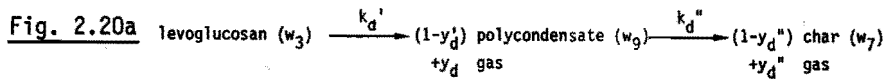

The carbonization is negligible in the isothermal experiments below 250°C. The decomposition of levoglucosan is then given by:

$$-\frac{dw_3}{dt} = kd'.w_3 \qquad (2.115)$$

$$\frac{dw_9}{dt} = (1-y_d').k_d'\, w_3 \qquad (2.116)$$

The total weight loss per unit time is then given by:

$$-\frac{dw_t}{dt} = -\frac{dw_3}{dt} - \frac{dw_9}{dt} = y_d'k_d'w_3 \qquad (2.117)$$

Initial conditions: for t=0 $w_3 = w_{30}$ (2.118)
$w_g = 0$

while w_{30} = initial weight of levoglucosan sample.
The amount of levoglucosan that has been decomposed at time t equals $w_{30} - w_3$. It follows that:

$$w_t = w_{30} - y_d'(w_{30}-w_3) \qquad (2.119)$$

where w_t = total weight at time t.

$$w_3 = w_{30} - \frac{w_{30}-w_t}{y_d'} \qquad (2.120)$$

Combination of eqs. (2.117) and (2.120) gives:

$$-\frac{dw_t}{dt} = k_d'(w_t - w_{30}) + y_d' k_d' w_{30}$$

which can be written as:

$$-\frac{dw_t}{dt} = k_d' w_t + (y_d' - 1) k_d' w_{30} \qquad (2.121)$$

Some weight loss may have occurred before the furnace of the thermobalance has reached the temperature where the measurement is to be carried out. In all isothermal experiments between 200 and 250°C this temperature will certainly have been reached before a weight loss of 20% has taken place.

$\frac{dw_t}{dt}$ for $w_t = 0.8 * w_{30}$ (20% weight loss) can be determined from the TG curve which is a plot of w_t vs time. The following equation can be derived for $w_t = 0.8 * w_{30}$:

$$-\left(\frac{dw_t}{dt}\right)_{w_t = 0.8 * w_{30}} = k_d' \cdot 0.8 w_{30} + (y_d' - 1) k_d' w_{30}$$

$$= k_d' \cdot w_{30} \cdot (y_d' - 0.2) \qquad (2.122)$$

The second step in the degradation of levoglucosan occurs at higher temperatures. The loss of weight due to this reaction is probably very small at temperatures between 200 and 250°C. The DTA peak for this reaction is observed at temperatures above 280-300°C (even for low heating rates).
The following relationship holds for large t in this case:

$$(w_t)_{t \to \infty} = (1 - y_d') \cdot w_{30} \qquad (2.123)$$

This expression is obtained from eq. (2.121) through substitution of $\frac{dw_t}{dt} = 0$ for $t \to \infty$. The value of k_d' for the temperature at which the experiment is carried out can be determined from eq. (2.122) when $y_d' = \left(\frac{dw_t}{dt}\right)_{w_t = 0.8 \cdot w_{30}}$ and w_{30} are known.

A dynamic TG curve of the polycondensation product of levoglucosan obtained by isothermal pyrolysis of levoglucosan between 200 and 250°C was measured using linear temperature rise. The weight loss that was measured was caused by the reaction:

$$\text{polycondensation product } (w_9) \xrightarrow{k_d''} \begin{matrix}(1-y_d'')\ \text{char} \\ +y_d''\ \text{gases}\end{matrix}$$

Assuming the reaction to be of first order in the polycondensation product the conversion equation is:

$$-\frac{dw_9}{dt} = k_d''.w_9 \qquad (2.124)$$

The rate of the char formation is given by:

$$\frac{dw_7}{dt} = (1-y_d'')k_d''\ w_9 \qquad (2.125)$$

A calculation similar to the derivation of eq. (2.121) leads to:

$$-\frac{dw_t}{dt} = k_d''.w_t + (y_d''-1)k_d''\ w_{90} \qquad (2.126)$$

y_d'' is determined from the total weight loss which is found when $\frac{dw_t}{dt} = 0$ Then:

$$0 = k_d''.w_t + (y_d''-1)k_d''.w_{90} \quad \text{or:}$$

$$y_d'' = \frac{-k_d''w_t+k_d''w_{90}}{k_d''w_{90}} = 1 - \frac{w_t}{w_{90}} \text{ for } \frac{dw_t}{dt} = 0 \qquad (2.127)$$

$\frac{dw_t}{dt}$ and w_t are determined as functions of T and k_d'' is calculated from eq. (2.126). E_d'' and k_{do}'' are determined by plotting ln k_d'' versus 1/T.

2.5.6 Experimental set up applied in the reaction kinetic investigation

2.5.6.1 Introduction

All thermogravimetric analyses were carried out in a Mettler Thermo-analyser 1/2 [2.43]. The cellulose used in the experiment was Merck 2351 native cellulose suitable for thin-layer chromatography. The furnace of the

thermobalance was flushed with argon at a flow rate of 4.5-5 liter/hour. Oxygen gas was excluded from the system in this way.

2.5.6.2 Isothermal pyrolysis of cellulose at temperatures between 180 and 230°C (atmospheric pressure)

Samples of cellulose (50-100 mg) were placed in an aluminium oxide crucible(fig.2.20).The crucible was heated in the thermobalance at a rate of about 25°C/min up to a temperature between 180 and 230°C. During the isothermal period the weight loss was recorded continually as a function of time. y_a and k_a can be calculated from the first 1.5-2% of weight loss (§ 2.5.5.2). Table 2.5 summarizes the values of y_a and k_a found at different temperatures.

Table 2.5 Reaction rate constant and gas yield factor of the dehydration of cellulose.

T (°K)	$k_a(sec^{-1})$	$y_a(-)$	$-\ln k_a$
514	$8.1*10^{-4}$	0.0268	7.12
500	$4.3*10^{-4}$	0.0250	7.75
486	$1.9*10^{-4}$	0.0230	8.56
478	$9.2*10^{-5}$	0.0219	9.29
467	$3.36*10^{-5}$	0.0200	10.30
463	$2.62*10^{-5}$	0.0180	10.55

Fig. 2.21 shows a plot of $-\ln k_a$ vs 1/T. The activation energy E_a and frequency factor k_{ao} determined from this plot are:

E_a = 32.8 kcal/mole, k_{ao} = $9.02*10^{10} sec^{-1}$

The correlation coefficient for the linear regression is 0.994.

2.5.6.3 Isothermal pyrolysis of cellulose at temperatures below 260°C

The experiments were carried out in a manner identical to that described in § 2.5.6.2. The experiment was terminated when the weight loss per unit of time had become zero. Table 2.6 summarizes the values for y_c and k_c obtained from the experimental data by means of the curve fitting

crucible
(ø 7 mm)

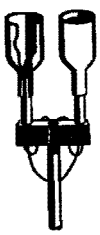

position of crucibles
in furnace for DTA/TGA
experiments

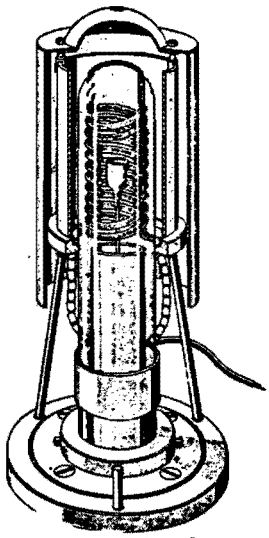

Furnace of Mettler
thermo-analyzer 1/2

Fig.2.20 Some details on the thermobalance

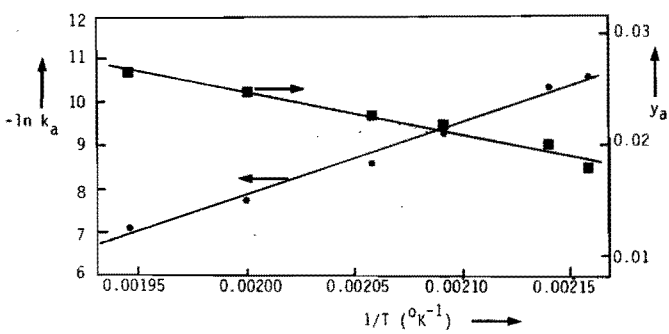

Fig.2.21 Plots of -ln k_a and y_a versus 1/T

method described in § 2.5.5.2 and in appendix 2.2 for different temperatures.

Fig. 2.22 shows a plot of - $\ln k_c$ vs. 1/T. The activation energy E_c and frequency factor k_{co} determined from the plot are:

E_c = 54.1 kcal/mole, k_{co} = $7.05*10^{17}$ sec^{-1}

The correlation coefficient of the linear regression is 0.997.

Table 2.6 Reaction rate constant and gas yield factor of reaction c at different temperatures.

T(^oK)	$k_c(sec^{-1})$	y_c	$-\ln k_c$
539	$7.5*10^{-5}$	0.74	9.50
528	$3.8*10^{-5}$	0.69	10.18
514	$7.1*10^{-6}$	0.74	11.85
500	$1.97*10^{-6}$	0.74	13.14
490	$5.04*10^{-7}$	0.74	14.50

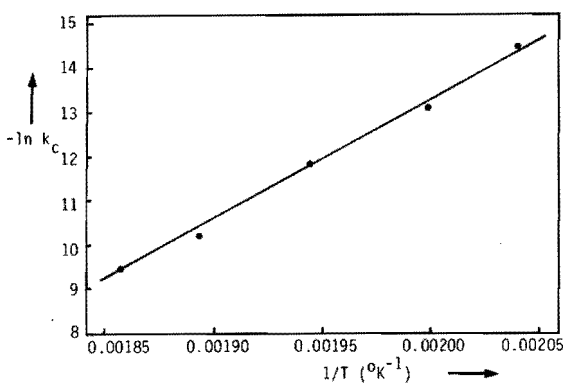

Fig.2.22 Plot of $-\ln k_c$ versus 1/T

2.5.6.4 Dynamic thermogravimetry of cellulose in vacuum atmosphere

A cellulose sample (30-60 mg) was placed in an alumunium oxide crucible inside the thermobalance. The furnace was evacuated to a pressure of 10^{-1}-10^{-2} Torr so that gaseous pyrolysis products were removed quickly. The sample was heated at a constant heating rate of 1-20^oC/min and cooled down again after it had reached a temperature of about 550^oC. The weight loss was recorded continually. DTA could not be carried out because of defects in the equipment. The temperature at which the weight

loss per unit of time was maximal and the conversion therefore was maximal was determined from the resulting curve of weight vs. time. Table 2.7 summarizes the values for T_{max} at different heating rates.

Table 2.7 Temperature of maximal cellulose conversion as a function of the heating rate.

heating rate $q(^oK/sec)$	T_{max} (^oK)	$1/T_{max}$ $(^oK^{-1})$	$-\ln(q/T^2_{max})$ (-)
0.0222	589	0.001698	16.56
0.0439	601	0.001678	15.92
0.0662	609	0.001642	15.54
0.1235	615	0.001626	14.93
0.2941	649	0.001541	14.17
0.3125	662	0.001510	14.16
0.5556	673	0.001486	13.61

Fig. 2.23 shows a plot of $-\ln(q/T^2_{max})$ versus $1/T_{max}$. The value of E_b calculated from the slope of the straight line that may be fitted to the data points is 24.6 kcal/mole, k_{b0} is found to be $1.66*10^7 sec^{-1}$. However, a straight line cannot accurately be fitted to the measured

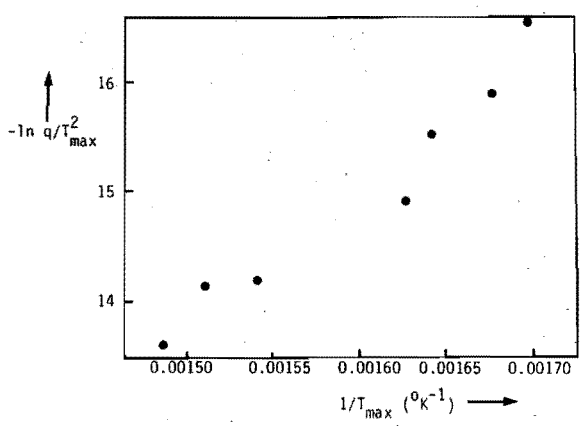

Fig.2.23 Plot of $\ln q/T^2_{max}$ versus $1/T_{max}$

data points of fig.2.23. The slope of the curve increases with decreasing heating rate. Applying linear regression to the four measured data points at the lowest heating rates (q=0.0222, 0.0439, 0.0662 and 0.1235 ^{o}K/sec) one finds an activation energy and frequency factor that are equal to E_b=40.2 kcal/mole, k_{b0}=1.05*10^{13} sec^{-1}. A discussion of the phenomenon is given in § 2.5.6.7.

2.5.6.5 Isothermal pyrolysis of levoglucosan in the temperature range 200-250^{o}C

A sample of 20-30 mg of levoglucosan (1,6-anhydro-β-D-glucopyranose, m.p. 180^{o}C) obtained from Raylo Chemicals Limited (Canada) was placed in a platinum crucible and covered with inert aluminium oxide powder. The crucible was placed in the thermobalance and the furnace was heated at a rate of 25^{o} C/min up to the temperature of investigation (between 200 and 250^{o}C). At that temperature the weight loss was recorded as a function of time.

k_d and y_d (or rather: k_d' and y_d') were determined by means of the method described in § 2.5.5.4. Values for k_d' at different temperatures are summarized in table 2.8.

Table 2.8 Reaction rate constant for isothermal pyrolysis of levoglucosan

T(^{o}K)	k_d'(sec^{-1})	- lnk_d'
511	3.94*10^{-4}	7.84
504	1.92*10^{-4}	8.56
495	1.00*10^{-4}	9.21
493	0.82*10^{-4}	9.41
483	0.33*10^{-4}	10.32
477	0.23*10^{-4}	10.68

The values that were determined hold for the polycondensation of levoglucosan, that is the d'-step. The gas yield factor y_d' was determined from the weight loss at 511^{o}K for t→∞ : y_d'=0.55 ± 0.02 (kg/kg levoglucosan). Fig. 2.24 shows a plot of -ln k_d' vs 1/T. The following value for the activation energy is found from the slope of the line: E_d' = 40.6 kcal/mole. The frequency factor is found to be 7.66*10^{13}sec^{-1}. The correlation coefficient of the linear regression is 0.997.

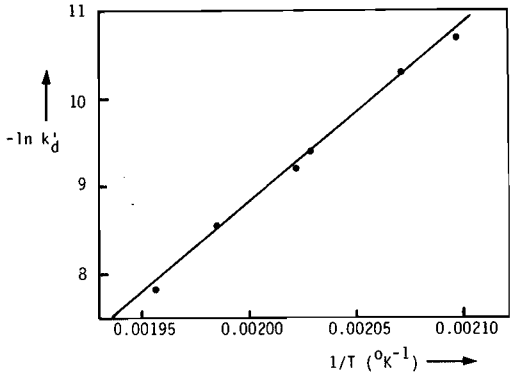

Fig.2.24 Plot of $-\ln k'_d$ versus 1/T

2.5.6.6 A DTA/TG-curve for cellulose

Fig. 2.25 represents a DTA/TG-curve for cellulose (Merck 2351 native cellulose). The furnace had been flushed with nitrogen at atmospheric pressure. The sample as well as the reference material (aluminium oxide) had been placed in platinum crucibles.The temperature difference between reference material and cellulose was measured by means of a Pt/PtRh thermocouple. This temperature difference and the weight loss of the cellulose sample were measured as a function of time during the linear

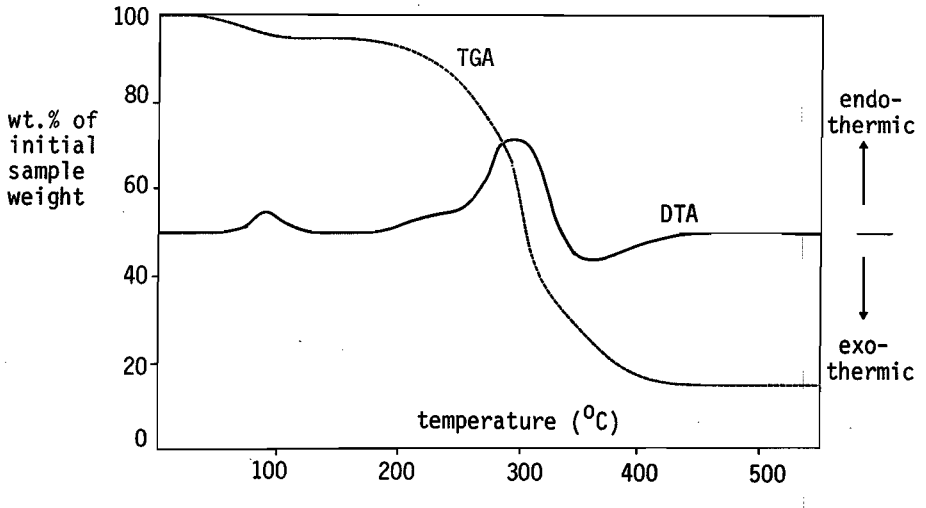

Fig.2.25 Combined DTA/TGA curve for cellulose

rise of the furnace temperature.The sample weight decreased about 5% at about 100°C and the DTA curve shows an endothermic peak: the water that is not chemically bond evaporates from the sample.
A slightly increasing endothermic DTA peak is measured at 280°C. The endothermic effect remains weak up to 300-310°C and then increases strongly. A considerable weight loss is measured together with the remarkably strong endothermic effect. Two endothermic conversions probably occur in this temperature range. Arsenau [2.12] ascribes the weak endothermic effect to the depolymerization of cellulose that produces levoglucosan. The consecutive strong endothermic effect is ascribed by Arsenau to evaporation of levoglucosan. Above 380°C the endothermic effect has disappeared and a weak but broad exothermic DTA peak is measured. The sample weight decreases up to 440°C. The effects in the temperature range above 380°C are ascribed to charring reactions of levoglucosan or dehydrocellulose. Arsenau observed a very weak endothermic effect at about 220°C which he ascribed to dehydration of cellulose. This endothermic effect is not visible in fig. 2.25. The weight loss during the dehydration reaction is very small (1-2%) and it is very difficult to find it by means of a TG curve.

2.5.6.7 Comments

1. Difficulties were encountered in the determination of the reaction kinetic parameters of the depolymerization reaction. The plot in fig. 2.23 was obtained from the data of experiments at 7 different heating rates. Linear regression of the data points of the 4 experiments with the lowest heating rates gives a straight line that is steeper than the straight line that might be fitted to all data points. The activation energy calculated from the straight line is substantially higher than the activation energy calculated when using all data points: E_b = 40.2 instead of 24.6 kcal/mole. It is possible that the temperature measured at maximum weight loss is not the actual temperature of the sample. The actual sample temperature may be lower than the measured temperature because of a thermal lag (see § 2.5.2). The thermal lag will be larger at higher heating rates. Moreover, the temperature distribution in the sample may be inhomogeneous at high heating rates. In that case the temperature should be measured as a function of the place in the sample as well. Akita

and Kase [2.16] have also used the Kissinger method for TG/DTA experiments in vacuum atmosphere.The heating rates that they have applied in their experiments were lower than was possible with the thermobalance that was used in our experiments:0.01-0.05 ^{o}K/sec. The activation energy for the depolymerization of cellulose they have calculated on the basis of these experiments is: E_b = 53.51 kcal/mole. It is noteworthy that Akita and Kase did in fact find an activation energy for the depolymerization of cellulose on the basis of their measurements at very low heating rate (53.51 kcal/mole), that is higher than the activation energy found here. In view of the limitations of the apparatus here it seems probable that the activation energy that Akita and Kase found is the more correct one.

2. The determination of the temperature at which the weight loss is maximal is not very accurate. Determination of T_{max} by means of DTA is much more accurate. The maximum in the DTA peak coincides with the temperature at which the cellulose conversion is maximal. As has been indicated above, it was not possible to carry out differential thermal analysis at the time the experiments were carried out because of defects in the equipment.
3. The activation energy and the frequency factor of the polycondensation of levoglucosan have been determined (§ 2.5.6.5). No values of E_d" and k_d" for the charring reaction of the polycondensation product could be found. Application of the method described in §2.5.5.4 gave no unambiguous value of E_d". It is felt to be likely that this reaction step does not proceed according to one single reaction but that it rather occurs according to a number of competitive and consecutive reactions. It would in that case be very difficult to obtain any information on the reaction kinetics of this step from the TG-curve.

2.6 The application of the models

The models derived in § 2.3.3 will be applied to calculate product distributions and reaction times for the pyrolysis of cellulose using the kinetic data obtained by the thermoanalytical experiments described in § 2.5.6 (see Chapter 7). The product distribution and reaction times will be compared to experimental findings obtained in pyrolysis experiments using shredded thin cardboard as a feedstock (§ 7.4).

Literature

2.1 P.M. Molton, T.F. Demmit, Reaction mechanisms in cellulose pyrolysis, Batelle, Washington (aug. 1977)

2.2 H.C. Elias, Macromolecules II, Wiley & Sons, New York (1977).

2.3 P.S. Maa, The influence of particle sizes and environmental conditions on high temperature pyrolysis of the cellulosic material Ph.D. Thesis, West Virginia University (1971).

2.4 A. Basch, M. Lewin, J. Polymer Science, Polym. Chem. Ed., 11, pp. 3071 (1973).

2.5 A. Pacault, G. Sauret, Compt. Rend. Acad. Scie. 246, pp. 608 (1958).

2.6 B.G. Ranby, J. Polym. Science, 53, pp. 131, (1961).

2.7 S. Patai, Y. Halpern, Isr.J. Chem., 8, pp. 655 (1970).

2.8 A. Broido, A.C. Javier-Son, A.C. Quano, E.M. Barrall, J. Appl. Polym.Sci., 17, pp. 3627 (1973).

2.9 R.C. Smith, H.C. Howard, J. Amer.Chem.Soc., 59, pp 234 (1937).

2.10 F.A. Wodley, J. Appl. Polymer Sci, 15, pp 835 (1971).

2.11 R.F. Schwenker Jr., E. Pascu, Chem. & Eng. Data Ser. 2, no. 1, pp 83 (1957).

2.12 D.F. Arsenau, Can. J. Chem., 49, pp 632 (1971).

2.13 F. Shafizadeh, Industrial pyrolysis of cellulosic materials, Appl. Polym. Symp. 28, John Wiley & Sons, pp. 153, New York, May 19-23 (1975).

2.14 N.M. Bikalis, L. Segal, Cellulose and cellulose derivatives 2nd ed., vol. V, part IV, V, pp. 1015, Wiley & Sons, New York (1971).

2.15 F. Shafizadeh, Y.L. Fu, Carbohydrate Research, 29, pp 113 (1973).

2.16 K. Akita, H. Kase, J. Polymer Science, Polym. Chem., A-1. vol. 5, no.4, pp 834 (1967).

2.17 F.J. Kilzer, A. Broido, Pyrodynamics 2, pp. 151 (1965).

2.18 S.L. Madorsky, V.E. Hart, S. Straus, J. of Research of Nat. Bureau of Standards, vol. 56, no.6, pp. 343 (1956).

2.19 W.K. Tang, W.K. Neill, J. Polymer Sci., part C, no. 6, pp. 65 (1964).

2.20 H.J.P. Venn, J. Textile Inst., 15, T 414 (1924).

2.21 F. Shafizadeh, Advances in carbohydrate chemistry, Pyrolysis and combustion of cellulosic materials, vol. 23, pp. 419, Academic Press (1968).

2.22 A. Bradbury, Y. Sakai, F. Shafizadeh, J. Appl.Polym.Sci., vol. 23, pp. 3271 (1979).

2.23 A. Broido, M. Weinstein, Thermal Analysis, vol. 3,proc. third ICTA Davos, pp. 285 (1971).
2.24 C.H. Bramford, J. Crank, D.H. Malan, Proc. Cambridge Phil. Soc., 42, pp. 166 (1946).
2.25 J.G. Rittmann, Computer study of the pyrolysis of porous solids, Ph.D. Thesis, Oklahoma State, Univ. Stillwater (1970).
2.26 H.C. Kung, F.M. Research Corporation, FMRC Serial no. 19721-6 (1972).
2.27 C.P.M. van Ginneken, W.J.A.H. Schoeber, M. Tels, Recycling Berlin '79, vol. 1, pp. 663, ed.K.J. Thomé-Kozmiensky (1979).
2.28 R.B. Bird, W.E. Stewart, E.N. Lightfoot, Transport Phenomena, John Wiley & Sons Inc., New York (1960).
2.29 C.P.M. van Ginneken, lecture notes (1979).
2.30 A.V. Luikov, Analytical heat diffusion theory, Academic Press, New York (1968).
2.31 L. Lapidus, Digital computation for chemical engineers, McGraw-Hill Book Company, New York (1962).
2.32 P.D. Garn, Thermoanalytical method of investigation, Academic Press, New York, (1965).
2.33 C.J. Keattch, D. Dollimore,An introduction to thermogravimetry, 2nd edition, Heyden & Sons Ltd., London (1975).
2.34 P.D. Bolkunevich, Khim. Drev., 3, pp. 78 (1979).
2.35 E.J. Murphy, J. of Polymer Sci., 58, pp. 649 (1962).
2.36 J.T. Langley, M.J. Drews, R.H. Barker, J. Appl. Polymer. Sci., 25, pp. 243 (1980).
2.37 J.K. Smith et al., Textile Research Journal,40, pp. 211 (1970).
2.38 P.C. Lewellen, W.A. Peters, J.B. Howard, 16th Int. Symp. on Combustion, Massachusetts, Inst. of Techn., pp. 1471 (1976).
2.39 P.K. Chatterjee, C.M. Conrad, Textile Research Journal, 36, no.6, pp 487 (1966).
2.40 P.K. Chatterjee, J. Appl. Polym.Sci., 12,pp. 1859 (1968).
2.41 A.E. Lipska, W.J. Parker, J. Appl. Polym.Sci., 10, pp. 1439 (1966).
2.42 A.J. Stamm, Ind. and Eng.Chem., 48-3, pp. 413 (1956).
2.43 Manual Mettler Thermo-analyser 1/2.
2.44 Computer Centre information, pp. 5.5, Eindhoven University of Technology.

List of symbols

		S.I.units
A	constant eq.(2.70)	
$\bar{A}$	matrix eq. (2.93)	
a	element of matrix $\bar{A}$	
B	constant eq. (2.71)	
$\bar{B}$	matrix eq. (2.93)	
Bi	Biot number	-
b	element of matrix $\bar{A}$	
C	constant eq. (2.72)	
c	element of matrix $\bar{A}$	
Cp, C_p	heat capacity	$J/kg.^oC$
D	constant eq. (2.73)	
E	activation energy	J/mole
e	emissivity	-
f	time level	
f	function	
F_o	Fourrier time	-
h	place step	m
h	heat transfer coefficient	$J/m^2.sec.^oC$
$h, \hat{H}$	enthalpy	J/kg
$\Delta H, \Delta\hat{H}$	heat of reaction	J/kg
j	place level	
k	time step	sec
k, k_p	reaction rate constant	sec^{-1}
k_{io}, k_{po}	frequency factor*)	sec^{-1}
l	slab thickness	m
l	plane of symmetry	m
L	half slab thickness	m
m	mass flux	$kg/m^2.sec$
P	constant eq. (2.74)	
O	truncation error	
Q	constant eq. (2.75)	
q	heat flux	$J/m^2.sec.$
q	heating rate	$^oC/sec$
R	gas constant	$J/mole.^oC$
R	constant eq. (2.84)	

*) Example: k_{ao} = frequency factor of reaction a.

R,r	radius	m
r	reaction rate	$kg/m^3.sec$
S	constant eq.(2.85)	
T	temperature	^oK, ^oC
$\bar{T}$	vector eq. (2.93)	
t	time	sec
Δt	period of time	sec
V	function value	
v	velocity	m/sec
W,w	weight	kg
x	place, distance	m
Δx	distance	m
y	element of vector $\bar{\bar{y}}$	
$\bar{\bar{y}}$	vector eq. (2.95)	

Greek symbols

α	constant eq. (2.68)	
α	heat transfer coefficient	$J/m^2.sec.^oC$
α	fraction decomposed	-
β	constant eq. (2.69)	
β	lumped parameter	sec^{-1}
ε	porosity	-
θ	weight factor	-
λ	thermal conductivity	$J/m.sec.^oC$
μ_n	solution characteristic eq.(2.40)	-
ρ	density	kg/m^3
σ	Stefan-Boltzmann constant	$J/sec.m^2.^oK^4$
$\emptyset$	heat flux	$J/m^2.sec$

Subscripts

a	reaction a
b	reaction b
c	reaction c
c	conduction
c	core
d	reaction d

eff	effective
f	at time f
g	gas
ga	gas a
gb	gas b
gc	gas c
gd	gas d
i	number
j	number
j	at place j
max	maximum
s	solid
s	surface
t	at time t
t	total
x	at place x
0	initial, virgin material
1	reaction, solid, component 1
2	reaction, solid, component 2
3	reaction, solid, component 3
4	solid, component 4
5	component 5
6	component 6
7	component 7
8	component 8
∞	environment

3. THE PYROLYSIS PILOT PLANT

3.1 Introduction

Experimental work on the low temperature pyrolysis of organic waste fractions were carried out in a pilot installation fitted with a spout-fluid bed reactor. Some of the characteristics that make this type of reactor particularly suited for the low temperature pyrolysis process were stated in section 1.6.

The pyrolysis experiments in the pilot plant are meant to demonstrate the suitability of the low temperature pyrolysis process to handle fractions from Dutch domestic waste. The experiments were expected to give us information about the following points:

a. the product distribution as a function of reaction conditions;
b. the environmental impact of the process;
c. properties of the pyrolysis products.

Besides, the experiments will provide insight into the technical limitations of the process and provide data for further technical and economic evaluation. Some data and products will be used to support the fundamental study of the pyrolysis process mentioned in Chapter 2.

General design principles for the pilot plant (or better: for the pyrolysis reactor) were:

1. A pyrolysis reactor was required in which relatively high yields of tar could be obtained. Tar is felt to be a more attractive fuel than either char or low calorific gas. Tar can easily be stored, can be transported in tank cars (eventually after dilution with water) and is easy to burn. The tar may be used as a Diesel oil substitute after dilution with water.

   This led us to investigate the types of reactors that are most suited to reach our aim, that is a reactor in which short residence times for the gaseous pyrolysis products can be obtained and tar yields may be high. Short residence times for waste materials and for gaseous pyrolysis products can easily be obtained in reactors in which the particles move under the influence of the flow of gases, f.i. fluidised beds, spouted beds and entrained beds. The entrained bed reactor was not considered because it requires very extensive pretreatment of the feedstock (§ 1.4 and 1.5). A choice had therefore to be made between fluidised, spouted and spout-fluid beds. The following characteristics

of the spout-fluid bed that will be discussed in more detail in § 3.3.2. led us to select this type of reactor: very good mixing in the solid phase, good heat transfer characteristics, relatively high gas flow rates through the apparatus and the possibility of introducing the feed into the reactor via the spoutpipe.

2. We wished to carry out pure pyrolysis as one of the aims of our investigation was to study the mechanism of pyrolysis and to develop a model of the conversion. We did not want to complicate this model by introducing oxidation reactions. Partial oxidation of the waste material is often used in pyrolysis processes to provide the heat required to bring the feed to reaction temperature,to evaporate the water in it and to compensate for the energy requirements of possible endothermic reactions and for heat losses.
   This led us to opt for electrical heating to meet these heat requirements in the reactor instead of introducing oxygen into the reactor in order to obtain the energy by partial combustion. An additional advantage of electrical heating is that is easy to control.
3. The maximum capacity of the reactor had to be in the order of 10 kg of waste/hour.

This chapter discusses how these general design requirements were met. An impression of the outcome of the design is given in the process scheme that is described in the next paragraph. The design of the apparatuses is described in more detail in succeeding paragraphs.

3.2 Process scheme

Before the pilot plant is discussed in more detail it may be useful to give a general impression of the plant by presenting the process scheme. Fig. 3.1 shows a scheme of the pilot plant used in the pyrolysis experiments. Three sections can be distinguished:

A. Feeding system

The solid feed is moved from a bunker to the spout gas line by means of a screw conveyor. The speed of the screw can be controlled to provide the desired feed rate. The feed material is entrained by the spout gas and is thus moved to the reactor by pneumatic transport.

B. Reactor

The reactor was already discussed in general terms in section 1.6. It is

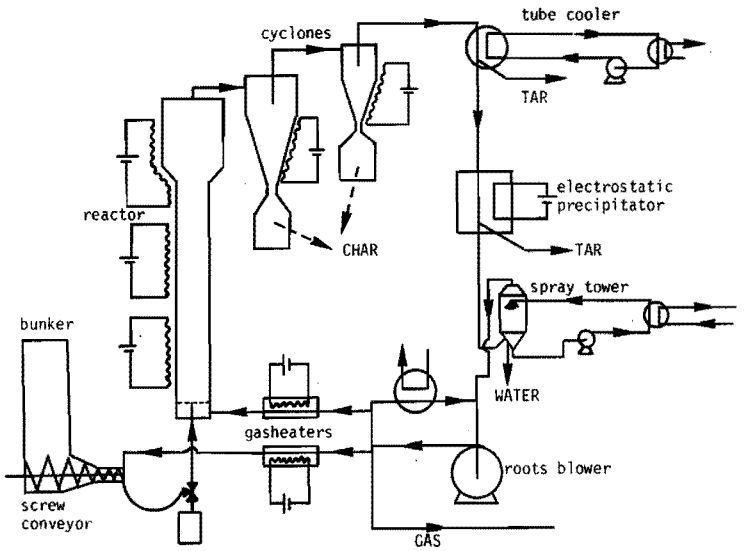

Fig.3.1 Pyrolysis pilot plant

sufficient for the moment to point out that the feed is mixed thoroughly with the sand present in the reactor and that the heat requirements for drying and pyrolysis of the feed in the reactor are met by electrically heating the fluidisation and spout gases and the reactor wall. The pyrolysis products leave the spout-fluid bed reactor through a disengagement space at the top. From this disengagement space most of the entrained sand flows back into the reactor bed.

C. Section in which the pyrolysis products are separated.

The pyrolysis products, inclusive of most of the char, enter a series of separation units. The char and some sand fines are separated in a series of 2 cyclones.These are operated at reaction temperature to prevent condensation of the volatiles. The gas stream that leaves the 2nd cyclone is cooled to about 120^{o}C in order to condense the tar (which is a mixture of organic compounds that condense at that temperature) while retaining most of the water in the gaseous phase. This tar condensation is carried out in a tube cooler. Oil is used as an external coolant. The oil is in its turn cooled externally by means of cooling water. Part of the tar condenses in very small droplets to form a mist. This mist is separated by means of an electrostatic precipitator that consists of a number of vertical tubes. A screw spindle has been fitted

in the axis of each tube and a voltage differential of about 15 kV is maintained between the spindles and the walls of the tubes. The tar droplets are separated at the tube walls. The tar flows down the tubes and is collected at the bottom of the electrostatic precipitator. The gas flow which has been freed of tar leaves the precipitator at temperatures above 100°C. The temperature of the gas is now reduced to about 25°C in a spray tower. Most of the water and light organic compounds separate from the gas. The water phase is collected in the bottom of the spray tower. Part of the water phase is cooled externally and is then introduced into the spraytower to act as a coolant.

The remaining gas flows to a Roots blower which is used as a simple gas circulation pump. Part of the repressurised gas is recycled to the reactor to serve as either spout or fluidisation gas. The gas that is not required for these purposes is discharged after samples have been taken from it.

The unit has been fitted out with several safety and control devices and with measurement apparatuses. These are not shown in fig. 3.1 but will be discussed later on.

3.3 Design of the pilot plant

3.3.1 Starting points of the design

The general design principles were already discussed in § 3.1.
The selection of a spout-fluid bed reactor with a capacity in the order of 10 kg of waste/hour led us to the design of a bed with a diameter of 15 cm and a (static) bed height of 25 cm. These dimensions were chosen on the basis of:

1. The data for a 400 tpd fluid bed pyrolysis installation designed by Burton and Bailie [3.1, 3.2] which were used to calculate the bed volume of the spout-fluid bed.
2. The results of the experiments at room temperature in a spout-fluid bed reactor that were carried out to investigate the mixing characteristics of the bed (§ 3.3.2). The bed height/bed diameter ratio was selected on the basis of these results.

The apparatus proved to be able to spout-fluidise a throughput of about 15 kg/hr of shredded domestic waste or shredded paper. The maximum heat flow that could be supplied by the electrical heating (see § 3.3.2)

limited the throughput that could be applied in pyrolysis experiments to about 10 kg/hr of dried, shredded domestic waste or shredded paper.
A factor that plays an important role in the design of the units for separation of the pyrolysis products is the total gas flow. As for the gas production, it was assumed that out of the maximum feed rate of 15 kg of waste per hour no more than 10 kg of wastes per hour could be converted to pyrolysis gas. This is a high estimate.
The composition of the pyrolysis gas was of course another important factor in the calculations. As the reactor was intended to be operated at widely diverging conditions a gas composition was assumed arbitrarily in order to be able to calculate physical constants of the gas. The assumed composition was:

35 vol.% hydrogen (H_2)
25 vol.% carbon monoxide (CO)
20 vol.% carbon dioxide (CO_2)
20 vol.% methane (CH_4)

This composition was based on data given in [3.1] for the pyrolysis of solid waste in a fluidised bed reactor. For physical properties of the pyrolysis gas see appendix 3.1.

As has been mentioned above, it was decided to meet all heat requirements in the reactor by electrically heating the fluidisation and spout gases and the reactor wall. It should be noted that the maximum temperature of the spout gas was limited by the fact that the spout gas is used to transport the feed into the reactor.

3.3.2 The reactor

The design of the reactor was the first step in the development of a pyrolysis system. From the beginning it was clear that a bed in which the particles move as a result of a gas flowing through the bed had certain advantages. The most important advantages of such a reactor are its excellent heat transfer characteristics that make it possible to have good control of the product distribution and to realize short residence times of waste materials in the reactor and the relatively high gas flow rates in the apparatus which effect short residence times for the gaseous pyrolysis products so tar yields can be high. A disadvantage is the small particle size that is required to handle the waste in such

type of reactor (see also § 1.4). Consequently, the waste materials have to be shredded. Shredding is a very expensive operation. Examples of this type of reactor are the fluidised bed, the spouted bed and the spout-fluid bed.
It should be noted that most (shredded) waste materials cannot be handled by themselves in any of the reactors just mentioned because of poor fluidisation properties. A fluidisation medium is needed to handle such materials. Sand is being used in most cases a fluidisation medium because of its physical and chemical properties (high melting point and chemical inertness). Sand was therefore selected for the present reactor also. A useful characteristic of the sand bed is that it acts as a thermal fly-wheel in case of disturbance in the supply of feed material.
To investigate which bed would offer the best possibilities for pyrolysing shredded domestic waste a number of experiments at room temperature were carried out in a bed of 15 cm diameter that could be operated as a fluidised bed, a spouted bed (with flat bottom) or a spout-fluid bed. Special attention was paid to its mixing and segregation characteristics. The performance of the bed was judged visually and by measuring concentration profiles and residence time variance for model compounds that were fed to the reactor as substitutes for shredded domestic waste. Theoretical work on spouted, fluidised and spout-fluid bed was done to support the experimental findings. The apparatus used to investigate the performance of the three types of beds had similar dimensions as the spout-fluid bed reactor used in the pyrolysis plant.
It is not necessary within the scope of this thesis to present all results of the investigation of the performance of the spout-fluid bed reactor. The discussion will be limited to the experimental findings that led us to select the spout-fluid bed reactor as pyrolysis furnace. In short:

1. In the spouted bed and the fluidised bed segregation of the model components occurred in certain regions of the bed in all circumstances. Segregation could, however, be avoided in the spout-fluid bed by appropriate choices of fluidisation and spout gas rates (visual observations, see also fig. 1.1). Measurement of concentration profiles in the bed confirmed this.
2. The spout-fluid bed can be operated as a packed bed, as a bubbling bed or as a bed with a fluctuating spout depending on fluidisation

and spout gas rates. See fig. 3.2A. The situation with bubbling bed or with a fluctuating spout is the most interesting one for the application of the bed as pyrolysis reactor. In this flow regime the gas near the axis of the reactor rises through the apparatus in large but separate bubbles. The mixing in the solid phase is good because of the turbulent motion in the bed and the waste material has sufficient residence time in the bed to react as no continuous gas spout exists between the spout opening and the top of the bed. If a continuous gas spout between the spout opening and the top of the bed (fig. 3.2B) did exist, the material that is introduced through the spout opening would be blown out of the reactor without having had time to react.

However, a flow regime with a continuous gas spout (stable spout) cannot be realised in the present spout-fluid bed because of the ratio of spout opening to bed diameter. A stable spout can exsist only at values of this ratio beneath a critical value (see § 4.2.2).

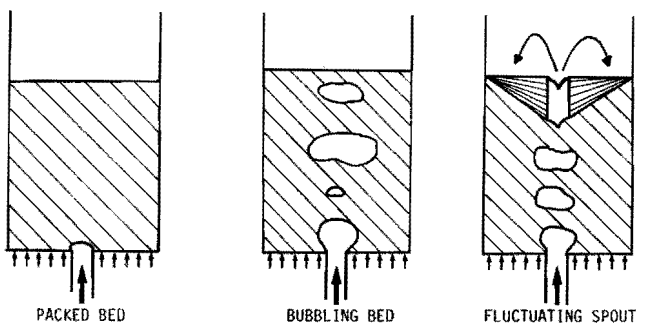

Fig.3.2A Flow regimes of the spout-fluid bed

Fig.3.2B Continuous gas spout (stable spout)

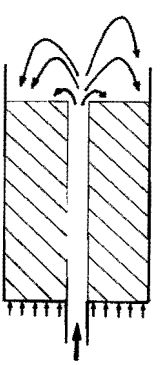

3. The result of the experiments in which the variance of the residence time was measured showed that the spout-fluid bed can be regarded as an ideal mixer in the solid phase when the fluidisation gas rate exceeds the minimum fluidisation rate. The spout gas rate should be sufficiently high in that case (see Chapter 4 for numerical values of gas flow rates).
4. The bed could be loaded with waste material up to about 7% of its weight without problems; higher loadings led to poor fluidisation and mixing.

It was decided on basis of the above results to use a spout-fluid bed with sand as fluidisation medium in the pyrolysis plant. Fig. 3.3 presents some details of the reactor that was constructed from heat resisting steel. The dimensions are summarized in table 3.1.

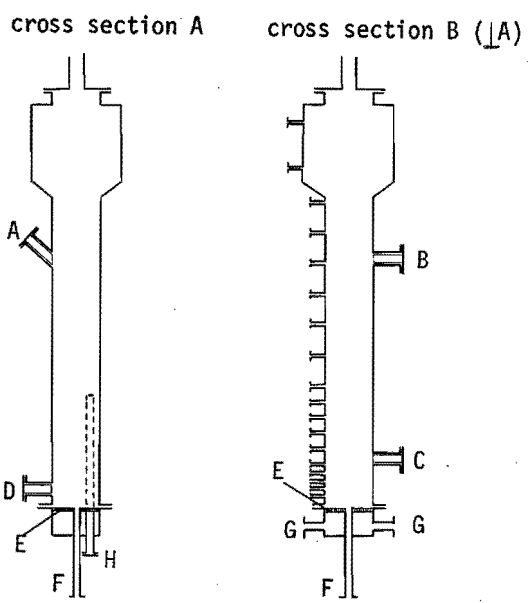

Fig.3.3 Diagram of spout-fluid bed reactor. For dimensions see table 3.1.

Some comments to fig. 3.3 are:
Some openings (Ø 40 mm) have been made in the reactor wall for possible alternative introduction of feedstock into the reactor (which is now being done through the spout gas opening) or to bring in the bed material

or additives to the bed. Of these openings (A,B,C and D) only A is being used to introduce the sand into the reactor before the start of a pyrolysis experiment. Additional openings (Ø 1/8") in the reactor wall serve to insert thermocouples or for pressure drop measurement. Most of them are located in the section just above the sieve plate as this is the most interesting part of the reactor. The sand bed (static height about 25 cm) is located here during the experiments so that the solid phase reactions will take place in this part of the reactor. There are 4 openings or tubes in the section of the reactor beneath the sieve plate E. These are the spout tube F and two openings through which the fluidisation gas is supplied to the reactor (G: Ø 25 mm). Pipe H (Ø 33 mm) is not being employed in the present situation but it may eventually used to accomodate an overflow (dotted lines) to collect sand and char from the bed. In that case the sand would be transported to a regenerator, another fluidised bed in which it would be heated by combustion of (part of) the char. The hot sand could then be recirculated to the pyrolysis reactor (via A), thus providing a large part of the heat input required in the reactor. It is still possible to extend the pilot plant with a sand regenerator if it should be desired to do so.
The sieve plate E is a nickel sieve plate prepared electrolytically that is resistant to the load exercised by the bed even at temperatures of 1000^{o}C. The pressure drop over the plate as a function of gas velocity is shown in fig. 3.4.

Table 3.1 Dimensions of spout-fluid bed reactor

Inner diameter reaction zone	150 mm
Height reactor	1,000 mm
Inner diameter disengagement space	280 mm
Height disengagement space	300 mm
Inner diameter spout opening	18 mm

The electrical heating of the reactor wall is an important subject that still has to be discussed in relation to the reactor. This heating together with the electrical heating of the fluidisation and, to lesser extent, the spout gases (see § 3.4.3) is needed to meet the heat input requirements in the reactor and to compensate for heat losses.

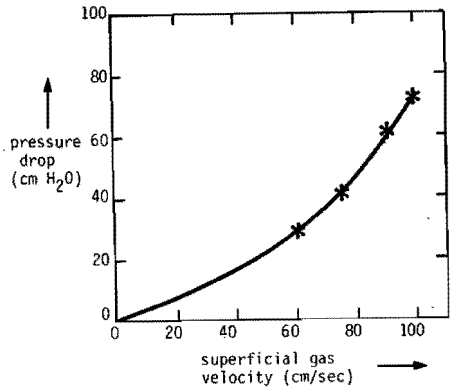

Fig.3.4 Pressure drop over sieve plate

Assuming that the heat content of the fluidisation gas is large enough for both fluidisation and spout gases to reach the reaction temperature, the electrical heating of the reactor wall will be used to heat the feedstock to reaction temperature, to heat the water in it to its boiling point, to evaporate the water, to heat the water vapor and to compensate for the energy requirement of possible endothermic reactions and for heat losses. In the calculations unfavourable process conditions were chosen to get an impression of what the maximum heat requirement in the reactor could be. These conditions were: domestic waste with a humidity of 33 1/3 wt.%, a maximum superficial gas velocity in the reactor of 1 m/sec, a reaction temperature of 600^{o}C and a maximum solid feed rate (15 kg of dry waste/hour). The temperature of the incoming waste was assumed to be 25^{o}C and no heat of reaction was taken into account. The calculations led to a heat requirement of 14 kW (estimated heat loss: 1 kW).
The maximum heat flow rate Q that can be transferred to the bed through the reactor wall is given by $Q = \alpha.\Delta T.A$. Here α is the heat transfer coefficient, ΔT the temperature difference between wall and bed and A the area of heat transfer. A and ΔT could easily be calculated for a bed height of 30 cm and the allowed maximum temperature for the heat resisting steel of 1000^{o}C. A relationship to calculate the heat transfer coefficient α was used that had been derived from a model based on Higbie's penetration theory [3.4]. The heat transfer coefficient calculated for the above situation in the pyrolysis reactor was: α = 283 J/m^2.sec.^{o}C (see appendix 3.2). The heat flux that is transferred to the reactor at operating conditions at a bed temperature of 600^{o}C is

Q = 16 kW. This would be enough to meet the calculated heat requirement (14 kW).

The electrical reactor heating consists of coils of Kanthal resistance wire [3.5]. The three sections of the reactor (bottom, middle and top section) are heated independently. The heating of the bottom section of the reactor consists of 2 heating coils arranged around the reactor as shown in fig. 3.5 (A). The coils are made of spiralised Kanthal DSD (molybdenumdisilicide)resistance wire with a diameter of 2 mm. The inner diameter of the spiral is 4 mm. The length of each wire is about 20 m. This results in a resistance of about 10 Ω. The coils were fixed to the reactor wall as follows: A layer of refractory cement was put on the wall. The spiralised coils were then wound on this layer. Finally, the space inside and between the spirals was filled with the cement (fig. 3.5, B).

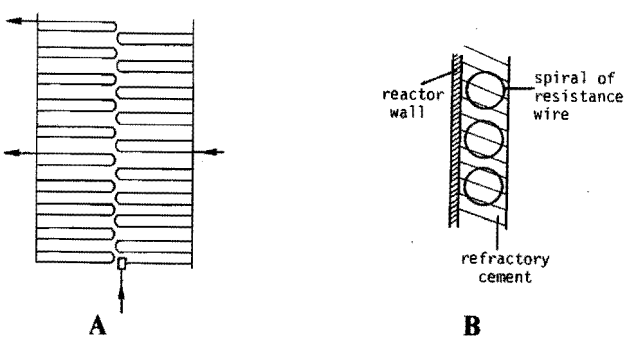

Fig.3.5 The heating coils around the bottom section of the reactor

The heating of the middle and top section of the reactor each consists of one coil. Both coils were made from non-spiralised Kanthal-A resistance wire (Ø = 1.3 mm, 1.1 Ω/m) which was wound around the reactor. The resistance wires are electrically insulated from the reactor wall by ceramic beads(fig. 3.6). The resistances of the middle section and the top section heating coil are 13 and 12 Ω respectively.

The installed maximum power of the reactor wall heatings is, at 220 V:

1. Bottom section: 9.5 kW.
2. Middle section: 3.7 kW.
3. Top section: 4.3 kW.

It should be noted that the heat transfer from coil to reactor wall is

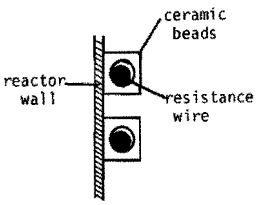

Fig.3.6 How the coils are placed at the middle and top section of the reactor

far better in case of the coils at the bottom section. The heat transfer from wire to beads and from beads to reactor wall in the two other sections is low because of poor contact.
The total maximum power of the reactor wall heatings (17.5 kW) is larger than the maximum heat flow to the reactor at operating conditions that was found from the above calculations (16 kW). The amount of heat that could be transferred to the waste material in practice was, however, limited because of the following reasons:

1. Most of the heat is required in the bed where the drying of the feed and the solid phase reactions take place. The maximum power of the heating coils at the bottom section of the reactor where the bed is located is, however, only 9.5 kW.
2. The heat losses through supportings of the reactor and as a result of imperfect insulation of the reactor have been underestimated.
3. The heat transfer from the coils at the middle and top sections of the reactor to reactor wall is poor.

The reactor was thermally insulated by means of a Fiberfrax Low Conductivity insulation blanket (appendix 3.3).
All data that are used to calculate the reactor and its accessoires and that have not been given so far are presented in appendix 3.4.

3.3.3 The feeding system

The feeding system was essentially simple: a bunker from which the feedstock for the pyrolysis reactor is moved to the pneumatic transport line (the spout pipe) by means of a screw conveyor. This screw conveyor, however, had to be of special design due to the poor transport properties of shredded domestic waste. A gastight bunker entrance was required because a risk of explosion would have existed if the pyrolysis gases

(which contain H_2) could have come into contact with the air.
The general operation of screw conveyors and the flow properties of shredded domestic waste will first be briefly discussed. The final design of a suitable screw conveyor will then be described.

3.3.3.1 The screw conveyor; general information

A screw conveyor consists in essence of a spiral screw rotating in a housing. The housing has a hopper on top of it to feed the screw with the material to be transported (fig. 3.7).
The behavior of a material in a screw is determined by the properties of the material and by those of the screw and housing. These properties can be divided into three groups [3.7]:

1. Particle flow parameters.
2. Properties of the apparatus as far as it is in contact with the particles (f.i. geometry,dimensions, surface roughness).
3. Properties of apparatus and particles together (f.i. coefficient of static and sliding friction).

If all of these properties and the relationships between them are known it should be possible to predict how a material is transported by the screw conveyor. However, some of the properties are hard to determine and not all of them are equally important for the behavior of the material in the screw.

Fig.3.7 Screw conveyor

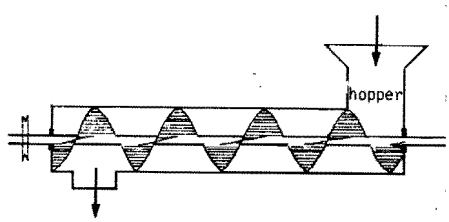

3.3.3.2 Properties of shredded domestic waste

Shredded domestic waste is a mixture of particles with different shape, size and density. The material is very porous when it has not been compressed. It is easy to compress, as a result of the geometries of some particles in it such as fibres, pellets, foils etc. It is therefore not possible to compare domestic waste to granular materials of which the behavior in a screw conveyor is well known and has been described in the literature.

An important property that determines the behavior of a material in a screw is its bulk density. The bulk density of non-compressed domestic waste is very small on account of the high porosity of the material. A second important property is the cohesion. The cohesion of domestic waste is large as a result of the variety in geometries that cause a cohesion by friction and as a result of strong capillar forces that result from the high moisture content of domestic waste. In addition a cohesion occurs in domestic waste which is being dried in the open, that is due to the presence of starch like components which act as glues. Another important property (which is related to the cohesion) is the flow behavior of the material and, indeed, shredded domestic waste must be regarded as a badly flowing (almost as a non-flowing) material.

3.3.3.3 The design of a screw conveyor for transporting shredded waste materials

Two factors more or less determine the final design of the housing of the screw:

a. the spout gas flow rate

b. the properties of the domestic waste.

The spout gas throughput should be kept low for the following reason: It is necessary to heat the fluidisation and spout gases as the electrical heating of the reactor wall is insufficient to meet the energy requirements in the reactor (see § 3.3.2). It is best to use the fluidisation gas for the heating as much as possible since heating of the spout gas may lead to undesirable pyrolysis of waste in the spout pipe or even in the screw. Note that the total gas flow is limited, too (see § 3.3.2). On the other hand, the velocity of the spout gas must be high enough to make pneumatic transport of the shredded waste through the spout pipe possible. To meet both requirements (low throughput and high velocity in the spout pipe) the spout pipe diameter should be small. Consequently, the diameter of the output opening of the screw must be small, too.

The properties of the domestic waste that are important in this context are its very great cohesion and small bulk density which may cause arching if the hopper is too narrow. The diameter of the hopper must therefore be relatively large to prevent arching and consequently the feed opening of the housing of the screw must be large, too.

A large feed opening and small output opening imply that a reduction of the diameter of the housing is necessary. The final design of the screw conveyor shows such a reduction (fig. 3.8).
In sections II and III a closed screw was used with a diameter almost equal to the inner diameter of section III of the housing. Section I is fitted with an open screw with a diameter almost equal to the inner diameter of the housing. If a closed screw had been used in section I, too much material would be transported from section I into section II and III which would have caused blockages. Reduction of the pitch in section I and increasing the pitch in sections II and III which would reduce the flow in I and increase the flow in sections II and III is no solution. The pitch in section I would become too small for the shredded material to sink in the groove of the screw. The pitch in II and III would become too large so that the material would tend to rotate with the screw instead of slipping along the screw blade. No material would then be transported.
To prevent rotation of the material in section III a counter screw has been fitted in this section. It is a spiral strip fitted to the inside of the housing which has been spiralised opposite to the direction of the screw blade. The counter screw forces the material to move forwards when it tends to rotate along with the screw.

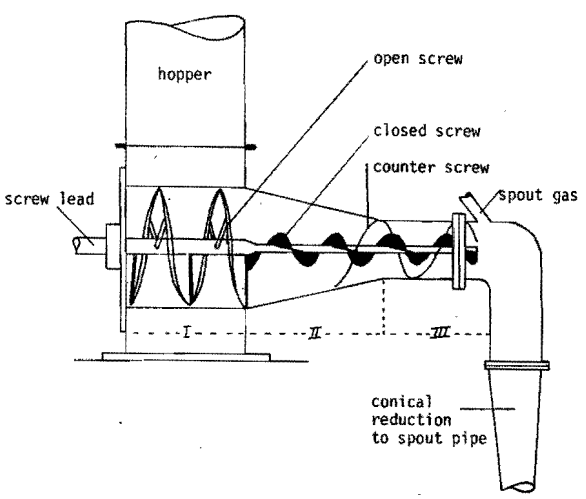

Fig.3.8 The screw conveyor

The screw is being driven by an electromotor with speed control. The solid particles flow caused by the screw conveyor has been measured for paper scrap and shredded domestic waste. The capacity of the screw conveyor was found to be a linear function of the rotational speed. The relative error was about 3 to 5% depending on material and capacity. The spout gas which transports the material to the reactor is introduced through a narrow pipe just above the output opening of the screw conveyor (fig. 3.8). The difference in diameters between this pipe and the throughput opening of the screw causes turbulences in the gas flow at the output opening of the screw conveyor which promotes smooth transport of the solid feedstock.

3.3.3.4 The bunker

The design of the bunker was very simple. A conical connecting piece was placed on top of the hopper (height 40 cm, Ø 12 cm). It acts as a transition to a glass bunker assembled from some pieces of Quick Fit pipe (Ø 5"). The bunker was fitted with a gastight system for refilling as its capacity was not sufficient for prolonged pyrolysis experiments. This system is a kind of sluice. It consists of a hinged cover and a flexible connecting piece that are alternatively opened and closed when the bunker is being refilled during an experiment (fig. 3.9). Nitrogen may be injected through a valve (not shown in fig. 3.9) to flush the bunker.

Fig.3.9 System for refilling

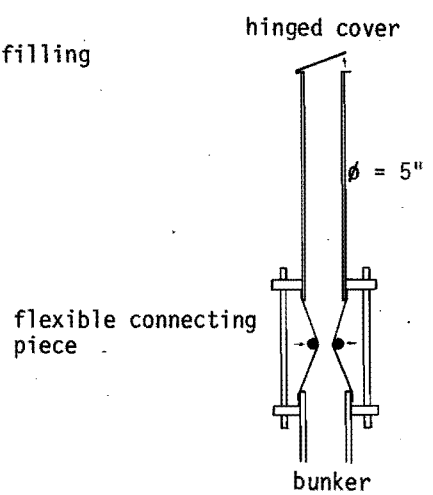

3.3.4 The separation units

3.3.4.1 Separation of solid particles

Char and fines of the sand are carried along in the gas stream leaving the reactor. A simple way to separate these solid particles from the hot gases is to make use of a cyclone.
Two cyclones were available in our laboratory that might be suitable for our purposes. It was therefore decided to carry out some calculations to see whether one of these would indeed be suitable rather than to design a new cyclone. The method proposed by Muschelknautz [3.8] was used to calculate the collection efficiency curve for both cyclones for both sand and char particles for the case of minimum gas flow rate through the apparatus. The collection efficiency curve is defined as the ratio of the weight of solid matter of a given particle diameter collected by the cyclone to the weight of solid matter of that diameter that had entered the cyclone. The shape of the collection efficiency curve is a function of the geometry of the cyclone.
The following data were used in the calculations:

Dimensions of the cyclones	: see fig. 3.10
Gas flow	: $2.65*10^{-3}$ m^3/sec (see appendix 3.5)
Viscosity of the gas	: $3.75*10^{-5}$ N.sec/m^2 (appendix 3.1, 800°C)
Density of sand particles	: 2600 kg/m^3[3.6]
Density of char	: 400 kg/m^3
Minimum diameter of char particles	: 30 μm
Minimum diameter of sand particles	: 80 μm

(It was found later on that particles < 30 μm were also present in the char: up to 3 wt.% of the char collected from the cyclones had a size below 30 μm. The reason might be, however, that this was the result of pulverisation of char particles in the cyclones themselves).

The calculations led to the conclusions that the sand fines (minimum diameter 80 μm) will be fully separated in both cyclones. The collection of the char particles (minimum diameter 30 μm) is unsatisfactory in either cyclone (see figs.3.11 and 3.12). It was therefore decided to calculate the efficiency curve for both cyclones in series so that the gas flow passes through cyclone 1 prior to entering cyclone 2. The

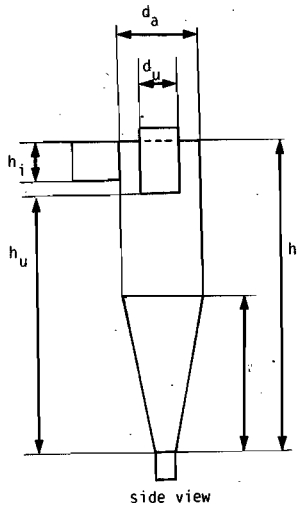

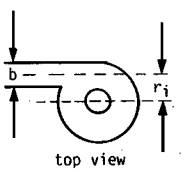

dimensions in mm:

	cyclone 1	cyclone 2
h	785	400
h_i	90	60
h_u	685	320
ℓ	360	240
d_a	180	120
d_u	90	60
b	45	30

Fig.3.10 Dimensions of the cyclones

Fig.3.11 Collection efficiency of cyclone 1

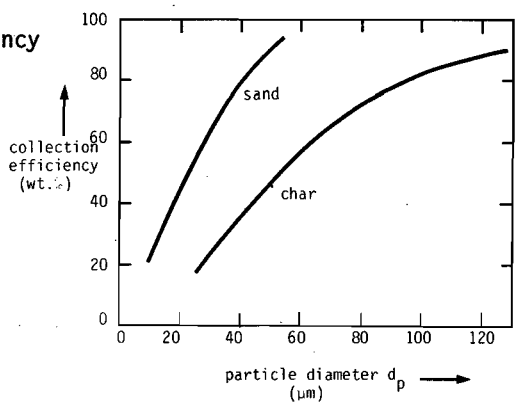

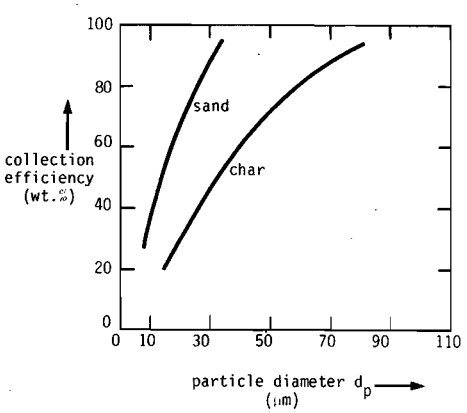

Fig.3.12 Collection efficiency of cyclone 2

collection efficiency is then given by:

$$\phi_{series} = \phi_1 + (100-\phi_1).\phi_2$$

where: ϕ_{series} = collection efficiency for both cyclones in series
ϕ_1 = collection efficiency cyclone 1 (fig. 3.11)
ϕ_2 = collection efficiency cyclone 2 (fig. 3.12)

The resulting collection efficiency curve for both cyclones in series is given in fig. 3.13. It was concluded from this curve that the collection of char particles would be satisfactory when the cyclones are used in series.

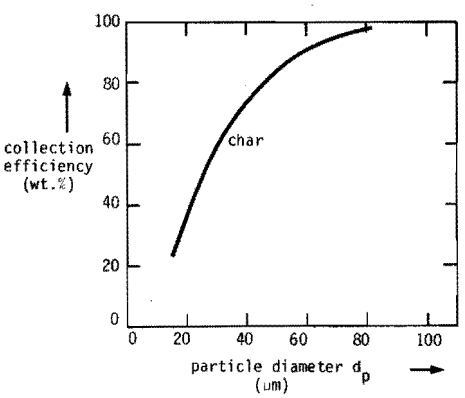

Fig.3.13 Collection efficiency curve for char in case of both cyclones in series

The pressure drop over the two cyclones was calculated from the relationship:

$$\Delta P = 4.02.\rho_g.v_i^2 \qquad [3.9]$$

where ΔP = pressure drop over the cyclone (N/m^2)
ρ_g = density of the gas (kg/m^3)
v_i = gas velocity at the entry of the cyclones (m/sec)

It is obvious that the pressure drop will be at a maximum for maximum gas flow rate. The pressure drop over both cyclones in series was therefore calculated for maximum gas flow rate. The following data were used in the calculations:

maximum glas flow : $29.8*10^{-3}$ m^3/sec (see appendix 3.5)
density of the gas : 0.23 kg/m^3 (appendix 3.1, 800°C, 1 atm).

Results:

	v_i (m/sec)	ΔP (N/m^2)
cyclone 1	7.4	51
cyclone 2	16.6	255

The maximum pressure drop over both cyclones (in the order of a few cm H_2O) was felt to be sufficiently low and it was therefore decided to use both cyclones in series in the pyrolysis pilot plant.

The cyclones are heated and insulated to prevent cooling of the gases and possible condensation of tar in the cyclones. Kanthal-A resistance wire is used (appendix 3.5). Fiberfrax Low Conductivity blanket has been applied for insulation.

3.3.4.2 Condensation and collection of the tar

The collection of the tar from the gas stream that leaves the cyclones was designed such that the condensation would occur in two steps. This did in fact happen. The gas stream is first cooled down to about 150°C in a tube cooler.Tarry compounds will condense from the gas as a result. Only part of the tar will be deposed on the walls of the cooler. The rest of the tar condenses to form a mist of very fine droplets. The gas stream is passed through an electrostatic precipitator to separate the tar mist from the gas. Most of the tar is collected during this second step. Both steps are discussed below.

A. Cooling of the gas in a tube cooler

Starting points for the design were:

1. It was decided to calculate the tube cooler as a gas cooler and not as a condensor as the tar content of the gas stream will be small. Relatively little heat is released by the condensation of relatively small amounts of tar compared to the large quantity of heat that has to be removed from the gas stream when this large gas flow is cooled to obtain a temperature drop of several hundreds of degrees Celsius.
2. The gas stream is made to flow inside the pipes to facilitate cleaning of the cooler.
3. It was decided to use a cooling oil as coolant instead of water so

that the temperature of the gas could be kept above 100°C. This is necessary to prevent the water present in the gas from condensing together with the tar.

4. Excess cooling surface was added to compensate for the heat effects of tar condensing in the cooler. These heat effects are:
   a. Extra release of heat of condensation. Assuming a maximum tar yield of 40 wt.% of the dry feed this effect can be 500 J/sec at most. In the worst case this accounts for about 15% only of the total amount of heat that has to be removed.
   b. Additional resistance to heat transport that results from the formation of a tar layer on the inside of the pipes.

The following differential equation describes the cooling process of gas flowing through a pipe:

$$-\frac{dT}{dx} = \frac{\alpha.\pi.d}{G.\rho.C_p} . (T-T_w)$$

where: T = gas temperature (°C)
T_w = wall temperature (°C)
x = length co-ordinate of pipe (m)
d = inner diameter of pipe (m)
α = heat transfer coefficient pipewall-gas ($J/m^2.sec^oC$)
G = gas flow through pipe (m^3/sec)
ρ = gas density (kg/m^3)
C_p = heat capacity of the gas ($J/kg.^oC$)

$\frac{\alpha.\pi.d}{G.\rho.C_p}$ is assumed to be constant. By introducing $G_n = n.G$ where:

n = number of parallel pipes
G_n = total gas flow through apparatus consisting of n parallel pipes,

this differential equation can be reduced to:

$$n.L = \frac{G_n.\rho.C_p}{\alpha.\pi.d} . \ln \{\frac{T_i-T_w}{T_u-T_w}\}$$

where L = length of the pipes (m)
T_i = gas temperature at entry of pipes (°C)
T_u = gas temperature at outlet of pipes (°C)

This relation was applied to design the tube cooler. The following aspects were taken into account:

a. The maximum gas flow through the cooler.
b. The temperature of the gas stream entering the cooler.
c. The need to ensure good operation of the cooler under all possible conditions (for this reason the cooler was designed for laminar flow of the gas).
d. The maximum length of the pipes that allows easy handling.
e. The minimum diameter of the pipes required to prevent obstruction by condensing tar.
f. The physical properties of the available coolant.
g. Addition of considerable excess cooling surface to compensate for the heat effects of tar condensing on the pipe wall (extra heat, extra resistance to heat transport).

A tube cooler that consists of 24 parallel pipes was designed and constructed on the basis of the calculations discussed in appendix 3.6. The dimensions of the pipes are length 2m, inner and outer diameter 15 and 18 mm respectively. The 24 pipes have been divided into two groups of 12 pipes. Each group is contained in a separate shell (108*100 mm). Baffle plates were fitted inside the shells between the pipes (see fig. 3.14).

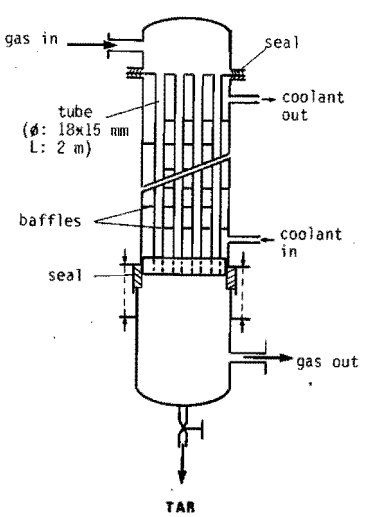

Fig.3.14 The tube cooler

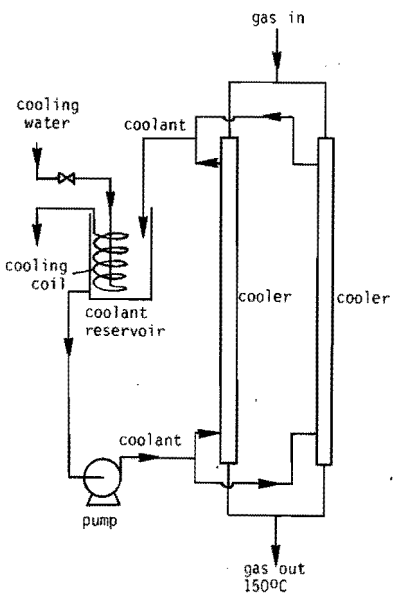

Fig.3.15 Tube cooler section

The coolant is pumped into a closed circuit from a reservoir. The coolant is split in two streams upstream from the condensor. The two streams flow through the shells in parallel and then come together again. The joint streams flow back into the reservoir where a water cooled cooling coil has been installed to remove the heat absorbed by the coolant in the tube cooler (fig. 3.15).

B. Collection of the tar.

Some tar is collected from the tube cooler (fig. 3.14). The remainder must be removed from the gas stream by some kind of filter or scrubber. On the basis of the experiences of several investigators in the field of waste pyrolysis that have been published at the time it was decided to use an electrostatic precipitator for removing the tar mist from the gas stream.

An electrostatic precipitator consists essentially of two electrodes that are placed in a gas stream. A sufficiently high voltage difference to achieve an electrical corona discharge is applied to the electrodes. The gas stream is partly ionised by this corona discharge. Some of the gas ions attach themselves to the particles to be collected. The particles thus acquire an electrical charge. They will be attracted by the collection electrode and they will be precipitated on it. Three important facets can be distinguished in the process of electrostatic precipitation:

1. Ionisation of the gas and the particles to be collected.
2. A sufficiently strong electrostatic field and a residence time of the gas in this field that is long enough for the particles to move to the collection electrode.
3. Removal of the collected particles and prevention of redispersal.

Ad 1. Ionisation

The gas is partly ionised when its is passed through a corona discharge. A corona discharge may occur in case of an extremely inhomogeneous electric field. This causes a partial break down of the insulating characteristics of the gas. The result is an ion current between the electrodes that sprays the particles with ions. The particles acquire a charge by this process. An undesiderable, complete breakdown of the insulating characteristics in some direction is called sparking. The voltage at which this will happen is known as the sparking potential. The sparking potential depends on the composition of the gas(f.i.on its moisture content),

on temperature and on the distance between the electrodes. Decreasing the moisture content and increasing the temperature lead to a decrease of the sparking potential.

Ad 2. Electrostatic field and residende time

The stationary velocity of a particle in an electric field can be found from a forces balance. The force of attraction that the electric field exerts on the charged particle is balanced by the friction forces on the particle. The below relation may be derived assuming laminar flow in the precipitator so that the friction forces obey Stokes'law:

$$N.\varepsilon.E = k_m.3\pi.\mu.d_p.u$$

where N = number of elemental charges
ε = elemental charge (C)
E = strength of electric field (V/m)
k_m = Stokes-Cunningham correction factor
μ = gas viscosity ($N.sec/m^2$)
d_p = particle diameter (m)
u = stationary migration velocity of particle (m/sec)

Rewriting gives:

$$u = \frac{N.\varepsilon.E}{k_m.3\pi.\mu.d_p}$$

The migration velocity is minimal for particles having a diameter of 1 μm (fig. 3.16, [3.9]). The migration velocity determines the residence time required for the particles to reach the collection electrode. In designing the electrostatic precipitator the calculations were therefore carried out for tar droplets with a diameter of 1 μm.

Ad 3. Removal of collected particles.

The removal of the collected tar is less difficult than the removal of dust particles: at the operation temperature (150°C in the present design) the tar is a liquid and can easily be drawn off.

The starting points for the design of the electrostatic precipitator were:

1. The electrostatic precipitator will consist of a number of parallel pipes each fitted with a wire in the centre.

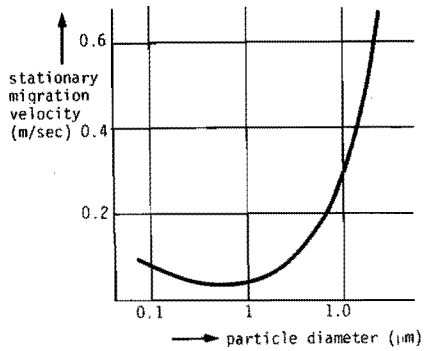

Fig.3.16 Stationary migration velocity u as a function of particle diameter. Air (20°C). Electrostatic potential gradient 3000 V/m [3.9]

2. The gas flows through the precipitator from the bottom upwards to prevent redispersed tar droplets from being entrained by the gas and being moved out of the apparatus. The collected tar is received in an electrically heated cone at the bottom of the precipitator where it can be drawn off.
3. In designing the electrostatic precipitator the calculations are carried out for tar droplets that have a diameter of 1 μm and for the maximum gas flow rate to be expected in the apparatus.
4. The operating temperature of the electrostatic precipitator in the design is fixed at 150°C. The tar is a liquid at that temperature so that it can easily be drawn off while the water present in the gas stream will not condense in the precipitator.
5. The electrostatic precipitator is designed for laminar gasflow in the apparatus.

The criterion for laminar flow is: Reynolds number < 2100. The gas flow in the pipes might, however, not be laminar even if the above criterion is met.Turbulences may occur due to all kinds of disturbances such as f.i. the presence of the central wire in the pipes, the deposition of tar on the pipe walls, entry effects of the pipe etc. Two kinds of flow regimes were therefore considered in the design of the electrostatic precipitator:

1. laminar flow of the gas in the pipes
2. fully developed turbulent gas flow even at Reynolds numbers below 2100.

1. Laminar flow through the pipes (detailed calculations: appendix 3.7)

The following relationships were used in the design calculations:

- Criterion for laminar flow:

$$Re = \frac{4.G_n.\rho}{n.\pi.d.\mu} < 2100 \qquad (3.1)$$

where G_n = gas flow rate (m^3/sec)
ρ = gas density (kg/m^3)
n = number of pipes (-)
d = pipe diameter (m)
μ = gas viscosity ($N.sec/m^2$)

- The stationary migration velocity:

$$u = \frac{N.\varepsilon.E}{k_m.3\pi.\mu.d_p} \qquad (3.2)$$

(The derivation of eq.(3.2) and the meaning of the symbols have been given at the beginning of this paragraph).

- The strength of electric field [3.9]:

$$E = \frac{V}{r.\ln\,(R_u/R_i)} \qquad (3.3)$$

where: E = strength of the electric field (V/m)
r = distance to centre of pipe (m)
R_u = internal radius of pipe (m)
R_i = external radius of wire (m)
V = voltage difference between pipe and wire (V)

- The number of elemental charges

$$N = 3.4*10^{5}.d_p.T \qquad (3.4)$$

(for $d_p \leq 1$ mm [3.9])

where: d_p = particle diameter (m)
T = absolute temperature (^oK)

- Stokes-Cunningham correction factor

$$k_m = 1 \text{ (for } d_p = 1 \text{ } \mu m) \qquad (3.5)$$

Combination of eqs. (3.2) through (3.5) and substitution of numeric values gives:

$$u = 1.07*10^{-7} . \frac{V}{r.\ln(R_u/R_i)} \text{ (m/sec)} \qquad (3.6)$$

The average migration velocity u_{av} for a particle between $r=R_i$ and $r=R_u$ is given by:

$$u_{av} = \frac{2\pi \int_{R_1}^{R_u} u.r.dr}{2\pi \int_{R_i}^{R_u} r.dr} \qquad (3.7)$$

Combination of eqs. (3.7) and (3.8) and rewriting yields:

$$u_{av} = 2.14*10^{-7} . \frac{V}{\ln(R_u/R_i)} . \frac{R_u-R_i}{R_u^2-R_i^2} \qquad (3.8)$$

- The time required for the particles to move from $r=R_i$ to $r=R_u$ is:

$$\Delta t = \frac{R_u-R_i}{u_{av}} = 4.67*10^6 . \frac{\ln(R_u/R_i)}{V} . (R_u^2-R_i^2) \qquad (3.9)$$

With $R_u/R_i = 3$ the equation may be rewritten to give:

$$\Delta t = 1.28*10^6 . \frac{d^2}{V} \text{ (sec)} \qquad (3.10)$$

- The superficial gas velocity in the pipes at maximum gas flow rate through the electrostatic precipitator is:

$$v_{sup,max} = \frac{G_n}{n.\frac{1}{4}\pi.d^2} \text{ (m/sec)} \qquad (3.11)$$

- The length L of the pipes in the electrostatic precipitator may then be calculated from:

$$L = \Delta t.v_{sup,max} \qquad (3.12)$$

- The sparking potential V as a function of d for a wire-in-tube precipitator is read from the graph shown in appendix 3.7 [3.9].

Table 3.2 summarizes the results of the calculations for different pipe diameters (d).

Table 3.2 Calculation of electrostatic precipitator for laminar flow.

d(m)	n(-) eq.(3.1)	V (kV)	Δt(sec) eq.(3.10)	$v_{sup,max}$ (m/sec) eq. (3.11)	L(m) eq.(3.12)
0.2	2	35	1.46	0.29	0.42
0.1	4	25	0.51	0.57	0.29
0.05	7	15	0.21	1.31	0.28
0.03	11	10	0.12	2.31	0.27
0.02	16	6	0.09	3.58	0.31

The following set of values was selected on the basis of practical considerations: d= 50 mm, n=7 pipes.

2. The influence of turbulences (detailed calculations: appendix 3.7)
To study the effect of turbulences it was decided to calculate the precipitator also while assuming that the particle concentration is homogeneous over the cross area of the pipes as a result of turbulent mixing. Postulating that particles that reach the pipe wall in period of time dt were at the beginning of that period at a distance dz from the wall (see fig. 3.17), the stationary migration velocity is given by:

$$u = \frac{dz}{dt} \qquad (3.13)$$

The displacement in the x-direction in period dt is then given by:

$$dx = v_{sup}.dt \qquad (3.14)$$

Fig.3.17 Piece of pipe

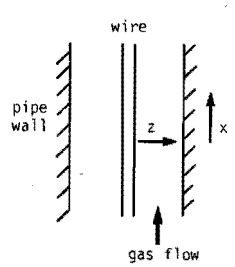

with v_{sup} = the average superficial gas velocity in the pipe (averaged over time). The decrease of particle concentration $\bar{c}$ with increasing length of co-ordinate x may be given by:

$$-\frac{d\bar{c}}{\bar{c}} = \frac{2\pi.R_u.dz}{\pi.(R_u^2-R_i^2)} \qquad (3.15)$$

Combination of eqs. (3.13), (3.14) and (3.15) yields:

$$-\frac{d\bar{c}}{\bar{c}} = \frac{2\ R_u}{R_u^2-R_i^2} \cdot \frac{u}{v_{sup}} .dx \qquad (3.16)$$

Substitution of eq. (3.6) and integration from x=0 to x=L leads to:

$$\frac{\bar{c}_u}{\bar{c}_i} = \exp.\{ - 2.14*10^{-7} \cdot \frac{V.L.}{v_{sup}.(R_u^2-R_i^2).\ln(R_u/R_i)} \} \qquad (3.17)$$

where: $\bar{c}_u$ = particle concentration at outlet of pipe (x=L)
$\bar{c}_i$ = particle concentration at entry of pipe (x=0)

The collection efficiency is defined as:

$$\eta = 1 - \frac{\bar{c}_u}{\bar{c}_i} \qquad (3.18)$$

For the case when d=50 mm and n=7 pipes (see 1.laminar flow) and η=99%. the length of the pipe (L) was calculated to be 1.30 m.
The dimensions of the apparatus were chosen on the basis of the above calculations for the electrostatic precipitator as summarized below:

number of pipes	: 7
length of pipes	: 1.30 m
inner diameter pipes	: 50 mm
diameter of central wire	: 15 mm

Fig. 3.18 presents a schematic diagram of the electrostatic precipitator. A Hippotronix R50B (maximum 60 kV and 5 mA) high voltage power supply unit was used.

The electrostatic precipitator was found to be rather inefficient in the pyrolysis experiments although it had been designed to have a collection efficiency of at least 99% for laminar flow rates while turbu-

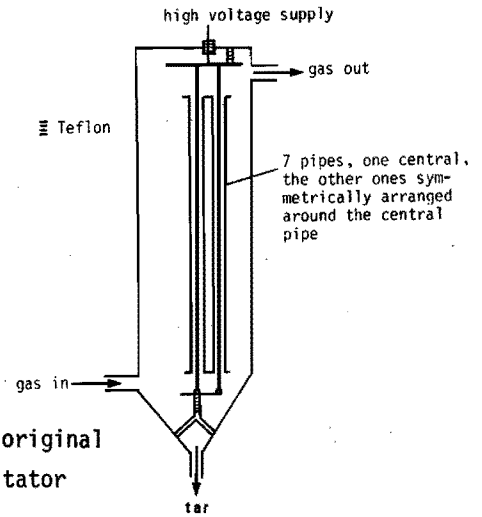

Fig.3.18 Schematic diagram of original electrostatic precipitator

lences are present in the gas stream. This indicates that errors had been made in the design. Potential sources for errors are:

1. It has not been taken into account that eq. (3.3) is no longer valid when charged gas (or other) particles are present and a current flows between the electrodes.Large deviations from this relation may occur especially near the corona.
2. The tar droplets were considered to be rigid spheres.
3. The nitrogen that is present in the gas in large quantities (especially during the start-up period) has a negative effect on the corona. The spark potential is decreased when considerable amounts of nitrogen are present in the gas.
4. The assumption that the particle (droplet) concentration is homogeneous over the cross area of the pipes as a result of turbulences may well be wrong.

We attempted at first to improve the performance of the electrostatic precipitator, that is to obtain a better collection efficiency and less breakdown of the voltage difference through introducing a number of minor modifications (f.i. different central electrodes, another way of centering of these electrodes without connecting these to the cone, etc.). But as the collection of tar from the gas stream remained unsatisfactory even when conditions were favourable (low gas flow rates, little tar production) a new electrostatic precipitator was constructed. The new precipitator was found to be more efficient because of the

following reasons:

1. 13 pipes were used instead of 7 (12 "active" pipes: one pipe is used for centering the electrodes, fig. 3.19). This reduces the gas flow rate in the pipes and improves the efficiency (eq. (3.19)).
2. Longer pipes were adopted (1.50 instead of 1.30 m) for better efficiency (eq. 3.17)).
3. Thinner central electrodes (6 mm) were applied for the better corona discharge.

The precipitator was provided with a steam jacket to keep the temperature of the gas in the precipitator above 100°C.

The new electrostatic precipitator was satisfactory as long as we continued to pyrolyse cardboard. It again failed when we began to pyrolyse fractions from shredded domestic waste. This might have been due to different behavior of the tar obtained in the latter experiments compared to the tar obtained in pyrolysis of cardboard. The tar obtained by pyrolysing domestic waste fractions has a lower dielectric constant which makes it less easy to separate in an electrostatic precipitator. It is much more viscous at lower temperature which results in the formation of tar bridges and stalactites that form a conductive connection between the central electrodes and pipe walls. To improve the operation

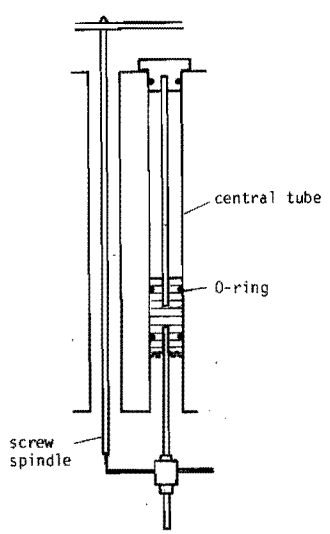

Fig.3.19 Centering of the electrodes

of the new precipitator some modifications were made that were meant to prevent tar from forming conductive connections. The distance between electrodes (and their suspension) and the conical bottom part of the precipitator were for instance increased by mounting a distance ring and all Teflon distance pieces were rippled.
These modifications led to the actual situation outlined in fig. 3.20. The modifications did indeed improve the performance of the electrostatic precipitator (see § 4.3.3).

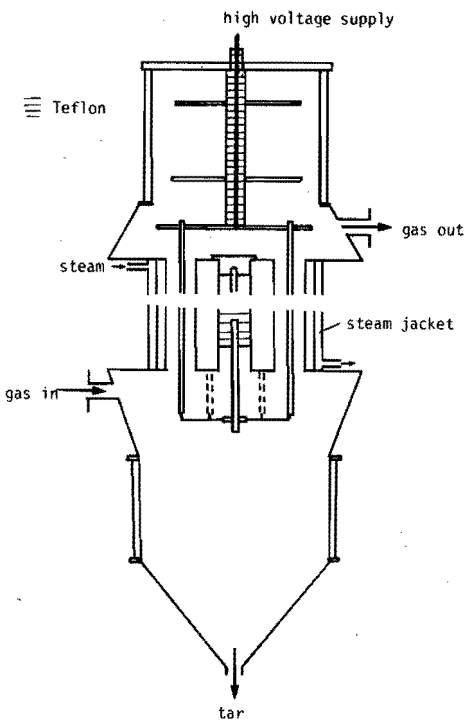

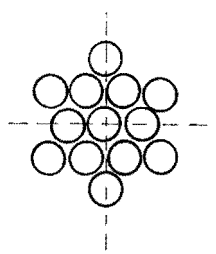
arrangement of the tubes

Fig.3.20 Electrostatic precipitator (modified)

3.3.4.3 Condensation of the water

The gas stream that leaves the electrostatic precipitator is cooled down from about 150°C to room temperature. The water present in the gas stream condenses together with most low-boiling organic compounds. At first we considered using a shell-and-tube heat exchanger.But it was found by calculating the heat and mass transport in this type of heat

exchanger that a very large area would be required to condense the water due to the poor mass transport of the water vapor. While the heat transport would be very good in the heat exchanger excessive formation of mist would occur. It was therefore decided to use direct water cooling in a cooling tower. The gas enters the cooling tower at the bottomside and is cooled in counterflow by a stream of droplets that are injected from a nozzle in the top of the tower. The gas leaves the tower at the top (see fig. 3.21).

In order to design a cooling tower it is necessary to make a reasonable estimate of the heat transfer from the gas to the water droplets. The heat transfer coefficient α for heat transport to a water droplet may be calculated from the Ranz-Marschall equation:

$$Nu_p = 2 + 0.6.\ Re_p^{\frac{1}{2}}.Pr^{1/3}$$

$$Nu_p = \frac{\alpha.d_p}{\lambda} \quad ; \quad Re_p = \frac{\rho.v_p.d_p}{\mu} \quad ; \quad Pr = \frac{C_p.\mu}{\lambda}$$

where: α = heat transfer coefficient ($J/m^2 sec.^oC$)
d_p = diameter of water droplet (m)
λ = thermal conductivity of the gas ($J/m.sec.^oC$)
ρ = gas density (kg/m^3)
v_p = rate of fall of water droplets (m/sec)
μ = gas viscosity ($N.sec/m^2$)
C_p = heat capacity of the gas ($J/kg.^oC$)

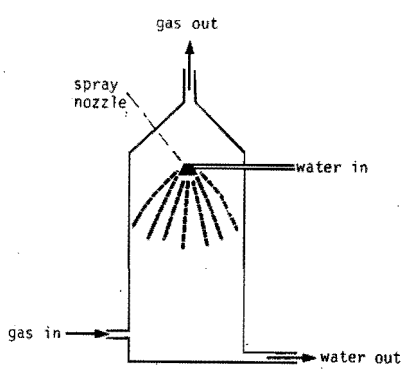

Fig.3.21 Scheme of spray tower

Some phenomena in the cooling tower may influence the Nusselt number Nu_d:

- There is not just one droplet in the cooling tower but a very large number of droplets. This may decrease the Nusselt number as a result of chanelling.
- The water vapor which has to be condensed moves to the water droplets and condenses giving off its heat of condensation and thus increasing the Nusselt number.

With these phenomena in mind a conservative estimate of the Nusselt number was made. α was calculated from the above equations (appendix 3.8)

The maximum amount of heat released in the cooling tower can be calculated from the assumed maximum water production during the pyrolysis and from the maximum gas flow that is to be cooled from 150^{o} to $25^{o}C$. The required total area of the water droplets then follows from:

$$A = \frac{\Delta Q}{\alpha . \Delta \bar{T}_{ln}}$$

in which:

A = total area of the water droplets (m^2)

ΔQ = the heat to be removed (J/sec)

$\Delta \bar{T}_{ln}$ = the logarithmic average temperature difference between water droplets and pyrolysis gas (^{o}C).

The calculations that were carried out on the basis of the above equations are presented in appendix 3.8. They led to the design and construction of the cooling tower shown in fig. 3.22. The condensation of the water from the gas stream and the spraying may cause a mist of very fine water droplets to be present in the outgoing gas stream. To remove this mist a couple of York mats have been placed just above the spray nozzle. These York mats are very fine nettings of thin, stainless steel wires. York mats have been placed just above the gas stream entry point also to demist the incoming gas stream.

The water level in the tower can be read from a gauge. A sketch of the complete spray tower installation is shown in fig. 3.23. Water is pumped from the water supply at the bottom of the spray tower into a heat exchanger(see also appendix 3.8) where the water is cooled by means of cooling water. From there the water flows back to the spray tower in

Fig.3.22 The spray tower

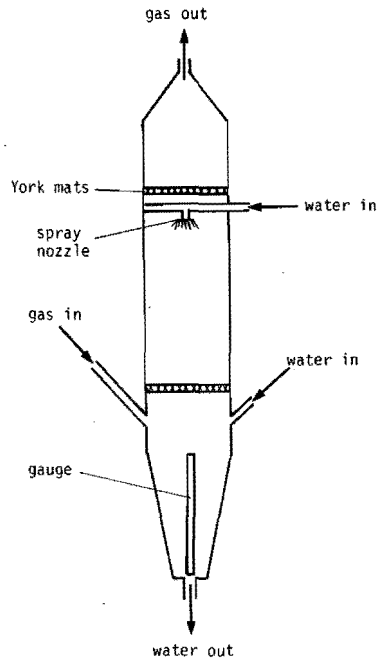

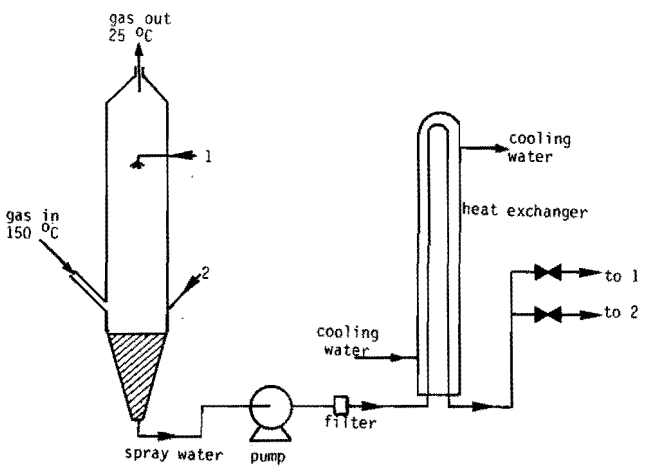

Fig.3.23 Complete spray tower system

two streams: one stream is led to the spray nozzle in the top of the tower while the other one carries the superfluous water to flow directly back into the water supply at the bottom of the tower. The water condensing from the gas stream is added to the water supply and is included in the closed spray water circuit. Water therefore has to be removed from the tower from time to time.

3.4 Additional data on the pyrolysis pilot plant

In this paragraph attention will be paid to some of the apparatuses that were not described so far but that nevertheless are required to ensure good operation of the pilot plant. Roots blower, pressure regulators and gas heaters are described. Some data on the measurement, control and safety devices will be presented.

3.4.1 The Roots blower

The gas that leaves the spray tower is compressed by means of a Roots blower. The Roots blower should be able to produce an increase of pressure of 0.5 atmosphere at the largest gas flow that may occur in the pilot plant. This calculated maximum gas flow is $11.5*10^{-3}$ m^3/sec. at 0^oC and 1 atm. A Roots blower was bought to meet these specifications. The choice of this apparatus was based on its low price also. A drawing of the Roots blower which is a displacement pump is presented in fig. 3.24. The Roots blower shows two disadvantages:

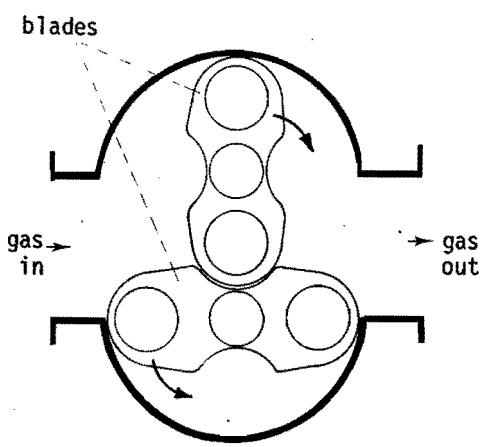

Fig.3.24 The Roots blower

1. The maximal increase of pressure is limited while the spaces between the two blades are not sealed very well. Gas will leak from the high pressure side to the low pressure side. More gas will leak when the pressure difference between high pressure and low pressure side is greater. In addition, the pressure head that the blower produces is limited by the increase in temperature of the gas. The gas is being compressed in the blower almost adiabatically which leads to an increase in gas temperature that increases as the pressure head increases. Our Roots blower can be used up to a highest temperature of $120^{o}C$.
2. As the Roots blower is a displacement pump it is impossible to control the flow by a valve in the outlet. The flow delivered by the blower is determined by the fixed number of revolutions per minute of the blades and the head (fig. 3.25).

It was decided to control the flow by recirculating the superfluous gas flow back to the suction side of the pump through a bypass rather than by varying the number of r.p.m. of the blades. The recirculated gas is cooled to prevent the temperature in the blower from rising too much. Two water cooled heat exchangers(pipe coolers) that were available were installed in the bypass for that purpose.

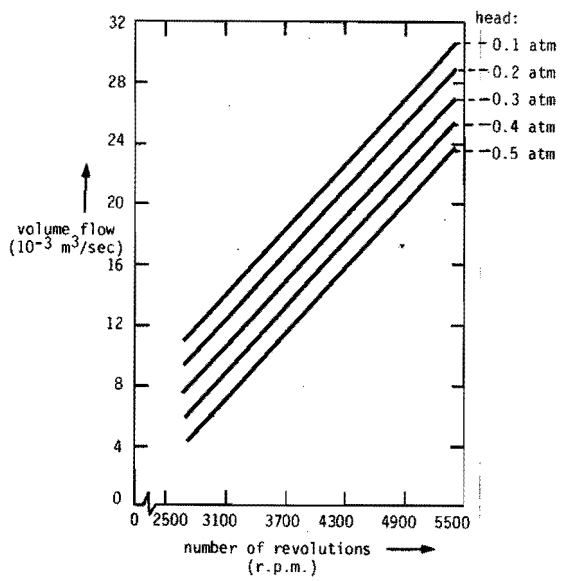

Fig.3.25 Flow delivered by the Roots blower

3.4.2 The pressure control

The gas stream is divided into four streams downstream from the Roots blower:

1. The fluidisation gas stream. The fluidisation gas flows through a gas heater to the space below the sieve plate of the reactor. This gas takes care of the fluidisation of the sand in the reactor.
2. The spout gas stream. This gas stream is also heated in a gas heater and is introduced into the reactor through the spout pipe.
3. The gas production flow. The gas that is produced by the pyrolysis process is blown off through a stack.
4. The bypass flow. The excess gas from the blower is recirculated to the suction side of the pump through a bypass.

It is important for good operation of the spout-fluid bed reactor that the flows of fluidisation and spout gas stream are approximately constant. The flows are adjusted by means of valves in the supply lines to the reactor. When the pressure upstream from these valves is constant the two flows may be assumed to be constant, too. The pressure control apparatus that keeps the pressure constant consists of two control valves (fig. 3.26). One control valve has been placed in the gas production line. The valve controls the flow of the gas that is blown off through this line. The flow is adjusted in such a way that the pressure at the delivery side of the blower remains constant. The volume delivery from the blower is constant in case of constant pressure at the delivery side and a fixed number of r.p.m. of the blades. A second control valve has been placed in the bypass to prevent too much gas from being blown off while not enough gas remains in the installation to

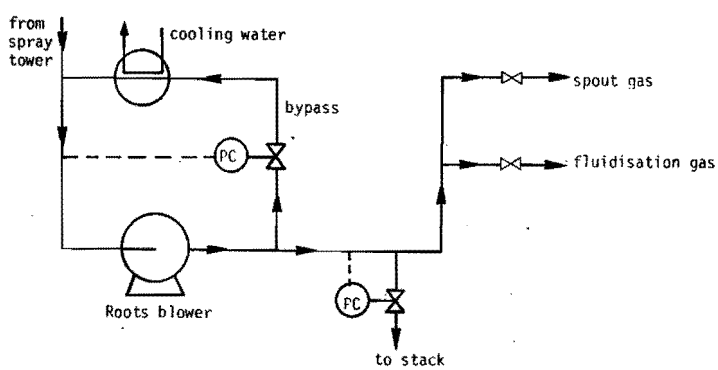

Fig.3.26 Pressure regulation system

provide the flow to the blower. The flow rate in the bypass is controlled in such a way that the pressure at the suction side of the blower is constant. Both control valves act proportionally (fig. 3.26).

3.4.3 The gas heaters

It has already been mentioned in § 3.3.2 that it is necessary to heat both the fluidisation gas and spout gas in order to meet the heat requirements of the reactor. The temperature of the spout gas is limited to a maximum of 200^{o}C as the spout gas stream is used to transport the solid feedstock into the reactor. Higher temperatures would cause the pyrolysis of the solid feed to start in the spout gas line.
It is clear from the fact that the heat required for heating the incoming gases in the reactor to reaction temperature must be provided by spout and fluidisation gas heaters that the fluidisation gas must be heated up to temperatures above reaction temperature.A special design of the fluidisation gas heater was needed to meet these requirements.

3.4.3.1 The fluidisation gas heater

After a couple of designs of a gas heater in which the heat was supplied to gas that flows through an externally heated pipe had proved unsuccessful it was decided to prepare a design in which the gas is heated directly by electrical heating coils. The gas flows through a pipe fitted on the inside with a spiralised resistance wire (Kanthal-A-strip). See fig. 3.27.

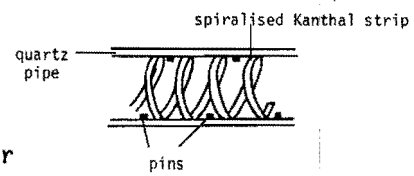

Fig.3.27 Principal design gas heater

Air heating experiments were carried out using heaters with different pipe diameters and different types of Kanthal-A strip. A theoretical model for a gas heater was developed from the results of these experiments. This model was used to design a gas heater that proved to be capable of heating the pyrolysis gases up to desired temperatures. See appendix 3.9. The heater was constructed according to the following design: Kanthal-A strip (5*0.5 mm) was spiralised with a thread of 7 mm inside

a quartz pipe of 18*15 mm. The length of the Kanthal strip is 9.5 m totalizing a resistance of 5.5 Ω so that the maximum power that can be generated at 220 V is 8.8 kW. The quartz pipe was mounted in a ceramic pipe (26*21 mm). This leaves some space for a thermocouple and the return lead of the resistance wire. The ceramic pipe was mounted in a stainless steel pipe (33.7*28.4 mm) to achieve gastight connections to the rest of the pyrolysis plant. The length of the gas heater is 1.50 m. The gas heater was insulated with Fiberfrax Low Conductivity blanket. A sketch of the fluidisation gas heater is presented in fig. 3.28.

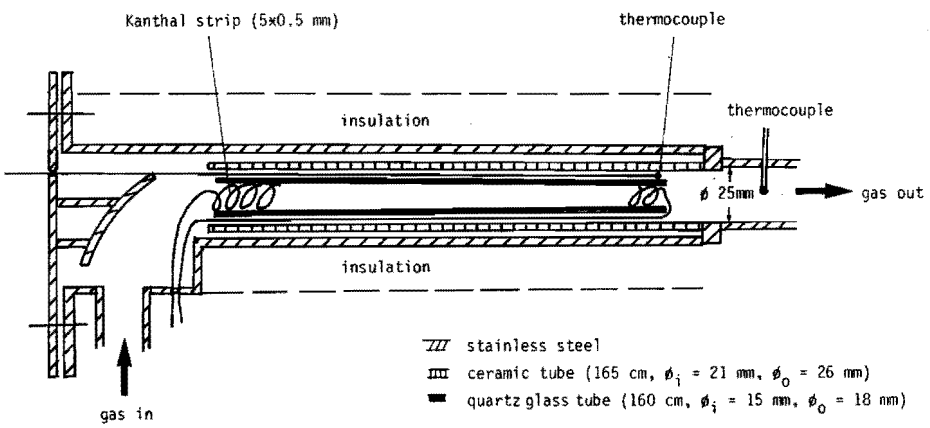

Fig.3.28 The fluidisation gas heater

3.4.3.2 The spout gas heater

An electrical furnace was available that could reach a maximum temperature of 600°C. The length of the furnace is 1 m and pipes with diameters of up to 60 mm can be used in it. It was decided on the basis of heat transfer calculations and practical considerations to use a stainless steel pipe that has an internal diameter of 25 mm for passing the gas flow through the furnace.

3.4.4 Measurement, control and safety devices

Measurement points. A scheme of the most important measurement points is presented in appendix 3.10. The scheme is,however, limited to temperature and pressure measurements. The points for measuring the oxygen concentration in the pilot plant for safety reasons (see below) and the

flow rate measurement are not shown in the scheme. These devices will be discussed in Chapter 4 together with the list of analyses.

Control devices. The pressure control has already been discussed in § 3.4.2. The semi-automatic control of the different heating elements will be discussed briefly below:

The electrical heating of the reactor is controlled by a couple of temperature controllers that adjust the temperature of the reactor wall. The wall temperature is measured by thermocouples that have been fastened to the outside of the reactor wall at three places: at the bottom, at the middle and at the top of the reactor (appendix 3.10: T_9, T_{10}, T_{11}). The power supplied to the coils around the bottom part of the reactor is adjusted by two different controllers. One of the coils is coupled to a Thysistor unit (adjustable temperature set point, power regulation by fast cycle intermitting action, 220 V, maximum current 25 A). The other coil is coupled to a manually controlled Variac transformer (maximum current 20 A) and to a Nieaf temperature controller that switches the heating on when the wall temperature T_9 falls below the set point temperature and switches it off when T_9 exceeds the set point temperature.

The electrical heating of the reactor wall at the middle and the top of the reactor both are controlled by Variac transformers(20 A) and Nieaf controllers that adjust wall temperatures T_{10} and T_{11}).

The heatings of both cyclones are also controlled by Variacs (20 A and 8 A) and Nieaf controllers that adjust wall temperatures T_{13} and T_{15}. The same is true for the electrical heating of the conical part of the electrostatic precipitator (8 A, T_{19}).

The power supplied to the fluidisation gas heater is adjusted by a Thyristor unit (40 A) that controls the temperature of the fluidisation gas at the outlet of the heater (T_3).

Safety devices. A large number of safety devices have been installed that can be divided into three groups:

1. devices that protect the apparatuses
2. devices that protect the process operation
3. devices that provide safety measures in connection with risks of explosion and drop out of current or pressure.

Some of these are described below. More details are given in appendix 3.11 where the other safety devices are presented also. All safety devices are fully automatic.

1. Devices for protecting the apparatuses. Among them are many devices that protect process apparatuses against excessive temperatures. Parts of for instance the Roots blower, the electrostatic precipitator and the pumps in the coolant circuits of condensor and spray tower have only limited resistance against high temperatures and must be protected against them.
2. Protection of process operation. Examples are: protection against excessive gas flow rates in the reactor (by controlling spout and fluidisation gas flows) and against malfunctioning of the Roots blower.
3. Safety measures in connection with risks of explosion and drop out of current and pressure. Protection against underpressure in the plant (risk of oxygen entering into the plant) and against too high oxygen concentration to prevent the formation of an explosive mixture of pyrolysis gas (hydrogen) and oxygen.
   Protection against drop out of electricity, of cooling water supply, of compressed air supply and of the Roots blower.

The carbon monoxide concentration inside the ventilated room in which the plant is installed is continously monitored as a measure to protect the operators of the pyrolysis plant against possible poisoning by carbon monoxide (one of the gaseous pyrolysis products). An alarm sounds when the concentration exceeds the limit of 25 ppm which is the M.A.C. value for CO.

Literature

3.1 R.S. Burton, R.C. Bailie, Combustion 45, pp. 13 (1974).

3.2 F.J. Jackson, Energy from solid waste, "Pyrolysis processes", pp. 106, Noyes Data Corporation, New Yersey (1974).

3.3 G.D. Mooiweer, M.Sc. Thesis, Eindhoven University of Technology, Laboratory for Physical Technology (aug. 1977).

3.4 H.S. Mickley, D.F. Fairbanks, AIChE Journal, vol. 1, no. 3, pp. 374 (1955).

3.5 Kanthal Handbook, Aktiebolaget Kanthal, Hallstahammar, Sweden (1961).

3.6 W.M.A. Kox, M.Sc. Thesis, Eindhoven University of Technology, Laboratory for Physical Technology (sept. 1975).

3.7 F.J.C. Rademacher, The vertical screw conveyor, Ph. D. Thesis, Eindhoven University of Technology (1972).
3.8 E. Muschelknautz, Chemie Ing. Techn. 44, pp. 63 (1972).
3.9 R.H.Perry, C.H. Chilton, Chemical Engineers'Handbook, McGraw-Hill, 5th edition, New York (1973).
3.10 R.B. Bird, W.E. Stewart, E.N. Lightfoot, Transport Phenomena, John Wiley and Sons, Inc., New York (1962).
3.11 D.A. Hougen, K.M. Watson, R.A. Ragatz, Chemical Process Principles, John Wiley and Sons, Inc., New York (1959).
3.12 International Critical Tables, Vol. V, McGraw Hill, New York (1929).
3.13 W.R. Gambill, Chemical Engineering, pp. 247, 28 aug. (1967).

List of symbols

		S.I. units
A	area	m^2
Cp,C_p	heat capacity	$J/kg.^oC$
$\bar{c}$	particle concentration	m^{-3}
D	internal pipe diameter	m
d	diameter, pipe diameter	m
E	strength of electric field	V/m
G	gas flow through pipe	m^3/sec
G_n	total gas flow	m^3/sec
ΔH_w	heat of evaporation of water	J/kg
k_m	Stokes-Cunningham factor	-
L	pipe length, distance	m
N	number of elemental charges	-
Nu	Nusselt number	-
n	number of pipes	-
Pr	Prandtl number	-
p	pressure	N/m^2
Δp	pressure difference	N/m^2
Q,ΔQ	heat flow rate	J/sec
Re	Reynolds number	-
R_i	radius of wire	m
R_u	internal radius of pipe	m
r	distance to centre of pipe	m

T	temperature	^{o}C, ^{o}K
ΔT	temperature difference	^{o}C
t	time	sec
Δt	period of time	sec
U	overall heat transfer coefficient	$J/m^2.sec.^{o}C$
u	gas flow rate	m/sec
u	stationary migration velocity	m/sec
v	velocity, fall velocity	m/sec
V	voltage difference	V
V	flow rate	m^3/sec
x	length co-ordinate	m
y	length co-ordinate	m
z	length co-ordinate	m

Greek symbols

α	heat transfer coefficient	$J/m^2.sec.^{o}C$
ϵ	elemental charge	C
ε	porosity	-
η	collection efficiency	-
λ	thermal conductivity	$J/m.sec.^{o}C$
μ	(gas) viscosity	N.sec/m
ρ	(gas) density	kg/m
τ	contact time	sec
Γ	hold up	m
$\emptyset$	diameter	m
$\emptyset$	collection efficiency cyclone	-

Subscripts

av	average
b	bulk
eff	effective
g	gas
h	domestic waste
i	internal
i	at entry
la	laminar flow
ln	logarithmic average

max	maximum
mf	minimum fluidisation
min	minimum
0	at $0^{o}C$ and 1 atm.
p	particle, droplet
s	solid phase
series	in series
sup	superficial
u	at outlet
u	external
w	wall, at wall
wg	water vapor
wl	water
y	at place y

4. THE PYROLYSIS EXPERIMENTS IN THE PILOT PLANT

4.1 Introduction

The general procedures concerning the start-up, operation and shut-down of the pyrolysis pilot plant will be discussed in this chapter. A scheme of the analyses that have been carried out will be presented. (Detailed descriptions of (some of) the analyses are given in an appendix). A description will be given of the preparation of organic fractions from shredded domestic waste.
The information given in this introductory paragraph has been confined to a discussion of the general proceedings and analyses in connection to the pyrolysis experiments carried out in the pilot plant.

Before the beginning of each experiment the unit is tested for gastightness. Air is introduced into the unit up to a pressure of about 0.2 ato. The pressure in the different parts of the plant is measured as a function of time. When the unit has been found to be gastight the Roots blower is started and the fluidisation medium (sand) is introduced into the reactor. The unit is flushed with nitrogen for reasons of safety (see Chapter 3) and all electrical heatings of the installation are switched on to bring the different parts of the plant to the desired temperatures. At the same time the high voltage power supply to the electrostatic precipitator is switched on. The warming up of the gaschromatographic analysis section and of the oxygen and carbon monoxide analysers is then in progress. As soon as the desired temperatures in the different parts of the unit have been reached the solid feeding is started. The end of the start-up period has now been reached and the beginning of the normal operation of the pyrolysis plant has begun.

Once the experiment has advanced this far the operators occupy themselves with a measurement and analysis b control and c trouble shooting.
a. Measurement and analysis.
All temperatures, the pressure drop over the spout gas line and the pressure of the gas at the outlet of the Roots blower are continuously recorded while the other pressure differences are recorded in a sequence (see Chapter 3). The operators may, however, select an individual pressure difference to be watched and recorded for a longer period of time. The solid feed rate, the spout gas flow rate and fluidisation gas flow rate are measured and recorded. The operators record voltage and current

flow of the high voltage power supply and the meter reading of the cumulative gasmeter in the gas production line from time to time. Samples are taken from the water in the spray tower at the beginning and end of each experiment. The gas is analysed on line as frequently as possible by means of a gaschromatographic system. The gaschromatographic analysis is confined to the determination of nitrogen, hydrogen,(oxygen), carbon monoxide, carbon dioxide and lower hydrocarbons like methane and ethane (see appendix 4.1). The samples from the spray water are analysed for total organic carbon content after the end of the experiment. [1])

b. Control.

There are a number of items that have to be watched and if necessary to be controlled manually by the operators such as the feeding system and the funtioning of the electrostatic precipitator. To check the proper functioning of the solid feed dosage system it suffices to look at the pressure drop over the spout gas line and the level of the waste in the bunker. The flow of the solid feedstock from the bunker into the screw conveyor may need to be kept going by rapping the bunker from time to time.

The bunker is refilled by the operators when this is required. The performance of the electrostatic precipitator is watched by reading the voltage and ampere meters of the high voltage supply. The voltage may be adjusted by manual control when it is considered too low for a proper functioning. Too high a voltage indicates sparking.

In addition, the bed temperature and thus the electrical heating of the reactor are watched continuously. When the temperature keeps falling below the set point temperature the bed temperature may be brought back to the desired temperature level by manual adjustment of the power supplied to the reactor wall heating and/or to the fluidisation gas heater or by reducing the solid feed rate.

It is of importance that the pressure in the pilot plant and the gas meter reading in the gas production line are checked to see whether there is a regular gas production. Stagnating gas production and/or decreasing pressure may indicate a leakage in the plant, that one of the heaters has dropped out or an obstruction of the solid feed dosage system. The operators must then intervene.

[1]) Study of the environmental impact of the process asked for other analysis of gas and water phase (see § 4.3.1).

c. Trouble shooting.

The operators spent a lot of time to trouble shooting especially in the initial stage of the pyrolysis experiments. But technical troubles in the relatively complicated installation demanded the attention of the operators in later experiments also. Trouble that repeatedly had to be faced were leakages through sealings and failures in electrical heaters (fuse failures, melting of lead-in wires of coils).

The normal shut-down procedure is self-explanatory. The solid dosage is stopped and all heaters (except for the heating of the electrostatic precipitator) are switched off. The pressure in the installation will decrease as a result of decreasing temperature. It is therefore necessary to inject nitrogen. When all the feed material present in the bed has been pyrolysed and the bed has cooled down to 300-400^{o}C the three-way valve below the reactor is switched into the position where the bed contents drop into the vessel under the reactor. When the installation has cooled that far the unit is flushed with air (instead of nitrogen). Finally the current to the electrostatic precipitator, the Roots blower and all other apparatuses is switched off. Samples from the water in the spray tower and from the tar from the electrostatic precipitator and condensor, from the char in both cyclones and from the feedstock are taken after the end of the experiment.

The list of analyses that are carried out for all experiments is presented in table 4.1. Additional analyses may be required to determine the properties of the pyrolysis products and to study the environmental impact of the pyrolysis process (see § 4.3.1).

Table 4.1 List of standard analyses.

Sample	Analyses
Feedstock	moisture content, ash content, elemental composition, heat of combustion
Gas	composition, heat of combustion
Tar	ash content, elemental composition, heat of combustion
Char	ash content, elemental composition, heat of combustion
Spray water	total organic carbon content

Note: the elemental analyses were confined in most cases to those for C, H, N and O.

See appendix 4.1 for more details of the analyses.

4.2 General information about experimental conditions

It has been mentioned above (§ 1.6, § 3.3.2) that the spout-fluid bed reactor when applied as a pyrolysis furnace is operated in a flow regime called fluctuating or bubbling spout regime. In this flow regime the gas near the axis of the reactor rises through the bed in large but separate bubbles. The nature of the flow regime depends on fluidisation and spout gas flow rates (fig. 4.1) when dimensions of the reactor and characteristics of the gas and the fluidisation medium are constant. The dimensions of the reactor are given in table 3.1. Relevant properties of the sand that was used as a fluidisation medium are:

- diameter of sand particles : 0.4 - 0.8 mm (average 0.57 mm)
- density of sand : 2510 kg/m^3
- bulk density : 1450 kg/m^3

The ratio of the diameters of the spout opening (1.8 cm) to the diameter of the bed (15 cm) is 0.12 for the spout-fluid bed reactor used in the pilot plant. This ratio is a useful design feature in that it determines whether a stable spout is possible. Above a critical ratio no stable spouting can occur. The spout gas that enters the reactor is immediately divided into large bubbles (bubbling or fluctuating spout). For sand particles of a particle size of 0.42-0.83 mm the critical ratio is 0.10 [4.2].

A stable spout regime is not possible for the spout-fluid bed reactor and the sand used in the plant according to the above criterion. Experimental findings have confirmed this. The occurence of a stable spout -

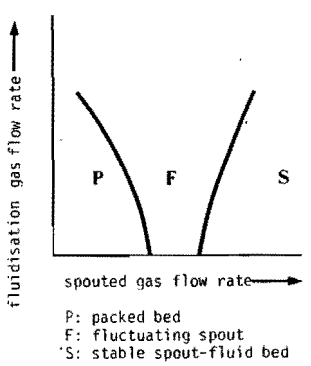

Fig.4.1 Flow regimes of the spout-fluid bed as a function of fluidisation and spout gas flow rate.

and thus a potential risk of feedstock introduced through the spout being immediately blown out of the reactor - is definitely impossible no matter how large the gas flows are that are supplied to the reactor through spout opening and sieve plate.

Concentration measurements (sand + 3 wt.% of shredded thin cardboard) were carried out in the spout-fluid bed reactor to obtain information about the mixing in the fluctuating spout regime. It was found that for very good solid mixing behavior of the bed the fluidisation gas flow rate must exceed the minimum fluidisation gas flow rate (u_{mf}). The solid mixing is excellent for fluidisation gas flow rates above $1.75*u_{mf}$ [4.3]. The minimum fluidisation gas flow rate for the sand used in the pyrolysis plant is u_{mf} = 22 cm/sec (superficial, [4.1]).
Three different aspects determine what spout gas flow rate is to be used: the pneumatic transport of the feedstock, sand particles falling into the spout pipe and the solid mixing behavior of the bed.

The pneumatic transport of the feedstock by the spout gas is assumed to occur smoothly when the linear velocity of the gas is above 15 m/sec [4.4]. The spout gas flow rate must also exceed the free fall velocity of the sand particles in air to prevent them from falling into the spout pipe. This velocity was calculated to be 6.9 m/sec at most depending on gas temperature and particle size of the sand but has been observed to be smaller than that. No lower limit of the spout gas flow rate for good solid mixing behavior has been determined exactly. The above concentration measurements used to describe the mixing behavior were, however, carried out at a minimum superficial spout gas velocity in the reactor u_{sp} = 22 cm/sec. Conservative calculations of both the minimum fluidisation and the minimum spout gas flow rate are summarized in table 4.2.
No upper limits have been found for the gas flow rates so far. The most critical part of the pyrolysis pilot plant appeared to be the electrostatic precipitator. For this reason it seems reasonable to connect the maximum flow rates of spout gas and fluidisation gas to the maximum gas flow rate that is allowable in the electrostatic precipitator. A conservative calculation led to a maximum gas flow rate of $20*10^{-3}$ m^3/sec at 20^oC at which the flow through the precipitator is still laminar.

It is stated for the sake of completeness that in the investigations

into the influence of a single reaction condition on the pyrolysis process all other conditions were kept as constant as possible.

Table 4.2 Minimum fluidisation and spout gas flow rates.

gas flow	criterion	actual gas flow rate (m^3/sec)	gas flow rate at 20°C (m^3/sec)
fluidisation gas	$u_{fl} > 1.75 * u_{mf}$ u_{mf} = 22 cm/sec (superficial)	$6.8*10^{-3}$ (at 400°C)	$3.0*10^{-3}$
spout gas	a. u_{sp} > 15 m/sec (linear)	$3.8*10^{-3}$ (at 150°C)	
	b. u_{sp} > 6.9 m/sec (linear)	$1.8*10^{-3}$ (at 150°C)	$2.7*10^{-3}$
	c. u_{sp} > 22 cm/sec (superficial)	$3.9*10^{-3}$ (at 150°C)	

4.3 Preparations of organic fractions from shredded domestic waste (Refuse Derived Fuels).

When domestic waste was used as material to be pyrolysed the feed had to be pretreated. Particle size, humidity and ash content of the domestic waste had to be reduced to make the material fit for processing in the pilot plant.

The domestic waste had to be shredded because domestic waste "as received" cannot be fluidised due to the presence of larger size particles in it. In addition, shredding of the waste was required to make transport of the waste through the spout gas line which has an inner diameter of 18 mm possible.

The limited heating capacity of the reactor made it necessary to reduce feed humidity to moderate values.

Strictly speaking, reduction of the ash content is not required. Nevertheless, ash content was reduced as inorganics do not decompose during the low temperature pyrolysis process but give rise to energy losses during the heating of the feed and cooling of the product stream or when ashes have to be drawn off from the bed.

What we have tried to accomplish is in fact the preparation of a refuse derived fuel (RDF). RDF is a fraction separated from domestic waste or refuse that can be used as a fuel and that consists largely of organic

compounds.

Most processes to prepare RDF make use of dry separation techniques like sieving, air classification and magnetic separation of ferro-metals. Dry separation techniques were used in the present investigation, too.

The following apparatuses for the preparation of RDF were available: a shredder with interchangeable sieve plate, a 120° zig zag air classifier and a trommelsieve installation with various sieve plates. A drying box and a large refrigerator (for storage of domestic waste or fractions from it) were also available.

The shredder was an Unicrex (Bohm Maschinenfabrik, Osnabruck) shredder in which the size reduction is accomplished by feeding the waste to two axes fitted with several knives and rotating at different speeds (see fig. 4.2). A sieve plate has been mounted below the axes through which the material leaves the shredder and which controls the degree of shredding. It should be noted that the Unicrex shredder differs from the hammer-mill shredders which are mostly used in waste handling practice. The Unicrex cuts the waste rather than beat it to pieces like a hammer-mill.

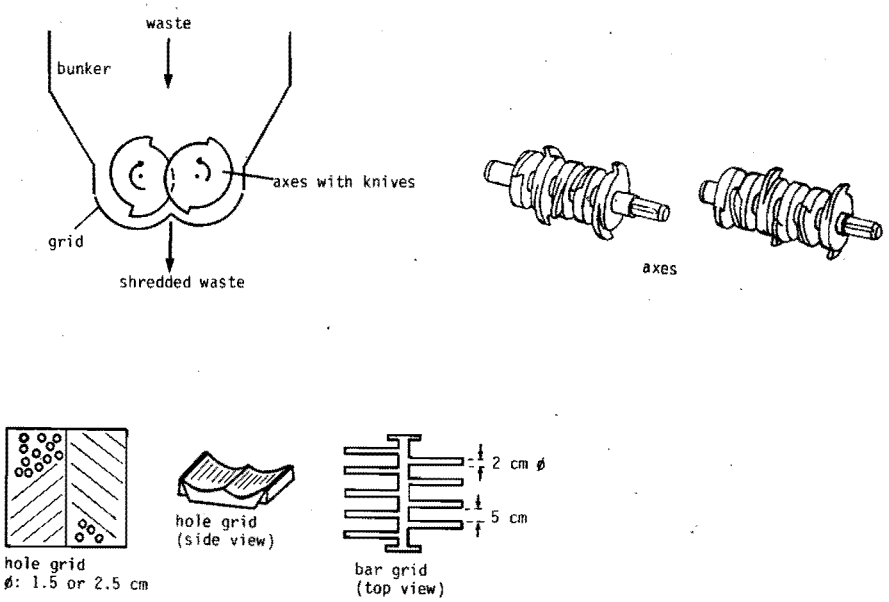

Fig.4.2 The Unicrex shredder

The apparatus used for air classification in the present investigation was a 120° zig zag air classifier. Air classification is a separation technique in which solid particles are classified according to their falling behavior in stagnant air. The particles are submitted to the drag of an upward flowing air stream in a vertical channel (in this case a zig zag shaped channel, see fig. 4.3). The result of the classification process is determined largely by the force balance between gravity and the mean air drag on the particles. In a zig zag air classifier the classification process takes place at every junction of two channel sections. A multi-stage classification is thus achieved. The solid particle feed to the classifier is separated in a "light" top fraction and a "heavy" bottom fraction.

The trommelsieve installation consists of a trommelsieve that rotates at an adjustable speed under a variable angle of inclination. The trommelsieve can be fitted with various sieve plates that have different sizes of perforations. See fig. 4.4.

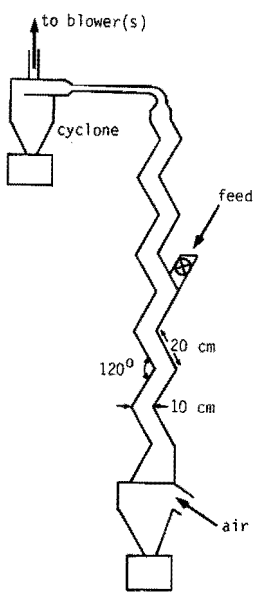

Fig.4.3 The 120° zig zag air classifier

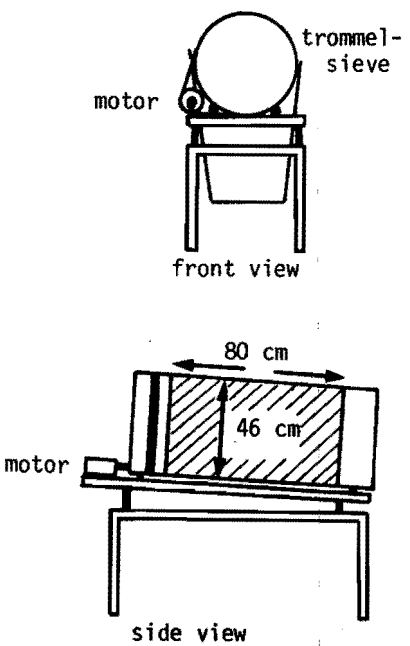

Fig.4.4 The trommelsieve installation

The procedure that we applied to prepare the fractions from shredded domestic waste on behalf of the pyrolysis experiments was developed on the basis of an extensive investigation of the influences on the quality and the yield of a RDF fraction of f.i. the degree of shredding and the air velocity in the air classifier. Freshly collected domestic waste was the starting material in all experiments. The waste was collected by the Eindhoven municipal sanitory services in working-class neighbourhoods without appartment buildings. The waste collected in this kind of neighbourhoods contains all possible components like f.i. garden waste which is not found in the domestic waste collected in districts full of appartment buildings. The size of the waste sample taken to prepare RDF fractions was in the order of 50-70 kg at a time. Some of the results of the investigation were:

1. A considerable reduction in ash content could easily be achieved by removing large pieces of glass and iron by handpicking.
2. Shredding of the waste was necessary before other separation steps could be taken. The separation units are not able to handle the larger size materials which are present in domestic waste "as received". In addition, a considerable reduction of the bulk volume of the waste is achieved which facilitates storage.
3. Shredding of the waste in the Unicrex shredder fitted with a hole grid with holes of 2.5 cm gave the best results. Seventy percent of the shredded waste did pass through a sieve with apertures of 1*1 cm^2. Use of the bar grid shown in fig. 4.2 in the shredder gave insufficient size reduction for further processing in the sieves or the air classifier. The use of the sieve plate with openings of 1.5 cm resulted in a far greater size reduction than was thought necessary. In addition, the shredding required excessive time and energy in that case.
4. Sieving of the waste shredded in the Unicrex shredder appeared not to be a satisfactory way to separate a fraction from the shredded waste that has a sufficiently reduced ash content. The reason for this is simple. By sieving one achieves a classification according to size but not to heat of combustion. Moreover, the Unicrex shredder forces many inorganic substances like glass splinters into such organic substances as textile and paper. Sieving does not then serve to remove the splinters from the organics anymore.
5. Air classification of the waste that had previously been shredded in

the Unicrex shredder resulted in a considerable reduction of the ash content of the waste that passed out of the classifier at the top end (= top fraction). Most of the inorganics (and some heavy organics) leave the air classifier through the bottom.

It is felt that the fact that better results are obtained through air classification than by trommelsieving is caused by the nature of the action of the air classifier. This apparatus classifies according to sizes as well as to densities of the particles. Inorganic substances are generally more dense than organic substances. In addition, the particles are submitted to a relatively rough treatment in the air classifier compared to that in the trommelsieve. Some of the agglomerates that often are present in organic waste may be broken up in the air.

6. The lowest ash contents were achieved in the top fraction at low air velocities in the zig zag air classifier. Under these circumstances the top fraction was of course very small, An example is given in table 4.3.

Table 4.3 Separation performance of the 120° zig zag air classifier. Feed: domestic waste shredded in the Unicrex shredder, moisture content 50 wt.%, ash content 24 wt.% (dry basis).

superficial air velocity (m/sec)	top fraction (wt.%)	ash content of top fraction (wt.%, dry basis)	bottom fraction (wt.%)	ash content of bottom fraction (wt.%, dry basis)
2.0	3.0	5	97.0	25
8.0	72.5	14	27.5	53

The following procedure for preparing a RDF fraction was developed on the basis of the above findings:

1. removal of large pieces of glass and iron by handpicking;
2. shredding in the Unicrex shredder fitted with a sieve plate with openings of 2.5 cm;
3. air classification at superficial air velocities of about 8 m/sec in the 120° zig zag air classifier.

It was mentioned above, however, that the RDF fraction has to meet certain requirements with respect to particle size and moisture content so that it can be processed in our pyrolysis pilot installation. Sieving and drying of the RDF fraction were therefore necessary.

Trommelsieving of the RDF obtained by the above procedure using a sieve plate with openings of 11 mm diameter proved to produce as undersize an organic fraction that can be transported in the spout gas line (inner diameter 18 mm). This undersize (about 75-80 wt.%) had a higher ash content than the oversize. It may therefore be attractive to shred the oversize so that it passes through the sieve, too. In this way both the yield and the ash content of the fraction to be used as pyrolysis feedstock are more satisfactory.

We investigated whether the order in which drying and separation were carried out did influence the final result of the preparation of a suitable RDF fraction. It was found that drying of the shredded waste before air classification did not greatly influence the separation process. The superficial air velocity in the classifier that is required to obtain an identical yield of top fraction was somewhat lower (about 6 m/sec instead of 8 m/sec for a yield of 70-80 wt.%). However, more energy is required for drying the total amount of shredded waste rather than drying the RDF fraction only in the case when the drying is the last step in the preparation.

The following procedure was finally applied for preparing a RDF fraction suitable for processing in the pilot plant on the basis of the above findings:

1. Removal of large pieces of glass and iron by handpicking.
2. Shredding of the waste in the Unicrex shredder (grid with holes of 2.5 cm diameter).
3. Air classification in the 120^{o} zig zag air classifier (at superficial air velocities of about 8 m/sec).
4. Sieving the top fraction in a trommelsieve (sieve openings: 11 mm diameter).
5. Drying the undersize.

When this procedure was followed 60-80 % (dry basis) of the organics present in the domestic waste was found in the fraction that is to be used as feedstock for the pyrolysis experiments. The reduction in ash content is 40-60%. An example is given below:

Freshly collected domestic waste:			Fraction to be used as feedstock (before drying):	
yield and composition (total basis, including moisture)	organics	: 33.2 wt.%	yield	: 53%
	ashes	: 27.4 wt.%	organics	: 42.1 wt.%
	moisture	: 39.4 wt.%	ashes	: 10.3 wt.%
			moisture	: 47.6 wt.%
yield and composition (dry basis)	organics	: 54.7 wt.%	yield	: 45.8%
	ashes	: 45.3 wt.%	organics	: 80.4 wt.%
			ashes	: 19.6 wt.%

The percentage of organics present in the waste that is recovered in the fraction which is to be used as feedstock amounts to (on dry basis)

$$\frac{80.4*45.8}{54.7} * 100\% = 67.3\%$$

The reduction in ash content is:

$$\frac{45.3-19.6}{45.3} * 100\% = 56.7\%$$

Table 4.4 shows some of the typical characteristics of the fractions from shredded domestic waste prepared according to the above procedure and used as feedstock in the pyrolysis experiments. [1])

Table 4.4 Data on domestic waste fractions used as feedstock.

Dimensions	passes a sieve with round apertures of 11 mm diameter
Moisture content (wt.%)	3 - 8
Ash content (wt.% on dry basis)	12 - 20
Elemental composition (dry basis)	
C (wt.%)	40 - 47
H (wt.%)	5 - 7
O (wt.%)	30 - 40
N (wt.%)	0.6- 1.5
S (wt.%)	0.2- 0.4
Cl (wt.%)	0.2- 0.4
Heat of combustion (kJ/kg)	16,000 - 17,000

[1]) The fraction used as feedstock in experiments no. IX and X (see next chapter) had somewhat higher moisture and/or ash contents.

4.4 Analysis and determinations in addition to standard analyses.

Some analyses have been carried out in addition to standard analyses (see table 4.1) to determine the nature of the pyrolysis products and to study the environmental aspects of the process in the case of pyrolysis of fractions from shredded domestic waste. See table 4.5.

Table 4.5 Analyses and determinations in addition to standard analyses.

Product	Analysis on/determination of:
Tar	chlorine, sulphur, viscosity, density, moisture content
Char	heavy metals, chlorine, sulphur.
Gas	HCl, PCB, polycyclic aromatics
Water phase	chlorine, BOD, PCB, polycyclic aromatics

Some analyses are briefly discussed below.

Tar fraction

- Determinations of chlorine and sulphur contents.
  The determinations of the chlorine and sulphur contents of the tar have been carried out by TNO - Utrecht (see standard analyses, appendix 4.1).
- Moisture content.
  The moisture content of the tar was determined according to ASTM D95-62 [4.5] which is based on azeotropic distillation of the water with toluene.
- Viscosity of the tar.
  The viscosity of the tar was determined by means of a Brookfield rotational viscosimeter. The immersion bodies LV 1,2,3 and 4 were used [4.6].

Char fraction

- Chlorine and sulphur content were determined by TNO-Utrecht (see above).
- Heavy metals. Samples of char and char ash were leached batchwise with water, diluted sulphuric acid,diluted hydrochloric acid and diluted nitric acid. Sulphuric acid was chosen to simulate the leaching process

by rainwater (rainwater in Holland has a pH = 4 due to the presence of CO_2 and SO_2 etc. [4.7]). Water was chosen to determine the minimum and nitric acid to determine the maximum amount of heavy metals that can be leached from the char or char ash. Hydrochloric acid was used because lead sulphate has a very small solubility product only. Its use also provided a comparison with leaching in which sulphuric acid was applied. A pH value below 4 was used for the acid solutions to obtain an intensified simulation of the natural leaching process. The percentages of Cr, Ni, Pb, Zn, Cd, Cu, Al and Fe in the leachates were measured by means of an atomic absorption spectrophotometer. These metals tested for were selected because of their poisonous nature and/or because it was expected that the metal in question would be present in large concentration.

Gas fraction

- HCl. The following arrangements were made to determine whether and in what concentration HCl was present in the pyrolysis gas: An extra gas sampling line was connected between delivery and suction side of the Roots blower. A valve, a rotameter and a gas wash bottle were installed in this line. The gas wash bottle was filled with a solution of NaOH in water (0.01-0.04 mole NaOH per litre) before the start of an experiment. A 0.01 n.NaOH solution should be more than sufficient for complete and rapid absorption of HCl in any scrubber [4.8]. In the course of an experiment a constant flow of gas was maintained through the gas wash bottle for a period of ½ - 1½ hr. After the experiment the amount of Cl^- absorbed by the NaOH solution was determined according to the method of Mohr [4.9].
- PCB, polycyclic aromatics.
  Sampling: an amount of gas (measured by means of a wet gas meter) is forced very slowly through a column packed with Tenax by the excess pressure that exists in the pilot plant unit. Components like PCB's, chloro alkanes, polycyclic aromatics etc. all are absorbed in this column.
  Analysis: desorption and subsequent analysis by capillary gas chromatography-mass spectrometry (GC-MS). The analysis (which is carried out in the laboratory of Instrumental Analysis at the Eindhoven University of Technology) is shortly discussed below (see water phase).

Water phase

- Biological oxygen demand (BOD) and chemical oxygen demand (COD).
  The BOD determinations were carried out by means of a Sapromat B6 (Voith, W-Germany). The oxygen pressure above the samples is held at a constant value during the measurements. Various nutrition salts solutions were added to the water to achieve a good environment for the micro-organisms to grow. The nutrition salts solutions used were K_2HPO_4 + Na_2HPO_4 in water, $MgSO_4$ in water, $FeCl_3$ in water, $CaCl_2$ in water and alkylthioureum in water. NaOH was applied in some cases to increase the pH value up to 6.5-7.0.
  The chemical oxygen demand was determined by means of a bichromate solution in the presence of an Ag^+-catalyst to promote complete oxidation of the organic compounds present in the water phase.
- PCB, polycyclic aromatics.
  Samples from the water phase were extracted, f.i. with butanol, ether, pentanol and analysed by capillary gas chromatography - mass spectrometry in the laboratory for Instrumental Analysis. The analysis is shortly discussed below:
  The water phase sample (about 200 ml) was extracted. The extract was concentrated by evaporating the solvent by passing nitrogen through it until a paste was obtained. The paste was injected into a Finnigan gas chromatograph (GC)/Mass spectrometer (MS) combination. The GC is fitted with a capillary column. The sample size is 2.5 µℓ, the split ratio equals 1:200. The mixture of components present in the paste is separated in the GC. The separated components are introduced into the MS through a direct coupling.The components are ionised and eventually cleaved into smaller ions. The ions are separated to their mass and the intensity of the separated bundles is measured as a function of mass. The separation takes place in high vacuum (1mPa).

Literature

4.1 J.M. Claessens, M.Sc. Thesis, Eindhoven University of Technology Laboratory for Physical Technology (april 1980).

4.2 K.B. Marthur, P.E. Gishler, AIChE Journal, 1, 157 (1955).

4.3 J.J.M. Mennen, M.Sc. Thesis, Eindhoven University of Technology, Laboratory for Physical Technology (october 1979).

4.4 M. Tels et.al. report "Process Development" Eindhoven University of Technology (1981).
4.5 ASTM Test D95-62, American Society for Testing and Materials, Philadelphia (1968).
4.6 Brookfield Synchro-lectric Viscometer, Brookfield Engineering Laboratories, Inc., Stoughton (Mass.).
4.7 Annual Survey 1979, KNMI/RVI, Zeist (Holland) (1980).
4.8 W. Leithe, The analysis of air pollutants, Ann-Arbor-Humphrey Science publ. Inc., London (1970).
4.9 W.J. Williams, Handbook of anion determinations, Butterworths & Co, Ltd., London (1979).
4.10 S.C. Jolly, Official, standarised and recommended methods of analysis, Publ. W. Heffer & Sons Ltd., (1963).
4.11 Kumpf, Maus, Straut, Bestimmung der Zusammensetzung fester Abfallstoffe, from Müll und Abfallbeseitigung, Erich Schmidt Verlag, Berlin (1973).
4.12 R.H. Perry, C.H. Chilton, Chemical Engineer's Handbook, 5th edition, McGraw-Hill Book Cy., New York (1973).
4.13 D.L. Wilson, Environmental Science & Technology, vol. 6, no. 13, pp. 1119 (1972).

List of symbols

		S.I.-units
ΔH	heat of combustion	J/kg
u_{fl}	fluidisation gas flow rate	m/sec
u_{mf}	minimum fluidisation gas flow rate	m/sec
$_{sp}$	superficial spout gas velocity	m/sec

Greek symbols

Ø	diameter	m

5. EXPERIMENTAL CONDITIONS AND RESULTS OF WASTE PYROLYSIS IN A SPOUT-FLUID BED REACTOR

5.1 Introduction

The experimental conditions and results of the pyrolysis of shredded thin cardboard and fractions from shredded domestic waste in the pilot plant described before are given first. Results are presented in terms of the dependences of product distributions and composition of the products on experimental conditions (§ 5.2 and § 5.3). The product distributions have been referred to moisture and ash free feedstocks. This makes a fair comparison possible between the outcomings of the experiments with shredded thin cardboard and those of the experiments with fractions from shredded domestic waste, as well as a comparison between the results of the experiments with fractions from shredded domestic waste mutually. The analysis data on the different feedstocks (tables 4.4 and 5.1) showed large differences in moisture as well as ash content of the cardboard and domestic waste fractions that have been used in the pyrolysis experiments. The composition of the products is given on an ashfree basis for the same reason. The specifications of the products obtained by pyrolysis of the domestic waste fractions that are required for judging their marketability and environmental aspects (§ 5.3) are given on total, "as is" basis. The ash content and the nature of the ash are factors that to a considerable extent determine the marketability and the environmental impact of the products and thus the potential usefulness of the pyrolysis process.

5.2 Pyrolysis experiments on shredded thin cardboard

5.2.1 Aim of experiments

The introductory pyrolysis experiments in the pilot plant were carried out with shredded thin cardboard as feedstock to facilitate the analysis and the interpretation of the results. It was mentioned above that the composition of the organic fraction from domestic waste which we wanted to pyrolyse varies enormously. It is almost impossible to take a representative sample of domestic waste. The varying solid feed composition, humidity and particle size complicate the interpretation of the results. It was decided to use a better defined material (cardboard) rather than domestic waste in the introductory experiments.

The decision to use shredded thin cardboard was based on the below considerations:

a. It is necessary to ensure obtaining results that may be used for predicting the behavior of shredded domestic waste under similar pyrolysis conditions that the chemical composition of the model substance is about the same as the average composition of the organic fraction from shredded domestic waste. A frequently used elemental formula for the organic part of West-European domestic waste is

   $C_6 H_{9.4} O_{3.8} N_{0.1} S_{0.01}$

   [5.1]. This explains why cellulose (elemental formula $(C_6 H_{10} O_5)_n$) is often chosen as a model substance (comp.Chapter 2). In this case the cellulosic material chosen was cardboard. The poor flow characteristics of shredded thin cardboard is another reason to use it as a model for shredded domestic waste. Both shredded thin cardboard and shredded domestic waste are materials that show difficult flow.

b. Computer input cards were selected as thin cellulosic material because the cards are easy to obtain. The use of thin shredded cardboard is motivated by the fact that we want to compare the experimental results obtained by pyrolysing shredded thin cardboard with the results obtained from the models developed for cellulose pyrolysis in Chapter 2. In these models the cellulose particles were assumed to be infinite, flat cellulose slabs. In addition, large numbers of domestic waste components are thin, f.i. newsprint, leaves etc.
   In the beginning of the investigation small pieces of computer cards were collected from a number of computer card punching machines present at the University. Later on the same waste material was provided to us by institutions having a much larger punching capacity.

c. Composition, size and ash content of the shredded cardboard were constant and its humidity was about constant, too. Table 5.1 shows some properties of the cardboard feedstock.

The experiments with shredded thin cardboard were meant in the first place to test the apparatuses and the control and safety devices and to make necessary alterations in it.
In the second place the experiments were meant to provide us with information about the influences of various reaction conditions on the pyrolysis process, especially on the product distribution and composition

Table 5.1 Data on thin shredded cardboard used as feedstock.

Dimensions	(mm^3)	3.4*1.6*0.18
Density	(kg/m^3)	900
Bulk density	(kg/m^3)	330
Moisture content	(wt.%)	5.7
Elemental composition	(wet basis)	
C	(wt.%)	41.9
H	(wt.%)	6.1
O	(wt.%)	50.7
Ash content	(wt.%)	1.3
Heat of combustion	(kJ/kg)	15,900

of the products. The influences of the following reaction conditions on the process were studied: pyrolysis temperature, gas flow rate in reactor, particle size of feedstock, humidity of the feed and solid feed rate. Finally the experiments with shredded thin cardboard were to provide us with intermediates of the pyrolysis reactions of a cellulosic material. The intermediates could then be used to study the reaction kinetics of the pyrolysis of cellulose (Chapter 2).

5.2.2 Experimental conditions and results

5.2.2.1 Experiments at different temperatures

In this series of 5 experiments the reaction temperature was varied. The other reaction conditions were kept constant at the nominal values indicated below:

Solid feed rate	7.85 kg/hr, $\pm$ 3%
Fluidisation gas flow rate	$3.53*10^{-3}$ m^3/sec, $\pm$ 4%
Spout gas flow rate	$3.77*10^{-3}$ m^3/sec, $\pm$ 4%
Total gas flow rate	$7.30*10^{-3}$ m^3/sec, $\pm$ 2%

Here, as in all tables in this chapter "m^3" when refering to gas volume stands for "m^3 of gas at 1 atm. of absolute pressure and at 20^oC". The reaction temperature varied less than 10^oC during each experiment. The departure of the actual solid feed rate from the nominal solid feed

rate exceeded 3% in experiment no. 1. Actual reaction conditions for all runs in this series are shown in table 5.2.

Table 5.2 Experimental conditions of series of experiments with shredded thin cardboard at different temperatures.

Exp.no. (-)	Temp. (^{o}C)	Solid feed rate (kg/hr)	Fluidisation gas rate (m^3/sec)	Spout gas flow rate (m^3/sec)	Total gas flow rate (m^3/sec)
1	439	5.9	$3.64*10^{-3}$	$3.60*10^{-3}$	$7.24*10^{-3}$
2	500	7.9	$3.44*10^{-3}$	$3.75*10^{-3}$	$7.19*10^{-3}$
3	530	7.7	$3.44*10^{-3}$	$3.90*10^{-3}$	$7.34*10^{-3}$
4	577	7.6	$3.54*10^{-3}$	$3.75*10^{-3}$	$7.29*10^{-3}$
5	594	8.1	$3.59*10^{-3}$	$3.83*10^{-3}$	$7.42*10^{-3}$

The product distributions obtained are presented in table 5.3 and summarized in fig. 5.1. Table 5.4 presents elemental compositions and heats of combustion of the tar and the char together with the total organic carbon (TOC) contents of the watery solutions produced and the compositions of the gases that were obtained. Composition data are shown for the char fractions collected in both cyclones. Heats of combustion are given for the char collected in the first cyclone only as the amounts of char that reach the second cyclone are very small. The properties of the various products are summarized in figs. 5.2, 5.3 and 5.4.

Table 5.3 Product distributions measured in series of experiments with shredded thin cardboard at different temperatures (basis moisture- and ashfree feed).

Experiment	Temperature (^{o}C)	Product distribution in wt.% char in both cyclones	tar	water phase	gas	total
1	439	23.2	22.9	43.7	7.3	97.1
2	500	9.8	38.1	43.7	11.1	102.7
3	530	7.4	38.6	32.7	17.5	96.2
4	577	6.3	-*)	-*)	32.2	-
5	594	5.5	19.8	35.5	35.1	95.9

*) not measured.

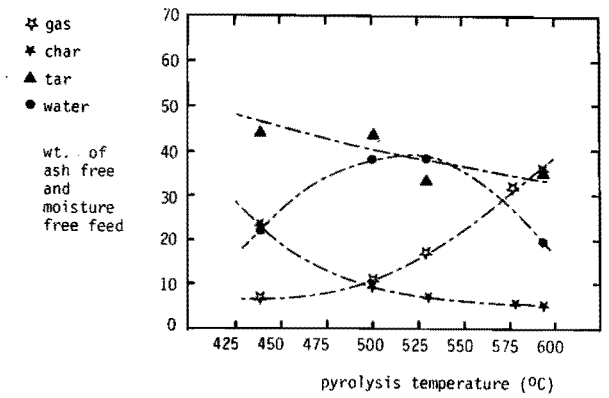

ERRATUM

Legend figure 5.1:
▲ tar must be ▲ water
● water must be ● tar

Fig.5.1 Pyrolysis experiments on shredded thin cardboard. Product distribution versus pyrolysis temperature (basis ash free and moisture free feed)

Table 5.4 Series of experiments with shredded thin cardboard at different temperatures. Properties of products (ashfree basis).

	Exp. no. →	1	2	3	4	5
	Temp. (°C) →	439	500	530	577	594
tar (from electro-	C (wt.%)	51.3	49.3	49.7	57.7*)	51.5
static precipitator	H (wt.%)	6.0	6.2	6.1	6.7	6.0
	O (wt.%)	42.7	44.5	44.2	35.6	42.5
heat of combustion	(kJ/kg)	19,900	20,250	20,150	-	20,500
char in 1st	C (wt.%)	61.3	76.2	89.1	90.5	89.8
cyclone	H (wt.%)	3.6	3.9	3.9	3.7	3.6
	O (wt.%)	35.1	19.9	7.0	5.8	6.6
heat of combustion		15,725	28,950	33,050	34,200	33,975
char in 2nd	C (wt.%)	70.5	70.7	73.5	77.4	74.6
cyclone	H (wt.%)	4.3	4.5	4.2	4.0	3.9
	O (wt.%)	25.2	22.3	22.3	18.6	21.5
gas	CO_2 (vol.%)	50	36.5	27	17.5	13.5
	H_2 (vol.%)	2	2	4	7	7.5
	CH_4 (vol.%)	2	4.5	7	13	11.5
	CO (vol.%)	46	55	59	59	64
	C_2H_6 (vol.%)	-	2	3	3.5	3.5
heat of combustion	(kJ/m³)	6,200	9,300	11,300	13,900	14,000
TOC of water fraction	(wt.%)	15.4	17.1	20.5	-**)	15.2

*) tar had been overheated
**) unreliable datum point

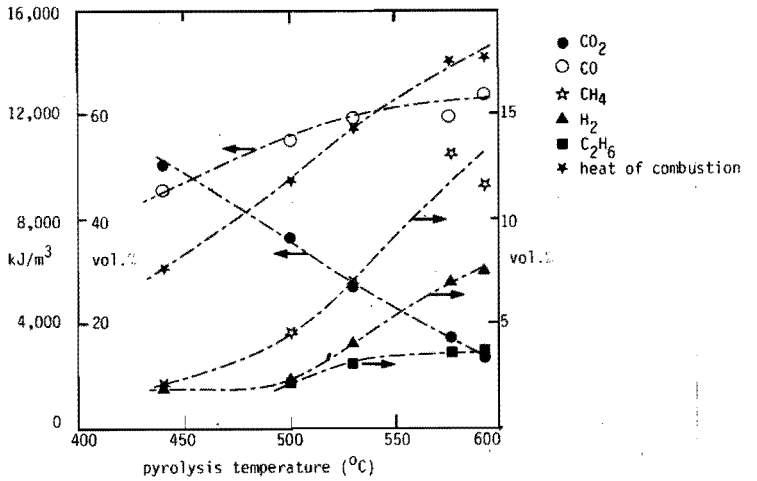

Fig.5.2 Pyrolysis experiments on shredded thin cardboard. Gas composition and heat of combustion of the gas versus pyrolysis temperature

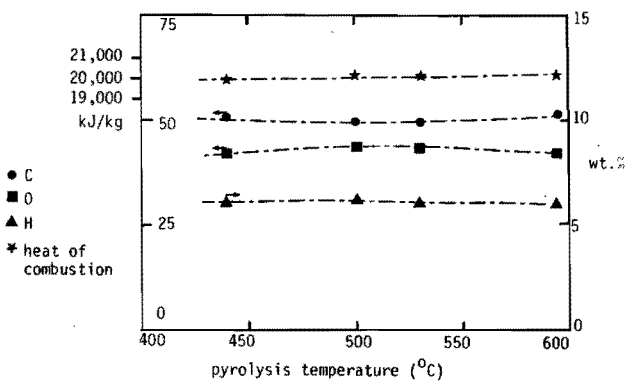

Fig.5.3 Pyrolysis experiments on shredded thin cardboard. Elemental composition and heat of combustion of tar (from electrostatic precipitator) versus pyrolysis temperature (on ash free basis)

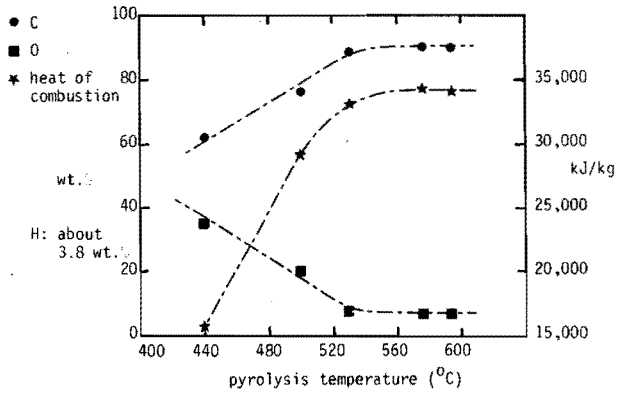

Fig.5.4 Pyrolysis experiments on shredded thin cardboard. Elemental composition and heat of combustion of char (from 1st cyclone) versus pyrolysis temperature (on ash free basis)

5.2.2.2 Experiments at different water content of the spout gas, different solid feed particle size, different solid feed rates and total gas rates.

During pyrolysis of (fractions from)wet domestic waste the water content of the gas in the reactor may be high. The influence of the water concentration was investigated for this reason in experiments nos. 6 and 7 by injecting steam into the spout gas. The amount of steam injected was equivalent to the water present in a solid feed containing 17.8 wt.% of water in experiment no. 6 and 24.3 wt.% of water in experiment no. 7.

The influence of the particle size of the feed was investigated in experiment no. 8 by using relatively large pieces of cardboard as a feedstock (particles of up to 8 mm in diameter as against 3.4*1.6*0.18 mm^3 in the other experiments).The cardboard used in this experiment has about the same moisture content and - expressed on ashfree basis - the same elemental composition as the shredded thin cardboard used in the other experiments. Data on the cardboard used in exp. no. 8 and a comparison of this cardboard to the thin cardboard used in the other experiments are presented in tables 5.5 and 5.6.

Table 5.5 Data on the larger size cardboard used in exp. no. 8.

Particle size: particle diameter		≤ 8 mm
particle thickness		1-2 mm
Moisture content	(wt.%)	6.6
Elemental composition (wet basis)		
C	(wt.%)	39.0
H	(wt.%)	5.6
O	(wt.%)	44.7
Ash	(wt.%)	10.7
Heat of combustion	(kJ/kg)	15,075

Table 5.6 Composition of the larger size cardboard compared to that of the thin cardboard used in the other experiments (on ashfree basis).

		larger size cardboard	standard cardboard
Elemental composition			
C	(wt.%)	43.7	42.5
H	(wt.%)	6.3	6.2
O	(wt.%)	50.0	51.3
Heat of combustion	(kJ/kg)	16,950	16,200

High gas flow rates were applied in experiments nos. 9 and 10 while in experiment no. 10 a high solid feed rate was used at the same time. Table 5.7 shows the reaction conditions used in these experiments. Table 5.8 presents the product distributions obtained in the experiments where steam was added to the spout gas. The table compares these product distributions to those obtained under similar conditions but without addition of steam to the spout gas. These last product distributions(a and b) were read from fig. 5.1 that summarizes data from experiments nos. 1 through 5. Table 5.9 shows properties of the products obtained in the experiments where water was added to the spout gas. These properties are again compared to those of products obtained under similar conditions but without addition of water to the spout gas. The last properties were read from figs. 5.2 through 5.4. Table 5.10 pre-

Table 5.7 Experimental conditions of the second series of experiments with shredded thin cardboard.

Exp.no. (-)	materials fed	rate at which materials fed (kg/hr)		total gas flow rate (m^3/sec)[1]	reaction temp.(°C)	[2]
6	standard cardboard + steam	7.1 1.0	8.1	$8.04*10^{-3}$(incl. of steam)	485	x
7	standard cardboard + steam	9.0 2.2	11.2	$7.47*10^{-3}$(incl. of steam)	453	x
8	larger size cardboard	5.5		$7.49*10^{-3}$	484	x
9	standard cardboard	7.0		$11.67*10^{-3}$	465	
10	standard cardboard	24.2		$11.86*10^{-3}$	463	x

[1]) m^3 of gas at 1 atm. of absolute pressure and 20°C.

[2]) It has been mentioned before that the electrostatic precipitator has been replaced by a new one in the course of this series of experiments. The runs carried out after the new electrostatic precipitator had been installed are marked with an "x" as experiments 6 through 10 have not been carried out in this sequence.

Table 5.8 Product distributions obtained in experiments with shredded thin cardboard at different water content of spout gas (different equivalent moisture content of solid feed) on basis of moisture - and ashfree feed.

Exp.no. (-)	Temperature (°C)	Equivalent moisture content of solid feed (wt.%)	Product distribution (wt.%) char	tar	water	gas	total
6	485	17.8	8.8	40.4	33.7	8.7	91.6
a*)	485	5.7	12	37	41	9	99
7	453	24.3	15.9	34.8	39.8	9.8	100.3
b*)	453	5.7	19	28	45	7	99

*) Data read from fig. 5.1.

sents the product distributions that were obtained in the experiment with larger size cardboard and in those where the solid feed rate and total gas flow rate were varied. The properties of the products obtained in these experiments are shown in table 5.11. For easy comparison tables 5.10 and 5.11 also provide data read from figures 5.1 through 5.4 that summarize experiments nos. 1 through 5.

Table 5.9 Properties of products (on ash free basis) obtained in experiments with shredded thin cardboard at different water content of spout gas.

		exp.no.→	6	a*)	7	b*)
tar (from	C	(wt.%)	49.8	50	51.2	50
electrostatic	H	(wt.%)	6.4	6.3	6.4	6.3
precipitator)	O	(wt.%)	43.8	43	42.4	42.5
char from	C	(wt.%)	79.9	74	79.3	65
1st cyclone	H	(wt.%)	4.3	3.75	4.3	3.75
	O	(wt.%)	15.8	22	16.4	31
char from	C	(wt.%)	70.2		71.0	
2nd cyclone	H	(wt.%)	2.6		4.2	
	O	(wt.%)	27.2		24.8	
gas	CO_2	(vol.%)	53.8	40	40.1	48
	H_2	(vol.%)	0.9	2.5	2.2	2
	CH_4	(vol.%)	3.9	3.5	5.5	2.5
	CO	(vol.%)	41.4	53.5	52.2	46.5
heat of cumbustion		(kJ/m^3)	6,750	8,600	8,075	6,600
TOC of water fraction		(wt.%)	15.8		12.5	

*) Data read from figs. 5.2 through 5.4.

Table 5.11 Properties of products (on ash free basis) obtained in experiments on shredded cardboard using different particle sizes, different solid feed rates and different total gas rates.

		exp.no.→	8	c*)	9	d*)	10
tar (from	C	(wt.%)	55.4	50	50.5	50	50.4
electrostatic	H	(wt.%)	6.9	6.3	6.4	6.3	6.1
precipitator)	O	(wt.%)	37.7	43	43.1	43.5	43.5
char from	C	(wt.%)	81.7	74	70.1	69	88.8
1st cyclone	H	(wt.%)	5.1	3.75	4.3	3.75	4.9
	O	(wt.%)	13.2	22	25.6	27	6.3
char from	C	(wt.%)	74.7		64.8		66.0
2nd cyclone	H	(wt.%)	5.0		4.6		4.8
	O	(wt.%)	20.3		30.6		29.2
gas	CO_2	(vol.%)	48.4	40	47	45	38.5
	H_2	(vol.%)	2.2	2.5	2	2	2
	CH_4	(vol.%)	8.0	3.5	3	3	2
	CO	(vol.%)	41.4	53.5	48	50.5	57.5
heat of combustion		(kJ/m^3)	8,350	8,600	6,750	7,200	7,500
TOC of water fraction		(wt.%)	11.4		10.4		13.8

*) Data read from figs. 5.2 through 5.4.

Table 5.10 Product distributions obtained in experiments on shredded cardboard using different particle sizes, different solid feed rates and different total gas rates (basis moisture- and ash free feed).

Exp.no. (-)	Temp. (^{o})	Gas flow rate (10^{-3} m^3/sec)*)	Solid feed rate (kg/hr)	Feed particle size (mm)	Product distribution (wt.%) char	tar	water	gas	total
8	484	7.49	5.5	< 8 * < 2	14.7	35.5	35.4	12.1	97.7
c**)	484	7.30	7.85	3.4*1.6*0.18	12	37	41	9	99
9	465	11.67	7.0	3.4*1.6*0.18	11.4	38.3	46.8	8.3	104.8
d**)	465	7.30	7.85	3.4*1.6*0.18	15	32	44	8	99
10	463	11.86	24.2	3.4*1.6*0.18	11.1	34.8	39.1	3.8***)	88.8 ***)

*) m^3 of gas at 1 atm. of absolute pressure and 20^{o}C.

**) Data read from fig. 5.1.

***) These values must be higher as a considerable gas leak was detected in the reactor afterwards.

5.2.2.3 Additional data on the experiments and products

A. The material balances given in the preceding paragraphs show deficits of a few wt.%. Table 5.12 shows a typical material balance.

Table 5.12 Material balance for exp.no.3 (basis ash free and moisture free feed = 100 wt.%).

	Input (wt.%)	Output (wt.%)					Difference (wt.%)
		tar	char in both cyclones	water phase	gas	total	
C	45.1	19.2	6.5	8.0	6.8	40.5	- 4.6
H	5.9	2.3	0.3	2.8	0.3	5.7	- 0.2
O	49.0	17.1	0.6	21.9	10.4	50.0	+ 1.0
Total	100.0	38.6	7.4	32.7	17.5	96.2	- 3.8

The deficit for carbon and the surplus of oxygen shown by the material balance of table 5.12 were found in the balances over most experiments. Apart from inavoidable inaccuracy in the elemental analysis the most important sources of errors are:

1. deposition of char type material on the walls of the reactor.
2. the aqueous products obtained contain some organic particles. These probably are very fine droplets of tar that have passed through the electrostatic precipitator. The presence of organic particles are apt to lead to low results in the total organic carbon analysis which measures carbon content of dissolved substances.
3. at the end of each experiment some tar is found to have adhered to the walls of the tar condensor and the electrostatic precipitator. This material was found to have a higher carbon content and a lower oxygen content than the tar which had been collected from these separation units in the normal manner and that has been sampled for use in the elemental analysis.

B. The density of the tar obtained in the pyrolysis experiments of shredded thin cardboard was 1100 $\pm$ 40 kg/m^3.

C. The tar contained about 4 wt.% of water (tar from electrostatic precipitator obtained in exp.no. 6).

D. The viscosity of the tar from the electrostatic precipitator, obtained in exp. no.6 is given in fig. 5.5 as a function of temperature and the amount of water that has been added to it.

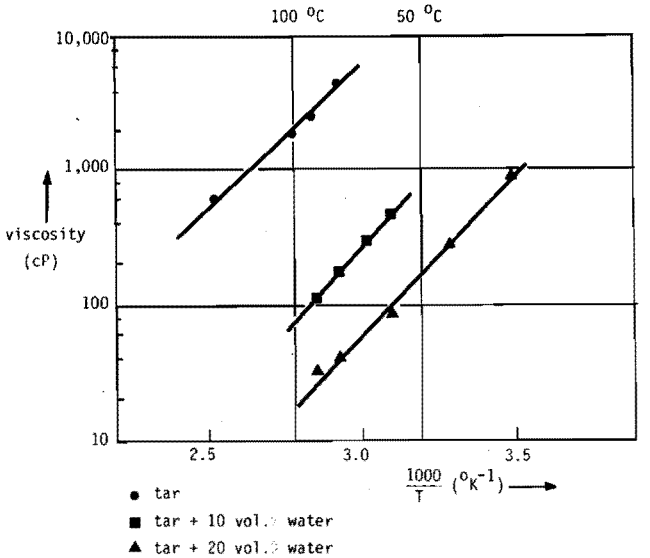

Fig.5.5 Viscosity of tar from electrostatic precipitator as a function of temperature and amount of water added to tar

5.3 Pyrolysis experiments with fractions from shredded domestic waste.

5.3.1 Aim of the experiments

It has been mentioned before that the pyrolysis experiments on fractions from shredded domestic waste were undertaken to demonstrate the suitability of the low temperature pyrolysis process for handling fractions from Dutch domestic waste. The experiments were to provide us with information about some technical aspects of the process, about the environmental impact of the process and about composition and properties of the products. In addition, an economic evaluation of the process was to be carried out. This evaluation was based also on the outcome of these experiments. The influence of various reaction conditions on the pyrolysis process was studied using shredded cardboard as a feedstock in the pyrolysis experiments. The reasons for carrying out these expe-

riments have been stated above (§ 5.2.1). A series of pyrolysis experiments using fractions from shredded domestic waste as a feedstock was planned, however, to verify if the results obtained in the experiments using cardboard as a feedstock give indeed a good picture of the pyrolysis of (organic) fractions from domestic waste.It was decided to investigate the influence of reaction temperature on the pyrolysis of fractions from shredded domestic waste in the same temperature range where the cardboard pyrolysis runs had been carried out as the reaction temperature is one of the most important factors influencing the pyrolysis process. Other conditions in this first series of experiments with fractions from shredded domestic waste were kept as identical as possible to those that were used in the cardboard pyrolysis experiments. The series of experiments was partly used also to study the properties of the pyrolysis products and, to a lesser extent, the environmental impact of the pyrolysis process. More information about environmental aspects of the low temperature pyrolysis of domestic waste were to be provided by the second series of experiments in which much attention was given to the possible occurence of components in (by)products that might be harmful to the environment. Additional analyses of a specific nature were required for this purpose (see § 4.4). Data on the domestic waste fractions that were used as a feedstock in the experiments have been given in table 4.4.

5.3.2 Experimental conditions and results

The conditions of the first experiments with fractions from shredded waste are not discussed and not shown in table 5.13. The separation of the tar mist from the gas was unsatisfactory in these experiments because of poor performance of the electrostatic precipitator. This was due to the fact that the tar obtained by pyrolysis of domestic waste fractions had quite different properties from that prepared through pyrolysis of cardboard. These 2 types of tar differed, f.i., in viscosity and dielectric constant. Some changes were therefore made in the design of the electrostatic precipitator to achieve better operation of the apparatus (Chapter 3). After this unexpected interruption two series of experiments on the organic fraction from shredded domestic waste have been carried out.

5.3.2.1 Experiments at different temperatures

Experimental data on the series of experiments at different reaction temperatures are given in table 5.13.

Table 5.13 Experimental conditions of series of experiments on organic fractions from shredded domestic waste at different temperatures.

exp.no.	solid feed rate (kg/hr)	moisture content of feed (wt.%)	ash content of feed (wt.%) on dry basis)	temp. (°C) **)	fluidisation gas rate*) (10^{-3} m^3/sec)	spout gas rate*) (10^{-3} m^3/sec)	total gas rate*) (m^3/sec)
I	5.0	8 ± 1	19 ± 1	451	3.35	4.06	7.41
II	4.1	3.0 ± 0.1	15 ± 2	453	5.06	5.18	10.24
III	5.2	5.9 ± 0.1	12.5 ± 0.2	478	3.49	4.43	7.92
IV	5.3	3.9 ± 0.1	12.3 ± 0.2	483	3.49	4.13	7.62
V	4.6	3.8 ± 0.1	18.5 ± 0.1	503	3.20	4.58	7.78
VI	5.5	2.9 ± 0.1	14 ± 0.5	524	3.30	4.43	7.73
VII	5.1	7.9 ± 0.2	12.3 ± 0.2	545	3.84	4.80	8.64

*) m^3 of gas at 1 atm. of absolute pressure and 20°C.
**) The variation in temperature in each experiment was less than 8°C.

The product distributions obtained are presented in table 5.14 and summarized in fig. 5.6. Table 5.15 presents elemental composition and heats of combustion of the tar and the char together with the total

Table 5.14 Product distributions measured in series of experiments with fractions from shredded domestic waste at different temperatures (basis moisture- and ash free feed).

exp.no.	temp. (°C)	Product distribution in wt.% gas	water phase	tar	char in both cyclones	total
I	451	15.6	34.9	19.4	20.4	90.3
II	453	13.4	40.3	8.4	20.8	82.9
III	478	16.2	38.4	15.7	22.3	92.6
IV	483	16.9	42.4	14.4	19.9	93.6
V	503	21.0	42.3	12.9	19.1	95.3
VI	524	21.7	38.9	19.3	14.6	94.5
VII	545	25.4	37.5	14.8	17.5	95.2

organic carbon contents of the water fractions produced and the compositions of the gases that were obtained. The properties of the various products are summarized in figs. 5.7, 5.8 and 5.9.

Table 5.15 Series of experiments on fractions from shredded domestic waste at different temperatures. Properties of products (ash free basis).

		exp.no. →	I	II	III	IV	V	VI	VII
		temp.(°C) →	451	453	478	483	503	524	545
tar (from	C	wt.%	81.9	81.6	81.1	79.7	77.9	81.9	81.8
electrostatic	H	wt.%	12.0	12.2	12.3	11.7	11.3	12.3	12.3
precipitator)	N	wt.%	0.9	0.6	0	0.7	1.3	0.5	0
	O[1]	wt.%	5.2	5.6	6.6	7.9	9.5	5.1	5.7
	S	wt.%	-[3]	-	-	-	-	0.1	0.1
	Cl	wt.%	-	-	-	-	-	0.1	0.1
heat of combustion[2]		kJ/kg	44,350	44,500	44,350	42,800	41,400	44,825	44,700
char (from	C	wt.%	69.7	78.4	71.5	83.0	81.4	81.7	81.0
1st cyclone)	H	wt.%	5.1	5.2	4.3	4.8	4.5	3.8	3.9
	N	wt.%	2.0	2.5	1.5	1.3	2.8	2.6	1.4
	O[1]	wt.%	23.2	13.9	22.7	10.9	11.3	6.8	10.7
	S	wt.%	-	-	-	-	-	1.1	0.8
	Cl	wt.%	-	-	-	-	-	4.0	2.2
heat of combustion[2]		kJ/kg	27,450	31,775	26,900	33,075	32,075	31,825	31,150
gas	CO_2	vol.%	54	56.5	50		46.5	39	33
	H_2	vol.%	2	2.5	3	not	3.5	4.5	5
	CH_4	vol.%	6	5	6	measured	7.5	9	9
	CO	vol.%	38	36	41		42.5	47.5	52
	C_2H_6	vol.%	-	-	-		-	-	1
heat of combustion[2]		kJ/m³	6,725	6,200	7,150		7,875	9,125	10,300
TOC of water fraction		wt.%	13.0	9.7	13.0	13.3	9.9	8.5	11.8

[1]) By difference. These figures include sulphur and chlorine content unless separate values for sulphur and chlorine content are given.

[2]) Calculated value.

[3]) - = not measured.

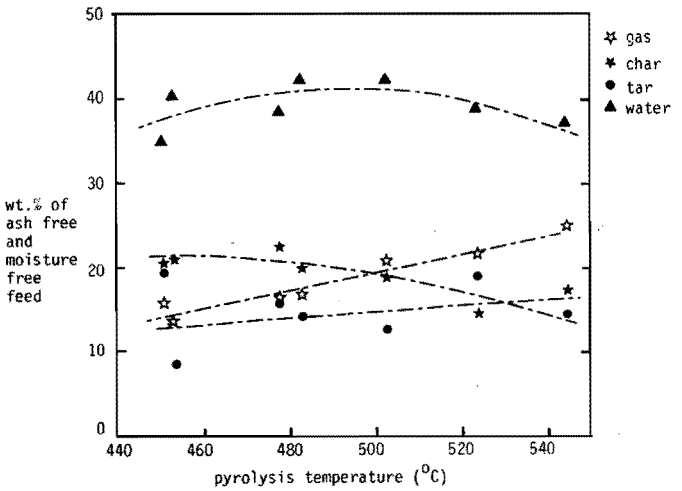

Fig.5.6 Pyrolysis experiments on fractions from shredded domestic waste. Product distribution versus pyrolysis temperature (basis ash free and moisture free feed)

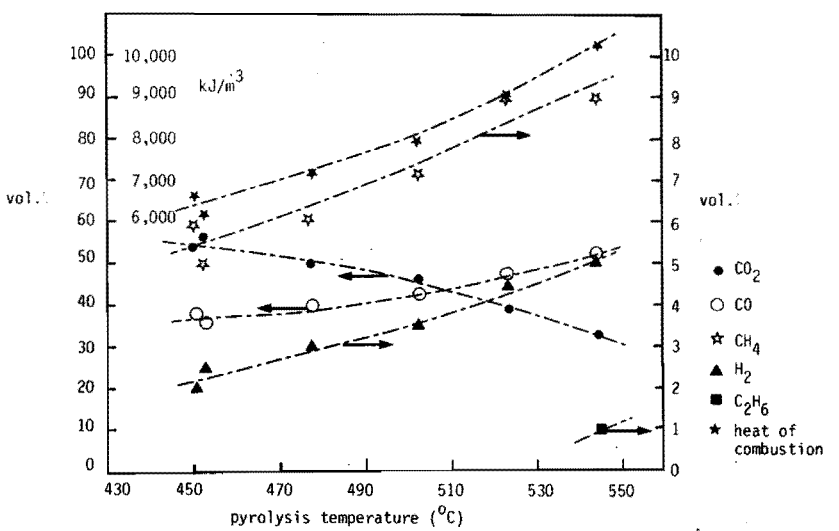

Fig.5.7 Pyrolysis experiments on fractions from shredded domestic waste. Gas composition and heat of combustion of the gas versus pyrolysis temperature.

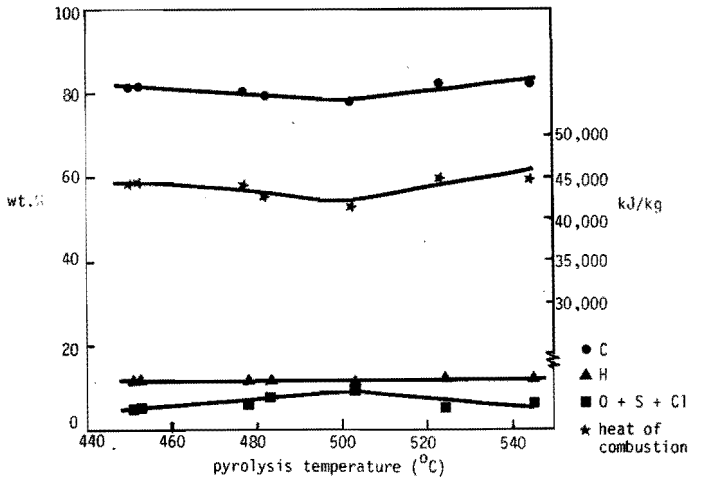

Fig.5.8 Pyrolysis experiments on fractions from shredded domestic waste. Elemental composition and heat of combustion of tar (from electrostatic precipitator) versus pyrolysis temperature (ash free basis)

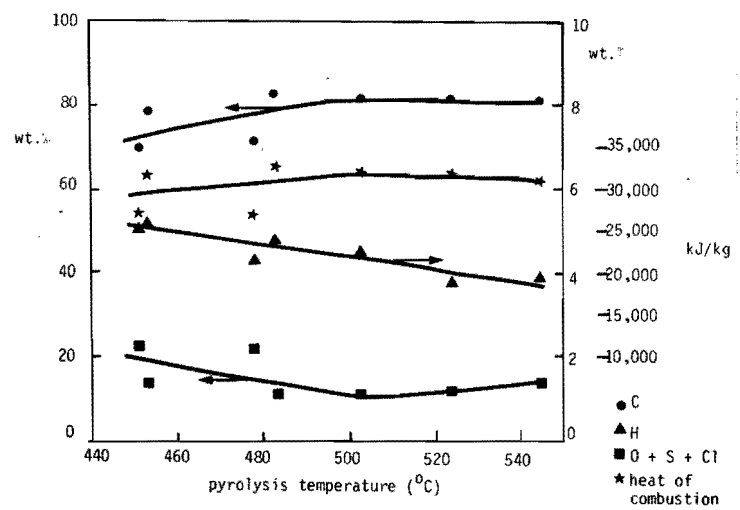

Fig.5.9 Pyrolysis experiments on fractions from shredded domestic waste. Elemental composition and heat of combustion of char (from 1st cyclone) versus pyrolysis temperature (ash free basis)

5.3.2.2 Other experiments

The experimental conditions of the other experiments on organic fractions from shredded domestic waste are given in table 5.16.

Table 5.16 Experimental conditions of second series of experiments on fractions from shredded domestic waste at different temperatures.

exp. no.	solid feed rate (kg/hr)	moisture content of feed (wt.%)	ash content of feed (wt.% on dry basis)	temp. (^{o}C)	fluidisation gas rate *) (10^{-3} m^3/sec)	spout gas rate *) (10^{-3} m^3/sec)	total gas rate *) (10^{-3} m^3/sec)
VIII	7.3	3.4	17.8	480-500	3.49	4.36	7.85
IX	8.5	12.0	32.2	512	4.03	4.21	8.24
X	8.8	8.2	34.5	399	4.13	4.21	8.34

*) m^3 of gas at 1 atm. of absolute pressure and 20^{o}C.

Additional information: after experiment no. VIII the 120^{o} zig zag air classifier used in the preparation of the RDF fractions was no longer available. A 105^{o} zig zag air classifier was used from them on.

The product distributions of the experiments that were carried out to investigate the presence of f.i. chlorine containing contaminants in the pyrolysis gas and the water fraction are presented in table 5.17. Table 5.18 presents the product distribution obtained in an experiment at extremely low pyrolysis temperature. The properties of the products obtained in the experiments(elemental compositions, heats of combustion etc.) are shown in tables 5.19 and 5.20.

Table 5.17 Pyrolysis experiments on fractions from shredded domestic waste to determine Cl containing contaminants in gas and water phase. Product distributions on basis of moisture- and ash free feed.

exp.no. (-)	temp. (^{o}C)	product distribution in wt.% gas	water phase	tar	char in both cyclones	total
VIII	480-500	17.1	32.4	24.0	22.6	96.1
IX	512	16.4*)	24.0	27.9	27.4	95.7

*) gas leak

Table 5.18 Pyrolysis experiment on a fraction from shredded domestic waste at very low pyrolysis temperature. Product distribution on basis of moisture- and ash free feed.

exp.no. (-)	temp. (^{o}C)	product distribution in wt.% gas	water phase	char in both cyclones	tar	total
X	399	13.6	31.0	28.8	22.8	96.2

Table 5.19 Pyrolysis experiments on fractions from shredded domestic waste to determine Cl containing contaminants in gas and water phase. Properties of products (ash free basis).

		exp.no. →	VIII	IX
		temp.(^{o}C) →	480-500	512
tar (from	C	wt.%	76.1	81.4
electrostatic	H	wt.%	10.6	12.2
precipitator)	N	wt.%	1.3	0.5
	O	wt.%	11.1	5.5
	S	wt.%	0.1	0.2
	Cl	wt.%	0.8	0.2
heat of combustion	(calculated)	kJ/kg	39,550	44,475
	(determined)	kJ/kg	38,950	-
char (from	C	wt.%	75.7	73.9
1st cyclone)	H	wt.%	5.6	4.8
	N	wt.%	2.5	2.4
	O	wt.%	12.0	15.1
	S	wt.%	0.5	0.4
	Cl	wt.%	3.8	3.4
heat of combustion	(calculated)	kJ/kg	31,800	29,550
	(determined)	kJ/kg	26,575	-
char (from	C	wt.%	71.6	72.2
2nd cyclone)	H	wt.%	4.4	4.6
	N	wt.%	2.2	2.5
	O	wt.%	17.8	17.1
	S	wt.%	0.6	0.5
	Cl	wt.%	4.2	3.1
gas	CO_2	vol.%	54	50
	H_2	vol.%	3.5	5
	CH_4	vol.%	8.5	10
	CO	vol.%	34	35
	HCl	ppm	< 5	< 5
heat of combustion		kJ/m^3	7,075	7,975
water phase	TOC	wt.%	10.0	12.2

Table 5.20 Pyrolysis experiment on a fraction from shredded domestic waste at very low pyrolysis temperature. Properties of products (ash free basis).

		exp.no.	X
		temp.(^{o}C)	399
tar (from	C	wt.%	76.4
electrostatic	H	wt.%	11.1
precipitator)	N	wt.%	1.0
	O	wt.%	11.0
	S	wt.%	0.2
	Cl	wt.%	0.3
heat of combustion *)		kJ/kg	40,400
char (from	C	wt.%	69.4
1st cyclone)	H	wt.%	6.4
	N	wt.%	3.3
	O	wt.%	17.6
	S	wt.%	0.4
	Cl	wt.%	2.9
heat of combustion *)		kJ/kg	30,175
gas	CO_2	vol.%	76.5
	H_2	vol.%	2
	CH_4	vol.%	4.5
	CO	vol.%	17
	HCl	ppm	< 7
heat of combustion *)		kJ/m^3	3,700
water phase	TOC	wt.%	13.3

*) Calculated value.

5.3.2.3 Additional data on the pyrolysis products

A. The char.

1. The density of the char particles (including air in pores) obtained in the pyrolysis experiments with shredded domestic waste fractions is 550 $\pm$ 50 kg/m^3.

2. The char obtained in the pyrolysis experiments on fractions from shredded domestic waste contains considerable amounts of ash. The chars obtained in experiments nos. I through IX have ash contents between 39.2 and 49.6 wt.%.
3. Leaching tests were carried out on the ash of the char. The amounts of heavy metals that were leached from the char ash are presented in table 5.21. In the last column of this table the norms are given that are mentioned in the Dutch Law on Chemical Wastes [5.1, 5.2, 5.3]. When any one of these norms is exceeded the material (in this case the char ash) is a chemical waste according to Dutch law.

Table 5.21 Amounts of heavy metals leached from char ash (in ppm = µg/g ash). Ash from char obtained in experiment no. II.

Metal	leaching with distilled H_2O (after 7 days)	leaching with H_2SO_4 0.8 n. (after 7 days)	boiling with HNO_3 1:1	Norms (Dutch law on Chemical Wastes
Fe	0	7640	11000	-
Al	0	45800	51600	-
Pb	0	0	0	5,000
Zn	2	1160	1530	20,000
Cd	0	8	8	50
Cr[1)]	64	140	150	Cr(VI)50 Cr(III)5,000
Cu	0	190	220	5,000
Ni	8	17	46	5,000

[1)] No distinction could be made in the tests between Cr(III) and Cr (VI).

B. The tar

1. The density of the tar obtained in the experiments on fractions from shredded domestic waste varies between 1060 and 1130 kg/m^3 at 20^{o}C.
2. The tars from the electrostatic precipitator obtained in the pyrolysis experiments on fractions from shredded domestic waste did have ash contents of less than 1 wt.% (0.1 to 0.9 wt.%), in most cases less than 0.3 wt.%. The ash content of tars from the tube cooler was somewhat higher but still less than 5 wt.%.

3. The water content of the tar is very low. A moisture content of only 0.2 wt.% was measured for the tar collected from the electrostatic precipitator in exp.no. V.
4. The viscosities of tars obtained in exps.nos. V and X respectively are shown as a function of the temperature in figs. 5.10 and 5.11. The viscosity measured by means of the Brookfield viscosimeter (Chapter 4) yielded somewhat different values for the viscosity when different immersion bodies and different speeds of rotation were applied. Increasing the speed of rotation led to a small decrease in the measured value of the viscosity. The use of a larger immersion body led to a decrease in the measured value of the viscosity, too. This indicates that the tar is not a Newtonian fluid but shows some resemblance to pseudo-plastic materials.
   The lines that are shown in figs. 5.10 and 5.11 are lines that were fitted to data points obtained with different immersion bodies and at different speeds of rotation of the bodies. Deviations have been observed from these lines up to 20%.
   The viscosity of the tar (or rather: ln η) as a function of reciprocal temperature may in very rough approximation be described by two straight lines with different slopes. The tar is highly sensitive to the temperature in the low temperature range but is far less sensitive to the temperature at higher temperatures (above about $90^{o}C$). This might be explained by assuming that the tars contain solid fractions that melt at temperatures of about 90-$95^{o}C$. It was observed during the viscosity determinations that the tar was not homogeneous at low temperatures.

C. Water fraction

1. The water phase has an unpleasant and burnt odor even after it has been diluted with 1000* its volume of water.
2. The pH value of the water phase can be as low as 3 (water phase of exp.no.I).
3. Values for BOD_9 (biological oxygen demand after 9 days) for the undiluted water phase were calculated from determinations carried out on strongly diluted solutions of the water phase. The period of 9 days appeared to be required to bridge the lag time period. The BOD_9 for the indiluted water phase obtained in this manner is up to 400

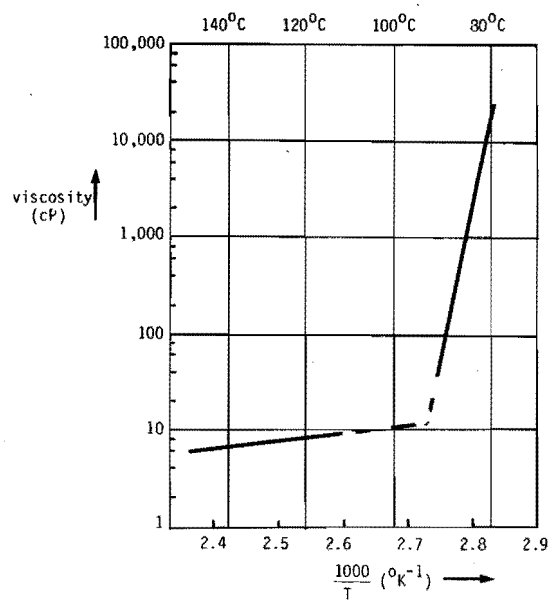

Fig.5.10 Viscosity of tar obtained in exp.no.V from electrostatic precipitator as a function of temperature

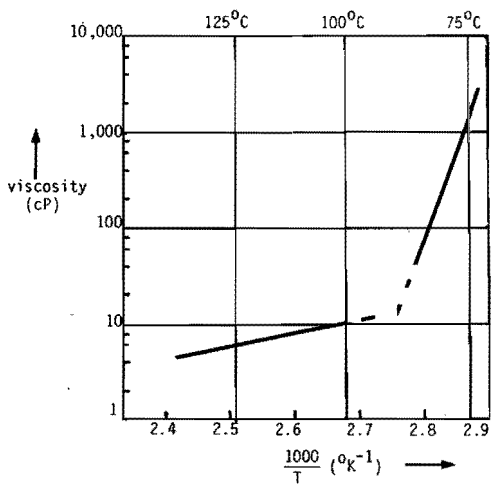

Fig.5.11 Viscosity of tar obtained in exp.no.X from electrostatic precipitator as a function of temperature

kg O_2/m^3 of water phase. The COD (chemical oxygen demand) was about 20% higher.

4. Samples were taken from the water collected in the cooling tower in the experiments VIII, IX and X. These samples were analysed for the presence of chlorine containing organic compounds and polycyclic compounds. Various extraction agents were used to extract the water samples (n-butanol, n-pentanol, di-ethylether etc) and the solutions thus obtained were analysed by means of GC/MS (see § 4.4). The results are presented in table 5.22 which summarizes the results obtained using different extraction agents. The water samples taken in experiments nos. VIII, IX and X all contained the same organic compounds. Only minor differences in peak heights in the chromatograms were observed. Figs. 5.12 and 5.13 present typical chromatograms obtained in analysing the water samples. Fig. 5.13 also shows mass spectra for selected mass fragments. Spectra showing a peak at a mass of 35 or 36 are typical for the presence of organic chlorine.
No chlorine containing organic compounds could be traced.

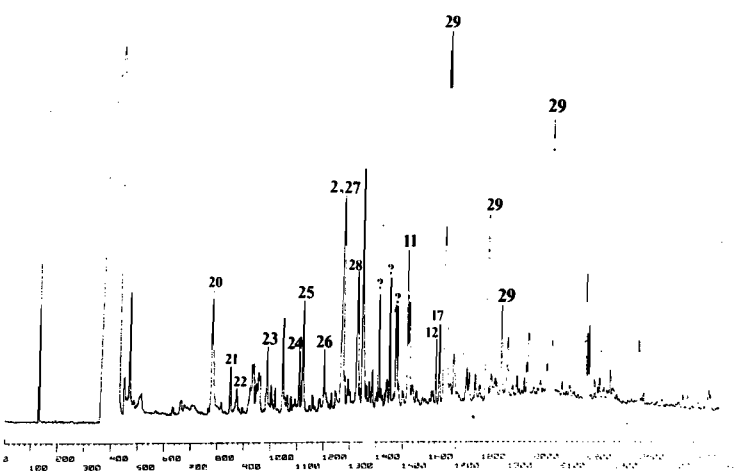

Fig.5.12 Chromatogram of water phase

Table 5.22 Organic compounds identified in water phase (numbers refer to peaks indicated in figs. 5.12 and 5.13).

1	acetone
2	2-hydroxy-3-methyl-1-cyclopentenone
3	3-methyl-2-cyclopentenone
4	5-methoxy-1,3-dimethyl-pyrazol
5	phenol
6	2-methoxy-phenol
7	4-methyl-phenol
8	3-methyl-phenol
9	3,4-dimethyl -phenol
10	3,4-dimethoxy-phenol
11	2-methylphenol
12	2,5-dimethylphenol
13	ethanone
14	heptanone
15	4-H-pyran-4-one, 3-hydroxy-2-methyl
16	quinoline
17	1,2-dimethoxy benzene
18	2H-azepin-2-one, hexahydro
19	benzoic acid
20	2-methyl-1-pentene
21	trimethyl pyrazine
22	imidazol
23	3,4-heptadiene
24	2-ethyl,6-methyl pyrazine
25	trimethyl pyrazine
26	cyclo-octene
27	pyrazol
28	2,4-dimethyl-cyclopentadione
29	O-furan-compounds
30	furanone

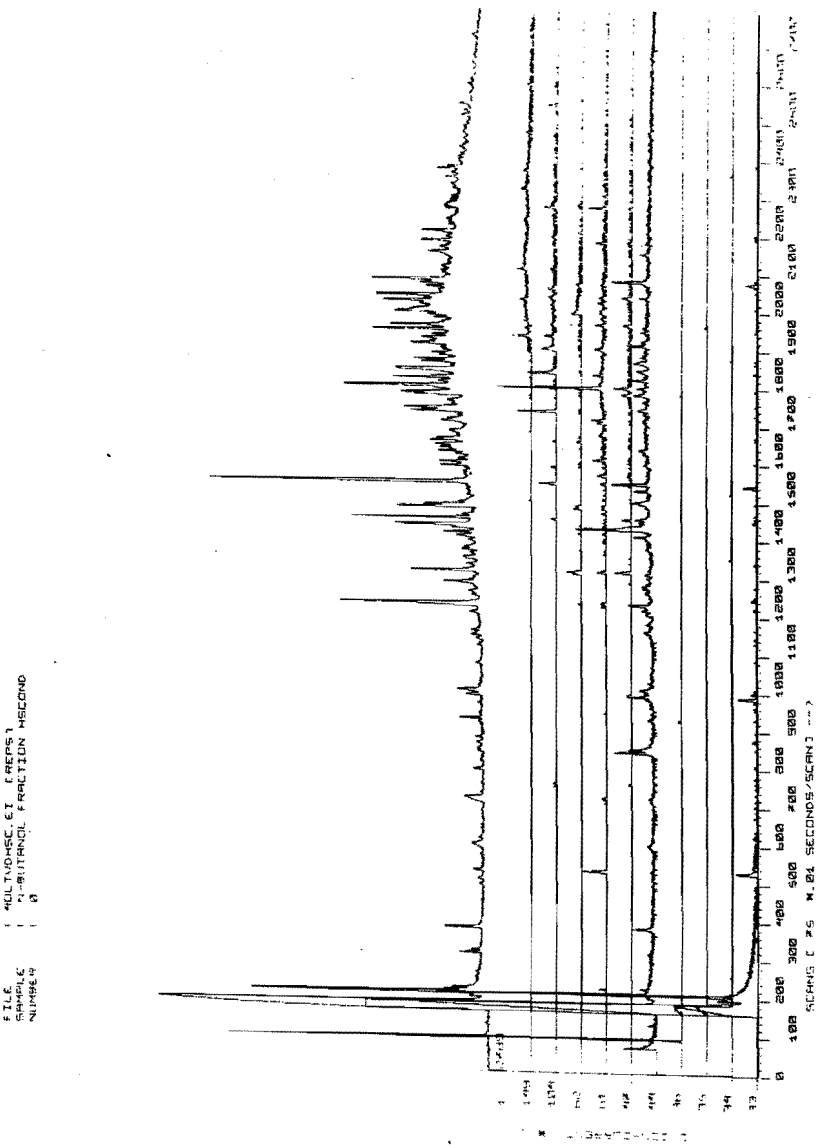

Fig.5.13 Chromatogram and mass spectrum of water phase

D. The gas phase

Unfortunately, the analysis of the gas phase with respect to the presence of chlorine containing organic compounds and polycyclic aromatics in it was not yet completed at the time when this thesis was published.

E. Additional information about the experiments

1. Not all materials that have been fed to the pyrolysis reactor during the experiments on fractions from shredded domestic waste did leave the reactor: some accumulation of material in the bed took place. The amount of material (almost entirely inorganic) that accumulated in the bed varied between 1-10 wt.% of the total input depending on the ash content of the feedstock and the gas flow rate in the reactor. This amount corresponds to 10-50 wt.% of the ash content of the feed.
2. Experiment no. X in which a very low pyrolysis temperature was applied showed an accumulation of material in the bed of 16 wt.% of the feed. Contrary to what was found in the other experiments, the material that had accumulated in the bed contained a considerable amount of organics. The fraction of the material > 1 mm did have an ash content of 48 wt.% only.

Literature

5.1 Staatsblad van het Koninkrijk der Nederlanden, jaargang 1976, 214 (1976).
5.2 Staatsblad van het Koninkrijk der Nederlanden, jaargang 1977, 435, (1977).
5.3 Tweede kamer der Staten Generaal, 2, zitting 1980 - 1981, 16524, nos. 1,2,3,4 (1981).

6. DISCUSSION OF EXPERIMENTAL RESULTS

6.1 Introduction

In this chapter the experimental results of the pyrolysis of shredded thin cardboard and fractions from shredded domestic waste in a spout-fluid bed reactor are discussed and compared to each other. An attempt is made to explain the observed influences of various process conditions on the pyrolysis and the differences that have been observed between the pyrolysis of cardboard and the pyrolysis of domestic waste fractions. The fundamental aspects that were discussed in Chapter 2 will be of help in explaining the observed phenomena. Attention will be paid to the environmental impact of the pyrolysis process.The properties of the products gas, tar, char and water phase will be discussed in some detail.

6.2 The pyrolysis of shredded thin cardboard

6.2.1 The influence of reaction temperature

From the results in § 5.2.2.1 (experiments at different temperatures: tables 5.3 and 5.4 and figs. 5.1 through 5.4) the following phenomena are seen to occur with increasing reaction temperature:

a. The tar yield shows a maximum at a reaction temperature of about 500-525^{o}C.
b. As tar yield decreases with increasing reaction temperature above 500^{o}C gas yield increases strongly.

It is felt that phenomena a. and b. may both be due to secondary cracking reactions of the pyrolysis tar that occur faster at higher temperatures and in which gaseous compounds are important products (see paragraphs 2.2.2.1 and 2.3.1).

c. The heat of combustion of the gas increases with increasing reaction temperatures. This is due to the fact that CO, H_2 and hydrocarbon contents of the gas increase with increasing reaction temperature whereas the CO_2 content of the gas decreases. These changes in gas composition are probably due to the occurrence at higher temperatures of other reactions that involve the release of less CO_2 and more CO, H_2 and hydrocarbons. The degradation of dehydrocellulose and the cracking of the tar (see also fig. 6.1, § 6.3.1) involve two sets of reactions that differ from each other in that they lead to the formation of two gases that have compositions which are not the same.

The shift to more CO and H_2 at the expense of CO_2 content of the gas cannot be ascribed to reactions like $C+CO_2 \rightleftarrows CO_2$ or $C+H_2O \rightleftarrows CO+H_2$ as these reactions play a role only at higher temperatures (above 700-800°C).

d. The amount of char produced per kg of cardboard decreases with increasing reaction temperature. With increasing reaction temperature more cellulose (cardboard) decomposes through depolymerization to tar while less cellulose decomposes to dehydrocellulose which reacts further to give char and gases.
e. The heat of combustion of the char increases with increasing reaction temperature up to a reaction temperature of about 530°C and then remains constant. This is due to an initial increase in the carbon content of the char. This initial increase in the carbon content of the char with increasing temperature might indicate that the conversion of the cardboard at temperatures below 530°C is not yet complete and that amounts of unreacted cellulose or dehydrocellulose still remain present in the char. Some unreacted cardboard particles were indeed found in the char collected from the cyclones in pyrolysis experiments at lower temperatures. In addition, it might be possible that the char obtained in pyrolysis experiments at lower temperatures carbonizes furthermore at higher temperatures.
f. Water yield decreases slowly with increasing temperature.
g. The elemental composition and heat of combustion of the tar appear to be independent of reaction temperature in the temperature range that was considered.

The changes that occur in product distribution and gas composition as reaction temperature increases appear to be those that were to be expected from increasing the cracking severity. Douglas, Webb and Daborn [6.1] found roughly the same changes in their batch experiments on the pyrolysis of paper in tubes. The present, continuous experiments in a spout-fluid bed reactor show a much higher yield of what Douglas c.s. define as "condensate products" (tar + water). This is probably due to the shorter residence time of the tar in the high temperature zone in the present experiments.

6.2.2 The influence of the water content of the spout gas, the solid feed particle size, the solid feed rate and the total gas flow rate

When the equivalent moisture content of the feed is increased by introducing steam into the spout gas, the following phenomena can be observed (see tables 5.8 and 5.9):
A higher moisture content of the feed leads to a relatively low water production during pyrolysis. The tar yield is seen to increase at increasing moisture content of the feed whereas char yield decreases. The influence on gas yield does not seem to be very great. An explanation might be that a water rich atmosphere surpresses the dehydration reaction and thus gives rise to a lower water production and lower char yield.
Increased moisture content of the feed has some effect on the properties of the products also: The carbon content of the char is higher and the oxygen content lower when steam has been introduced into the spout gas. No change in properties of the tar is observed. The nature of the influence of the moisture content of the feed on the gas composition is not quite clear, but the effect does not seem to be very great.

Increasing the particle size of the solid feed results in higher char and gas yields (table 5.10). This may be due to the fact that pyrolysis tar produced inside a reacting particle must find its way to the gas surrounding the particle by diffusing through a hot layer of char. Inside this layer the tar may be subject to cracking. Thus char and gas yield might increase as the length of the diffusion path of the tar is increased, i.e. with greater feed particle size. This might also explain the higher carbon contents of tar and char on ash free basis that occur in the pyrolysis of larger pieces of cardboard. At larger feed particle size the CH_4 and CO_2 contents of the gas are seen to be higher (table 5.11).

Tar yield increases as gas flow rates are increased while less char is produced (table 5.10). This may be due to a shorter residence time of the tar in the high temperature zones which would result in a reduction of secondary cracking. Increasing the gas flow rate seems to have little influence on the elemental compositions and heats of combustion of the tar and char and on the composition of the gas (table 5.11).

Increasing the solid feed rate appears to have little influence on the process as long as the capacity of the reactor or the separation units are not exceeded.

6.2.3 Properties of the pyrolysis products

The pyrolysis gases produced had heats of combustion between 6,200 and 14,000 kJ/m^3 depending on the pyrolysis temperature (table 5.4). This is of course much lower than the heat of combustion of many natural gases (order of 30,000 - 35,000 kJ/m^3).

The pyrolysis tars had a heat of combustion of about 20,000 kJ/kg. This is about half the heat of combustion of a typical no. 6 fuel oil (42,500 kJ/kg). The high viscovity is a disadvantage of pyrolysis tar. This disadvantage may, however, be overcome by adding water to the tar (fig. 5.5).

The pyrolysis char produced here is not a high grade fuel. The elemental composition and heat of combustion of the char have been given in Chapter 5 on ash free basis. The char produced contains ash. As the ash content of the cardboard feedstock is constant and as this ash is almost entirely found back in the char, the ash content of the char increases with increasing pyrolysis temperature because the char yield decreases with increasing reaction temperature. The ash content of the char increases from 16 wt.% in experiment no.1 (at 439^{o}C) up to 28.5 wt.% in experiment no. 5 (at 594^{o}C). The heat of combustion (on total basis) varies from about 17,000 to 26,000 kJ/kg. The pyrolysis char produced thus is less attractive as a fuel than commercial charcoal (ash content 2-3 wt.%, heat of combustion 28,000 - 30,000 kJ/kg). But the low sulphur content is of course advantageous. The char is less suited to be applied as an activated carbon because of its high ash content[6.2].

6.3 The pyrolysis of organic fractions from shredded domestic waste

6.3.1 The influence of reaction temperature

It is seen that as reaction temperature increases (tables 5.14 and 5.15 figs. 5.6 through 5.9):

a. Gas yield increases strongly.
b. The heat of combustion of the gases increases with increasing reaction temperature, due to an increase of CO, H_2 and hydrocarbon contents of the gases with increasing reaction temperature whereas the CO_2 content of the gases decreases.
c. The amount of char produced decreases with increasing reaction temperature.

d. The heat of combustion of the char increases with increasing reaction temperature up to a reaction temperature of about 500°C, due to an increase of carbon content. Above about 500°C the heat of combustion very slowly decreases due to a slightly decreasing hydrogen content whereas carbon content remains constant.

The above phenomena are the same as those that were found in the pyrolysis experiments using shredded thin cardboard as a feedstock (§ 6.2.1).

e. Water production shows a maximum at a reaction temperature of about 500°C.

f. Tar yield seems to increase slowly with increasing reaction temperature. It is hard to judge whether this is really so as the scatter in the data points is rather great.

g. The heat of combustion of the tar is about constant in the temperature range that was considered. Indeed, the heat of combustion does show a minimum at about 500°C due to a minimum in the carbon content but this minimum is, however, shallow. The drop in heat of combustion is only about 7%.

The above phenomena may be explained on the basis of the below simplification of the scheme of the pyrolysis reaction mechanism (fig. 6.1) which has already been discussed in Chapter 2.

Fig. 6.1 Simplified reaction scheme of cellulose pyrolysis.

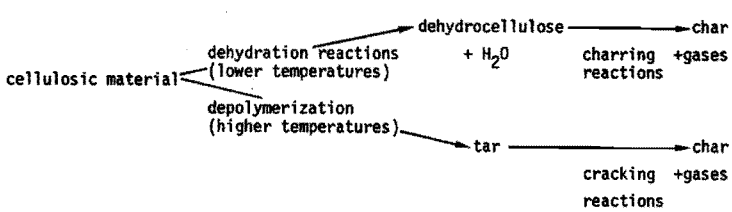

In the below discussion the term "charring reactions" is used to indicate the reaction of dehydrocellulose giving char and gases and the term "cracking reactions" refers to the reactions in which the tar is cracked to give also char and gases. The results of the cardboard pyrolysis experiments that have been discussed before are used to support the explanation of the phenomena observed in the pyrolysis experiments using domestic waste fractions as a feedstock.

Comparison of the results of cardboard pyrolysis on the one hand and pyrolysis of organic domestic waste fractions on the other shows that there are some interesting differences:

1. The char yield in the pyrolysis experiments on organic domestic waste fractions is high and - up to 500°C - almost constant. The experiments on shredded thin cardboard show a sharp decrease of char yield with increasing reaction temperature.
2. The yield of the water phase increases slightly with increasing temperature in the experiments on domestic waste fractions up to a reaction temperature of 500°C. The experiments on cardboard show a decrease of water yield with increasing reaction temperature.
3. The tar yield from pyrolysis of domestic waste fractions is low and does not increase strongly with increasing reaction temperature. In cardboard pyrolysis there is a sharp rise of tar yield with increasing reaction temperature up to 500-525°C. The tar yield decreases at higher reaction temperatures. The tar yield in cardboard pyrolysis is much higher than that obtained in domestic waste pyrolysis in the temperature range that was considered.

The above differences may be due to the influences of the differences in feedstock: Comparison of tables 4.4 and 5.1 shows a considerable difference in ash content of cardboard and domestic waste fractions. In addition, the feedstock particle size shows great differences, too: the cardboard used has uniform dimensions and is very thin (d=0.18 mm) whereas the domestic waste fractions have a particle size distribution going from dust to pieces of 11 mm thickness. The influences that these differences in ash contents and particle sizes may have are discussed separately below.

A. Ash content

It is felt that some of the inorganic compounds present in the domestic waste fractions may as positive catalysts on the dehydration. reactions dominating at lower temperatures (see also paragraph 2.2.2.1). This may explain the slight increase in the yield of the water phase that occurs with increasing temperature in the domestic waste experiments up to 500°C, the high char yield and the low tar production in comparison to cardboard pyrolysis. At higher reaction temperatures the depolymerization reactions appear to become more important than the

dehydration reactions. This might explain the decrease in char and water yield at temperatures above 500°C. The steady increase of gas yield with increasing reaction temperature can be explained by the fact that at higher temperatures the rate of both charring and cracking reactions become greater, which results in increased gas production. That char yield does not also increase with increasing reaction temperature may be explained by assuming that the cracking reactions (which are part of the depolymerization branch of the reaction scheme (fig. 6.1) and may dominate at higher temperatures) yield less char than the charring reactions. Indeed, in the thermoanalytical experiments on cellulose carried out to determine reaction kinetic parameters it is found that the "char yield factor" (= 1 minus gas yield factor) for the tar cracking reactions is only about half the char yield factor for the charring reaction (0.15 and 0.26 kg char/kg reactant respectively). See also Chapter 7. In addition, the char yield was found to decrease with increasing reaction temperature in the experiments on cardboard too, which in fact confirms the latter argument.

B. Feed particle size

The particle size of the shredded domestic waste fractions is on the whole greater than that of the cardboard particles used in the pyrolysis experiments. The larger size may give rise to heat transport limitations and to an increase of secondary cracking reactions of the tar. Limitations in heat transport lead to lower heating rates for the material inside a pyrolysing particle. Lower heating rates may cause a greater part of the cellulosic material to be decomposed according to the dehydration reactions which dominate at lower temperatures. This might explain the slight initial increase in water yield with increasing reaction temperature (assuming incomplete cellulose conversion in the lower temperature range). It might also explain the high char yield in the experiments on domestic waste fractions.
In addition, the length of the diffusion path of the tar through a hot layer of char is increased in case of larger feed particle size (see § 6.2.2). Tar yield will be lower in this case as the tar may be subject to cracking inside this hot layer of char.

Apart from the above discussed influences of ash content and feed particle size the fact remains, of course, that the chemical compositions of

cardboard and domestic waste fractions are not the same. The differences in chemical composition may well influence the differences in pyrolysis behavior of the two feedstocks.

6.3.2 Other pyrolysis experiments

The experiments VIII, IX and X were carried out mainly to investigate some of the environmental aspects of the pyrolysis process, in particular to investigate the presence of chlorine containing organic compounds in the gas and water phases as well as the presence of HCl in the gas. The outcomings of these experiments will therefore be discussed in more detail in the next paragraph (§ 6.3.3) in which attention is paid to the properties of the products obtained in pyrolysing domestic waste fractions. The discussion of the results of the experiments nos. VIII, IX and X in the present paragraph will be limited to a comparison of these experiments with the pyrolysis experiments on fractions from shredded domestic waste that were carried out to investigate the influence of reaction temperature.

Experiment no. VIII

The reaction temperature has been varied during this experiment in the temperature range 480-500°C. The product distribution obtained (table 5.17) is not entirely in line with the product distributions obtained in previous experiments with shredded domestic waste fractions (fig. 5.6): Char and gas yield of experiment no. VIII show good agreement with the yields of char and gas that can be read from fig. 5.6 for the reaction temperatures concerned. The tar yield obtained, however, is higher than is read from fig. 5.6 while the yield of water phase of experiment no. VIII is lower than the water yield to be expected from fig. 5.6 for the reaction temperatures of this experiment.
The chemical composition and heat of combustion of the tar (table 5.19) also show some differences from those that can be read from fig. 5.8: carbon and hydrogen contents are lower and (O+S+Cl)-content is higher, which results in a lower heat of combustion.
No explanation can be given for the observed differences. It might be, however, that the (chemical) composition of the domestic waste fraction used as a feedstock in experiment no. VIII happened to be different from the global composition given in table 4.4. Unfortunately, no elemental analysis has been carried out for the waste fraction used in this

experiment. The speculation that has been given here therefore cannot be shown to be correct.
The observed differences are, in any case, not so great that the analyses of water phase and gas phase cannot be considered representative of all experiments in the discussion of the product properties (§ 6.3.3).

Experiment no. IX

The shredded domestic waste fraction used as feedstock in this experiment is different from the fractions used before in two respects:

1. A 105^{o} zig zag air classifier was used instead of a 120^{o} zig zag air classifier (see § 4.3) to prepare the fractions for experiments nos. IX and X. The use of a different zig zag air classifier had some effect on the composition of the waste fractions as the superficial gas flow rate through the classifier could not be raised as high as in the 120^{o} zig zag air classifier due to limited blower capacity. As a consequence the average particle size of the feedstock prepared thus was smaller than that of the previously prepared waste fractions. The ash content of the fraction prepared thus was higher than that of the previous prepared waste fractions which is rather surprising (see § 4.3).
2. The moisture content of the waste fraction is about twice the average moisture content of the waste fractions used as feedstock in previous pyrolysis experiments.

The influence of the above differences in feedstock composition on the pyrolysis process are contradictory in some respects. A higher moisture content leads to relatively low water production and high tar yields while char yield is lower. On the other hand, a higher ash content leads to more char and less tar production. Smaller particle size again leads to higher tar yields and decreased char and gas yields (§ 6.2.3).
When the results of pyrolysis experiment no. IX are compared with the results of the experiments nos. I through VII (§ 5.3.2.1, tables 5.14 and 5.15 and figs. 5.6 through 5.9) it is seen that both char and tar yields are higher while the water yield is lower. Gas yield is also lower. This may, however, be due to a gas leak. The carbon content of the char is lower while the gas composition is somewhat different too: H_2 and CH_4 contents are higher and CO content lower.
It should be noted, however, that the differences in composition of the

products are not very great.

Experiment no. X

As in experiment no. IX the waste fraction used as feedstock in this pyrolysis experiment was prepared using the 105° zig zag air classifier. (see above).

The reaction temperature was extremely low in this experiment (399°C). This resulted in incomplete conversion of the waste materials in the spout-fluid bed reactor. This is concluded from the increased accumulation of material in the bed and from the fact that the material accumulated in the bed contained considerable amounts of organics: the > 1mm fraction of this material did have an ash content of only 48 wt.% (§ 5.3.2.3). The ash content of the material accumulated in the bed in other experiments was almost 100%.

The carbon content of the char is low and oxygen content is high compared to that of the chars obtained at pyrolysis experiments above 500°C. This also might indicate that the conversion was incomplete.

The pyrolysis gas obtained in experiment no. X is a very low calorific value gas. The heat of combustion amounts to only about 3700 kJ/m^3. This is due to the high carbon dioxide content of the gas, which is 76.5 vol.% (table 5.20).

It is felt on the basis of the above results that is not attractive to pyrolyse domestic waste fractions at temperatures below about 450°C because of incomplete conversion of the waste and the relatively low values of the heats of combustion of the fuels obtained.

6.3.3 Additional data on pyrolysis products

As was indicated above, the chararcteristics of the pyrolysis products will be discussed on the basis of their total (that is not ash free and not moisture free) composition.

The char

The char obtained in pyrolysing fractions from shredded domestic waste is not a high grade fuel for several reasons:

1. Its ash content is very high: about 40-50 wt.% on total basis. This is not surprising. About 50-90% of the inorganics present in the waste fractions end up in the char while the rest remains in the bed (§ 5.3.2.3).

2. As a result of its high ash content and the presence of oxygen in it the heat of combustion of the char is not high (16,000 - 20,000 kJ/kg).

The corresponding data for commercial charcoal are: ash content 2-3 wt.% heat of combustion 28,000 - 30,000 kJ/kg.

Furthermore, the char contains a few weight percents of chlorine (2-3 wt.% on total basis), to a large extent in inorganic compounds.

Although the char ash contains heavy metals, these metals do not exceed the limits which would make the material a chemical waste according to Dutch law. It is doubtful, however, whether this is true in the case of chromium. It was not possible to distinguish between Cr(III) and Cr(VI) in our leaching experiments. The total amount of Cr in the char ash remains far below the norm for Cr(III) but just exceeds the norm that the law sets for Cr(VI) (see table 5.21).

The low sulphur content of the char (0.1-0.5 wt.% on total basis) is of course advantageous.

The char collected from the cyclones is a powder-like material (90% of it has a particle diameter between 40 and 600 μm) that may easily be co-fired in powdered-coal fired power plants.

Attempts to reduce the ash content of the char by washing the char with water were unsuccessful.

The tar

The ash content of the tar collected from the electrostatic precipitator is low (0.1-0.9 wt.%, in most cases < 0.3 wt.%) This tar has a heat of combustion of 40,000 - 45,000 kJ/kg which is roughly equal to the heat of combustion of a typical no. 6 fuel oil (42,500 kJ/kg). The pyrolysis tar shows some similarity to no. 6 fuel oil in other respects too (table 6.1).

Like the char, the tar contains relatively little sulphur. The viscosity of the tar is about the same as that of fuel no. 6 at 90°C, but the tar viscosity increases rapidly with decreasing temperature so that at room temperature the tar is almost a solid. Contrary to the tar obtained in pyrolysis of shredded thin cardboard the tar discussed here contains little or no water (0.2 versus 4.0 wt.%). Attempts to dissolve water in the tar obtained in pyrolysis of domestic waste fractions in order to lower its viscosity were not very succesful. The tar solves only a few weight percents of water. We have not investigated how easily the tar can be emulgated with water.

Table 6.1 Some properties of no. 6 fuel oil and pyrolysis tar (§ 5.3.2.3).

		no. 6 fuel oil [6.3]	pyrolysis tar produced in present experiments from shredded domestic waste
Carbon content	wt.%	85.7	76-82
Hydrogen content	wt.%	10.5	11-12
Sulphur content	wt.%	0.7-3.5	0.1-0.2
Chlorine content	wt.%	-	0.1-0.8
Ash content	wt.%	<0.5	0.1-0.9
Nitrogen content	wt.%	2.0	0-1.3
Oxygen content	wt.%		5-11
Heat of cumbustion	kJ/kg	42,500	40,000-45,000
Density	kg/m^3	980	1060-1130
Viscosity	cP at 90^{o}C	75	50 (fig.5.10)

An advantage of the tar is its low sulphur content compared to that of no. 6 fuel oil. The presence of chlorine in the pyrolysis tar is, of course, an unattractive characteristic.
The heat of combustion of the tar on a volume basis is even higher than that of no. 6 fuel oil (44-50*10^9 J/m^3 and 42*10^9 J/m^3 resp.).

The gas phase

The pyrolysis gases produced are low calorific value gases. The heats of combustion of the gases are in the range of 6,200 - 10,300 kJ/m^3. This is of course much lower than that of many natural gases (30,000 - 35,000 kJ/m^3).
The HCl content of the gases is not very high. The gases obtained contained 5-7 ppm HCl. This is not surprising as the temperatures at which the pyrolysis experiments have been carried out are relatively low. The decomposition of chlorine containing inorganic constituents in the waste is prevented. The HCl is released during pyrolysis mostly by the decomposition of organic compounds which contain chlorine [6.4].
It should be noted, however, that some HCl may be captured by steel surfaces in the high temperature zone (reactor and cyclones).

In addition, the above figures for HCl content of the gas should be regarded as indicative. They are in no way representative. It is a fact that all chlorine present in PVC is released as HCl during low temperature pyrolysis. More PVC being present in domestic waste consequently leads to the formation of more HCl.
It is regretted that no definite answer can be given now to the question whether chlorine containing organic compounds are present in the gas. The analyses in question were not completed yet (see § 5.3.2.3).

The water phase

The total organic carbon content of the water phase is high (8-13 wt.%) partly because of the presence of tar constituents in the water phase (as a result of a less than complete separation efficiency of the electrostatic precipitator).
The biological oxygen demand (BOD) of the water phase was found to be up to 400 kg O_2/m^3. The chemical oxygen demand (COD) was about 20% higher. The difference in BOD and COD might in part be due to the presence of solid particles in the water phase that were oxidized in the COD determinations but not in the determinations of the BOD. We are inclined to conclude from these data that the organic contaminants present in the water phase can destroyed completely by means of aerobic biological purification of the water phase.
Table 5.22 summarizes the organic compounds that have been identified in the water phase. An important conclusion is that no chlorine containing organic compounds could be traced in the water phase. The organic compounds mentioned in table 5.22 all are compounds that normally can be found in many types of waste water streams. All the compounds are in principle bio-degradable.
Considering the pH value, the odor of the water phase and the presence in it of a large number of organic compounds it will be clear that the water phase must be treated before it can be discharged.

6.3.4 Comments

1. The properties of the tar have been discussed on the basis of the results obtained for the tar collected from the electrostatic precipitator. Actually, a minor part of the tar is separated from

the gas stream in the tube cooler. This tar contained more ash than the tar collected from the electrostatic precipitator (up to 5 wt.% and up to 0.9 wt.% resp.). The oxygen content of the tar from the tube cooler is somewhat higher than that from the electrostatic precipitator while the carbon and hydrogen contents are lower. Only very little tar was separated in the tube cooler.

2. Small differences in the elemental composition of the chars collected from cyclone 1 respectively cyclone 2 were also observed (table 5.19).
3. The determination of the elemental composition of individual char and domestic waste samples are found to be subject to errors because of the combination of the inhomogenety of the samples and the very small sample sizes used in the elemental analysis. Elemental analysis of char and domestic waste samples in duplicate revealed differences in the order of several wt.% in carbon content and of about 1 wt.% in hydrogen content.
4. The calculated heats of combustion showed excellent agreement with the experimentally determined heats of combustion of the products obtained in pyrolysis of shredded thin cardboard because of the homogenety of the samples. The agreement between the calculated heats of combustion and experimentally determined heats of combustion of the tar obtained in pyrolysis of domestic waste fractions was very good too (see table 5.19). The agreement was less good in cases of the domestic waste fractions and of the char obtained in pyrolysis of these fractions. Relative differences between calculated and experimentally determined heats of combustion of up to 10% were observed. No systematic error was observed. The inhomogenety of the samples combined with the relatively small sample sizes in the experimental determination of the heats of combustion as well as the elemental analysis on which the calculations of the heats of combustion were based again caused these differences.
5. The reaction temperature given in Chapters 5 and 6 are average temperatures. The actual bed temperature were functions of time and - to lesser extent - of the place in the bed. The departure of the local bed temperature from the average bed temperature was only 1-5^{o}C (1^{o}C in most cases) because of the very good mixing in the bed. The temperature variations during the course of a pyrolysis experiment could, however, amount to as much as 10^{o}C.

6. The figures given for the heavy metals contents of the char are in no way representative but should be regarded to be indicative. It will be recalled that it is all but impossible to take a representative sample of domestic waste.

Literature

6.1 E. Douglas, M. Webb, G.R. Daborn. The pyrolysis of waste and product assessment, Symposium on the treatment and recycling of solid wastes, Manchester (January 11th, 1974).

6.2 J. Zielinski, P. Przywarska, Trans. Recycling Berlin'79, vol. 1, pp. 707 (1979).

6.3 G.M. Mallan, C.S. Finnay, AIChE symposium series, vol. 69, no. 133, pp 56 (1973).

6.4 R. Schmidt, Proceedings of the 2nd International Symposium M.E.R. pp 9.67 (October 1981).

7. APPLICATION OF THE MATHEMATICAL MODELS OF CELLULOSE PYROLYSIS

7.1 Introduction

This chapter discusses the results of the calculations of product distributions and conversion times made from the mathematical models derived in § 2.3.3. Some of the parameter values used in the models were taken from literature while others were determined experimentally. The models were first tested for the sensitivity of the calculated product distributions and conversion times to the physical transport and reaction kinetic parameters (§ 7.2.2). The parameter values used in this case were all taken from literature. On the basis of the results of these calculations we decided to carry out thermoanalytical experiments in order to obtain more reliable kinetic data (see § 2.5) and to determine experimentally those physical transport parameters for which the models are most sensitive and for which few literature data were available (§ 7.2.3).

The results obtained from the general model and the lumped parameter model were then compared to each other (§ 7.3). This was done to see whether the simplified method of calculating the temperature history inside a pyrolysing particle that results from applying the lumped parameter model (§ 2.3.3.4) leads to results that agree with the results of the general model.

Finally, the results that have been obtained by using the experimentally determined kinetic data in the models are discussed (§ 7.4). These results are of course compared to the product distributions that were obtained experimentally in cardboard pyrolysis (§ 5.2).

7.2 Sensitivity analysis of the general model

7.2.1 Introduction

Before a sensitivity analysis could be undertaken we had to test the accuracies of the computer programs that had been written to calculate the numerical solutions of the models which have been discussed in Chapter 2. These tests were carried out in two ways. First, an imaginary case of a pyrolysis conversion was set up that had been simplified to the point where the differential equations that institute the model could be solved analytically. The simplifying assumptions were:

a. the pyrolysis involves one chemical reaction only;
b. the influence of convective heat transport is negligible and
c. the coefficient of thermal conductivity is constant.
The analytical solution of our model for this case was calculated and compared to the numerical solution that was obtained by means of our computer programs.
In the second place the computer programs that have been set up to calculate the numerical solutions of the models were applied to the model that Rittmann [7.1] has developed (see § 2.3.2). Rittmann used a different method to derive relationships from the differential equations that describe the heat transport and chemical conversions (method of integral relations). The parameter values used in this comparison were of course those selected by Rittmann. These values are summarized in appendix 7.1.
Excellent agreements were obtained in both of these tests.It was concluded that the computer program we had written to calculate the numerical solutions of our general model is sufficiently accurate.

7.2.2 Testing the sensitivity of the general model for different parameter values

The sensitivity analysis has been carried out only for the general model that assumes tar evaporation. But it will be clear that the results are valid for the general model without tar evaporation too. Unless stated otherwise the parameter values used in the calculations are those that are presented in appendix 7.1. The meaning of the symbols has already been given in § 2.3.3.2.
It is evident that the temperature at which the pyrolysis is carried out has a great influence on the product distribution as well as on the reaction time. Both the reaction rates and the driving force for heat transport are highly dependent on this temperature. The reaction temperature is, however, only one of the parameters that we wanted to investigate the influence of.
Reliable values for a fairly large number of other parameters were not available from literature. All of these parameters had in principle to be determined experimentally. To reduce the experimental work load we decided to find those parameters to the values of which the model is especially sensitive. The values of these parameters then

would have to be examined carefully through experiments.
Not all results of the sensitivity analysis will be presented here. Some of the results are shown in diagrams, however, to illustrate the sensitivity of the model to the values of a number of parameters.

Slab thickness

Although the thickness of the pyrolysing cellulose slab is one of the independent parameters, just like the reaction temperature, it was decided to investigate the influence of slab thickness on the pyrolysis process in order to see whether its influence is so small that we may assume that the heat transport inside the particle is not a limiting factor. If this were so the reaction limited conversion rate model (§ 2.3.3.5) should provide a good description of pyrolysis. Fig. 7.1 presents the product distribution, expressed in wt.% of the original cellulose, as a function of half slab thickness (L) for the case that convective heat transfer to the slab predominates (T_∞ = 600°C and heat transfer coefficient = 83.8 J/m^2.sec.°C). Figs. 7.2 through 7.5 present the mass concentration of the unreacted cellulose as a function of the dimensionless distance x/L from the slab centre with time elapsed since the start of the pyrolysis as parameter.
It was concluded from the above results that the slab thickness has substantial influence on the product distribution (fig. 7.1) as well as on the reaction time (figs. 7.2 through 7.5). Only for small values

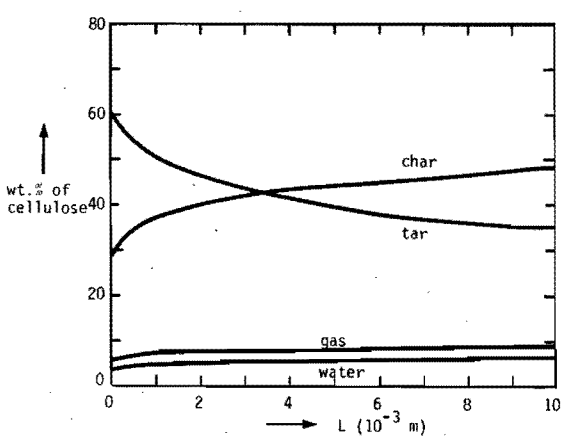

Fig.7.1 Calculated product distribution as a function of half slab thickness (T = 600°C, heat transfer coefficient = 83.8 J/m^2.sec.°C)

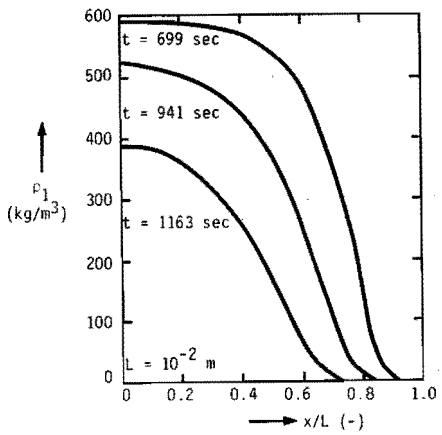

Fig.7.2 Calculated mass concentration of unreacted cellulose as a function of dimensionless distance x/L from slab centre (parameter: time elapsed since start of pyrolysis). $L=10^{-2}$ m.

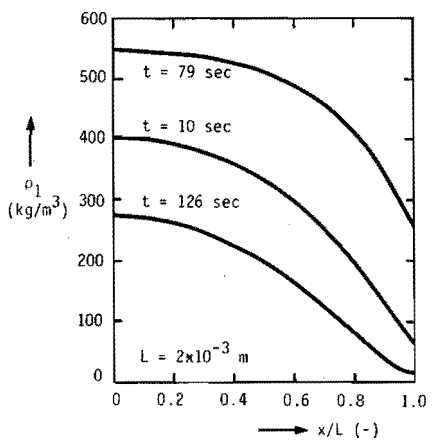

Fig.7.3 Calculated mass concentration of unreacted cellulose as a function of dimensionless distance x/L from slab centre (parameter: time elapsed since start of pyrolysis). $L=2\times10^{-3}$ m

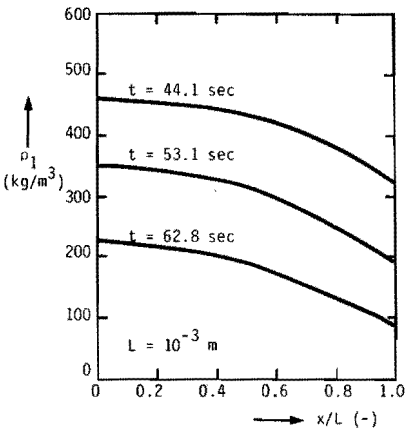

Fig.7.4 Calculated mass concentration of unreacted cellulose as a function of dimensionless distance x/L from slab centre (parameter: time elapsed since start of pyrolysis). L=10^{-3} m

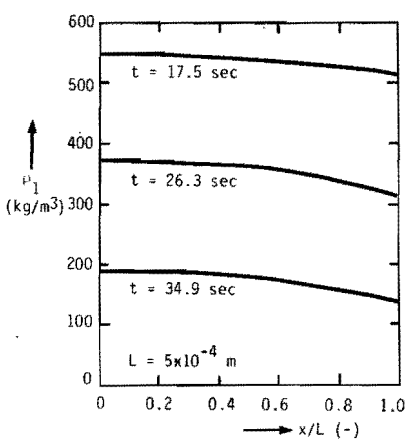

Fig.7.5 Calculated mass concentration of unreacted cellulose as a function of dimensionless distance x/L from slab centre (parameter: time elapsed since start of pyrolysis). L=5x10^{-4} m

of slab thickness do the reactions take place almost homogeneously and are concentration profiles rather flat (fig. 7.5).

Thermal conductivity (λ)

Char production and reaction time (90% conversion) are presented as a function of λ(for $L = 10^{-3}$m, $T = 600^{o}C$, $Nu = 2$) in fig. 7.6. The influence of λ on reaction time is rather great.

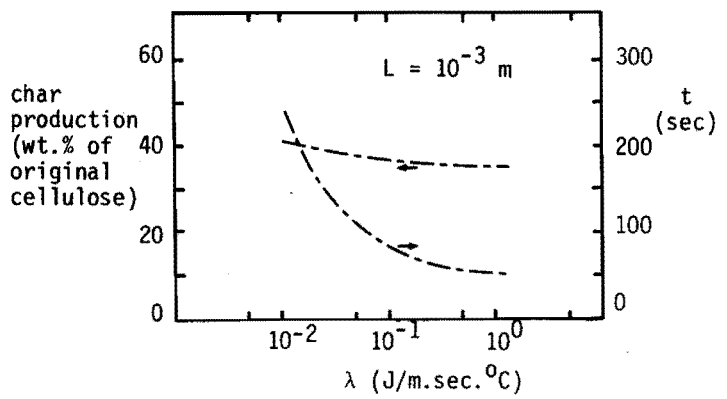

Fig.7.6 Calculated char production and reaction time as a function of thermal conductivity λ ($T = 600^{o}C$)

Reaction kinetic parameters

To illustrate the influence of the values of the reaction kinetic parameters on the pyrolysis process described by the general model with tar evaporation an example is given in fig. 7.7 of the influence of the value of one of the frequency factors (k_{bo}) on the char production (for $L = 10^{-3}$m, $T = 600^{o}C$, $Nu = 2$). Variation of k_{bo} has a great effect on the char production. Similar effects were observed when the values of the other reaction kinetic parameters were varried.

The general conclusions were: the product distribution obtained with the general model with tar evaporation is highly sensitive to the values of the reaction kinetic parameters while the reaction time required for a given cellulose conversion is sensitive to the values of heat transport parameters (f.i. λ). Much attention should therefore be paid to obtaining reliable data for the thermal conductivity of cellulose that is being subjected to pyrolysis and for the reaction kinetic parameters.

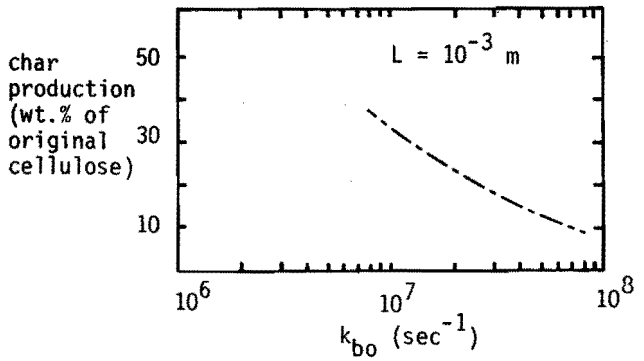

Fig.7.7 Calculated char production as a function of frequency factor k_{bo} (T = 600°C)

Measurements to establish values for the reaction kinetic parameters have already been discussed in Chapter 2. The determination of the thermal conductivity of cellulose being subjected to pyrolysis (or rather: for cellulose and for the char obtained by pyrolysing cellulose) is described in appendix 7.2.

The sensitivity of the general model with tar evaporation, that of the general model without tar evaporation as well as that of the reaction limited conversion rate model for the values of some of the parameters will be discussed in § 7.4 in which the results are given that have been obtained with those models using the experimentally determined kinetic data.

7.3 Comparison of lumped parameter model to general model (with tar evaporation)

The lumped parameter model (see § 2.3.3.4) was developed for cases where the sensitivity of the product distribution obtained with the general model with tar evaporation for the thickness of the cellulose slab is relatively small. The lumped parameter temperature history is exact when all physical parameters are constant, the material is homogeneous and has constant composition, the reactions do not influence the heat transport and Fourrier time is sufficiently large before the decomposition starts.

The parameter values used in the lumped parameter model and those applied in the general model with tar evaporation were identical (see appendix 7.1). The value of μ_1^2 in eq. (2.50) is given as a function of Biot number in fig. 7.8. Some of the results of the comparison of the lumped parameter model to the general model with tar evaporation are given below. Figs. 7.9 and 7.10 present the product distributions obtained with the general model with tar evaporation and the lumped parameter model for identical parameter values. The product distributions are given as functions of slab thickness in fig. 7.9 and as functions of reaction temperature in fig. 7.10. The maximum relative difference in the product distributions obtained with the two models is about 15%. This agreement is very good considering the simplicity of the description of the temperature history in the lumped parameter model. It was, however, decided not to use the lumped parameter model before it had been tested for more reliable data of the reaction kinetic parameters and heat transport parameters as it might be that the agreement would be less good in that case.

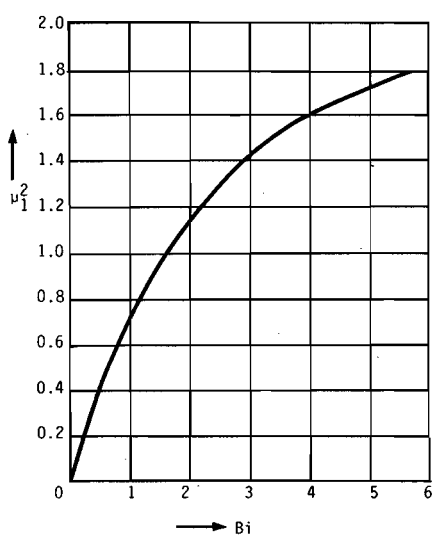

Fig.7.8 Value of μ_1^2 (eq.2.50) as a function of Biot number

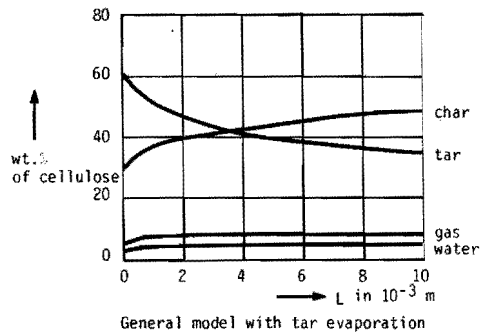

Fig.7.9 Product distributions as a function of half slab thickness obtained with the general model with tar evaporation and the lumped parameter model for identical parameter values.

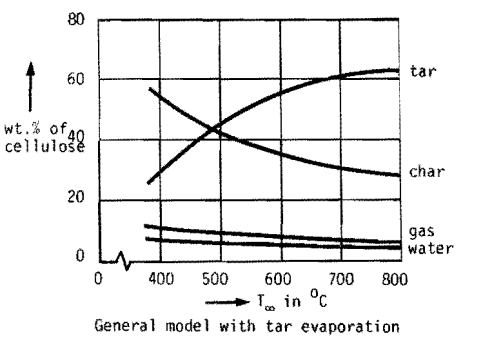

Fig.7.10 Product distributions as a function of reaction temperature obtained with the general model with tar evaporation and the lumped parameter model for identical parameter values.

7.4 Results of modelling the cellulose pyrolysis on the basis of experimentally determined kinetic data

7.4.1 Calculation of product distributions using the experimentally determined kinetic data and physical transport parameters

The parameter values used in the calculations were partly taken from literature, partly obtained in experimental work carried out as part of the present investigation. The value of each parameter and its source are briefly discussed below.

A. Reaction kinetic parameters (symbols: see fig. 2.14)

- The dehydration reaction (reaction a): § 2.5.6.2:

E_a = 32.8 kcal/mole
k_{ao} = $9.02*10^{10}$ sec^{-1}
y_a = 0.025 kg H_2O/kg cellulose

The kinetic data obtained in our thermoanalytical experiments for reaction a are in reasonable agreement with those we found in literature when these parameter values are ascribed to the dehydration reaction (table 2.2).

Assuming that water is indeed the only gaseous product formed in the dehydration reaction the fractional gas yield factor corresponds to the loss of 1 water molecule per 4 β-1,4-glucopyranose monomer units of the cellulose molecule.

- The dehydration of dehydrocellulose (reaction c): § 2.5.6.3:

E_c = 54.1 kcal/mole
k_{co} = $7.05*10^{17}$ sec^{-1}
y_c = 0.74 kg gases/kg dehydrocellulose

The maximum amount of char formed from the cellulose in the dehydration step is given by: $(1-y_a)*(1-y_c)$ = 0.975*0.26 = 0.254 kg char/kg cellulose. The char residue amounts to 0.254*162.14 = 41 atomatic mass units (a.m.u.) per monomer unit (162.14 a.m.u.). This corresponds to a residue per cellulose monomer consisting of 3 carbon atoms and 5 hydrogen atoms (assuming that no oxygen is present in the char).

- The depolymerization of cellulose (reaction b)

E_b = 53.5 kcal/mole
k_{bo} = $1.05*10^{17}$ sec^{-1}
y_b = 1 kg levoglucosan/kg cellulose

values obtained by Akita and Kase [7.2] see § 2.5.6.7

- The degradation of levoglucosan:

E_d = 40.5 kcal/mole
k_{bo} = $7.66*10^{13}$ sec^{-1}
y_d = 0.85 kg gases/kg levoglucosan

The activation energy and frequency factor used in the models are those that have been obtained for the polycondensation of levoglucosan (§ 2.5.6.5). It has already been indicated in § 2.5.6.7 that no values could be obtained for the kinetic parameters of the charring reaction of the polycondensation product. The value of the fractional

gas yield factor y_d applies, however, to the polycondensation reaction and the charring reaction together. The gas yield factor of the polycondensation was found to be 0.55 kg of gases/kg levoglucosan (§ 2.5.6.5). The gas yield factor for the polycondensation and for the charring reaction together was calculated from the final char residue yield in experiments in which the polycondensation products obtained by isothermal pyrolysis of levoglucosan (§ 2.5.6.5) were subjected to further degradation in dynamic TG. The amount of char residue is in that case given by: $(1-y_d')*(1-y_d'') = 1-y_d$. The value obtained by this method was: y_d = 0.85 kg gases/kg levoglucosan.

B. Physical transport parameters

- The thermal conductivity of the solids.
  The thermal conductivities of cellulose (paper) and of the char obtained in pyrolysis experiments with shredded thin cardboard as a feedstock have been determined experimentally (see appendix 7.2). The values obtained were:
  λ_{paper} = 0.116 J/m.sec.^{o}C
  λ_{char} = 0.109 J/m.sec.^{o}C
  The value of the thermal conductivity of the solids that Rittmann has used in his calculations was λ = 0.113 J/m.sec.^{o}C [7.1]. It was decided on the basis of the relatively small difference between λ_{paper} and λ_{char} to use a constant thermal conductivity for the solids in the models. The value of this constant thermal conductivity was chosen equal to that which Rittmann has used and which lies in between the values of the thermal conductivity of paper and char.
  So: λ = constant = 0.113 J/m.sec.^{o}C.

The values of the following physical parameters used in the models were chosen equal to those which Rittmann has used (appendix 7.1):

- heat capacity of the solids (C_{p1}, C_{p2}, C_{p3}, C_{p4})
- Nusselt number (Nu). The below calculations were carried out for convective heat transfer to the cellulose slab.
- initial mass concentration cellulose (ρ_o)
- initial temperature of cellulose particle (T_o)

The following physical transport parameter values for the gaseous products were estimated from the values of these parameters for CO_2 and steam in the temperature range 100-600^{o}C:

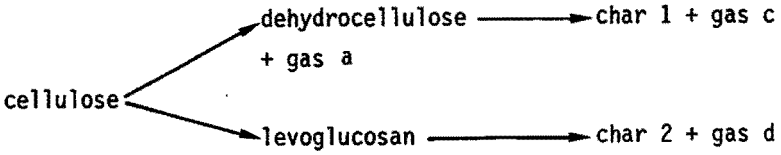

Total solids = cellulose + dehydrocellulose + char 1 + char 2
Total gases = gas a + gas c + gas d
t = reaction time required to reach a given conversion

7.4.1.1 Results obtained with the general model with tar evaporation

The results of the calculations are presented in table 7.2 for a cellulose conversion of 100% as a function of the reaction temperature.
As a result of the calculation procedure the cellulose conversion is not exactly 100%. This is true also for the tables summarizing the calculations in the next paragraphs.

Table 7.2 General model with tar evaporation. Product distributions and reaction times at different reaction temperatures (T)

T(^{o}C)		400	450	500	550	600
t(sec)		1.39	0.74	0.55	0.45	0.39
cellulose	(wt.%)	1.07	0.25	0.04	0.03	0.04
dehydrocellulose	(wt.%)	1.10	0.14	0.02	0.01	0.01
char 1	(wt.%)	19.93	17.97	17.07	16.37	15.92
levoglucosan	(wt.%)	19.18	28.74	32.59	35.45	37.20
gas a	(wt.%)	1.99	1.78	1.68	1.61	1.57
gas c	(wt.%)	56.66	51.13	48.55	46.55	43.37
levoglucosan	(wt.%)	19.18	28.74	32.59	35.45	37.20
total solids	(wt.%)	22.10	18.36	17.13	16.41	15.97
total gases	(wt.%)	58.65	52.91	50.23	48.16	46.94

These results will be discussed together with those obtained with the general model without tar evaporation after these last results have been presented (see below).

- thermal conductivity of the gases (λ_{ga}, λ_{gb}, λ_{gc}, λ_{gd})
- heat capacity of the gases (C_{pga}, C_{pgb}, C_{pgc}, C_{pgd})

C. The heats of reaction

No quantitative data could be found in literature for the heats of reaction of the different reactions that take place during the pyrolysis of cellulose. The sensitivity of the models for the heats of reactions proved to be low (see § 7.4.3). It was therefore arbitrarily decided to use for reactions a,b en c the values of the heats of reaction that Rittmann has used in his calculations. For reaction d, the degradation of levoglucosan (gas b) to char and gases, we used the same value as for reaction c in which dehydrocellulose decomposes to yield char and gases also.
The parameter value used in the models are summarized in table 7.1.

Table 7.1 Paramater values used in the model

parameter	value	unit	parameter	value	unit
k_{ao}	$9.02*10^{10}$	sec^{-1}	ΔH_a	69135	J/kg
k_{bo}	$1.05*10^{17}$	sec^{-1}	ΔH_b	691350	J/kg
k_{co}	$7.05*10^{17}$	sec^{-1}	ΔH_c	-394700	J/kg
k_{do}	$7.66*10^{13}$	sec^{-1}	ΔH_d	-394700	J/kg
E_a	32.8 [1]	kcal/mole	$\lambda_{1,2,3,4}$	0.113	J/m.sec.°C
E_b	53.5	kcal/mole	$\lambda_{ga, gb, gc, gd}$	0.0419	J/m.sec.°C
E_c	54.1	kcal/mole	$C_{p1,2,3,4}$	2304,5	J/kg.°C
E_d	40.5	kcal/mole	$C_{pga,gb,gc,gd}$	2000	J/kg.°C
y_a	0.025	-	T_o	300	°K
y_b	1	-	ρ_o	600	kg/m³
y_c	0.74	-	Nu	2	-
y_d	0.85	-	R	1.986	cal/mole,°K

[1]) This value has been changed later on, see table 7.1[2]

The calculations were carried out for half slab thickness L = 0.00009 m as the results are compared to experimental results obtained in pyrolysis experiments in which shredded thin cardboard (d=0.18 mm) was used as feedstock. The terms used in the tables that summarize the results obtained by using the models are defined in the below reaction scheme:

7.4.1.2 Results obtained with the general model without tar evaporation

The results of the calculations are presented in table 7.3 and figs. 7.11 through 7.16. Table 7.3 presents the product distribution as a function of reaction temperature at 100% cellulose conversion while in figs. 7.11 through 7.16 plots are given of the temperature profile within the cellulose slab and the mass concentrations of the different products as functions of the dimensionless place inside the slab for a reaction temperature of 500°C. The time elapsed since the start of the pyrolysis is given as a parameter.

Table 7.3 General model without tar evaporation. Product distributions and reaction times at different reaction temperatures.

T (°C)		400	450	500	550	600
t (sec)		1.18	0.58	0.42	0.34	0.30
cellulose	(wt.%)	0.75	0.41	0.09	0.12	0.12
dehydrocellulose	(wt.%)	0.20	0.06	0.02	0.01	0.01
char 1	(wt.%)	19.16	16.65	15.63	14.96	14.51
char 2	(wt.%)	3.46	5.12	5.81	6.12	6.38
levoglucosan	(wt.%)	0.48	0.37	0.12	0.13	0.13
gas a	(wt.%)	1.89	1.63	1.54	1.48	1.43
gas c	(wt.%)	54.66	47.29	44.50	42.58	41.36
gas d	(wt.%)	19.46	28.75	32.88	34.69	36.19
levoglucosan	(wt.%)	0.48	0.37	0.12	0.13	0.13
total solids	(wt.%)	23.57	22.24	21.55	21.21	21.02
total gass	(wt.%)	76.01	77.67	78.92	78.75	78.98

The product distributions obtained with both general models have been plotted as functions of reaction temperature in figs. 7.17 (levoglucosan yield), 7.18 (total solids yield) and 7.19 (total gases yield).

The plots of levoglucosan yield as a function of reaction temperature calculated from the general model without tar evaporation (see f.i. fig. 7.17) show that levoglucosan yield is about zero in all cases. The levoglucosan yield calculated from the general model without tar evaporation can sometimes be somewhat higher than zero for low temperatures only. This is because the rate of degradation of levoglucosan

may be smaller than the rate of formation of levoglucosan in that case.

Fig.7.11

Calculated temperature as a function of dimensionless distance x/L from slab centre (parameter: time elapsed since start of pyrolysis). General model without tar evaporation.

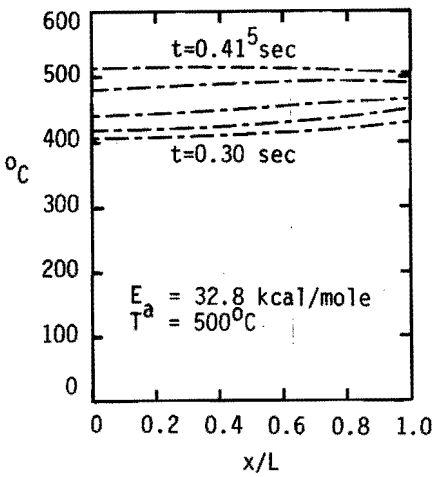

Fig.7.12

Calculated concentration of unreacted cellulose as a function of dimensionless distance x/L from slab centre (parameter: time elapsed since start of pyrolysis). General model without tar evaporation.

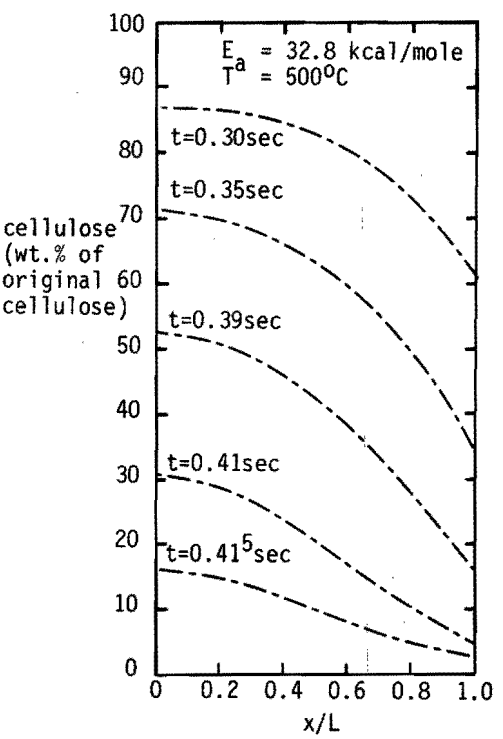

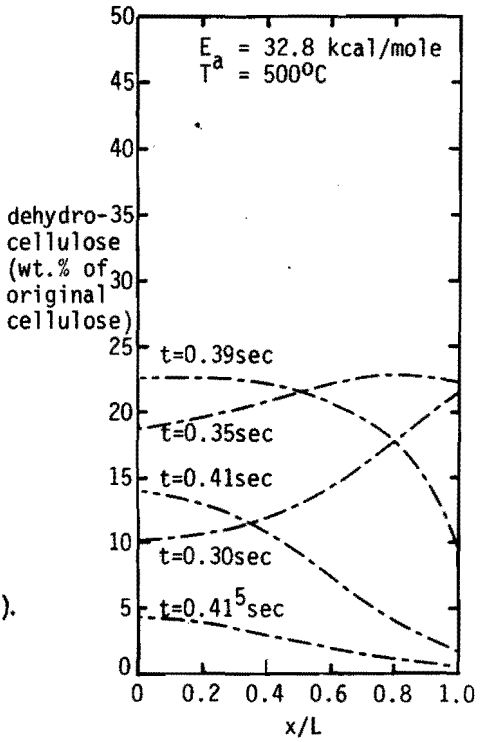

Fig.7.13

Calculated concentration of dehydrocellulose as a function of dimensionless distance x/L from slab centre (parameter: time elapsed since start of pyrolysis). General model without tar evaporation.

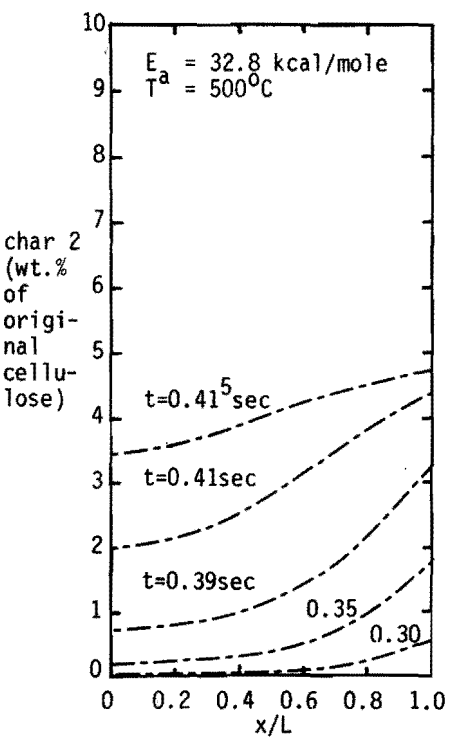

Fig.7.14

Calculated concentration of char 2 as a function of dimensionless distance x/L from slab centre (parameter: time elapsed since start of pyrolysis). General model without tar evaporation.

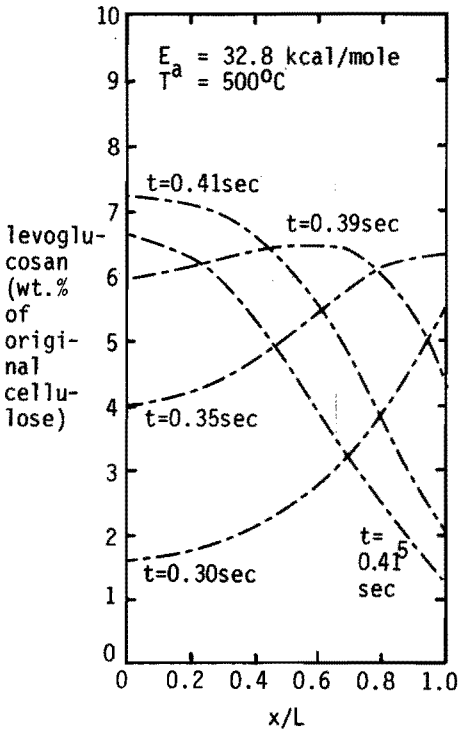

Fig.7.15

Calculated levoglucosan concentration as a function of dimensionless distance x/L from slab centre (parameter: time elapsed since start of pyrolysis). General model without tar evaporation.

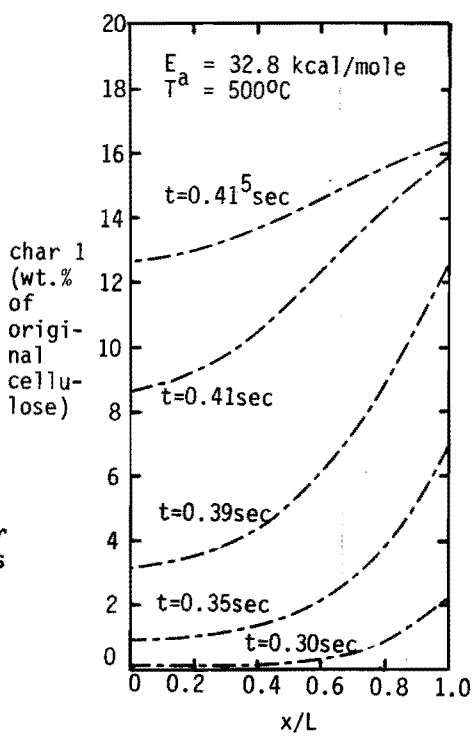

Fig.7.16

Calculated concentration of char 1 as a function of dimensionless distance x/L from slab centre (parameter: time elapsed since start of pyrolysis). General model without tar evaporation.

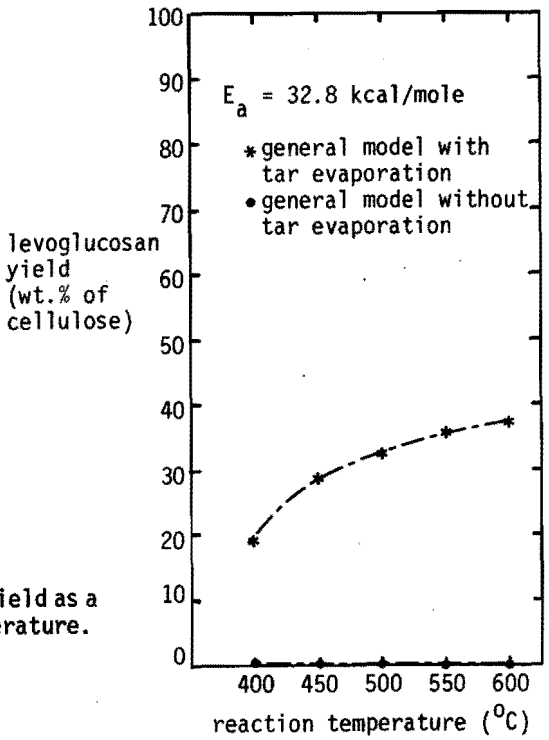

Fig.7.17

Calculated levoglucosan yield as a function of reaction temperature.

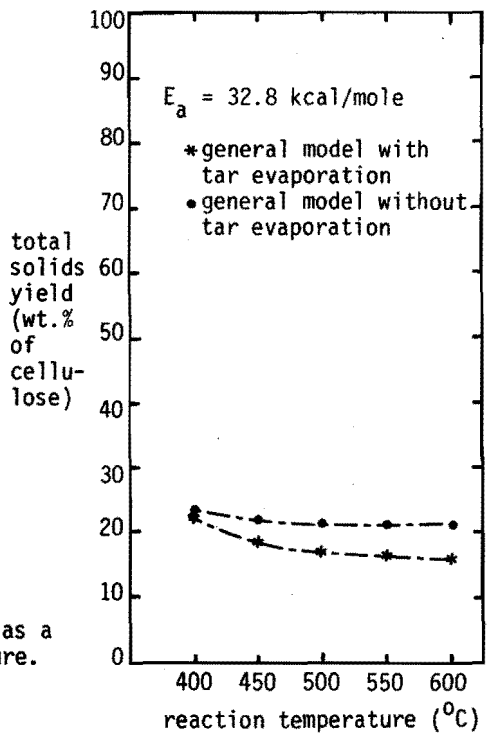

Fig.7.18

Calculated total solids yield as a function of reaction temperature.

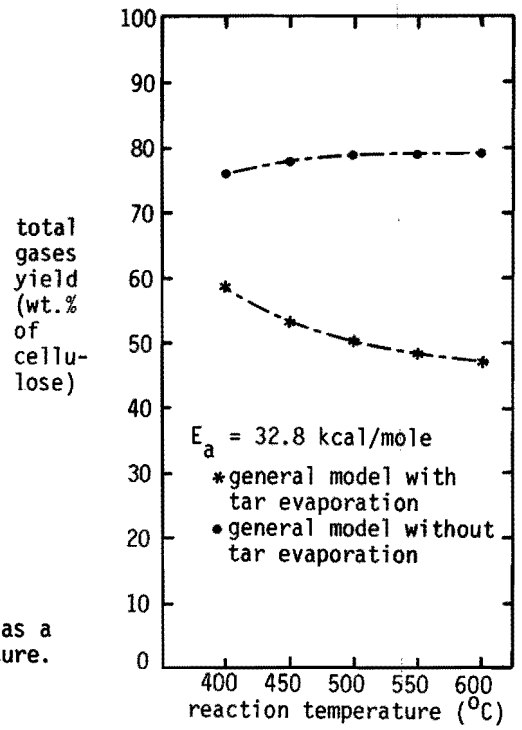

Fig.7.19
Calculated total gases yield as a function of reaction temperature.

Table 7.4 indicates how much of the cellulose has been decomposed through dehydration (and consecutive reaction) and how much through depolymerization (and consecutive reaction).

Table 7.4 Percentage of cellulose decomposed through dehydration and through depolymerization

	reaction temperature (°C)→	400	450	500	550	600
General model without tar evaporation (table 7.3)	through dehydration (%)	76	66	62	59	57
	through depolymerization (%)	24	34	38	41	43
General model with tar evaporation (table 7.2)	through dehydration (%)	81	71	67	65	63
	through depolymerization (%)	19	29	33	35	37

Discussion:
Although the temperature profiles inside the pyrolysing cellulose slab are rather flat (fig. 7.11) the concentration profiles of cellulose

and its pyrolysis products are on the contrary far from flat. Considerable concentration gradients exist inside the pyrolysing slab. The cellulose concentration profiles inside the slab with a thickness of 0.18 mm are rather steep in contrast with the results obtained with the models for small values of the slab thickness using values of the reaction kinetic parameters taken from literature (fig. 7.5, d = 1 mm). The reactions apparently do not take place homogeneously throughout the slab even when slab thickness is very small.

It was concluded from figs. 7.11 through 7.16 that the temperature history has been different for different places inside the slab. The lumped parameter model would therefore not be very useful to calculate product distributions in this case.

It is seen from table 7.4 that the cellulose mainly decomposes through dehydration even at higher temperatures. Many investigators assume, however, that the depolymerization of cellulose predominates at temperatures above 300-350^{o}C (see Chapter 2). In addition, the calculated total solids yield (fig. 7.18) is too high and the calculated levoglucosan yield (fig. 7.17) is too low compared to the experimental results we obtained in pyrolysis experiments using shredded thin cardboard as feedstock (see paragrapgh 7.4.2). This also indicates that the depolymerization reaction does in fact play a more important role than the models predict.

It was therefore concluded that it is necessary to adapt the values of some of the kinetic parameters in such a way that the dehydration reaction becomes less important in the high temperature range. We have attempted to achieve this by varying the values of the activation energy and frequency factor of the dehydration reaction (reaction a) within the limits of the experimental errors that may have been made in the determination of E_a and k_{ao}. The experimental error in E_a was estimated to be in the order of 20% at most.

We decided to carry out model calculations using the parameter values presented in table 7.1 except for a reduction of the value of E_a by 10 and 20% respectively. The values of the frequency factors k_{ao} that were used together with these values of E_a were calculated from the experimentally determined reaction rate at 190^{o}C (see § 2.5.6.2). We obtained the following sets of values:

E_a = 29.5 kcal/mole (0.9*32.8), k_{ao} = 2.3 $10^9 sec^{-1}$
E_a = 26.2 kcal/mole (0.8*32.8), k_{ao} = 6.2 $10^7 sec^{-1}$

7.4.1.3 The influence of E_a on the product distributions obtained with the general models with and without tar evaporation

The relatively small changes that were made in E_a have dramatic influences on the product distributions obtained with the general models. The product distributions and reaction times obtained with the general models using E_a = 29.5 kcal/mole and E_a = 26.2 kcal/mole are summarized in tables 7.5 through 7.8. The figs. 7.20 and 7.21 present the yields of levoglucosan, total solids and total gases following from the general models using E_a= 32.8, E_a = 29.5 and E_a = 26.2 kcal/mole. Fig. 7.22 shows how the percentages of cellulose decomposed through either dehydration or depolymerization change dramatically with relatively small changes in E_a (plots for the general model without tar evaporation).

Although the amount of cellulose decomposed through dehydration (and consecutive charring) decreases strongly with decreasing values of E_a (fig. 7.22) the effect on the yields of levoglucosan, total solids and total gases is relatively small in case of the general model without tar evaporation (fig. 7.21). This is because the depolymerization and consecutive tar cracking reaction yield char and gases in this case just like the dehydration and consecutive charring reaction.

The effect of decreasing values of E_a on the product distributions obtained from the general model with tar evaporation is rather great (fig. 7.20). This is due to the fact that in this case the levoglucosan does not decompose into char and gases. The products of dehydration and the charring reaction that follows upon dehydration are completely different from the product of the depolymerization of cellulose (levoglucosan).

The above results will be discussed in more detail in paragragh 7.4.2 in which the results obtained with the models are compared to the experimental data obtained by pyrolysing shredded thin cardboard.

Table 7.5 General model with tar evaporation. Product distributions and reaction times obtained for E_a = 29.5 kcal/mole.

T (^oC)		400	450	500	550	600
t (sec)		9.55	2.10	1.21	0.91	0.78
cellulose	(wt.%)	0.01	0.06	0.02	0.02	0.02
dehydrocellulose	(wt.%)	0.04	0.05	0.00	0.00	0.00
char 1	(wt.%)	16.23	12.00	10.13	9.20	8.64
levoglucosan	(wt.%)	35.94	52.54	60.01	63.68	65.88
gas a	(wt.%)	1.60	1.19	1.00	0.91	0.85
gas c	(wt.%)	42.21	34.16	28.84	26.19	24.60
levoglucosan	(wt.%)	35.94	52.54	60.01	63.68	65.88
total solids	(wt.%)	16.28	12.11	10.05	9.22	8.66
total gases	(wt.%)	43.81	35.35	29.84	27.10	25.45

Table 7.6 General model without tar evaporation. Product distributions and reaction times obtained for E_a = 29.5 kcal/mole

T (^oC)		400	450	500	550	600
t (sec)		8.40	1.27	0.73	0.55	0.46
cellulose	(wt.%)	0.02	0.14	0.02	0.02	0.03
dehydrocellulose	(wt.%)	0.05	0.02	0.00	0.00	0.00
char 1	(wt.%)	15.03	10.46	8.57	7.66	7.09
char 2	(wt.%)	6.11	9.08	9.99	10.49	10.82
levoglucosan	(wt.%)	0.01	0.05	0.02	0.02	0.02
gas a	(wt.%)	1.48	1.01	0.84	0.75	0.70
gas c	(wt.%)	42.76	29.20	24.38	21.76	20.13
gas d	(wt.%)	34.55	50.72	56.62	59.47	61.33
levoglucosan	(wt.%)	0.01	0.05	0.02	0.02	0.02
total solids	(wt.%)	21.21	19.70	18.58	18.17	17.94
total gases	(wt.%)	78.79	80.93	81.84	81.98	82.16

Table 7.7 General model with tar evaporation. Product distributions and reaction times obtained for E_a = 26.2 kcal/mole.

T (^oC)		400	450	500	550	600
t (sec)		18.86	6.23	2.35	1.80	1.57
cellulose	(wt.%)	0.01	0.00	0.01	0.03	0.00
dehydrocellulose	(wt.%)	0.02	0.00	0.00	0.00	0.00
char 1	(wt.%)	9.26	5.75	4.47	3.97	3.70
levoglucosan	(wt.%)	63.52	77.26	82.33	84.28	85.35
gas a	(wt.%)	0.91	0.57	0.44	0.39	0.36
gas c	(wt.%)	26.35	16.40	12.74	11.31	10.57
levoglucosan	(wt.%)	63.52	77.26	82.33	84.28	85.35
total solids	(wt.%)	9.29	5.75	4.48	4.00	3.70
total gases	(wt.%)	27.26	16.97	13.18	11.70	10.93

Table 7.8 General model without tar evaporation. Product distributions obtained for E_a = 26.2 kcal/mole

T (^oC)		400	450	500	550	600
t (sec)		15.64	2.09	1.00	0.71	0.57
cellulose	(wt.%)	0.01	0.06	0.02	0.02	0.02
dehydrocellulose	(wt.%)	0.02	0.00	0.00	0.00	0.00
char 1	(wt.%)	8.28	4.50	3.34	2.80	2.49
char 2	(wt.%)	10.10	12.33	13.08	13.37	13.55
levoglucosan	(wt.%)	0.01	0.02	0.01	0.02	0.02
gas a	(wt.%)	0.81	0.44	0.33	0.28	0.24
gas c	(wt.%)	23.56	12.79	9.49	7.95	7.05
gas d	(wt.%)	57.21	69.87	74.18	75.77	76.78
levoglucosan	(wt.%)	0.01	0.02	0.01	0.02	0.02
total solids	(wt.%)	18.41	16.89	16.44	16.19	16.06
total gases	(wt.%)	81.58	83.10	84.00	84.00	84.07

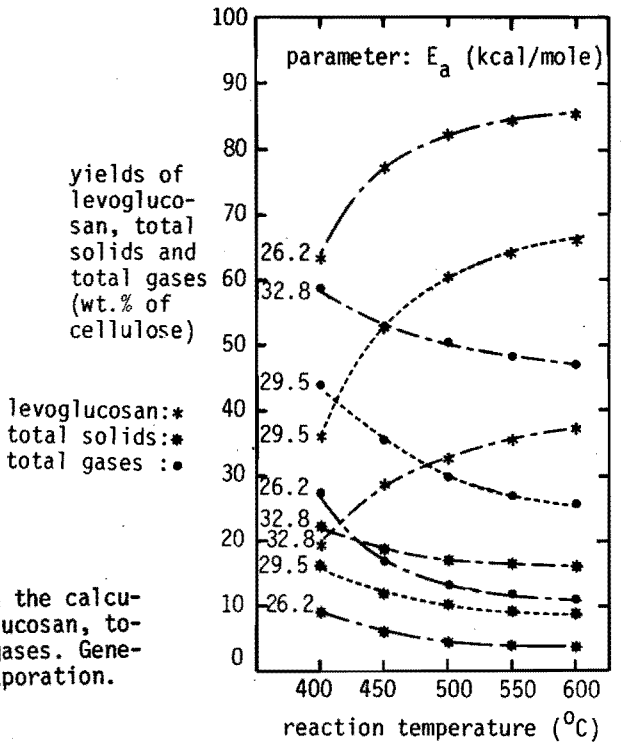

Fig.7.20

The influence of E_a on the calculated yields of levoglucosan, total solids and total gases. General model with tar evaporation.

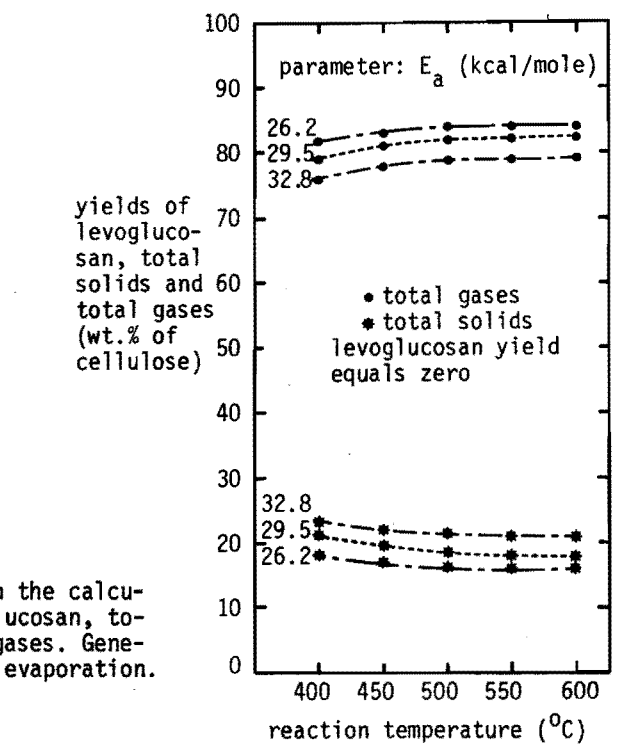

Fig.7.21

The influence of E_a on the calculated yields of levoglucosan, total solids and total gases. General model without tar evaporation.

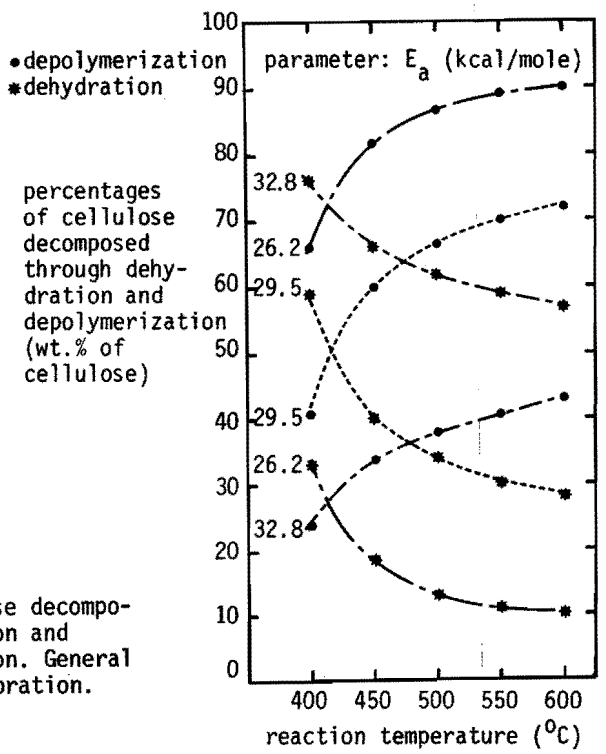

Fig.7.22

Percentages of cellulose decomposing through dehydration and through depolymerization. General model without tar evaporation.

7.4.1.4 Results obtained with the reaction rate limited conversion model

The results obtained with this model are summarized in table 7.9 and fig. 7.23. The depolymerization of cellulose predominates at temperatures above about 450-500°C in this case. It was therefore not necessary to adapt the activation energy of the dehydration reaction in this case. However, the model does not present a realistic description of the pyrolysis conversion of cellulose. The reaction times required to obtain 99.9% conversion of cellulose calculated from this model are unrealisticly short especially at higher temperatures (even if the value of E_a is reduced to 26.2 kcal/mole, results not shown here). In addition, the levoglucosan decomposes almost completely into char and gases. It is therefore impossible to obtain a levoglucosan yield when using this model which approaches the experimentally found tar yield.

Table 7.9 Product distributions and reaction times required to obtain 99.9% cellulose conversion obtained from the reaction rate limited conversion model (E_a = 32.8 kcal/mole)

T (^oC)		400	450	500	550	600
t (sec)		2.70	0.37	0.05	0.01	0.00
cellulose	(wt.%)	0.10	0.10	0.10	0.10	0.10
dehydrocellulose	(wt.%)	1.27	0.08	0.02	0.01	0.00
char 1	(wt.%)	20.46	15.45	9.66	5.42	2.95
char 2	(wt.%)	2.68	5.83	9.25	11.76	13.18
levoglucosan	(wt.%)	0.02	0.03	0.06	0.14	0.42
gas a	(wt.%)	2.05	1.53	0.95	0.53	0.29
gas c	(wt.%)	58.23	43.97	27.51	15.42	8.39
gas d	(wt.%)	15.20	33.02	52.44	66.63	74.67
levoglucosan	(wt.%)	0.02	0.03	0.06	0.14	0.42
total solids	(wt.%)	24.51	21.46	19.03	17.29	16.23
total gases	(wt.%)	75.48	78.52	80.90	82.58	83.35
percentage cellulose decomposed:						
through dehydration	(%)	82	61	38	21	12
through depolymerization	(%)	18	39	62	79	88

It was concluded that the reaction rate limited conversion model does not provide a good description of the conversions involved in the pyrolysis of cellulose. It follows that heat transfer is one of the factors that limit the rate of the low temperature pyrolysis of thin slabs of cellulose.

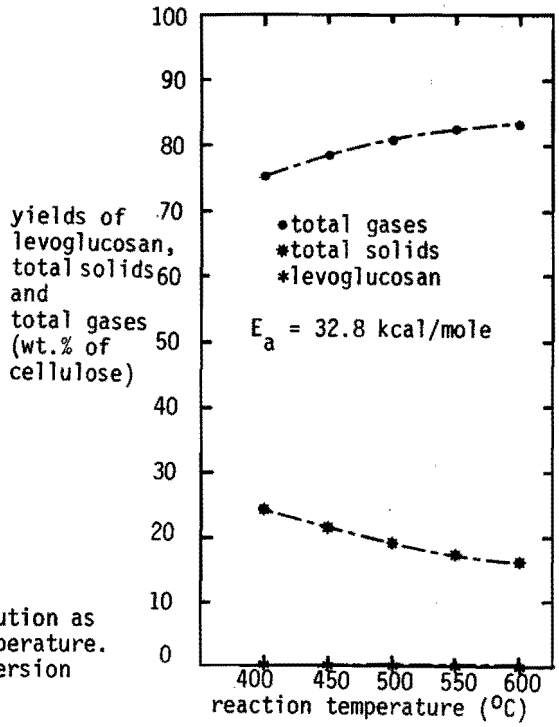

Fig.7.23

Calculated product distribution as a function of reaction temperature. Reaction rate limited conversion model.

7.4.2 Comparison of product distributions obtained from the models to those obtained in pyrolysis experiments using shredded thin cardboard as a feedstock

The product distributions obtained from the models were compared to the experimental product distributions found in the above pyrolysis experiments where shredded thin cardboard was used as a feedstock (see § 5.2.2).

Figs. 7.24 through 7.32 present the experimentally determined product distributions together with the product distributions calculated from the general models with and without tar evaporation at values of E_a of 32.8, 29.5 and 26.2 kcal/mole. The figures show the experimental tar yield (to be compared to calculated levoglucosan yield), the experimental char yield (to be compared to calculated total solids yield) and the sum of the experimental water and gases yield (which is to be compared to calculated total gases yield).

When it is assumed that a macro-kinetic aspects do not play a role in

the pyrolysis conversion (see § 2.3.3) that b the simplifications of the chemical reactions and the heat transport in the models give a sufficiently accurate description of reality and that c the parameter values used together with the models are sufficiently accurate the experimental curves must lie in between the curves obtained with the general model with tar evaporation and the curves calculated from the general model without tar evaporation.

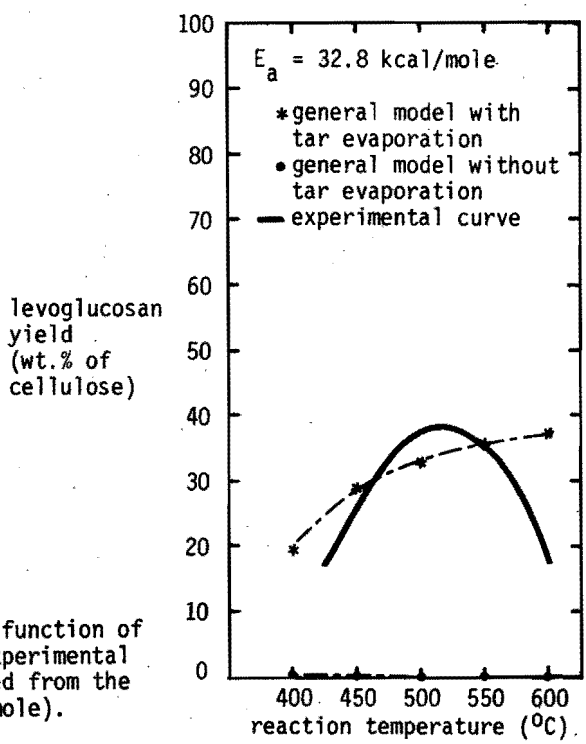

Fig.7.24

Levoglucosan yield as a function of reaction temperature. Experimental curve and curves obtained from the models (E_a = 32.8 kcal/mole).

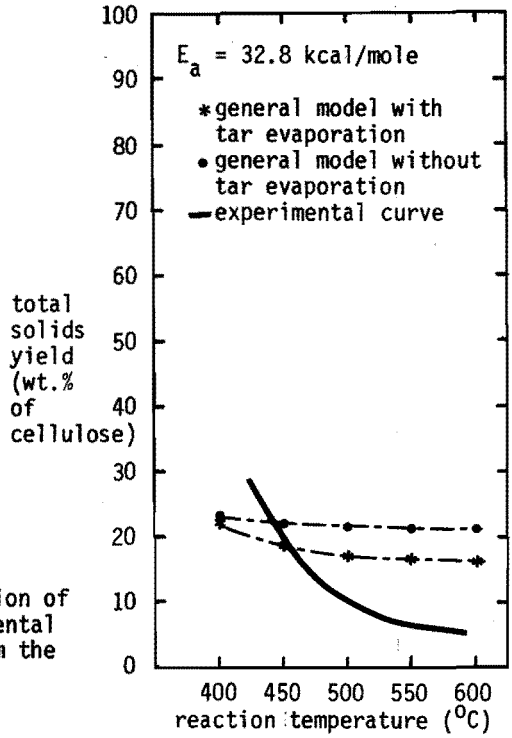

Fig.7.25

Total solids yield as a function of reaction temperature. Experimental curve and curves obtained from the models (E_a = 32.8 kcal/mole).

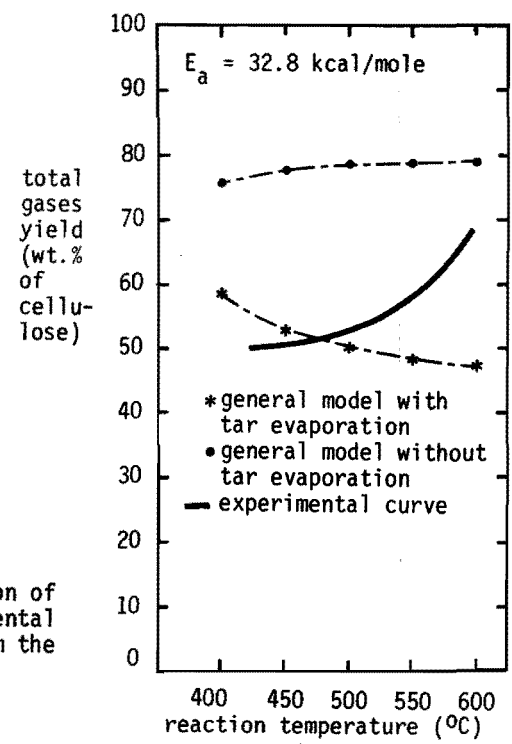

Fig.7.26

Total gases yield as a function of reaction temperature. Experimental curve and curves obtained from the models (E_a = 32.8 kcal/mole).

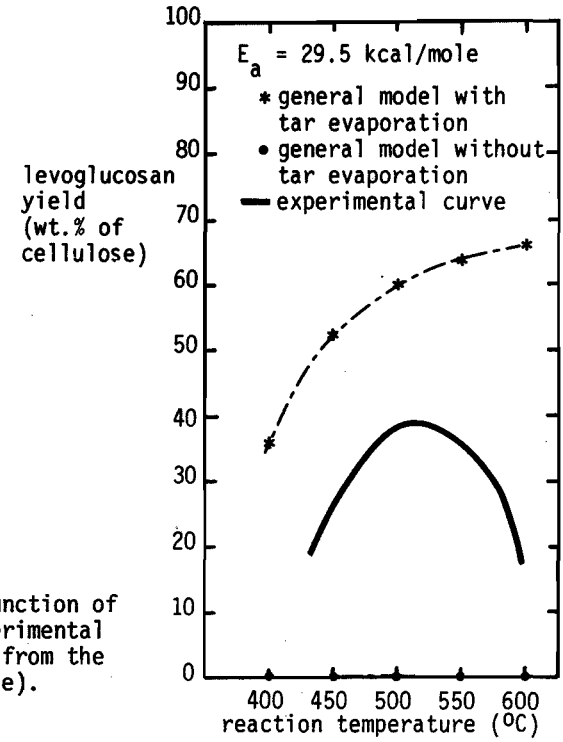

Fig.7.27

Levoglucosan yield as a function of reaction temperature. Experimental curve and curves obtained from the models (E_a = 29.5 kcal/mole).

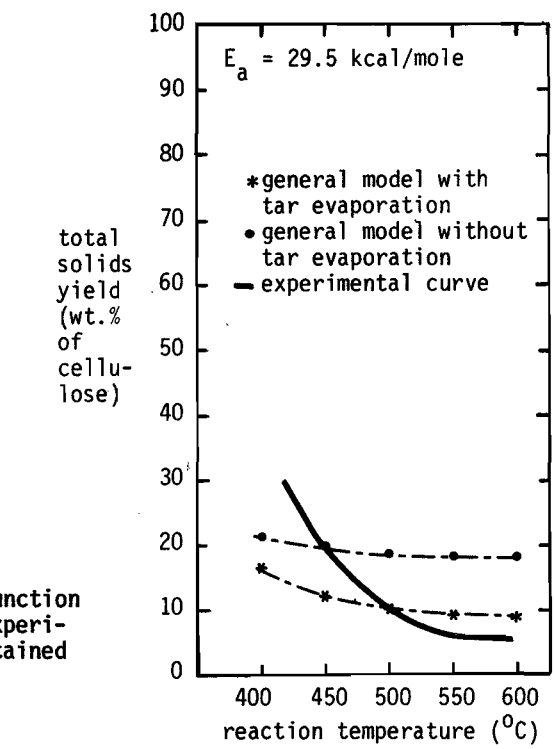

Fig.7.28

Total solids yield as a function of reaction temperature. Experimental curve and curves obtained from the models (E_a = 29.5 kcal/mole).

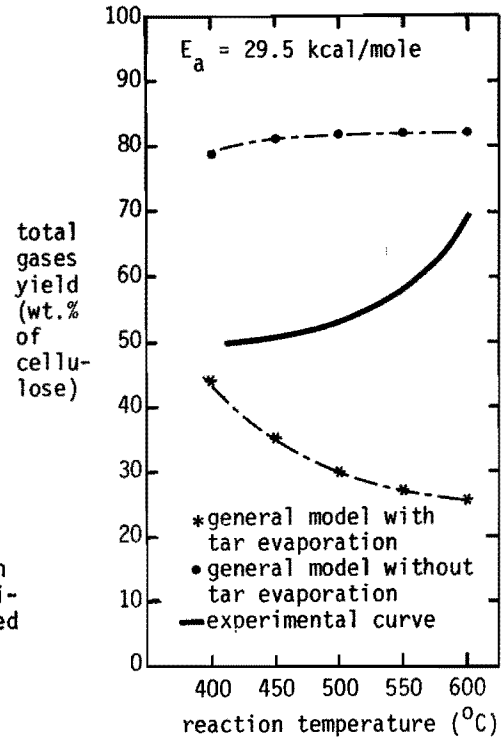

Fig.7.29

Total gases yield as a function of reaction temperature. Experimental curve and curves obtained from the models (E_a = 29.5 kcal/mole).

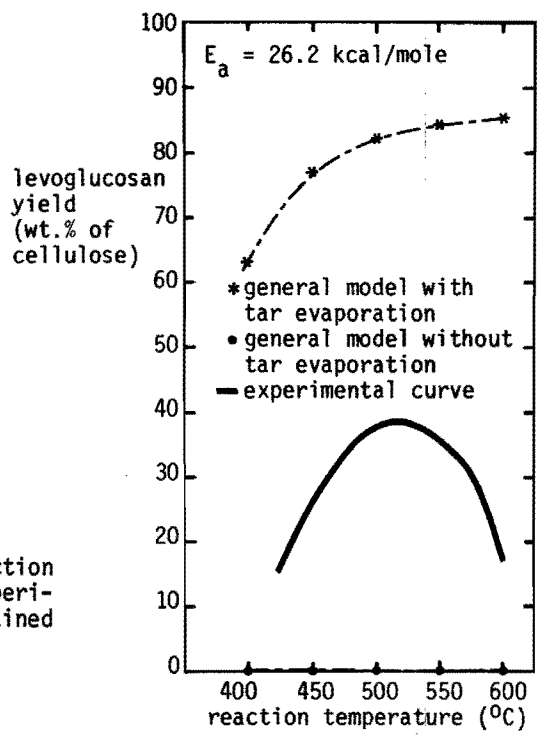

Fig.7.30

Levoglucosan yield as a function of reaction temperature. Experimental curve and curves obtained from the models (E_a = 26.2 kcal/mole).

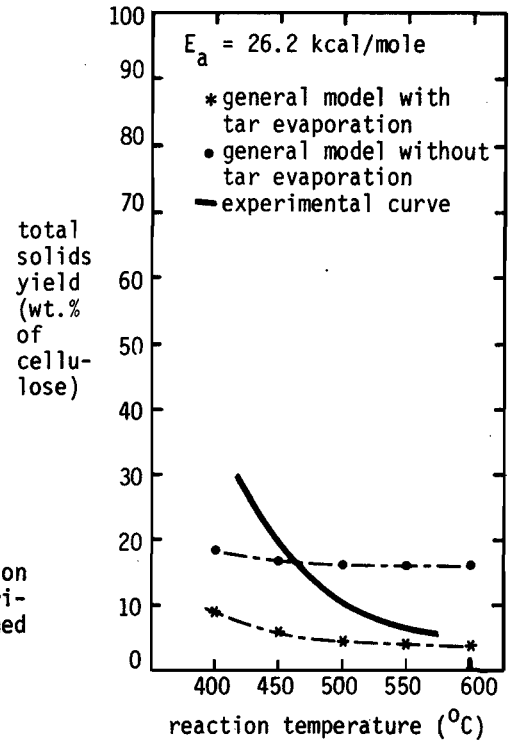

Fig.7.31

Total solids yield as a function of reaction temperature. Experimental curve and curves obtained from the models (E_a = 26.2 kcal/mole).

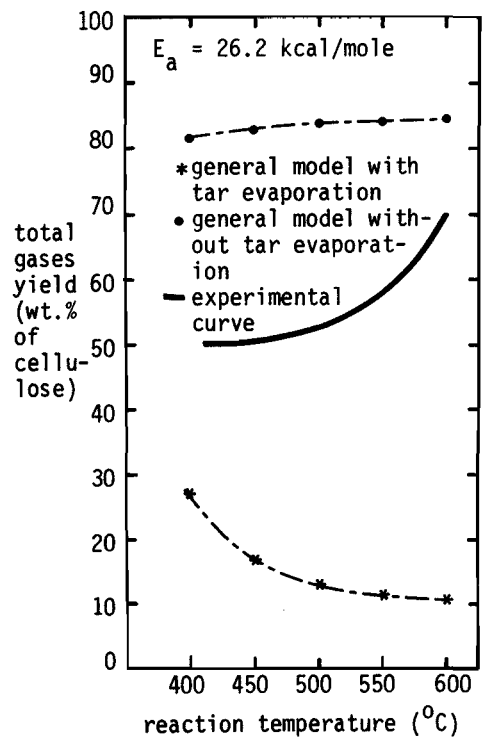

Fig.7.32

Total gases yield as a function of reaction temperature. Experimental curve and curves obtained from the models (E_a = 26.2 kcal/mole).

When the graphs for different values of E_a are compared it is seen that the best results are obtained when using E_a = 26.2 kcal/mole together with the models: the experimental curves of the yields of levoglucosan, total gases and total solids all lie in between the curves obtained with the general model with tar evaporation and the general model without tar evaporation, except for the total solids yield in the low temperature range (reaction temperatures below 450-500°C). See figs. 7.30, 7.31 and 7.32.
But then it has been observed (§ 6.2.1) that the pyrolysis of cardboard in the spout-fluid bed reactor had not been completed at reaction temperatures below about 500°C. The residence time of part of the cardboard particles in the spout-fluid bed reactor was apparently insufficient under these circumstances for the pyrolysis to be complete. Macro-kinetic aspects apparently do play a role in the cellulose pyrolysis in the low temperature range.
This point is illustrated by tables 7.10 and 7.11 and by figs. 7.33 through 7.35. It has been assumed there that cellulose conversion was 80% at 400°C and 90% at 450°C.

The illustration is not correct because the reaction time required to reach 80% cellulose conversion at 400°C is more than twice the reaction time required to reach 90% cellulose conversion at 450°C. Thus the ratio of the reaction times at 400°C resp. 450°C to the unknown average residence times cannot be the same. This is true even though the average residence time at 450°C may well have been somewhat shorter than that at 400°C because the fluidisation and spout gas flow rates at 20°C and 1 atm. were the same in all experiments so that actual gas velocities were higher at 450°C than at 400°C. Note that for the experiments at 500°C and higher the ratios of the reaction times required to obtain 100% cellulose conversion to the unknown average residence times may not be relevant. The reason is that the compositions of the particles no longer change after 100% cellulose conversion has been reached. Although the illustration of tables 7.10 and 7.11 and figs. 7.33 through 7.35 is thus not exact it is nevertheless shown as it gives some impression of the role of the macro-kinetics at pyrolysis temperatures below 500°C.

Table 7.10 Product distributions and reaction times obtained with the general model with tar evaporation for E_a = 26.2 kcal/mole. Incomplete cellulose conversion at low temperatures.

T (^oC)		400	450	500	550	600
t (sec)		4.22	1.99	2.35	1.80	1.57
cellulose	(wt.%)	19.68	9.30	0.01	0.03	0.00
dehydrocellulose	(wt.%)	3.22	0.69	0.00	0.00	0.00
char 1	(wt.%)	6.51	4.94	4.47	3.97	3.70
levoglucosan	(wt.%)	51.31	70.37	82.33	84.28	85.35
gas a	(wt.%)	0.73	0.50	0.44	0.39	0.36
gas c	(wt.%)	18.52	14.05	12.74	11.31	10.57
levoglucosan	(wt.%)	51.31	70.37	82.33	84.28	85.35
total solids	(wt.%)	29.41	14.93	4.48	4.00	3.70
total gases	(wt.%)	19.25	14.55	13.18	11.70	10.93

Table 7.11 Product distributions and reaction times obtained with the general model without tar evaporation for E_a = 26.2 kcal/mole. Incomplete cellulose conversion at low temperatures.

T (^oC)		400	450	500	550	600
t (sec)		3.56	1.31	1.00	0.71	0.57
cellulose	(wt.%)	19.91	9.31	0.02	0.02	0.02
dehydrocellulose	(wt.%)	2.84	0.41	0.00	0.00	0.00
char 1	(wt.%)	6.10	4.15	3.34	2.80	2.49
char 2	(wt.%)	7.69	10.85	13.08	13.37	13.55
levoglucosan	(wt.%)	1.91	1.58	0.01	0.02	0.02
gas a	(wt.%)	0.68	0.42	0.33	0.28	0.24
gas c	(wt.%)	17.33	11.82	9.49	7.95	7.05
gas d	(wt.%)	43.67	61.57	74.18	75.77	76.78
levoglucosan	(wt.%)	1.91	1.58	0.01	0.02	0.02
total solids	(wt.%)	36.54	24.72	16.44	16.19	16.06
total gases	(wt.%)	61.68	73.81	84.00	84.00	84.07

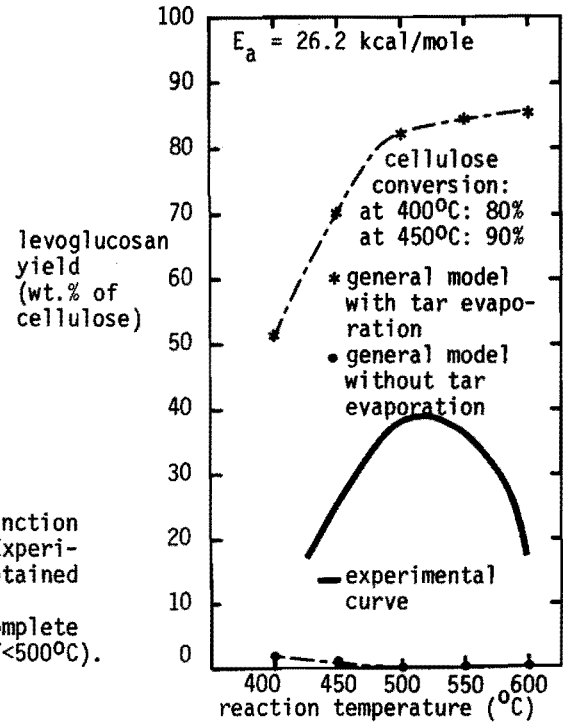

Fig.7.33

Levoglucosan yield as a function of reaction temperature. Experimental curve and curves obtained from the models (E_a = 26.2 kcal/mole, incomplete cellulose conversion for T<500°C).

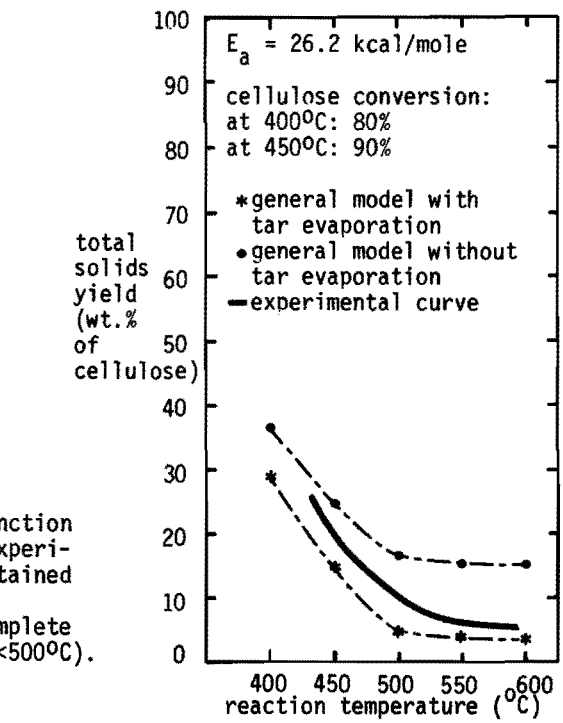

Fig.7.34

Total solids yield as a function of reaction temperature. Experimental curve and curves obtained from the models (E_a = 26.2 kcal/mole, incomplete cellulose conversion for T<500°C).

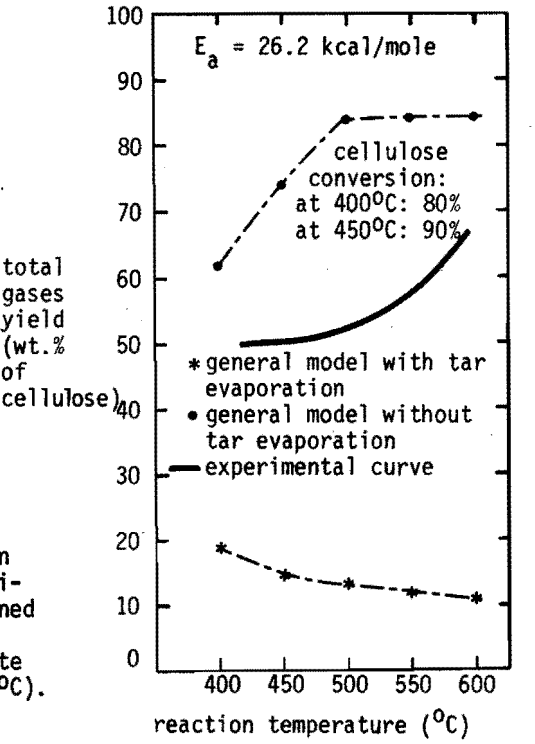

Fig.7.35

Total gases yield as a function of reaction temperature. Experimental curves and curves obtained from the models (E_a = 26.2 kcal/mole, incomplete cellulose conversion for T<500°C).

7.4.3 Closer examination of the influence of the values of some critical physical parameters on the results obtained from the general models.

Before the general findings of modeling the cellulose pyrolysis are discussed the sensitivity of the general models for the values of some of the physical parameters is investigated. The validity of the values of some parameters used in the calculations is open to doubt. This is especially true for the heats of reaction and the heat transfer coefficient for convective heat transport to the cellulose particles. The influence of the values of these parameters on the results of the model calculations are summarized in tables 7.12 and 7.13.

To demonstrate the relative insensitivity of the results of the calculations to the value of Nu, the fact that it is highly improbable that Nu should be lower than 2 has been disregarded (table 7.13).

Table 7.12 The influence of heats of reaction (general model without tar evaporation, E_a = 29.5 kcal/mole, T = 500°C).

		$\Delta\hat{H}_a$ = 69135 J/kg $\Delta\hat{H}_b$ = 691350 J/kg $\Delta\hat{H}_c = \Delta\hat{H}_d$ = -394700 J/kg (see table 7.1)	$\Delta\hat{H}_a = \Delta\hat{H}_b$ = 1000 J/kg $\Delta\hat{H}_c = \Delta\hat{H}_d$ = -1000 J/kg
t (sec)		0.73	0.63
cellulose	(wt.%)	0.02	0.02
dehydrocellulose	(wt.%)	0.00	0.00
char 1	(wt.%)	8.57	7.71
char 2	(wt.%)	9.99	10.52
levoglucosan	(wt.%)	0.02	0.02
gas a	(wt.%)	0.84	0.76
gas c	(wt.%)	24.38	21.92
gas d	(wt.%)	56.62	59.63
levoglucosan	(wt.%)	0.02	0.02
total solids	(wt.%)	18.58	18.25
total gases	(wt.%)	81.84	82.31

It is concluded from table 7.12 that the general model is not very sensitive to the heats of reaction. Changing the values of the heats of reaction with a factor 70 to 400 does hardly change the product distribution or reaction time.

Table 7.13 The influence of Nusselt number (general model without tar evaporation, E_a = 29.5 kcal/mole, T = 500°C)

		Nu = 20	Nu = 2	Nu = 0.2
t (sec)		0.46	0.73	3.08
cellulose	(wt.%)	0.00	0.03	0.09
dehydrocellulose	(wt.%)	0.00	0.00	0.01
char 1	(wt.%)	6.99	8.57	12.22
char 2	(wt.%)	10.83	9.99	7.79
levoglucosan	(wt.%)	0.06	0.02	0.03
gas a	(wt.%)	0.69	0.84	1.21
gas c	(wt.%)	19.85	24.38	34.80
gas d	(wt.%)	61.57	56.62	44.14
levoglucosan	(wt.%)	0.06	0.02	0.03
total solids	(wt.%)	17.82	18.59	20.11
total gases	(wt.%)	82.11	81.84	80.15

The influence of Nusselt number on the product distribution and reaction time is also indicated in fig. 7.36.

The influence of Nusselt number which determines the heat transfer coefficient to the slab is somewhat greater, especially with respect to reaction time. Changing the Nusselt number from 20 to 0.2 increases the reaction time by a factor of 7. However, the changes in the product distributions are relatively small (fig. 7.36).
It was felt on the basis of the above findings that the results obtained from the general models using the parameter values that are summarized in table 7.14 can be maintained.

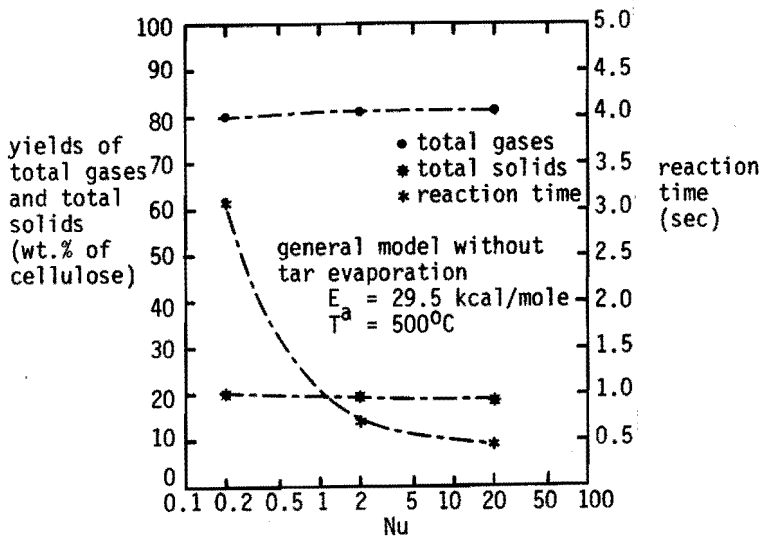

Fig.7.36

Influence of Nusselt number on product distribution and reaction time. General model without tar evaporation (E_a = 29.5 kcal/mole, T=500°C).

Table 7.14 Final values of the parameters used in the models

parameter	value	unit	parameter	value	unit
k_{ao}	$6.2*10^7$	sec^{-1}	ΔH_a	69135	J/kg
k_{bo}	$1.05*10^{17}$	sec^{-1}	ΔH_b	691350	J/kg
k_{co}	$7.05*10^{17}$	sec^{-1}	ΔH_c	-394700	J/kg
k_{cd}	$7.66*10^{13}$	sec^{-1}	ΔH_d	-394700	J/kg
E_a	26.2	kcal/mole	$\lambda_{1,2,3,4}$	0.113	J/m.sec.°C
E_b	53.5	kcal/mole	$\lambda_{ga,gb,gc,gd}$	0.0419	J/m.sec.°C
E_c	54.1	kcal/mole	$C_{p1,2,3,4}$	2304.5	J/kg.°C
E_d	40.5	kcal/mole	$C_{pga,gb,gc,gd}$	2000	J/kg.°C
y_a	0.025	-	T_o	300	°K
y_b	1	-	ρ_o	600	kg/m^3
y_c	0.74	-	Nu	2	-
y_d	0.85	-	R	1.986	kcal/mole,°K
			L	0.00009	m

7.4.4 Discussion

1. Apart from the influence of reaction temperature on the pyrolysis process, the influence of particle size for instance may also be predicted from the general models. Table 7.15 presents the product distribution and reaction time obtained with the general model without tar evaporation for different thickness of the cellulose slab (L = 1/2 d).

Table 7.15 Influence of particle size (general model without tar evaporation, E_a = 29.5 kcal/mole, T = 500°C).

		d = 1 mm	d = 0.18 mm
t (sec)		9.23	0.73
cellulose	(wt.%)	0.06	0.02
dehydrocellulose	(wt.%)	0.01	0.00
char 1	(wt.%)	15.25	8.57
char 2	(wt.%)	5.99	9.99
levoglucosan	(wt.%)	0.02	0.02
gas a	(wt.%)	1.51	0.84
gas c	(wt.%)	43.41	24.38
gas d	(wt.%)	33.91	56.62
levoglucosan	(wt.%)	0.02	0.02
total solids	(wt.%)	21.31	18.58
total gases	(wt.%)	78.83	81.84
cellulose decomposed through:			
dehydration	(%)	60	34
depolymerization	(%)	40	66

It is seen that increasing particle size leads to increasing reaction time and to more cellulose decomposing through dehydration.
Only part of the levoglucosan in fact decomposes into char and gases. In table 7.16 the product distributions are presented for the cases where 25, 50 or 75% of the levoglucosan produced during the pyrolysis decomposes into char and gases.

Table 7.16 Product distributions for different particle size and different percentages of levoglucosan decomposing into char and gases (E_a = 29.5 kcal/mole, T = 500°C)

percentage of levoglucosan decomposing		75% *)		50%		25%	
particle size (mm)		d=1	d=0.18	d=1	d=0.18	d=1	d=0.18
cellulose	(wt.%)	0.06	0.02	0.06	0.02	0.06	0.02
dehydrocellulose	(wt.%)	0.01	0.00	0.01	0.00	0.01	0.01
char 1	(wt.%)	15.25	8.57	15.25	8.57	15.25	8.57
char 2	(wt.%)	4.49	7.50	2.99	5.00	1.50	2.50
levoglucosan	(wt.%)	9.98	16.66	19.96	33.32	29.94	49.97
gas a	(wt.%)	1.51	0.84	1.51	0.84	1.51	0.84
gas c	(wt.%)	43.41	24.38	43.41	24.38	43.41	24.38
gas d	(wt.%)	25.45	42.48	16.97	28.32	8.48	14.16
levoglucosan	(wt.%)	9.98	16.66	19.96	33.32	29.94	49.97
total solids	(wt.%)	19.81	16.09	18.31	13.59	16.82	11.10
total gases	(wt.%)	70.37	67.70	61.89	53.54	53.40	39.38

*) Thus: levoglucosan = 0.25 * [char 2 + levoglucosan + gas d (table 7.15)].

It follows from table 7.16 that as particle size increases total solids yield increases as does total gases yield while levoglucosan yield decreases. Similar trends have been observed in our pyrolysis experiments when cardboard of different particle size were used as feedstocks (see § 6.2.2).

2. It was not possible to distinguish between water and other gases in the models as water is the gaseous product of the dehydration reaction (gas a) while gases c and d also contain water. An extra check on the calculated product distributions on the basis of the experimental water yield could therefore not be carried out.
3. It was not expected that macro-kinetic aspects would play a role in the pyrolysis process. These aspects have therefore not been included in the models which were set up to describe the pyrolysis of single cellulose particles. It was assumed that the residence time of the particles in the reactor would be long compared to the

reaction time. It was observed in the experiments on cardboard, however, that the residence time of part of the cardboard particles in the reactor was insufficient for the pyrolysis to be complete at reaction temperatures below about 500°C.

4. It was not to be expected that the models can describe the experimental results really accurately:
   a. The levoglucosan produced may evaporate during the pyrolysis and be collected as a pyrolysis product. But the levoglucosan may also remain in the particle and there decompose into char and gases. It seems probable that in actual fact the levoglucosan will partly evaporate and that the percentage of the levoglucosan that evaporates depends on the temperatures within the particle. In order to obtain accurate results it is therefore necessary that an effective transport rate coefficient for levoglucosan is incorporated into the model. This effective transport rate coefficient must be temperature dependent. We have made no attempt to incorporate such an effective transport rate coefficient.
   The reason is that we feel that deriving the temperature dependent values of such an effective transport rate coefficient far exceeds the discriminating powers of both our experiments and the models. In addition, the effect indicated under point b below may intervene. This being the case the best we could hope for was that the experimental product distribution curve would lie in between the curve predicted by the general model without tar evaporation (effective transport rate coefficient equal to 0) and that obtained from the general model with tar evaporation (effective transport rate coefficient infinitely large).
   b. The pyrolysis experiments were carried out in a spout-fluid sand bed. The char layers formed at the outside of the pyrolysing particle may be partly removed by abrasion, f.i. through the movement of the sand present in the bed, during the reaction.
   c. Macro-kinetic aspects which have not been included in the models do play a role in the pyrolysis process: the cellulose conversion is incomplete at reaction temperatures below about 500°C and the levoglucosan evaporated from the pyrolysing particle may be sub-

ject to cracking reactions in the bulk gas. However, the effect of the latter phenomenon can at the most be comparable to that which results from assuming that the levoglucosan remains in the particle and is there subject to cracking reactions (general model without tar evaporation).

d. The four-step reaction model is a drastic simplification of the reality. The pyrolysis of cellulose proceeds through a very complex series of competitive and consecutive reactions.

e. The physical processes were also simplified in the models.

It was found, however, that the product distributions obtained from the general models with and without tar evaporation which incorporate chemical as well as physical conversion rate limitations approximate the experimental product distributions of cellulose pyrolysis up to one order of magnitude. To obtain this result the value of the activation energy of the dehydration reaction had to be reduced to a value of 20% lower than the value which was experimentally determined (this being the lower limit of experimental error). In addition, the cellulose conversion for reaction temperatures below 500^{o}C must be assumed to be incomplete.

It is felt that the models do contribute to a better understanding of what is happening during the pyrolysis in spite of the above mentioned shortcomings of the models. We hope that this better understanding may stimulate industrial execution of pyrolysis.

Literature

7.1 J.G. Rittmann, A computer study of the pyrolysis of porous solids, Ph.D. Thesis, Oklahoma State, Univ. Stillwater (1970).

7.2 K. Akita, H. Kase, J. Polymer Science, Polym. Chem. A-1, vol. 5, no.4, pp. 834 (1967).

7.3 R.H. Perry, C.H. Chilton, Chemical Engineers Handbook, 5th edition, McGraw-Hill Book Company, New York (1973).

List of symbols

		S.I. units
Bi	Biot number	-
C_p	heat capacity	J/kg.^oC
d	slab thickness	m
d	particle size	m
d	sample thickness	m
E	activation energy	J/mole
G	mass	kg
ΔH	heat of reaction	J/kg
k	reaction rate constant	sec^{-1}
k_o	frequency factor	sec^{-1}
L	half slab thickness	m
Nu	Nusselt number	-
n	number of thermocouples	-
p	porosity	-
R	gas constant	J/mole.^oK
T	(reaction) temperature	^oC, ^oK
t	reaction time	sec
ΔT	temperature difference	^oC
V	sample volume	m^3
v	ratio of thermal conductivities	-
ΔV	voltage difference	V
x	distance from slab centre	m
y	gas yield factor	-

Greek symbols

λ	thermal conductivity	J/m.sec.^oC
μ_1	see eq. (2.50)	-
ρ	density	kg/m^3
ρ	mass concentration	kg/m^3
Ø	heat flux	J/m^2.sec
Ø	diameter	m

Subscripts

a	reaction a
b	reaction b
c	reaction c
c	char
char	char
d	reaction d
d'	reaction d' (fig. 2.20a)
d"	reaction d" (fig. 2.20a)
g	powder
g	gases
ga	gas a
gb	gas b
gc	gas c
gd	gas d
l	gas, air
paper	paper
tot	total
o	initial
1	reaction, solid 1
2	reaction, solid 2
3	reaction, solid 3
4	reaction, solid 4
∞	continuous phase, environment

8. PROCESS DESIGN AND ECONOMIC EVALUATION OF A PYROLYSIS PLANT ON TECHNICAL SCALE

8.1 Introduction

This chapter discusses the process design of a pyrolysis plant for domestic waste on technical scale. This includes the design of an installation for the preparation of an RDF fraction from the waste and the recovery of f.i. iron from the waste, the design of a reactor system and of apparatuses for the separation of the individual pyrolysis products from the product stream. The economics of the process are discussed and compared to those of conventional incineration of domestic waste. Attention will also be paid to environmental aspects of the process.

The basic reference data for the design were:

1. capacity: 100,000 tons of domestic waste per year
2. combination of recovery of certain waste components and of pyrolysis
3. low temperature pyrolysis in a spout-fluid bed reactor. Low temperature and application of a spout-fluid bed reactor are selected in order to maximize tar production. Tar is felt to be a more attractive fuel than char or low calorific value gas (see § 3.1).

The design of the pyrolysis part of the plant was based on the results obtained in the above pilot plant experiments on shredded thin cardboard (§ 5.2) as insufficient data on the pyrolysis of organic fractions from domestic waste were available at the time when the present calculations were made. The consequences of the use of data based on cardboard pyrolysis instead of on pyrolysis of domestic waste fractions will, however, be discussed in the final paragraphs of this chapter.

Installations with a capacity of 50,000 and 200,000 tons/year will also be dicussed in the economic evaluation.

A simplified process scheme of the plant is shown in fig. 8.1.

No detailed calculations will be presented in this chapter to promote surveyability. Detailed calculations are, however, shown in lit. no. [8.1].

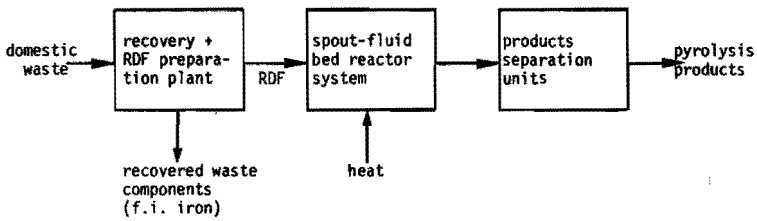

Fig.8.1 Simplified process scheme of pyrolysis plant

8.2 Design of a plant for recovery of waste components and RDF preparation

8.2.1 Introduction

A waste separation plant was designed in which some components of the domestic waste are recovered and in which an RDF fraction is prepared as a feedstock for the pyrolysis reactor. RDF (Refuse Derived Fuels) indicates a concentrate of the organic materials from domestic waste. Two flow schemes have been adopted that pursue different separation aims:

1. preparation of an RDF fraction for pyrolysis that includes paper, plastics and organics.
2. preparation of an RDF fraction for pyrolysis that includes organics only while plastics and paper are recovered separately for recycling purposes.

The final design of the waste separation plant was based on the process scheme of an existing material-from-waste recovery plant developed by TNO/Esmil [8.2]. The composition of the domestic waste which was used as a feedstock to the separation plant in the design calculations is presented in table 8.1.

8.2.2 Details on the design

Both flow schemes (figs. 8.2 and 8.3), the motivation why different types of apparatuses were selected and the order of the apparatuses in the schemes are discussed below together with data on the output streams of the separation plant. The numbers shown refer to the flows indicated in figs. 8.2 and 8.3.

Table 8.1 Composition of Dutch domestic waste (in kg/100 kg domestic waste "as is" [8.3])

components	wt.% wet basis	wt.% dry basis	wt.% water
organics like garden and kitchen waste	48	19	29
paper	22	15	7
plastics	6	6	-
rest of organics	5	4	1
glass	12	12	-
iron	3	3	-
inorganics	4	4	-
total	100	63	37

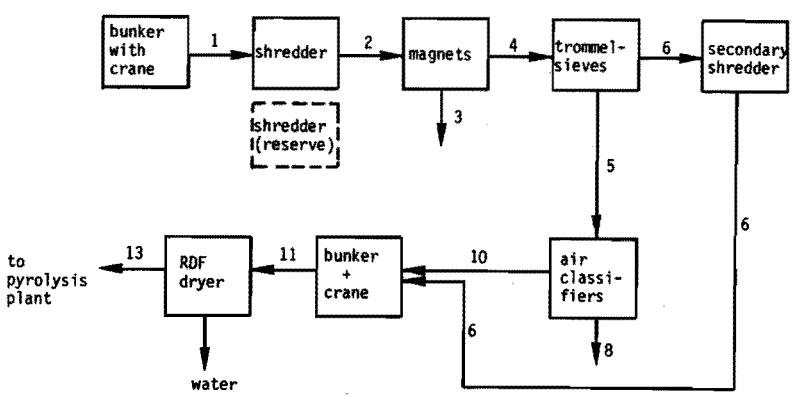

Fig.8.2 Waste separation plant. Flow scheme 1 (no recovery of paper and plastics)

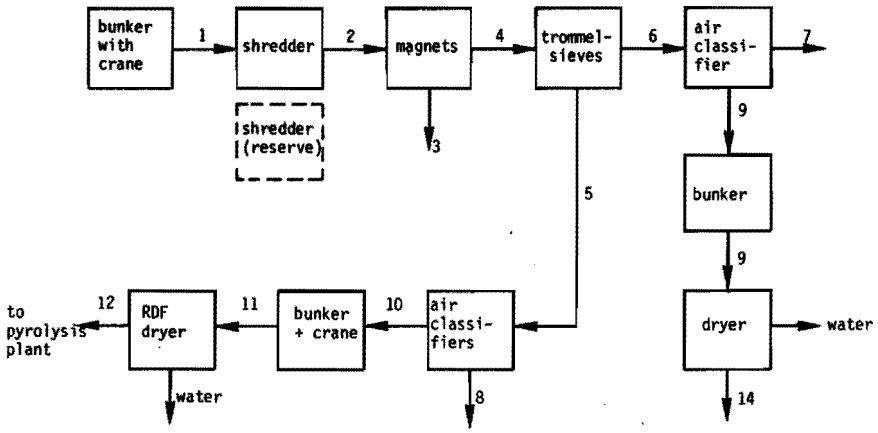

Fig.8.3 Waste separation plant. Flow scheme 2 (recovery of paper and plastics)

- Bunker (flow schemes 1 and 2)
  The bunker was meant for dealing with peaks and stagnancies in the domestic waste supply. The crane takes care of the transport of the waste from bunker into the shredder.
- Shredder (flow schemes 1 and 2)
  The shredder (a flail mill) tears the bags and shreds the organic material. It also serves to desagglomerate the waste. Carpets and other large, massive pieces must be removed first.
- Magnets (flow schemes 1 and 2)
  The magnets remove iron (3) from the waste. They are located downstream from the shredder as the iron is more desaggregated here and upstream from the other separation units in order to relieve the load on these apparatuses.
- Trommelsieves (flow schemes 1 and 2)
  The trommelsieves classify the waste particles according to their sizes. Most of the paper and plastics and some organics pass out of the sieves in the oversize stream (6).

The flow schemes differ from here on and are therefore discussed separately.

Flow scheme 1

- Secondary shredder
  Stream 6 (paper and plastics) is fed into a shredder where the plas-

tics and paper are shredded to ensure smooth transport into the pyrolysis reactor. The paper and plastics have not been shredded in the primary shredder in order to save energy and because this would have had a bad influence on the separation performance of the trommelsieves.

- Air classifiers (feed: stream 5)
  The organic material is cleaned of glass and inorganics as far as possible in the air classifiers. The air classifiers classify according to the fall behavior of the particles in stagnant air (see also Chapter 4). The relatively light organic materials pass out of the classifiers in the top fraction (10). Glass and inorganics drop out of the classifiers at the bottom (8).

Flow scheme 2

- Air classifier plastics/paper (feed: stream 6)
  Stream 6 is sprayed with water. The paper is moistened selectively and the fall behavior of the paper is thus changed so that it differs more from the fall behavior of the plastics. Separation of paper and plastics by means of air classifying is now possible.
- Bale press and bunker
  Storage of the paper (9) is necessary to bridge the difference in operation times of the waste separation plant and the dryer. The waste separation plant is operated 16 hours/day except in the week ends. The pyrolysis unit is operated continuously. The dryer is also operated continuously as the heat for drying of the paper is provided by the pyrolysis unit.
- Dryer (for drying the paper (9))
  The paper must be dried again to prevent it from rotting. The paper is dried by trommel-drying.

Both flow schemes (figs. 8.2 and 8.3) show a bunker and dryer for the RDF fraction to be used as pyrolysis feedstock (stream 10 or streams 10 + 6 = stream 11). Drying of the RDF fraction appeared to be advantageous with respect to reactor design (see § 8.3). It was concluded that it would be attractive to dry the feed to the pyrolysis reactor to moderate humidity. It was therefore decided to bring the moisture content of the RDF fraction down to about 15 wt.% in a trommel-dryer. A bunker for storing the RDF fraction was necessary then because of the difference in operation times of the waste separation plant and

pyrolysis unit (see above).

The waste separation plant can be operated according to two flow schemes (1 and 2) depending whether it is thought attractive to recycle paper and plastics or to feed them to the pyrolysis unit. The material flows inside the waste separation plant is shown in tables 8.2 and 8.3 for flow schemes 1 and 2 respectively.

Table 8.2 Material flows for flow scheme 1 (input 100 kg domestic waste "as is")

Flow (kg)↓ Stream no.→	1	2	3	4	5	6	8	10	11	13
organics (garden, kitchen waste)	48	48	-	48	39	9	8	31	40	22
paper	22	22	-	22	4	18	2	2	20	17
plastics	6	6	-	6	2.5	3.5	1	1.5	5	5
rest of organics	5	5	-	5	4	1	1	3	4	4
glass	12	12	-	12	12	-	10	2	2	2
iron	3	3	3	-	-	-	-	-	-	-
inorganics	4	4	-	4	4	-	3	1	1	1
total	100	100	3	97	65.5	31.5	25	40.5	72	51
total (tons/hr) *)	33	33	1	32	22	10	8	14	24	17

*) The waste separation plant is operated for 3000 hrs in a year.
A capacity of 100,000 tons/year corresponds to 33 tons/hr.

Table 8.3 Material flows for flow scheme 2 (input 100 kg domestic waste "as is").

Flow (kg)↓ Stream no.→	1	2	3	4	5	6	7	8	9	10	12	14
organics (garden, kitchen waste)	48	48	-	48	39	9	6	8	3	31	17	2
paper	22	22	-	22	4	18	-	2	18	2	2	15
plastics	6	6	-	6	2.5	3.5	3	1	0.5	1.5	1.5	0.5
rest of organics	5	5	-	5	4	1	1	1	-	3	3	-
glass	12	12	-	12	12	-	-	10	-	2	2	-
iron	3	3	3	-	-	-	-	-	-	-	-	-
inorganics	4	4	-	4	4	-	-	3	-	1	1	-
total	100	100	3	97	65.5	31.5	10	25	21.5	40.5	26.5	17.5
total (tons/hr) *)	33	33	1	32	22	10	3	8	7	14	9	6

*) The waste separation plant is operated for 3000 hrs in a year. A capacity of 100,00 tons/year corresponds to 33 tons/hr.

The output of the waste separation plant is

a. for flow scheme 1:
   stream 3 (iron)
   stream 8 (inorganics that have to be disposed of)
   stream 13 (dried RDF fraction (15 wt.% water) which is used as feedstock for pyrolysis)

b. for flow scheme 2:
   stream 3 (iron)
   stream 7 (from which plastics may be separated and sold)
   stream 8 (inorganics that have to be disposed of)
   stream 12 (dried RDF fraction (15 wt.% water) which is used as feedstock for pyrolysis)
   stream 14 (paper which is sold after cleaning)

Table 8.4 summarizes the data that are required for the design of the pyrolysis unit.

Table 8.4 Data on feedstock for pyrolysis

	Flow scheme 1	Flow scheme 2
Dried RDF fraction flow (tons/hr) [1]	6.9	3.8
Composition	see table 8.2 (stream no.13)	see table 8.3 (stream no. 12)
Moisture content (wt.%)	15	15
Heat of combustion (kcal/kg)	3000	2300
Particle size (m)	< 0.1	< 0.1

[1]) The pyrolysis unit is operated continuously. This corresponds to 7000 operating hrs/year.

The investment costs of the apparatuses for the waste separation plant are given in table 8.5.

Table 8.5 Equipment costs

Apparatus	costs (Dfl. in 1981)
bunker for storing domestic waste	500,000
crane	300,000
2 trommelsieves	180,100
3 cyclones	76,300
3 air classifiers	120,000
3 blowers	121,500
2 primary shredders (one reserve) 1 secondary shredder	1,215,000
2 belts + magnets	58,600
bunker for storing paper	185,000
trommel-dryer (for paper)	25,000
bunker for storing RDF	441,700
crane	300,000
trommel-dryer (for RDF)	685,000
total equipment costs	4,208,200

8.3 Design of pyrolysis reactor

8.3.1 Introduction

The design of the spout-fluid bed reactor was the most critical part of the design of the pyrolysis unit. The design had to based on the experiences we had with the relatively small spout-fluid bed reactor installed in the pilot plant described before (Chapter 3). No data on existing spout-fluid bed reactors were found in literature nor were larger scale spout-fluid beds available in our laboratory that might have provided us with more insight in the factors that determine the up-scaling of this type of reactor.

It was quite clear, however, that linear up-scaling was not possible. The gas production in the reactor is proportional to bed volume and thus to bed diameter to the power three, assuming constant bed height to bed diameter ratio and constant loading of the bed. The gas velocity resulting from this gas production is inversely proportional to the square of bed diameter. Linear up-scaling would therefore lead

to rapidly increasing gas velocities in the bed that increase with increasing bed diameter so that the bed material might be blown out of the reactor at larger diameter values.

Some of the factors that played an important role in the design of the spout-fluid bed reactor were:

1. The minimum fluidisation gas flow rate that is allowable to ensure good solid phase mixing in the bed.
2. The minimum spout gas velocity required for pneumatic transport of the RDF. It is recalled that the feed is introduced into the reactor together with the spout gas.
3. The maximum spout gas flow rate that is allowed to prevent the bed from operating in the stable spout regime (see Chapter 4).
4. The ratio of bed diameter to spout diameter.
5. The maximum flow rate of the gas that passes out of the reactor that is allowed to prevent the bed material from being entrained by this gas flow.
6. The minimum ratio of bed height to bed diameter that still ensures good solid mixing behavior in the bed.

Part of the above factors are determined by the characteristics of the fluidisation medium that is used. It was decided to use the same fluidisation medium that we had applied in the experiments in the pilot plant, i.e. sand particles with diameters in the range of 400-800 μm and with a density of 2600 kg/m^3. The reason is that all the experience we had in spout-fluidising was based on investigations in which only this material had been used.

The choice of this sand as a fluidisation medium also determines the minimum fluidisation gas flow rate (u_{mf}) and the maximum gas flow rate in the reactor that has to be observed to prevent the sand particles from being blown out of the reactor. u_{mf} was calculated to be 22 cm/sec. The fall velocity of the smallest sand particles (400 μm) was calculated to be about 2 m/sec.

The six above factors are now discussed quantitatively:

1. Good solid phase mixing in the spout-fluid bed is ensured when the fluidisation gas flow rate exceeds 1.75*u_{mf} (see Chapter 4). It was decided therefore to apply a fluidisation gas flow rate (at the sieve plate) of 40 cm/sec.

2. Smooth pneumatic transport of the RDF fraction (particles < 10 cm) is ensured at linear spout gas velocities of about 10-15 m/sec or larger. A linear spout gas velocity of 15 m/sec was therefore chosen in the design.
6. The ratio of bed height (H) to bed diameter (D) applied in the experiments in the pilot plant was about 1.5. Studies of the mixing characteristics of spout-fluid beds at different values of this ratio showed, however, that reduction of the value of this ratio to about 1 does not affect the mixing behavior in the spout-fluid bed. Therefore H/D = 1 was adopted.

The above factors 3,4 and 5 are closely related to each other. The total gas flow rate (factor 5) results from the fluidisation gas flow, the spout gas flow and the gas production in the bed. The fluidisation gas flow has already been discussed (factor 1). The spout gas velocity has been chosen (factor 2) and equals 15 m/sec (linear). It is therefore necessary not to use a large spout diameter in order to keep the superficial spout gas flow rate and thus the total gas flow rate in the reactor relatively low. In addition, the superficial spout gas flow rate being relatively low prevents the bed from operating in the stable spout regime (factor 3). A ratio of bed diameter to spout diameter of 10-15 was selected on the basis of these considerations. The gas production in the bed can be reduced by drying the feed (less water vapor in the reactor) and by decreasing the waste loading of the bed. It was decided to dry the feed to a humidity of 15 wt.% (see § 8.2). The maximum gas flow rate in the reactor must not exceed 2 m/sec to prevent the smallest sand particles from being entrained by the gas. The gas flow rate at the top of the reactor may be reduced by the use of a disengagement zone on top of the reactor.
The above findings are summarized in table 8.6 together with additional data on the temperature of the flows that are introduced into the reactor.

Nothing has been said so far about the way the heat requirements in the pyrolysis process were going to be met. Two alternatives were adopted in the design of the reactor:

1. introduction of less than stoechiometric amounts of air into the reactor. Combustion of part of the feed or pyrolysis products in the reactor to provide the required heat.

Table 8.6 Data used in designing the spout-fluid bed reactor.

fluidisation medium	sand; $400<d_p<800\mu m$; ρ = 2600kg/m^3
fluidisation gas flow rate (m/sec)	0.40
spout gas velocity (m/sec)	15
maximum gas flow rate in reactor (m/sec)	2
ratio of bed height to bed diameter	1
ratio of bed diameter to spout diameter	10-15
temperature feedstock (RDF directly from dryer)	80^{o}C
temperature spout and fluidisation gas entering the ractor (recirculated pyrolysis gas)	150^{o}C

2. the use of a second, fluidised bed in which the fluidisation medium is heated (by off gases from a furnace in which part of the pyrolysis products are burned). The hot fluidisation medium is then recirculated to the pyrolysis reactor.

Introduction of air into the reactor is a relatively simple way to provide the heat. A disadvantage is of course that large amounts of nitrogen are introduced into the reactor so that the calorific value of the pyrolysis gas is reduced while the gas flows in the reactor and in the apparatuses for separation of the pyrolysis products are increased. The second option is a more complicated and a relatively expensive one. It requires a second bed and sand transport lines between this bed and the pyrolysis reactor.

The design of the reactor will be discussed below for both alternatives. The design of the reactor was based on the maximum throughput (6.9 tons/hr., table 8.4).and was carried out for reaction temperatures for which tar yield was expected to be maximal. Maximum tar yield was achieved in the pyrolysis experiments on shredded cardboard at reaction temperatures of about 500-525^{o}C (see § 5.2.2; it is repeated here that the process design was based on the pyrolysis experiments on cardboard, see § 8.1). In the case of the reactor with an external sand heater the calculations were therefore carried out for a reaction temperature of 500^{o}C. In the case of the reactor with partial combustion the calculations were carried out over a wider temperature range. The reason is that part of the tar is burned to provide the required heat. Maximum net tar production may therefore occur at reaction temperatures that differ from those for which maximum tar yield was found in the pyrolysis experiments on cardboard.

8.3.2 Reactor design for the case of partial combustion

The gas flow rate in the reactor above the bed was calculated from:

$$v_p = (u_f + \frac{v_{sp}}{c^2}) \cdot \frac{T_r}{T_{in}} \cdot \frac{P_r + \rho_b.g.h_{bed}}{P_r} + \frac{Q_{prod}}{\frac{1}{4}.\pi.d_b^2} \qquad (8.1)$$

where v_p = gas flow rate above the bed (m/sec)
u_f = fluidisation gas flow rate at the bottom of the bed (m/sec)
v_{sp} = linear spout velocity (m/sec)
c = ratio of bed diameter to spout diameter
T_r = reaction temperature (^oK)
T_{in} = temperature of spout and fluidisation gas entering the reactor (^oK)
P_r = pressure in reactor above the bed (N/m^2). P_r was fixed at 1.2 atm. to provide the head required for the products separation units.
ρ_b = bulk density of sand (kg/m^3)
g = gravitational acceleration (m/sec^2)
h_{bed} = static bed height (m)
d_{bed} = bed diameter (m)
Q_{prod} = net gas production (m^3/sec)

Q_{prod} = flow rate of gaseous pyrolysis products (including tar and water vapor) plus combustion gases produced in the reactor minus the amount of air that was introduced into the reactor. The air is introduced into the reactor through the fluidisation gas.

The below trial-and-error method was used to calculate the reactor diameter:

- A reactor diameter was selected on the basis of rough calculations.
- Fluidisation and spout gas flows were calculated from the data given in table 8.6 and from the reactor diameter.
- The heats required to heat the feed, to heat the fluidisation and spout gases and to evaporate the water in the feed were calculated (see also table 8.4).
- The amount of air required for the combustion that provides the required heat was calculated from the heats of combustion and from the composition of the components that are oxidized. This amount of

air and the amount of the combustion gases produced were not very sensitive to what components were assumed to be oxidized (feedstock or various pyrolysis products). It was assumed that gaseous pyrolysis products would burn more easily than either char or feedstock. The calculations were therefore carried out on the assumption that the heat requirements in the reactor are met by combustion of the pyrolysis gas and part of the tar. It was further assumed that the gas is converted entirely to CO_2 and H_2O and the tar to H_2O and equimolar amounts of CO_2 and CO.

- The amounts of gaseous pyrolysis products and combustion gases that are formed in the reactor are calculated.
- v_p is calculated from eq. (8.1).

The bed diameter was increased or decreased depending on the value of v_p that was calculated and the procedure was started all over again. The calculations were initially carried out for a reaction temperature of 600°C. This resulted in a reactor diameter of 2.70 m and a spout diameter of 18 cm (c=15). The maximum gas flow rate above the bed v_p = 1.95 m/sec in that case. The results for different reaction temperatures are summarized in table 8.7 for the above reactor diameter.

Table 8.7 Compositions and sizes of flows that are introduced into the reactor or that pass out of it (reactor diameter = 2.70 m, spout diameter = 18 cm). Input: 6900 kg RDF/hr.

reaction temperature (°C)→		450	500	550	600
v_p (m/sec)		1.77	1.76	1.97	1.95
Q_{spout}	(m^3 at 20°C and 1 atm/hr)	1500	1500	1500	1500
Q_{fluid}	(m^3 at 20°C and 1 atm/hr)	9050	9050	9050	9050
Q_{air}	(m^3 at 20°C and 1 atm/hr)	4310	3380	4750	5340
Q_{out}*)	(m^3 at 20°C and 1 atm/hr	16,550	15,370	16,200	15,100
	(actual m^3/hr)	36,500	36,300	40,700	40,240
Composition of gas that passes out of reactor (vol.%):	N_2	33.5	33.4	36.9	40.9
	H_2O	53.9	49.9	47.2	43.9
	CO	4.7	5.6	3.0	1.5
	CO_2	7.4	10.6	11.9	11.8
	tar	0.5	0.5	1.0	1.5
	rest **)	-	-	-	0.4
tar (kg/hr)		360	1040	1315	1055
char (kg/hr)		1334	626	465	406

*) Q_{out} = flow rate of gas that passes out of the reactor

**) rest = CH_4, C_2H_6, H_2

The static bed height equals the bed diameter (2.70 m). The bed will expand during operation, and the reactor must therefore be higher. In addition, the reactor was provided with a disengagement space on top of it. The gas velocity is halved in this disengagement space. A sketch of the reactor is given in fig. 8.4.

The resulting flow scheme for maximizing tar yield is presented in fig. 8.5. This scheme anticipates upon the designs of the products separation units that are discussed in the next paragraphs. The reaction temperature is 500°C. The net product is tar. Other pyrolysis products are burned in a furnace to provide the heat required for drying of the RDF fraction. Some comments to the flow scheme (fig. 8.5):

	N_2	H_2O	CO	CO_2	tar
- composition of gas that passes out of the reactor (vol.%)	33.4	49.9	5.6	10.6	0.5 (=0.32 kg tar/sec)

	N_2	H_2O	CO	CO_2
- composition of gas that passes out of the scrubber (vol.%)	25.4	62.3	4.3	8.0

	N_2	O_2	CO_2	H_2O
- composition of drying air (vol.%)	73.1	18.3	3.0	5.6 (= 0.035 kg H_2O/kg dry air)

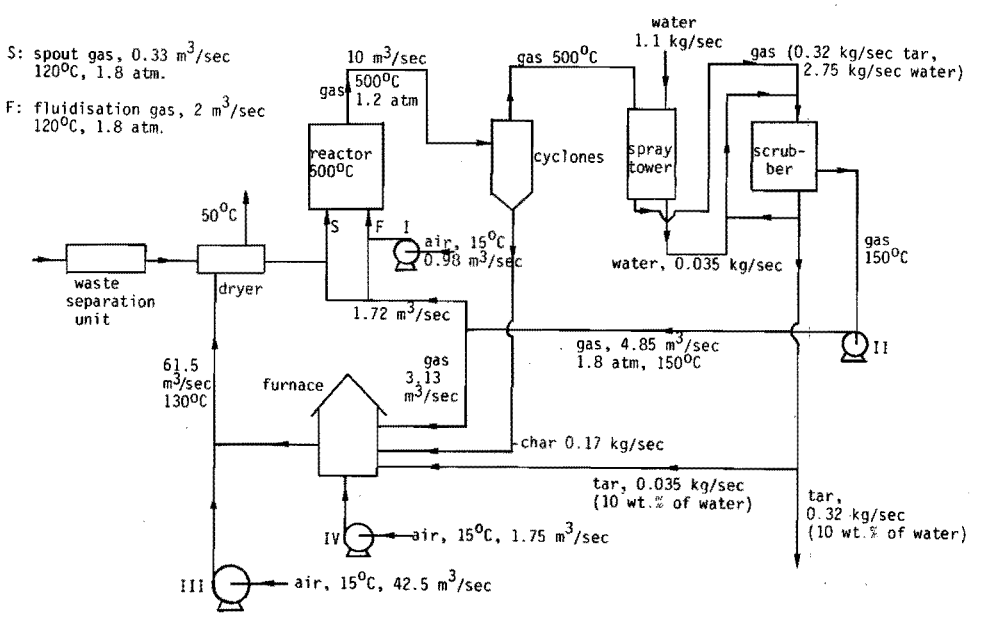

Fig.8.5 Flow scheme (reactor with partial combustion at maximum tar yield)

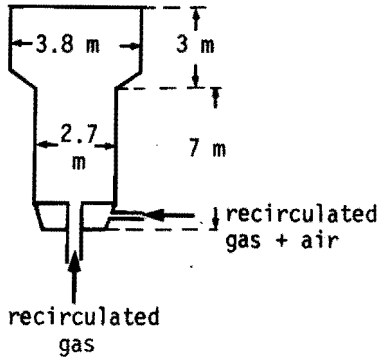

Fig.8.4 Sketch of the reactor with partial combustion.

Additional data on the reactor system:
Ash is removed from the bed semi-continuously by means of overflows. The RDF fraction is introduced into the reactor through the spout pipe. A sluice is required in the feeding system as the pressure in the reactor just below the sieve plate is about 1.8 ata. The RDF is dosed into the spout pipe by means of a vibratory conveyor. The construction materials used in the reactor system are:

- spout pipe: 10 CrMo 9 10 steel (thickness 5 mm). Very hard steel is required because of the eroding action of the waste in the spout pipe.
- sieve plate: steel that has been nickel-plated in an electrolytical process (thickness 12.2 mm).
- reactor wall: 15 mm construction steel with a refractory lining (Chamotte Y42 bricks, 42% Al_2O_3) to protect the reactor wall against erosion by the sand.
- insulation: 200 mm Fiberfrax low conductivity blankets.

The equipment costs (apparatuses directly related to the reactor) are summarized in table 8.8. The equipment costs of the remaining apparatuses will be presented later on.

Table 8.8 Equipment costs.

Apparatuses	costs (Dfl. in 1981)
reactor (including sieve plate, bricks and insulation)	175,600
solid feed dosage system	116,000
blowers (inclusive of electro motors)	266,500
furnace	750,000
total equipment costs	1,308,100

8.3.3 Reactor design for the case of an external sand heater

A simplified diagram of the reactor system for the case that an external sand heater is used is presented in fig. 8.6.

The reactor

Relationship (8.1) (see § 8.3.2) was used for calculating the reactor diameter in this case also. Q_{prod} (= net gas production flow, m^3/sec) consists of pyrolysis gases, tar and water vapor that are produced in the reactor. Q_{prod} could be calculated directly from the product distributions obtained in pyrolysis experiments on cardboard (§ 5.2.2) and from the amount of water present in the feed (15 wt.%). The reaction temperature that was selected is 500°C (in order to maximize tar yield, see also § 8.3.1). The reactor diameter was now calculated from eq. (8.1) using the data presented in table 8.6 (with c=10). The reactor diameter resulting from the calculation was 1.60 m. The reactor dimensions are presented in fig. 8.7. The flow scheme is presented in fig. 8.8.

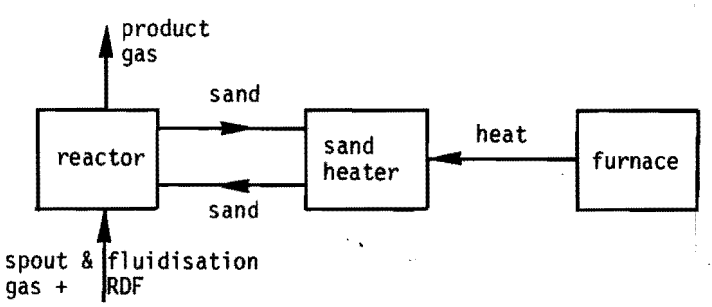

Fig.8.6 Simplified scheme of reactor system (reactor with external sand heater)

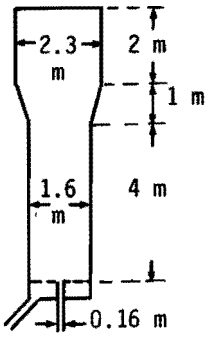

Fig.8.7 Reactor dimensions (reactor with external sand heater)

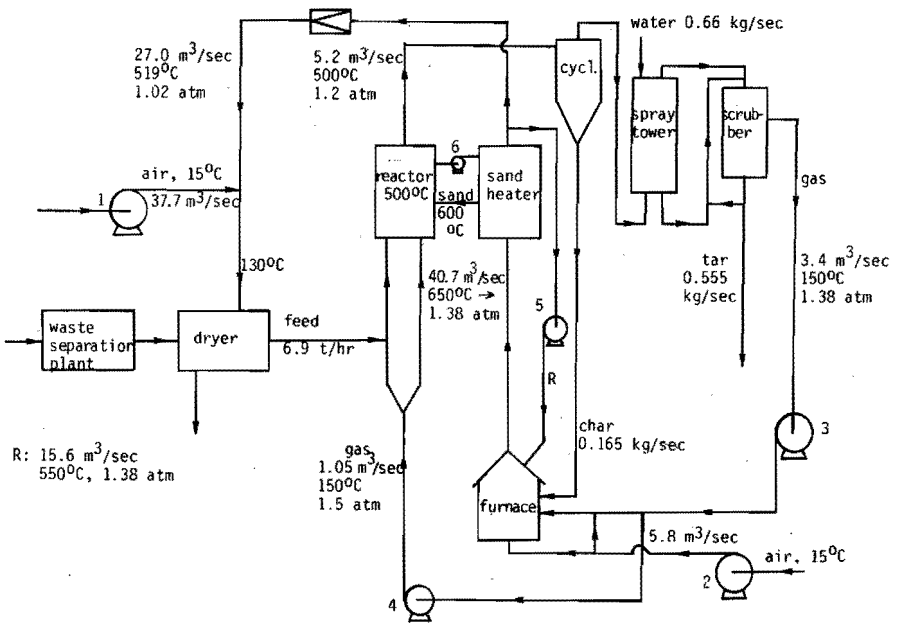

Fig.8.8 Flow scheme (reactor with an external sand heater at maximum tar yield)

The heat requirements in the reactor for heating the spout and fluidisation gases, for heating the feed and to evaporate the water present in the feed were now calculated. The heat requirements in the reactor were: 2.6 MW (temperature of spout and fluidisation gas = 150°C, reaction temperature = 500°C).

The furnace

Part of the products from the pyrolysis process are burned in a furnace to generate hot gases. The hot gases are used for heating the sand in the sand heater and for drying the RDF fraction. It should be noted that only very little char is deposed on the sand. It is therefore not possible to heat the sand in the sand heater by combustion of char deposed on the sand only. The process scheme of the furnace section is presented in fig. 8.9.

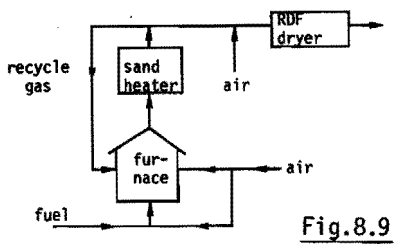

Fig.8.9 Furnace section

The pyrolysis products are burned with primary combustion air. Secondary combustion air and recirculated combustion gases are introduced into the furnace to cool the gas flow that leaves the furnace to the required temperature.

The heat required in the reactor was calculated to be 2.6 MW (see above). The heat required in the dryer for the RDF fraction is 4.8 MW. Extra heat must be provided by the furnace to compensate for cooling of the gas flow to the RDF dryer due to expansion (1.2 → 1.02 atm.). Char, pyrolysis gas and low boiling organic compounds are burned in the furnace. The results of the calculations are presented in fig. 8.10.

The sand heater

The sand heater consists of two fluid beds in series (fig. 8.11). It was decided to use two beds in series in which the gases flow countercurrently to the sand because the off gases from the furnace can be cooled down in this way to temperatures below the final temperature of the sand. More efficient use is therefore made of the heat content of these gases than in case of one fluidised bed only. The temperature profile is given in fig. 8.12. The superficial gas velocity in the beds is 2 m/sec. The bed height in each bed is 50 cm. Both beds are cylindrical and the dimensions are: diameter 5 m, height 10 m.

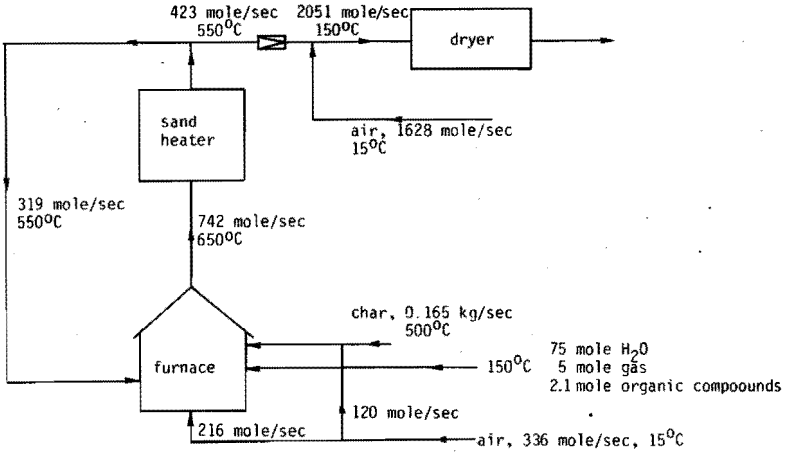

Fig.8.10 Flows in furnace section

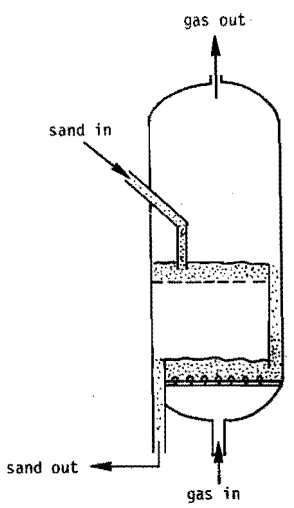

Fig.8.11 Sand heater

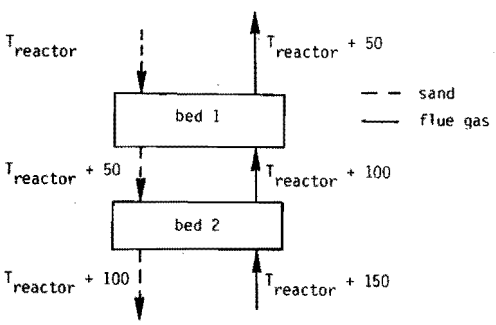

Fig.8.12 Temperature profile in sand heater (°C)

Sand circulation system

Steam was selected as transport medium as it does not give rise to undesirable reactions in either the pyrolysis reactor or the sand heater. The steam provides a gas lock between sand heater and reactor to prevent the oxygen that is present in the gas entering the sand heater from getting into the reactor (see fig. 8.13).

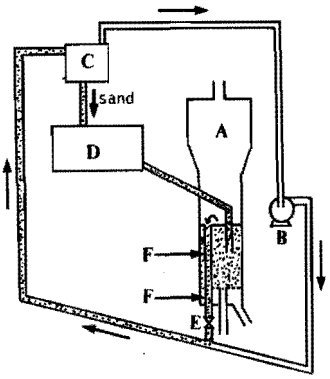

A reactor
B blower
C gas-solid separator
D sand heater
E slide valve
F steam

Fig.8.13 Sand circulation system

The equipment costs (apparatuses directly related to the reactor, see fig. 8.8) are summarized in table 8.9.

Table 8.9 Investment costs of apparatuses

Apparatuses	costs (Dfl., in 1981)
Feed dosage system (sluices, belt conveyors, screw conveyors)	102,000
Reactor system (including insulation, refractory lining etc.)	79,000
Furnace	750,000
Sand heater	600,000
Blowers etc.	575,500
Total equipment costs	2,106,500

An alternative to the above system (globally existing of reactor, sand heater and furnace) may be possible in which no separate furnace is required. In that case the sand is heated in the sand heater by combustion of the pyrolysis gas, low boiling organic compounds and the char which is injected into the beds of the sand heater. The char is thus burned in a series of 2 fluid beds. The off gases from the sand heater are mixed with air. The resulting gas flow is then used for

drying the RDF feedstock.
The above alternative is attractive in that it reduces the number of apparatuses. The equipment costs would thus be reduced.
A complicating factor may be, however, that the temperature in the sand heater might rise above the softening temperature of the glass that is present in the sand. This might lead to a situation where the sand particles stick together so that proper fluidisation of the sand beds in the sand heater might become difficult or even impossible. Also, smaller and/or partly combusted char particles might be blown out of the fluid beds without having burned entirely.

8.4 Separation of the products from the gas that passes out of the reactor

8.4.1 Separation of the char

The char is separated immediately downstream from the reactor. The separation takes place at temperatures almost equal to reaction temperature and at a pressure of about 1.2 atm (see § 8.3). The char particle size is in the range 10-600 μm. The separation efficiency in the char separation unit must be insensitive to process conditions such as temperature, composition and flow rate of the gas and the amount of char.
It was decided to use one or more cyclones for this purpose because of the below reasons:

- a cyclone is a simple, relatively cheap apparatus that separates particles of not too small sizes with little loss of pressure.
- the separation efficiency is relatively independent of composition and temperature of the gas and of the amount of char.
- the gas flow rate does influence the efficiency substantially. This problem can easily be solved by applying more than one cyclone in parallel and by operating the required number of cyclones depending on gas flow rate.

The method of Krambrock [8.4] was used to calculate the dimensions of the cyclones and the pressure drop over them. A computer program was set up to calculate the various ratios of the dimensions of the cyclone for 6 types of cyclones. The size of the cyclone was calculated for each type in such a way that it separates particles of a given

minimum diameter. The number of cyclones that are placed in parallel was a variable in these calculations. The pressure drop over the cyclone was also calculated in the computer program.
The calculations have been carried out for both process schemes indicated below:
A. Reactor with partial combustion at maximum tar yield (fig. 8.5).
B. Reactor with sand heater at maximum tar yield (fig. 8.8).
The calculations led to the selection of cyclones which show dimensions that were slightly different only for the two process schemes. It was decided to use standard dimensions in both cases. The dimensions of the standard cyclone were: height 2.60 m, diameter 0.80 m. The results are summarized in table 8.10.

Table 8.10

process scheme	number of standard cyclones	pressure drop (mm H_2O)	total equipment costs of cyclones (Dfl., in 1981)
A	5	200 to	25,000
B	4	250	20,000

8.4.2 Separation of the tar

The tar must be separated from the gas by condensation. It is necessary to cool the gas flow that passes out of the cyclones to about 150°C to condense all tar. The following apparatuses have been considered for gas cooling and tar condensation:
1. a shell-and-tube heat exchanger/condensor
2. a spray tower (gas cooling by evaporation of water).
It was observed in the pilot plant experiments that part of the tar condenses to form a mist. It is therefore necessary to use a mist separator downstream from the above apparatuses for gas cooling and tar condensation. Two alternatives have been considered:

1. an electrostatic precipitator
2. a scrubber
Calculations were carried out for all four of these apparatuses for tar collection.

The shell-and-tube heat exchanger/condensor

The shell-and-tube heat exchanger/condensor was calculated as a heat exchanger with extra resistance to heat transport due to the presence of a tar layer on the exchange surface and with extra cooling surface to compensate for the heat of condensation of the tar. The calculations were based on the method described by Kern [8.5]. The results of the calculations are summarized in tables 8.11 and 8.12.

Table 8.11 Shell-and-tube heat exchanger/condensor for process scheme A (reactor with partial combustion)

area of heat exchange	(m^2)	803
number of tubes	(-)	1916
length of tube bundles	(m)	3
tube diameter	(m)	0.035
shell diameter	(m)	1.82
pressure drop process gas	(atm)	0.025
pressure drop coolant	(atm)	1.40
temperature of coolant entering the heat exchanger	(^oC)	120

Table 8.12 Shell-and-tube heat exchanger/condensor for process scheme B (reactor with external sand heater).

area of heat exchange	(m^2)	495
number of tubes	(-)	1012
length of tube bundles	(m)	3.5
tube diameter	(m)	1.32
shell diameter	(m)	0.035
pressure drop process gas	(atm)	0.033
pressure drop coolant	(atm)	1.34
temperature of coolant entering the heat exchanger	(^oC)	120

The equipment costs of the shell-and-tube heat exchanger/condensor including pumps and blowers are presented in table 8.13.

Table 8.13 Equipment costs (heat exchanger/condensor)

Process scheme	equipment costs (Dfl., in 1981)
A	375,400
B	206,800

The spray tower

The flows in a spray tower are presented in fig. 8.14 for the cases that the gas is cooled co-currently or counter-currently to the water droplets.

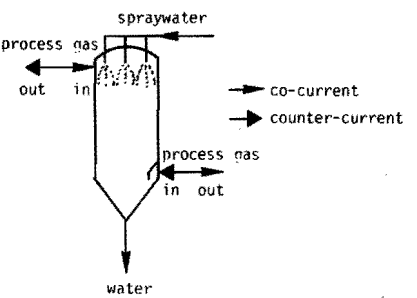

Fig.8.14 Spray tower

A computer program was written in which the column is divided from the top downward into sections in which a constant temperature increase or decrease of the gas dT occurs. The fall velocity of the water droplets, the heat transfer coefficient and the area of heat transfer were calculated for each section of the column. These data were used to calculate the length dH of this section. The total length of the column was found by adding the dH's over the entire temperature range. The results of the calculations are not shown here but will be briefly discussed below.

The calculations for various sizes of water droplets, spray water flow rates and for co-current as well as counter-current operation showed that the co-current operation leads to columns of acceptable dimensions. The columns for counter-current operation must have very large diameter to ensure that the gas flow rate remains below the fall velocity of the water droplets. It was therefore decided to apply co-current operation. The columns that are required then have a diameter of 2.5 m and heights of 9 m and 5 m for process schemes A and B respectively. The equipment costs of the spray towers are presented in table 8.14.

Table 8.14 Equipment costs of the spraytowers (Dfl., in 1981).

	process scheme A	process scheme B
column	100,000	50,000
spray system	20,000	20,000
total equipment costs	120,000	70,000

The electrostatic precipitator

The electrostatic precipitation process can be divided into two stages which can be described separately:

1. charging of the particles in the corona
2. migration of the charged particles to the collector and precipitation on the collector.

It was decided to use a single stage wire-and-tube precipitator where both stages occur within the same tube. This geometry is recommended for the removal of liquid mists with large droplet concentrations because in such apparatus the precipitated liquid is easy to remove. The calculations were based on the model for the electrostatic precipitation process that was published by Crawford [8.6]. The below data were used in the calculations:

- gas: temperature, pressure, flow rate and composition, viscosity and density
- tar: average droplet size, concentration, dielectric constant
- precipitator: number of tubes, diameters of tube and wire
- collection efficiency

The influence of some of the above data on the electrostatic precipitation process were calculated first:

- diameter of wire: decreasing wire diameter leads to better operation of the precipitator. A diameter of 4 mm was selected for reasons of stability of the construction.
- tube diameter: increased tube diameter leads to a minor improvement of the precipitation process.

Table 8.15 summarizes the results of the calculations for a collection efficiency of 99%. The symbols used in the table are:

d = tube diameter

n = number of tubes

L = tube length

A = cross area of the precipitator

Table 8.15 Dimensions of electrostatic precipitator

n	d = 0.12 m		d = 0.24 m		d = 0.50 m	
(-)	L(m)	A (m^2)	L(m)	A(m^2)	L(m)	A(m^2)
500	320	6.5	266	26	-	-
1000	- *)	-	133	52	123	255
3000	53	39	67	104	-	-
4000	40	52	33	208	-	-

*) - = not calculated

The scrubber

A scrubber is an apparatus in which dust particles or mists can be collected from a gas by means of a liquid stream that flows co-currently or counter-currently to the gas. Different types of scrubbers are known that each have an efficiency that is highly dependent on the particle sizes of the dust or mist. The sizes of the tar droplets are in the order of 1-20 µm. A scrubber type that is very suitable for separating particles of this size is the venturi-scrubber (fig. 8.15).

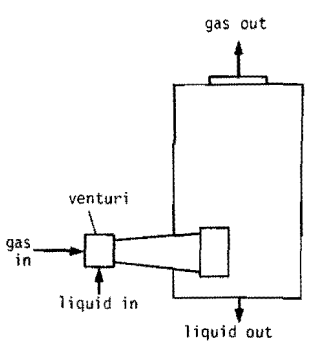

Fig.8.15 Venturi scrubber

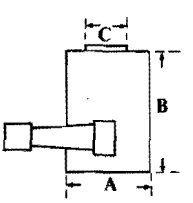

Fig.8.16 Dimensions of the scrubber (see table 8.16)

An efficiency of 99% can be reached in this scrubber for particles of 10 μm. A secondary mist is created in the scrubber by radial injection of a liquid into the venturi throat. The liquid is thus distributed throughout the gas. The droplet size of the secondary mist is in the order of 150-200 μm. This secondary mist collects the fine tar droplets. Agglomeration of the scrubbing droplets to form larger size droplets takes place in the wider part of the scrubber. The droplets are subsequently separated from the gas by means of a cylone. The separated scrubbing liquid is recirculated to the venturi throat. The gas passes out of the scrubber at the top side.
The calculations of the scrubber were based on methods described in lit.no. [8.7]. The scrubbing liquid that is used in the design is tar to which 10 wt.% of water have been added in order to reduce the viscosity. The operating conditions are: temperature 150°C, pressure 1.2 atm. The resulting scrubbers are presented in table 8.16 and fig. 8.16 for process schemes A and B.

Table 8.16 Data on the scrubber

	Process scheme A	Process scheme B
Cross area of throat (m^2)	0.15	0.13
A (fig. 8.16, m)	4.20	3.13
B (fig. 8.16, m)	1.99	1.51
C (fig. 8.16, m)	1.09	0.79
Flow rate of scrubbing liquid (m^3/sec)	0.032	0.014

The equipment costs are presented in table 8.17.

Table 8.17 Equipment costs of scrubber unit (Dfl., in 1981)

	Scheme A	Scheme B
scrubber	23,710	13,480
blower (+ motor)	18,600	11,100
pump (+ motor)	3,800	2,860
total equipment costs	46,110	27,440

Discussion

A co-current spray tower was selected as gas cooler/condensor instead of the shell-and-tube heat exchanger because the equipment costs are lower (comp. tables 8.13 and 8.14) and because it was expected that the heat exchanger should rapidly become fouled by the condensing tar. Because of the high viscosity of the tar this might even lead to obstructions. The heat exchanger would thus have to be shut down for cleaning from time to time.

The scrubber was selected as tar collection apparatus. The enormous dimensions of the electrostatic precipitator and the high electricity costs that were to be expected led to this selection. The fact that the tar itself can be used as scrubbing liquid makes the application of the scrubber even more attractive.

8.5 Resulting process schemes

The process scheme A and B that result from the above designs are presented in figs. 8.17 and 8.18. It will be recalled that the schemes show differences in reactor design:

Scheme A: reactor with partial combustion

Scheme B: reactor with external sand heater

Symbols used in figs. 8.17 and 8.18:

Apparatuses:

CY = cyclone(s)
FE = feeding devices
FU = furnace
RE = reactor
SA = sand heater
SC = scrubber
SP = spray tower
TA = tar storage
TR = trommel-dryer
WA = waste separation plant

Flows:

a = air
ch = char
co = combustion gases
d = domestic waste
g = gas (incl. water vapor)
rd = refuse derived fuel
re = recycle gas
sa = sand
st = steam
t = tar
w = water

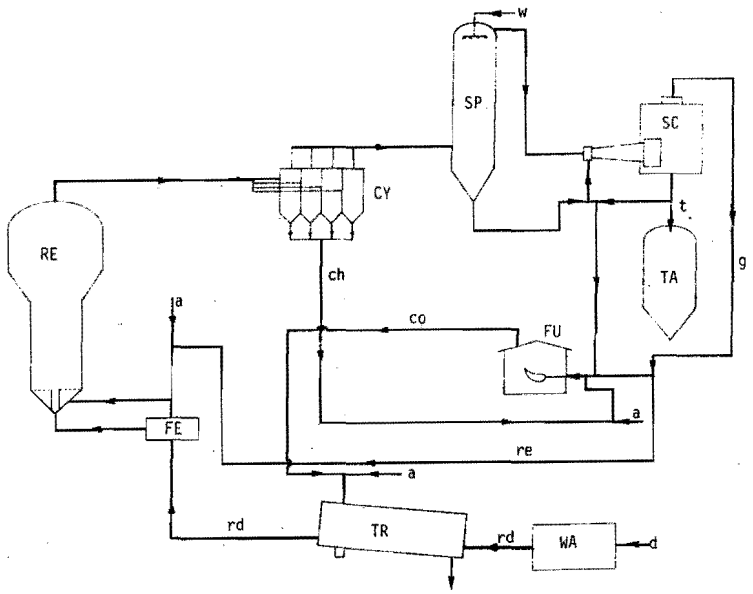

Fig.8.17 Process scheme A (reactor with partial combustion)

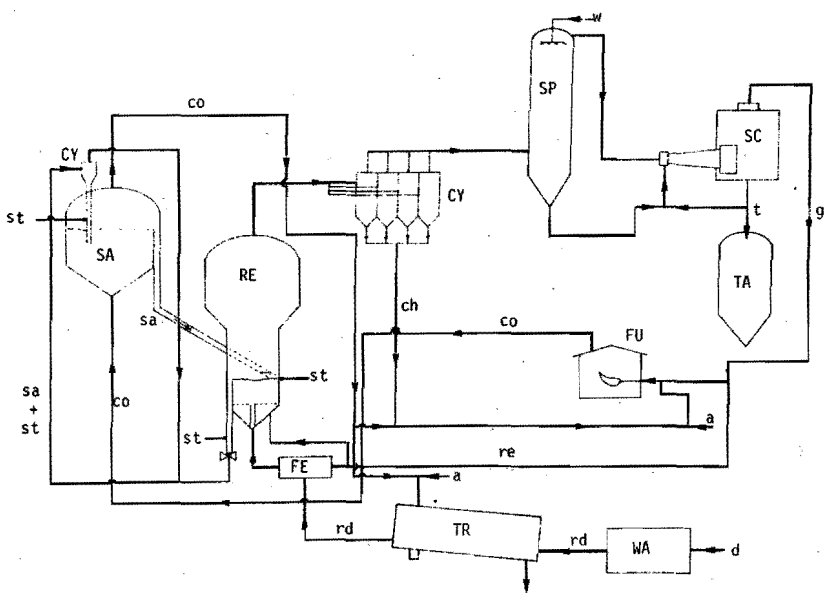

Fig.8.18 Process scheme B (reactor with an external sand heater)

It is seen from these schemes that the water fraction is not separated from the gas. The water produced during the pyrolysis process is contaminated with organic compounds and must therefore be purified before it may be drained off. However, the costs of purification of the water fraction produced in pyrolysis of domestic waste are high. It was decided therefore not to separate the water fraction from the gas but to apply oxidation of the water fraction. The water fraction is burned in the furnace together with the pyrolysis gas (and eventually part of the char or tar). This implies that the gas is used for meeting part of the heat requirements of the process and that the gas is not a product that can be sold. Char and tar only are such products in the above process schemes.
The thermal efficiency of the process was calculated for both process schemes using the following definition: the thermal efficiency is the ratio of the heat of combustion of the net pyrolysis product flow to the sum of the heat of combustion of the domestic waste and the externally supplied energy (electricity). The results of the calculations are presented in table 8.18.

Table 8.18 Thermal efficiency calculations.

Process scheme	heat of combustion net product flow (tar) in J/year	electricity in J/year	heat of combustion input (domestic waste) in J/year	thermal efficiency (%)
A	$1.44*10^{14}$	$0.21*10^{14}$	$6.16*10^{14}$	23
B	$2.49*10^{14}$	$0.33*10^{14}$	$6.16*10^{14}$	38

8.6 Investment and operating costs

8.6.1 Calculations of the costs

The equipment costs of the total plant are given in table 8.19 for both schemes.

The capital costs which include - apart from the equipment costs - also the costs for buildings and foundations, site work, installation, instrumentation, piping, utility equipment, procurement, taxes etc. were calculated according to the method of Peters and Timmerhaus [8.8]. In this method the capital costs are estimated from the equip-

ment costs as follows: Each of the cost factors included in the capital costs is expressed in a percentage of the equipment costs. Addition of these cost factors results in an estimate of the capital costs which is found by multiplying the equipment costs with a factor that depends on the nature of the process. The factor that was applied in the present calculations is 3.87. The results are summarized in table 8.20.

Table 8.19 Equipment costs of pyrolysis plant (Dfl., in 1981)

	Process scheme A	Process scheme B
Waste separation plant (table 8.5)	4,208,200	4,208,200
Reactor system (tables 8.8 and 8.9)	1,308,100	2,106,500
Cyclones (table 8.10)	25,000	20,000
Spray tower system (table 8.14)	120,000	70,000
Scrubber system (table 8.17)	46,100	27,440
Storage of products	110,000	150,000
Total equipment costs	5,817,400	6,582,140

Table 8.20 Capital costs (Dfl., in 1981)

Process scheme	capital costs (Dfl., in 1981)
Process scheme A	22,513,340
Process scheme B	25,472,880

The annual costs were calculated as indicated below [8.8]:

1. Interest and depreciation

   Assumptions: - the plant is depreciated in 10 years (n)
   - the interest on capital is 13% (i)
   - the costs that result from interest and depreciation are calculated on an annuity basis.

   The resulting capital recovery factor

$$\left(= \frac{i*(1+i)^n}{(1+i)^n-1} \right)$$

equals 0.1843 in that case.

2. Energy costs.
   These were calculated for electricity only. The calculations were based on the total installed power. The yearly costs followed from the product of total installed power * hours of operation * kilo-Watthour price.
   Hours of operation: for waste separation plant 3000 hrs/year
   for pyrolysis unit 7000 hrs/year
   KiloWatthour price: Dfl. 0.12/kWh.
   Total installed power: waste separation plant 437 kW
   pyrolysis unit including separation units:
   Scheme A 655 kW
   Scheme B 1118 kW
3. Personnel costs.
   Total production staff: 40 men (4 shifts for the pyrolysis unit). Average costs of one staff member are estimated at Dfl. 60,000/year.
4. Costs for maintenance: 8% of total capital investment.
5. Management etc.: 15% of personnel costs.
6. Laboratory: 15% of personnel costs.
7. Stock (chemicals, reserve parts, etc.): 15% of costs for maintenance.
8. Insurancies: 1% of capital investment.
9. Overhead: 60% of (3.+4.+5.)
10. Administration: 50% of personnel costs.
11. Marketing: 5% of total annual costs.

The final results are presented in table 8.21.

Table 8.21 Annual costs for pyrolysis plant (Dfl., in 1981).

Process scheme	annual costs (Dfl., in 1981)
A	14,957,610
B	16,408,440

The costs for disposal of the inorganic rest from the waste separation plant are not included in these figures. These costs amount to Dfl. 600,000 (24,000 tons at Dfl. 25.-/ton).
It is necessary to estimate the benefits of the sale of the products

in order to be able to calculate the net costs per ton of domestic waste. The only possible way to do this seems to be to connect the prices of the pyrolysis products to those of comparable fossile fuels. The following prices were adapted:

Char: 50% of the price of coals that have the same heat of combustion (the ash content of the char is high).

Tar: 75% of the price of fuel oil with the same heat of combustion. The heat of combustion of the tar must be corrected for the 10% of water that has been added to it in the scrubber.

The resulting prices are: char Dfl. 61.25/ton, tar Dfl. 133.50/ton. The benefits are summarized in table 8.22.

Table 8.22 Benefits of sale of pyrolysis products (Dfl., in 1981).

Scheme	net tar production (kg/sec)	net char production (kg/sec)	benefits (Dfl/ year)
A	0.32	-	1,076,540
B	0.555	-	1,867,130

The price of the iron recovered in the waste separation plant (3000 tons/year) was fixed at Dfl. 250.-/ton. The paper price was assumed to be Dfl. 200.-/ton, the plastics were assumed to have zero value. The net costs per ton of domestic waste can now be calculated (table 8.23). It is recalled here that the figures presented here are those for the case that plastics and paper are not recovered but are included in the feedstock to the pyrolysis reactor.

The various costs factors are summarized in table 8.24.

Table 8.23 Net annual costs and net costs per ton of domestic waste (in Dfl., in 1981) for an input of 100,000 tons of domestic waste/year. Plastics and paper are not recovered but are also pyrolysed.

	Scheme A	Scheme B
Annual costs (table 8.21)	14,957,610	16,408,440
Costs of disposal of inorganics	600,000	600,000
Benefits of sale of iron	- 750,000	- 750,000
Benefits of sale of pyrolysis products (table 8.22)	-1,076,540	-1,867,130
Net annual costs (Dfl. in 1981)	13,731,070	14,391,310
Net costs per ton of domestic waste (Dfl.)	137.31	143.91

Table 8.24 Cost factors and resulting net costs for process schemes A and B

	Process scheme A		Process scheme B	
	costs	cost per ton (Dfl.)	costs	cost per ton (Dfl.)
Capital costs	22,513,340 Dfl		25,472,880 Dfl	
Amortization costs	4,419,210 Dfl/year	41.49	4,694,650 Dfl/year	46.94
Operating costs:				
- Labor & Administration	4,933,010 Dfl/year	49.33	5,340,820 Dfl/year	53.41
- Maintenance, power, utilities	3,138,750 Dfl/year	31.39	3,494,270 Dfl/year	34.94
- Overhead	2,736,640 Dfl/year	27.37	2,878,700 Dfl/year	28.79
- Disposal inorganics	600,000 Dfl/year	6.00	600,000 Dfl/year	6.00
Total operating costs	11,408,400 Dfl/year	114.09	12,313,790 Dfl/year	123.12
Total plant costs	15,557,610 Dfl/year	155.58	17,008,440 Dfl/year	170.08
Credits:				
- Tar	1,076,540 Dfl/year	10.77	1,867,130 Dfl/year	18.67
- Iron	750,000 Dfl/year	7.50	750,000 Dfl/year	7.50
Total credits	1,826,540 Dfl/year	18.27	2,617,130 Dfl/year	26.17
Net costs	13,731,070 Dfl/year	137.31	14,391,310 Dfl/year	143,91

8.6.2 Discussion

The net costs per ton of domestic waste calculated above are valid for the case where a complete waste separation plant is available, i.e. one has the choice to recover the plastics and paper or not to do so. It is also possible, however, to calculate the design of systems in which the choice of what to produce (paper, plastics, tar) is either entirely fixed or entirely free. Calculations for these systems and intermediate systems have been carried out. Some of the conclusions were:

1. One must pay for flexibility: the gross costs per ton of domestic waste increase with increasing flexibility of the system. This is not surprising as more apparatuses are required for flexible systems than are being operated at any single point in time.
2. Systems and modes of operation which include the recovery of plastics and paper show lower net costs per ton than do systems where paper and plastics are pyrolysed. This can be understood from the below considerations: the mass flow of solid/liquid products is larger in cases where paper and plastics are recovered and: the assumed paper price is higher than that of the tar.

Calculations were carried out to investigate the influence of the product prices on the net costs per ton of domestic waste. The conclusion was that the systems in which paper and plastics are excluded from the feedstock for the pyrolysis unit but are recovered are relatively cheap even if the paper price is reduced to zero or tar prices are tripled. This is because smaller pyrolysis units can be used in these cases (smaller throughput in pyrolysis unit).

Summarizing the above discussion it was found:
Systems in which paper and plastics are excluded from the feed to the pyrolysis unit are relatively cheap. Systems in which the recovery of paper and plastics is optional are relatively cheap when they are operated in such a way that paper and plastics are recovered. The (minimum)net costs per ton of domestic waste for these systems (product prices as indicated above) vary between Dfl. 90.85 and Dfl. 109.45.

Global calculations have also been carried out to investigate the influence of the throughput on the economics of the process. These calculations were carried out for a throughput of 50,000 and 200,000 tons

of domestic waste per year. The paper and plastics were not recovered but pyrolysed and process scheme A was adopted. It was concluded that a throughput of 50,000 tons/year is not very attractive as the net costs per ton of domestic waste were about Dfl. 190/ton in this case as compared to Dfl. 137.31/ton for a throughput of 100,000 tons/year. Increasing the throughput to 200,000 tons/year hardly affected the net costs per ton of domestic waste.
It should be kept in mind, however, that these calculations were very rough only.

The design calculations were based on the experimental results obtained in pyrolysis experiments on shredded thin cardboard as insufficient data on pyrolysis of RDF fractions were available at the time when the designs were computed. It appeared later on, however, that the product distributions as well as the compositions of the products obtained in pyrolysis experiments on RDF fractions were different from those obtained in pyrolysis experiments with cardboard feed. Large differences between runs on cardboard and on RDF were observed in tar and char yields as well as in the heat of combustion of the tar (see Chapter 5). It was decided therefore to investigate to what extent these differences did affect the design calculations. Calculations were carried out on the basis of the results obtained in pyrolysis experiments on RDF fractions for a pyrolysis temperature of 500^{o}C. The calculations were confined to calculating the gas flow rates in reactor and products separation units as the gas flow rate was the most important factor in designing these apparatuses.
The gas flow rates that resulted from these calculations hardly differed from those that have been calculated on the basis of the results obtained in pyrolysis experiments on cardboard feedstock (§ 8.2 through § 8.5) both for the reactor with partial combustion (process scheme A) and for the reactor with an external sand heater (process scheme B). In fact, the gas flow rates were 3 and 2% lower for the reactor with partial combustion and the reactor with an external sand heater respectively.
It was concluded that these minor differences would hardly affect the design of the reactor or that of the products separation units.
The net yield of products was calculated for the reactor with partial combustion (scheme A). See table 8.25.

Table 8.25 Net yield of products (reactor with partial combustion, scheme A).

	net tar yield (kg/sec)	net char yield (kg/sec
Calculations based on cardboard pyrolysis	0.32	-
Calculations based on pyrolysis of RDF fractions	0.166	0.285

The heats of combustion of the tar and the char obtained in the pyrolysis of RDF fractions differed from those obtained in cardboard pyrolysis. Consequently the benefits that result from the sales of these products are different, too. The product prices were estimated in the same way as had been done above. This resulted in a price of Dfl. 39.20/ton for the char and Dfl. 261.50/ton for the tar from domestic waste. The benefits from selling the products are then Dfl. 1,375,440/year which is about 28% higher than the benefits calculated for process scheme A based on cardboard feedstock (see table 8.22). As a result the net costs per ton of domestic waste reduce to Dfl. 134.30/ton (were Dfl. 137.31).
The thermal efficiency was calculated for process scheme A. The thermal efficiency based on RDF pyrolysis was calculated to be 40% (was 23%).

The above process design was based on data such as product distributions and composition of the products obtained in experiments that were carried out in a pyrolysis pilot plant that has a capacity of 10 kg/hr only. The product distributions and composition of the pyrolysis gas in the larger scale pyrolysis plant calculated above might differ from those obtained in the pyrolysis experiments in the pilot plant because the residence time of the gaseous products in the reactor is larger in the large scale units than in the pilot plant. This might lead to more cracking so that tar yield might decrease and more gas might be produced.

8.7 Concluding remarks

1. The water fraction produced in the pyrolysis process is contaminated with organic compounds. Both aerobic and anaerobic purifications are very expensive. A simple and relatively cheap solution was found: the water is not condensed from the pyrolysis gas but is introduced in a furnace where the organic compounds are burned together with the pyrolysis gas. The heat thus generated is used for drying the feed to the pyrolysis plant.
2. The reactor with partial combustion is preferable to the reactor with external sand heater on the basis of its simplicity and because it is assumed to be more dependable. In addition, the reactor with partial combustion is relatively cheap.
3. Recovery of paper and plastics must be an option in the plant as an alternative for the pyrolysis of these waste components because of the high benefits from selling these products. In addition, the costs of the pyrolysis unit can be reduced when paper and plastics are excluded from the pyrolysis. The pyrolysis unit can be smaller in that case because of the smaller throughput.
4. The assumed paper price in the above calculations (Dfl. 200.-/ton) is rather high considering the present market situation for recovered paper. On the other hand, no economic value has been ascribed to the recovered plastics while it seems highly probable that there is a market for these plastics. The amount of plastics involved is 3600 tons/year.
5. The following process schemes were found to be the most attractive ones on the basis of the above remarks 2 and 3.

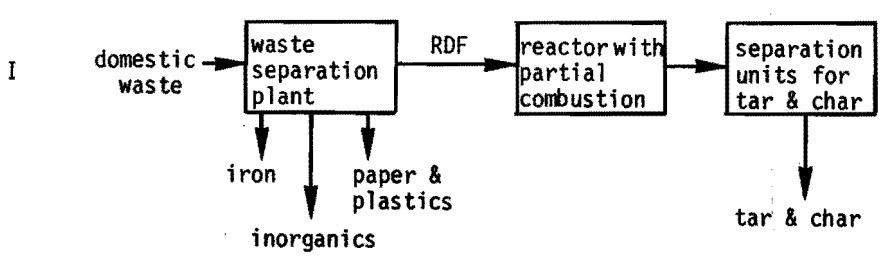

II

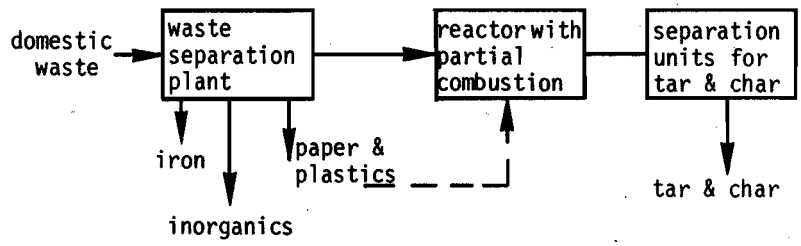

The main difference between both of these schemes is the size of the pyrolysis unit that is required. The pyrolysis unit in scheme II (= process scheme A,fig. 8.17) must be calculated for a larger throughput (organics + plastics and paper).

6. The net costs per ton of domestic waste that were calculated using the product prices indicated above were:
   Scheme I: Dfl. 90.- to Dfl. 95.-/ton; products: iron, paper, plastics and tar and char.
   Scheme II: Dfl.110.-/ton; products: iron, paper, plastics and tar and char.
   Dfl.135.-/ton to Dfl. 140.-/ton; products: iron and tar and char.
7. The net costs per ton of domestic waste for scheme II are substantially higher than the net costs per ton for conventional incineration of domestic waste (Dfl. 70.- to Dfl. 100.-/ton). The net costs per ton for scheme I are comparable to those of incineration.
   It should be noted that the net costs per ton of domestic waste calculated here for pyrolysis are based on the assumption that the pyrolysis plant is depreciated in 10 years which, as far as we know, is a considerably shorter period than that in which incineration units are depreciated.

Literature

8.1 M. Tels, C.P.M. van Ginneken et.al., report Procesontwikkeling, Eindhoven University of Technology, Laboratory for Physical Technology (1981).

8.2 T.N.O. Social Technology Section, Dokumentationblatt 37 D, Apeldoorn (1980).

8.3 S.V.A. report 3000, Amersfoort (1979).
8.4 W. Krambrock, Aufbereitungstechnik, no. 7 (1971).
8.5 D.Q. Kern, Process heat transfer, McGraw-Hill Book Cy., New York (1950).
8.6 M. Crawford, Air pollution control theory, McGraw-Hill Book Cy., New York (1976).
8.7 H.E. Hesketh, Journal of the air pollution control association, 24, pp. 939 (1974).
8.8 M.S. Peters, K.D. Timmerhaus, Plant design and economics for chemical engineers, Chem. Eng. Series 1968, McGraw-Hill Book Cy., New York (1968).

List of symbols

		S.I. units
A	cross area	m^2
c	ratio of bed diameter to spout diameter	-
D	bed diameter	m
dH	section length	m
dT	temperature increase/decrease	^oC
d_{bed}	bed diameter	m
d_p	particle diameter	m
g	gravitational acceleration	m/sec^2
H	bed height	m
H	column length	m
h_{bed}	static bed height	m
i	interest	%
L	tube length	m
n	number of tubes	-
n	period of depreciation	year
P_r	pressure in reactor	N/m^2
Q_{air}	air flow	m^3/sec
Q_{fluid}	fluidisation gas flow	m^3/sec
Q_{out}	out going gas flow	m^3/sec
Q_{spout}	spout gas flow	m^3/sec
T_{in}	temperature of gas entering reactor	^oK
T_r	reaction temperature	^oK

u_f	fluidisation gas flow rate	m/sec
u_{mf}	minimum fluidisation gas flow rate	m/sec
v_p	gas flow rate above the bed	m/sec
v_{sp}	linear spout gas velocity	m/sec

Greek symbols

ρ	density	kg/m^3
ρ_b	bulk density	kg/m^3

9. CONCLUSIONS

1. Combination of low temperature operation (up to about 600^{o}C) and application of a spout-fluid bed reactor in waste pyrolysis leads to relatively high tar yields.
   The tar obtained in low temperature pyrolysis of the organic fraction of domestic waste resembles no. 6 fuel oil in f.i. heat of combustion, density and carbon, hydrogen and ash content. The pyrolysis tar produced contains less sulphur than no. 6 fuel oil. Disadvantages of the tar are its high viscosity and the presence of some chlorine in it.

2. The gases and chars produced in low temperature pyrolysis of the organic fraction of domestic waste have relatively low heats of combustion. The char contains considerable amounts of ash.

3. It was concluded with respect to the environmental impact of the pyrolysis process that:
   a. The HCl content of the pyrolysis gases produced is not very high.
   b. The organic contaminants present in the water phase produced are bio-degradable. No chlorine containing organic compounds were found to be present in the water phase.
   c. The char ash contains heavy metals. The heavy metals contents of the ash of the chars that were produced in the present investigation by pyrolysis of organic waste fractions are, however, low so that the char ash is not a chemical waste according to Dutch law.

4. The pyrolysis experiments on shredded cardboard and on shredded domestic waste fractions in a spout-fluid bed reactor showed that the conversion is incomplete at reaction temperatures below about 500^{o}C and at the residence times of the solid particles that were used.

5. A technical and economic evaluation of the low temperature pyrolysis process in a spout-fluid bed reactor was carried out for a plant with a capacity of 100,000 tons of domestic waste/year and a combination of material recovery and pyrolysis. This evaluation

showed that the net costs of pyrolysis inclusive of RDF feedstock preparation are from Dfl. 90 tot Dfl. 140 per ton of domestic waste. These costs are comparable to or higher than the net costs per ton of domestic waste for conventional incineration (Dfl. 70 to Dfl. 100) depending on the process scheme of the pyrolysis plant and the way it is operated. It is to be noted that the period of depreciation for the pyrolysis apparatus was taken to be 10 years whereas the above published costs of incineration are most often based on periods of depreciation in the order of 25 years.

6. The models of cellulose pyrolysis derived here do not give accurate predictions of experimental product distributions obtained in spoud-fluid bed pyrolysis. This is due to the simplifications of chemical and physical processes in the models and to the uncertainty as to what amount of levoglucosan (tar components) is removed from the solid particles during pyrolysis. The models cover the limiting cases: It is assumed that levoglucosan either evaporates completely from the pyrolysing particle or that it remains in the particle and is there subjected to cracking reactions. In practice, however, the tar will partly evaporate and partly remain in the particle. The tar evaporated from the pyrolysis particle may in addition be subject to cracking in the bulk gas. It was furthermore assumed in deriving the models that the reaction time of the particles was small compared to their residence time in the reactor. The models therefore assume that the cellulose conversion is complete. It was observed in pyrolysis experiments that the conversion is incomplete at reaction temperatures below about $500^{o}C$. Despite all of these shortcomings of the models, the experimentally determined curves of product distribution vs. reaction temperature were found to lie in between the limiting curves predicted by the models.

7. The models of cellulose pyrolysis derived here that incorporate conversion rate limitations due to chemical reactions as well as to physical transport provide a good insight in what factors govern the pyrolysis process. The present models are valid only in cases where the residence time of the solid particles is appreciably longer than the pyrolysis reaction time.

Appendix 2.1. Numerical evaluation of the general model

The principles of the numerical evaluation of the heat transport equation have been discussed in paragraph 2.4.2. This appendix deals with the details of the discretisation of the heat transport equation (with boundary conditions) and reaction rate equations as well as some considerations about the stability of the computation process. A scheme of the computer program is given.

Stability

An error is introduced at any time level as a result of truncation of the Taylor series and the limited computing accuracy. This error influences the calculations at higher time levels. When the error remains constant or decreases with increasing number of time spacings the computing process is said to be stable. No mathematical correct stability criterion for the case when the coefficient matrices $\bar{A}$ and $\bar{B}$ are non-linear functions of the function value was found in the literature. It was therefore decided to look for conditions that will yield stable computations empirically. We took the computing process to be instable when it yielded physically unacceptable values for the variables. Temperatures that strongly oscillate with time and place are for instance physically unacceptable. This means that there is a possibility that not every instable calculation was identified as such and that results of instable computations that are physically acceptable are wrongly interpreted as being stable. To protect ourselves against this happening we set up an overall heat balance over a part of the flat slab that has a unit area. The amount of heat supplied to this part of the slab must be equal to the sum of:

- the heat content of this part of the flat slab
- the heat of reaction
- the heat removed by the gases that are produced

A further check on the stability of the computation was carried out by comparing the results to analytical solutions for the case of constant coefficients and to numerical solutions obtained by other methods (f.i. method of integral relations, see Chapter 7 [2.25]).

Variable coefficients and boundary conditions

The coefficients in the heat transport equations (eqs. 2.16 and 2.36) like $k_a, k_b, k_c, k_d, \lambda_{eff}, \rho_1, \rho_2, \rho_3, \rho_4$ are non-linear functions of the

variable T_i as is the heat flux in boundary condition (eq. 2.19b). It is necessary for reasons of computing technique to maintain the linearity of the set of equations. There are a number of possibilities to approximate the coefficients and the heat flux at the new time level:

a. taking the values at the previous level
b. linear extrapolation of coefficients and flux from two previous levels
c. linear extrapolation of temperature and mass concentration
d. iteration after one of the above methods a,b,c.

Linear extrapolation of temperature and mass concentration was preferred for approximation of the coefficients and boundary conditions at the new time level.

Spacing in the grid

The spacing between two successive points of the grid at the horizontal co-ordinate axis in fig.2.16 is determined by the number of place steps on the one hand and by the place stepsize distribution on the other hand. The lower limit for the spacing between the points of the grid is determined in practice by the computation time required for calculating the process. The upper limit is given by the accuracy of calculation that is desired. The latter is being checked by calculating the process with different spacings in the grid and comparing the results.

A constant place stepsize was chosen because of the fact that a large mass concentration gradient $\frac{\partial \rho}{\partial x}$ may occur at every place. The spacing between points of the grid 0 and 1 (= step h_1) has, however, been chosen very small because of the boundary condition at the centre of the slab, which is being discretised by a first order approximation.

The same requirements apply to the size of the time steps.In the computation process the time step is calculated according to the below criteria:

- the temperature change at the surface of the slab (x=L) that occurs in one time step may not exceed an allowable relative change in temperature difference between surface temperature and the bulk temperature of the surrounding gas phase.
- the change in mass concentration that occurs in one time step may not exceed an allowable relative change at any place within the slab.

The maximum time step that meets both criteria is chosen in the course of the computing process. The allowable changes in temperature and mass concentration have been determined empirically.

Discretisation of the heat transport equation

The discretisation of the heat transport equation that follows from the general model with tar evaporation is shown here. The discretisation of the heat transport equation that follows from the general model without tar evaporation is analogous.

The transport of heat inside the infinite flat slab is given by eq. (2.16):

$$(\rho_1 C_{p1} + \rho_2 C_{p2} + \rho_3 C_{p3}) \cdot \frac{\partial T}{\partial t} = - \left[\int_0^x (k_a \rho_1 C_{pga} + k_b \rho_1 C_{pgb} + k_c \rho_2 y_c C_{pgc}) dx \cdot \right] \frac{\partial T}{\partial x} +$$

$$+ \frac{\partial}{\partial x} (\lambda_{eff} \cdot \frac{\partial T}{\partial x}) - (k_a \rho_1 \Delta \hat{H}_a + k_b \rho_1 \Delta \hat{H}_b + k_c \rho_2 \Delta \hat{H}_c) \qquad (2.16)$$

$j_{max}-1$ relations can be set up for every time level between the variables T_o, T_1, T_2, $\ldots\ldots T_j, \ldots\ldots T_{jmax}$ in the Crank-Nicholson discretisation scheme (fig. 2.18, $\theta = 1/2$). When this scheme is used the general relation between the three variables at the next level and the three variables at the previous level is: [1)]

$$(\rho C_p)_{j,f+\frac{1}{2}} \cdot (\frac{T_{j,f+1} - T_{j,f}}{k_{f+1}}) = \frac{1}{h_j + h_{j+1}} \lambda_{j+,f+1} \cdot (\frac{T_{j+1,f+1} - T_{j,f+1}}{h_{j+1}}) - \lambda_{j-,f+1} \cdot$$

$$\cdot (\frac{T_{j,f+1} - T_{j-1,f+1}}{h_j}) + \lambda_{j+,f} \cdot (\frac{T_{j+1,f} - T_{j,f}}{h_{j+1}}) - \lambda_{j-,f} (\frac{T_{j,f} - T_{j-1,f}}{h_j}) -$$

[1)] Some terms have been replaced by symbols or words to facilitate reading the equations:

$$\rho C_p = \rho_1 C_{p1} + \rho_2 C_{p2} + \rho_3 C_{p3} \; ; \; \text{convection} = \int_o^x (k_a \rho_1 y_a C_{pga} + k_b \rho_1 C_{pgb} + k_c \rho_2 y_c C_{pgc}) dx$$

$$\text{heat of reaction} = k_a \rho_1 \Delta \hat{H}_a + k_b \rho_1 \Delta \hat{H}_b + k_c \rho_2 \Delta \hat{H}_c$$

$$(-)\ (\text{convection})_{j,f+\frac{1}{2}} \cdot \tfrac{1}{2} \cdot \left(\frac{T_{j+1,f+1} - T_{j-1,f+1}}{h_j+h_{j+1}} + \frac{T_{j+1,f}-T_{j-1,f}}{h_j+h_{j+1}}\right) -$$

$$(-)\ (\text{heat of reaction})_{j,f+\frac{1}{2}} \qquad (1)$$

Fig. 1 illustrates the indices that have been used in eq. (1).

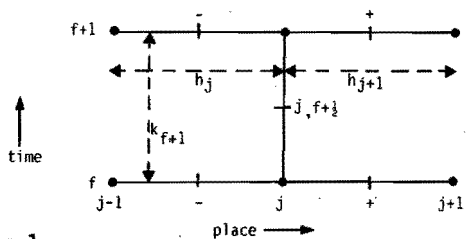

Fig.1

The set of equations is now written in the form of a matrix:

$$b_{j-1}\cdot T_{j-1,f+1} + a_j \cdot T_{j,f+1} + c_j \cdot T_{j+1,f+1} = y_j \qquad (2)$$

The coefficients in eq.(2) are given by:

$$b_{j-1} = \frac{-\lambda_{j-,f+1}}{(h_j+h_{j+1}).h_j} - \frac{(\text{convection})_{j,f+\frac{1}{2}}}{2(h_j+h_{j+1})} \qquad (3)$$

$$a_j = \frac{(\rho C_p)_{j,f+\frac{1}{2}}}{k_{f+1}} + \frac{\lambda_{j+,f+1}}{(h_j+h_{j+1}).h_{j+1}} + \frac{\lambda_{j-,f+1}}{(h_j+h_{j+1}).h_j} \qquad (4)$$

$$c_j = \frac{-\lambda_{j+,f+1}}{(h_j+h_{j+1}).h_{j+1}} + \frac{(\text{convection})_{j,f+\frac{1}{2}}}{2(h_j+h_{j+1})} \qquad (5)$$

$$y_j = T_{j+1,f} \cdot \left| \frac{\lambda_{j+,f}}{(h_j+h_{j+1}).h_{j+1}} - \frac{(\text{convection})_{j,f+\frac{1}{2}}}{2(h_j+h_{j+1})} \right| +$$

$$T_{j,f}\left[\frac{(\rho C_p)_{j,f+\frac{1}{2}}}{k_{f+1}} - \frac{\lambda_{j+,f}}{(h_j+h_{j+1}).h_{j+1}} - \frac{\lambda_{j-,f}}{(h_j+h_{j+1})h_j}\right] +$$

$$T_{j-1,f}\cdot\left[\frac{\lambda_{j-,f}}{(h_j+h_{j+1}).h_j} + \frac{(\text{convection})_{j,f+\frac{1}{2}}}{2(h_j+h_{j+1})}\right] -$$

$$(\text{heat of reaction})_{j,f+\frac{1}{2}} \qquad (6)$$

Eq.(6) does not hold at the boundaries of the grid (fig. 2.16) where j=0 and $j = j_{max}$. For j=0 and $j = j_{max}$ the boundary conditions must be applied.

Boundary conditions

Two coefficients are available for both boundary conditions to maintain the tridiagonal form of the coefficient matrix $\bar{\bar{A}}$: a_o and c_o for the boundary condition at x=0 and b_{jmax-1} and a_{jmax} for the boundary condition at x=L . The boundary conditions can therefore be given in terms of a function value or of the first derivative towards place. The boundary at the centre of the slab is given by:

$$\frac{\partial T}{\partial x} = 0 \text{ for } x=0$$

First order discretisation of this derivative gives:

$$\frac{T_{1.f+1}-T_{0,f+1}}{h_1} = 0 \text{ whence: } T_{0,f+1} = T_{1,f+1} \qquad (7)$$

The coefficients in matrix $\bar{\bar{A}}$ therefore are:

$$a_o = 1 \qquad (8)$$

$$c_o = -1 \qquad (9)$$

$$y_o = 0 \qquad (10)$$

The discretisation of the boundary condition at the outside of the slab for the case that $(\lambda.\frac{\partial T}{\partial x})_{x=L}$ = constant (eq. 2.19a) is given by:

$$\lambda_{jmax-\frac{1}{2},f+1} \cdot \left(\frac{T_{jmax,f+1}-T_{jmax-1,f+1}}{h_{jmax}}\right) = \text{constant} \qquad (11)$$

The coefficients in matrix $\bar{\bar{A}}$ are (see eq. 2):

$$b_{jmax-1} = -\frac{\lambda_{jmax-\frac{1}{2},f+1}}{h_{jmax}} \qquad (12)$$

$$a_{jmax} = \frac{\lambda_{jmax-\frac{1}{2},f+1}}{h_{jmax}} \qquad (13)$$

$$y_{jmax} = \text{constant} \qquad (14)$$

The energies required for reaction, heat capacity and convection are not included in these coefficients. It was therefore decided to approximate the boundary conditions (case 1 and 2: eqs. (2.19a) and (2.19b) with the aid of an energy balance. The balance has been set up for the outer half of the outer slice of the slab at time level f+1. The location of the slice for which an energy balance is set up is indicated schematically in fig. 2.

Fig. 2

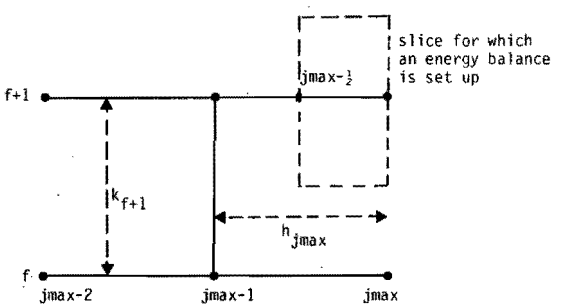

Heat balance:

accumulated heat = incoming heat - outflowing heat

$$\text{accumulated heat} = \frac{h_{jmax}}{2} \cdot (\rho C_p)_{jmax-\frac{1}{4},f+1} \cdot \left(\frac{T_{jmax,f+1}-T_{jmax,f}}{k_{f+1}}\right) +$$

$$(\text{heat of reaction})_{jmax-\frac{1}{4},f+1} \cdot \frac{h_{jmax}}{2}$$

incoming heat $= (\text{convection})_{jmax-\frac{1}{4},f+1} \cdot (T_{jmax-\frac{1}{2},f+1} - T_{ref})$ (case 1)

$= (\text{convection})_{jmax-\frac{1}{4},f+1} \cdot (T_{jmax-\frac{1}{2},f+1} - T_{ref}) + h_{eff} \cdot (T_{cont.phase} - T_{jmax,f+1})$ (case 2)

$$\text{out flowing heat} = \lambda_{jmax-\frac{1}{2},f+1} \cdot \left(\frac{T_{jmax,f+1} - T_{max-1,f+1}}{h_{jmax}} + \right.$$

$$\left. + (\text{convection})_{jmax-\frac{1}{4},f+\frac{1}{2}} (T_{jmax,f+1} - T_{ref})\right)$$

When T_{ref} is set equal to $T_{jmax-\frac{1}{2},f+1}$ the convection term in the equation for the incoming heat drops out. The temperature difference $(T_{jmax,f+1} - T_{jmax-\frac{1}{2},f+1})$ in the convection term in the equation for the outflowing heat is approximated by: $\frac{T_{jmax,f+1} - T_{jmax-1,f+1}}{2}$

The coefficients b_{jmax-1}, a_{jmax} and y_{jmax} are now given by (see eq.(2)):

$$b_{jmax-1} = -\frac{\lambda_{jmax-\frac{1}{2},f+1}}{h_{jmax}} - \frac{(\text{convection})_{jmax-\frac{1}{4},f+\frac{1}{2}}}{2} \qquad (15)$$

$$a_{jmax} = \frac{h_{jmax} \cdot (\rho C_p)_{jmax-\frac{1}{4},f+1}}{2.k_{f+1}} + \frac{\lambda_{jmax-\frac{1}{2},f+1}}{h_{jmax}} + \frac{(\text{convection})_{jmax-\frac{1}{4},f+\frac{1}{2}}}{2}$$

(case 1) (16)

$$a_{jmax} = h_{jmax} \cdot \frac{(\rho C_p)_{jmax-\frac{1}{4},f+1}}{2k_{f+1}} + \frac{\lambda_{jmax-\frac{1}{2},f+1}}{h_{jmax}} + \frac{(\text{convection})_{jmax-\frac{1}{4},f+\frac{1}{2}}}{2} + h_{eff}$$

(case 2) (16')

$$y_{jmax} = h_{jmax} \cdot \frac{(\rho C_p)_{jmax-\frac{1}{4},f+1} \cdot T_{jmax,f}}{2.k_{f+1}} - \frac{h_{jmax}}{2} \cdot (\text{heat of reaction})_{jmax-\frac{1}{4},f+1} +$$

$+$ constant (case 1)

(17)

$$y_{jmax} = \frac{h_{jmax} \cdot (\rho C_p)_{jmax-\frac{1}{4},f+1} \cdot T_{jmax,f}}{2.k_{f+1}} - \frac{h_{jmax}}{2} \cdot (\text{heat of reaction})_{jmax-\frac{1}{4},f+1} +$$

$+ h_{eff} T_{cont.phase}$ (case 2)

(17')

Discretisation of the reaction rate equation

The reaction rate equations (eqs. 2.1) through (2.3))with the initial conditions ($\rho_1=\rho_{1,0}$ and $\rho_2=\rho_3=0$ for t=0) describe the mass concentrations of the solids as functions of time and temperature. Integration of eq.(2.1)from t=0 to t=t gives:

$$\frac{\partial\rho_1}{\partial t} = - k_a\rho_1 - k_b\rho_1 \quad (2.1) \qquad \int_{\rho_{1,0}}^{\rho_1} \frac{d\rho_1}{\rho_1} = - \int_0^t (k_a+k_b).dt \quad (18)$$

$$\text{or: } \ln\left(\frac{\rho_1}{\rho_{1,0}}\right)_t = - \int_0^t (k_a+k_b).dt \quad (19)$$

The conversion at t+Δt may be written as:

$$\ln\left(\frac{\rho_1}{\rho_{1,0}}\right)_{t+\Delta t} = - \int_0^t (k_a+k_b).dt - \int_t^{t+\Delta t} (k_a+k_b).dt \quad (20)$$

It follows that:

$$\left(\frac{\rho_1}{\rho_{1,0}}\right)_{t+\Delta t} = \left(\frac{\rho_1}{\rho_{1,0}}\right)_t . F(\Delta t) \quad (21)$$

Assuming that k_a and k_b are constant during Δt (assuming that Δt is very small) F(Δt) is given by:

$$F(\Delta t) = \exp(-(k_a+k_b).\Delta t) \quad (22)$$

The conversion at every point of the grid can be determined during a time interval from equation (22) by calculating k_a and k_b for every point of the grid as a function of the temperature. Repeated application of eq. (21) gives the mass concentration. Combination of eqs. (21) and (22) gives:

$$\left(\frac{\rho_1}{\rho_{1,0}}\right)_{t+\Delta t} = \left(\frac{\rho_1}{\rho_{1,0}}\right)_t . \exp(-(k_a+k_b).\Delta t) \quad (23)$$

$$\text{Or: } (\rho_1)_{f+1} = (\rho_1)_f.\exp(-(k_a+k_b).k_{f+1}) \quad (24)$$

The following equations can be derived in the same way as eq. (24):

$$(\rho_2)_{f+1} = (\rho_2)_f.\exp(-k_c.k_{f+1}) + (1-y_a).(\rho_1)_f.(1-\exp(-k_a.k_{f+1})) \quad (25)$$

$$(\rho_3)_{f+1} = (\rho_3)f + (1-y_c).(\rho_2)_f.(1-\exp(-k_c.k_{f+1})) \quad (26)$$

Scheme of computer program: fig. 3

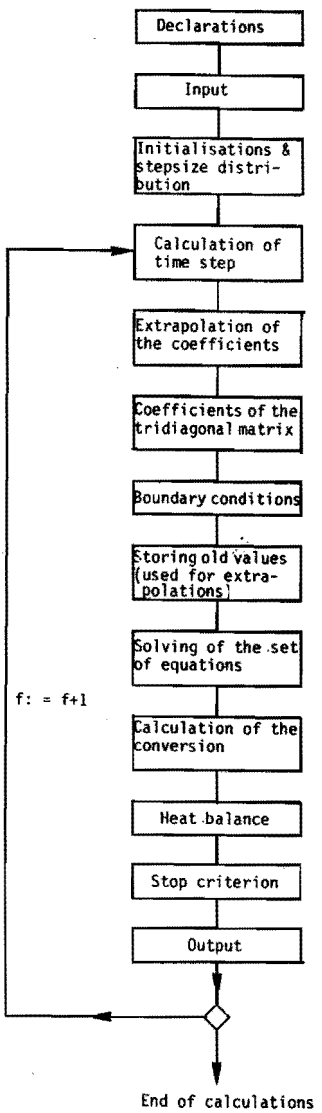

Fig.3 Scheme of computer program

Appendix 2.2. Curve fitting method used to determine k_a,k_c,y_a and y_c.

In the course of the isothermal thermogravimetric analysis of cellulose at temperatures below 260°C the weight (w_t) of the sample is recorded as a function of the time (t). The resulting curve should in theory be described by eq. (2.104), which is shown in § 2.5.5.2.
The values for k_a,k_c,y_a and y_c were calculated by means of the so-called Gauss Newton Choleski method in which k_a,k_c,y_a and y_c are determined from a number of data points (w_t,t) in such a manner that the sum of the squares of the deviations of the data points from the theoretical curve given by eq. (2.104) is as small as possible (Basis of the computation is the least square method [2.44]). Input data for the program are:
- about 20 data points (t,w_t)
- starting values for k_a,k_c,y_a and y_c

The starting values must be fairly accurate to allow the computing process to converge to a reliable result. The following methods were used to obtain the starting values:

1. starting values for k_a and y_a

   The first derivative of the sample weight towards time (dw_t/dt) for t=0 is equal to $-y_a k_a$. (Differentiation of eq. (2.104) or eq. (2.105) and substitution of t=0). Thus:

$$w_t'(o) = \left(\frac{dw_t}{dt}\right)_{t=0} = -y_a k_a \qquad (1)$$

   The second derivative for t=0 is given by:

$$w_t''(0) = \left(\frac{d^2 w_t}{dt^2}\right)_{t=0} = k_a^2 . y_a \qquad (2)$$

   Combination of eqs. (1) and (2) yields:

$$k_a = - \frac{w_t''(0)}{w_t'(0)} \qquad (3)$$

   and

$$y_a = \frac{w_t'(0)^2}{w_t''(0)} \qquad (4)$$

The following equation holds for small t:

$$w_t''(0) = \frac{w_t'(t)-w_t'(0)}{t} \qquad (5)$$

The first derivative can be determined from the slope of the tangent to the w_t vs t curve.

2. Starting value for k_c

The conversion of cellulose into dehydrocellulose will be (almost) complete for large t. For t=t (large t) let:

A = amount of dehydrocellulose at $t=t_1$ (grams)

B = amount of char at $t=t_1$ (grams).

For $t>t_1$ it follows that:

$$w_t(t) = \underbrace{B+(1-y_c).A.(1-\exp[(t_1-t).k_c])}_{\text{char}} + \underbrace{A.\exp.[(t_1-t).k_c]}_{\text{dehydrocellulose}}$$

$$= B+A(1-y_c)+A.y_c.\exp.[(t_1-t).k_c] \qquad (6)$$

Similarly for $t_2>t_1$:

$$w_t(t_2) = B+A(1-y_c)+A.y_c.\exp.[(t_1-t_2).k_c] \qquad (7)$$

and for $t_3>t_1$:

$$w_t(t_3) = B+A(1-y_c)+A.y_c.\exp.[(t_1-t_3).k_c] \qquad (8)$$

By definition: $w_t(t_1) = A+B$ (9)

Combination of eqs. (7), (8) and (9) gives:

$$\frac{w_t(t_1)-w_t(t_3)}{w_t(t_1)-w_t(t_2)} = \frac{1-\exp[(t_1-t_3).k_c]}{1-\exp[(t_1-t_2).k_c]} \qquad (10)$$

$w_t(t_1)$, $w_t(t_2)$ and $w_t(t_3)$ were measured respectively for t_1, t_2 and t_3. The value for k_c that was used as starting value for the least squares calculation was calculated from eq. (10).

3. Starting value for y_c

The limit value of w_t for $t \to \infty$ is given by (see eq. (2.104)):

$$\lim_{t\to\infty} w_t(t) = (1-y_a)(1-y_c).w_t(0) \qquad (10)$$

$(1-y_a)(1-y_c)$ can be calculated by taking the residual weight of the sample after pyrolysis batch experiments with very large reaction periods. It follows for y_c that:

$$y_c = 1 - \left| \lim_{t\to\infty} \frac{w_t(t)}{w_t(0)} \cdot \frac{1}{(1-y_a)} \right| \qquad (12)$$

The starting values obtained by the above methods were used as input data for the Gauss Newton Choleski procedure together with a number of data points (t, w_t).

Appendix 3.1 Physical properties of the pyrolysis gas.

Values and relationships used in the design calculations.

physical property of the gas (at 0°C and 1 atm)				relationship used in calculation of the property at other temperature (T, °K) or pressure (p,atm) [3.10, 3.11, 3.12].
name	symbol	value	unit	
density	ρ_o	0.9	kg/m^3	$\rho_1 = \rho_o \cdot \frac{p_1}{p_o} \cdot \frac{T_o}{T_1}$
viscosity	μ_o	$1.4*10^{-5}$	N.sec/m^2	$\mu_1 = \mu_o \cdot \{\frac{419}{T+146}\} \cdot \{\frac{T}{273}\}^{3/2}$
				$\frac{\partial \mu}{\partial p} = 0$ (for 0<p<10 atm)
thermal conductivity	λ_o	0.05	J/m.sec.°C	$\lambda_1 = \lambda_o \cdot \{\frac{373}{T+100}\} \cdot \{\frac{T}{273}\}^{3/2}$
				$\frac{\partial \lambda}{\partial p} = 0$ (for 0<p<10 atm)
heat capacity	Cp_o	1600	J/kg.°C	$Cp_1 = 1302.3+1.104*T-0.873*10^{-4}*T^2 - 0.796*10^{-7}*T^3$
				$\frac{\partial Cp}{\partial p} = 0$ (for p<3.5 atm).

Appendix 3.2 Calculation of the heat transfer coefficient from reactor wall to spout-fluid bed

The penetration theory of Higbie was applied to estimate the heat transfer coefficient. A relation for the heat transfer coefficient is derived on the basis of this theory in [3.4]:

$$\alpha = \frac{2}{\pi} \cdot \sqrt{\frac{\lambda_{eff} \cdot \rho_s \cdot Cp_s}{\tau}}$$

where: λ_{eff} = effective thermal conductivity in the bed (J/m.sec.^{o}C)

ρ_s = density of solid phase packet (kg/m^3)

Cp_s = heat capacity of solid phase packet (J/kg.^{o}C)

τ = contact time of solid phase packet with the wall (sec.)

λ_{eff} may be calculated from:

$$\frac{1}{\lambda_{eff}} = \frac{1-\epsilon}{\lambda_s} + \frac{\epsilon}{\lambda_g}$$

in which ϵ = porosity of the bed

λ_s = thermal conductivity of solid phase

λ_g = thermal conductivity of the gas

A conservative value of 4 seconds was assumed for the contact time on the basis of visual observations [3.6]. Using the numeric values (appendix 3.1 and 3.4) of the other physical properties in the relations for λ_{eff} and α the heat transfer coefficient α was calculated to be 283 J/m^2.sec.^{o}C.

Appendix 3.3 Thermal insulation of the reactor

Fiberfrax Low Conductivity insulation blanket (density 100 kg/m^3) was chosen as the insulation of the reactor must be resistant to high temperatures. This insulation material contains large amounts of Al_2O_3 and Si_2O_2. The maximum temperature it can continously be exposed to is 1260^{o}C. The thermal conductivity of the Fiberfrax is a function of temperature. A plot of the thermal conductivity versus the average temperature according to ASTM-C177-63 is given below. The average temperature is defined as half the sum of the temperature at the inside and

the temperature at the outside of the insulation. The thickness of the insulation was calculated as a function of the heat loss and the temperature on the outside of the insulation that could be tolerated. This led to an insulation thickness of 8-10 cm. This insulation blanket is enclosed in an aluminium jacket. The same Fiberfrax Low Conductivity insulation blanket was used to insulate the cyclones and fluidisation gas heater.

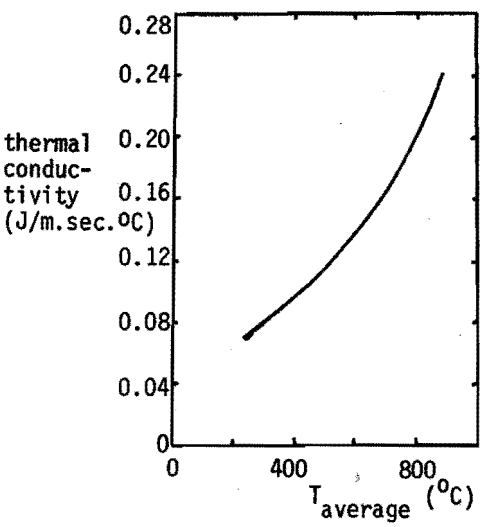

Appendix 3.4 Data employed in design of reactor

The following data have been used together with the data given in the text of § 3.3.2 in calculations regarding the design of the reactor and its accessoires:

symbol	description	numeric value	unit
Cp wℓ	heat capacity of water	4190	J/kg.^{o}C
Cp wg	heat capacity of water vapor	1840	J/kg.^{o}C
Cp h	heat capacity of domestic waste (dry basis)	2200	J/kg.^{o}C
ΔH_w	heat of evaporation of water	$2.3*10^6$	J/kg
ϵ	porosity of sand bed	0.5	-
λ_s	thermal conductivity of solid phase	0.39	J/m.sec.^{o}C
λ_g	thermal conductivity of gas (at 400^{o}C)	0.09	J/m.sec.^{o}C
ρ_s	bulk density of sand	1400	kg/m^3
Cp_s	heat capacity of sand	1200	J/kg.^{o}C

Appendix 3.5 The cyclones. Data on gas flow rates and electrical heating

A. Calculation of the minimum gas flow through the cyclones

The gas flow through the cyclones is at a minimum when the reactor is operated at minimum fluidisation gas flow rate (u_{mf}) and zero gas production. The value of the minimum fluidisation gas flow rate that has been used in the design calculations is 15 cm/sec. Experimental determination of the u_{mf} in the spout fluid bed resulted in a value of 22 cm/sec for the sand used in the pyrolysis experiments. The minimum gas flow through the cyclones was therefore found to be:

$$u_{mf} * \frac{\pi}{4} \cdot (\text{reactor diameter})^2 = 0.15 * \frac{\pi}{4} * (0.15)^2 = 2.65*10^{-3} \text{ m}^3/\text{sec.}$$

B. Calculation of the maximum gas flow through the cyclones

The maximum superficial gas flow in the reactor (apart from gas produced by pyrolysis) is assumed to be 1 m/sec which corresponds to a flow of $17.7*10^{-3}$ m^3/sec. The maximum gas production is 10 kg/hr (§ 3.3.1) which corresponds to a gas flow of $3.1*10^{-3}$ m^3/sec (1 atm., 0^{o}C). The maximum

temperature at which the cyclones will be operated is 800°C and the pressure in the cyclones is atmospheric. The gas flow due to gas production will therefore show a maximum value of $12.1*10^{-3}$ m³/sec (800°C, 1 atm). The maximum total gas flow that enters the cyclone will be $29.8*10^{-3}$ m³/sec in that case.

C. The electrical heating of the cyclones

Cyclone 1 is fitted with two electrical heating coils of Kanthal-A resistance wire. One coil has been wound around the entry of the cyclone (42 Ω), the other one around the body of the cyclone (46 Ω). The two coils are connected in parallel. The maximum power that can be absorbed by the two coils at 220 V is $(220)^2*(\frac{1}{46} + \frac{1}{42})$ = 2200 Watt.
Cyclone 2 has been fitted with one coil only made of Kanthal-A resistance of 38 Ω and absorbs 1275 Watt at 220 V.

Appendix 3.6 Detail on the design of the tube cooler

The design was based on the relationship:

$$n.L = \frac{G_n.\rho.C_p}{\alpha.\pi.d} .\ln \{\frac{T_i-T_w}{T_u-T_w}\}$$

See text of § 3.3.4.2 for the meaning of the symbols.
The physical properties of the gas used in the calculations were supposed to be constant throughout the cooler.Their numerical values were calculated using the equations shown in appendix 3.1 at an average temperature:

$$T_{av} = \frac{T_i+T_u}{2}$$

To ensure good operation at any gas flow rate that was to be expected in the cooler it was decided to calculate the cooler for laminar flow of the gas. The heat transfer coefficient α may be estimated from the Nusselt number. In case of almost stationary flow inside a pipe Nu reaches the limiting value of 3.66.This value was used in designing the cooler: $\alpha = \frac{3.66*\lambda}{d}$ (λ: thermal conductivity of the gas, J/m.sec.°C).
For practical reasons the length and the internal diameter of the pipe were chosen to be 2 m and 15 mm respectively. The wall temperature T_w was assumed to be equal to the temperature of the coolant flowing around the

pipes. We thus assumed that the resistance to heat transport is entirely located in the gas phase at the inside of the pipe. The coolant was selected on the basis of price, availability and physical properties. The choice fell on UCON hft 14 cooling oil. In the dimensioning of the cooler the temperature of the coolant - and T_w - was chosen to be 100^oC. In the below table (that summarizes the calculations) n_{min} is the minimum number of parallel pipes required to cool the maximum gas flow from the temperature indicated to 150^oC. The minimum of parallel pipes necessary for operation under laminar flow conditions in the cooler is also given (n_{la}) in the table. The following relationship was used as the criterion for laminar flow:

Reynolds number = $\frac{4.G_n.\rho}{n.\pi.d.\mu} < 2100$ (μ: viscosity of the gas, N.sec/m^2)

The minimum number n_{la} is thus given by: $n_{la} = \frac{G_{n,max}.\rho}{525.\pi.d.\mu}$

$T_i(^oC)$	$G_{n,max}$ (m^3/sec)	$G_{n,max}*\rho$(kg/sec)	α(J/m .sec^oC)	n.L (m)	n_{min}	n_{la}
300	$21.0*10^{-3}$	$10.36*10^{-3}$	18.3	30.1	16	17
500	$20.4*10^{-3}$	$8.38*10^{-3}$	20.7	34.0	17	14
800	$20.8*10^{-3}$	$6.83*10^{-3}$	24.4	32.3	17	10

A cooler consisting of 24 parallel pipes was designed and constructed on the basis of the above calculations. Compared to the calculated number of 17 pipes that are required the 24 pipes included represent an excess cooling surface of 40%.

Appendix 3.7 Details on the design calculations for the electrostatic precipitator

Data used in the calculations (for meaning of the symbols: § 3.3.4.2):

(maximum)gas flow : $(G_n*\rho) = 10.4*10^{-3}$ kg/sec (appendix 3.6)
Viscosity of pyrolysis gas : $\mu = 2*10^{-5}$ N.sec/m^2 (appendix 3.1, 150^oC)
Viscosity of nitrogen : $\mu_{N2} = 2.3*10^{-5}$ N.sec/m^2 (150^oC)
Droplet diameter : $d_p = 1\ \mu m = 10^{-6}$ m
Gas density : $\rho = 0.58$ kg/m^3 (appendix 3.1, 150^oC)
Elemental charge : $\varepsilon = 1.6*10^{-19}$C

Ratio R_u/R_i [1] : $R_u/R_i = 3$

Sparking potential [2] : $V = 0.5*V$ (read from fig. 1).

1) The ratio R_u/R_i must meet the criterion $R_u/R_i > 2.72$ to make corona discharge possible [3.9].

2) The factor 0.5 is due to the increased operating temperature of the electrostatic precipitator (150^oC).

1. Laminar gas flow through the pipes

eq.(3.1): $$R_e = \frac{4.G_n.\rho}{n.\pi.d.\mu} < 2100 \longrightarrow n.d. > 0.315$$

Combination of eqs. (3.2) through (3.5) yields:

$$u = \frac{3.4*10^5.T.\varepsilon.V}{3.\pi.\mu.r.\ln(R_u/R_i)}$$

Substitution of the above data (μ_{N2} is a conservative assumption for start-up period) gives:

$$u = 1.06*10^{-7}.\frac{V}{r.\ln(R_u/R_i)} \qquad \text{eq.(3.6)}$$

eq.(3.7): $$= u_{av} = \frac{2\pi\int_{R_i}^{R_u} u.r.dr}{2\pi\int_{R_i}^{R_u} r.dr}$$

Combination of eqs.(3.6) and (3.7) and rewriting yields:

$$u_{av} = 2.14*10^{-7}.\frac{V}{\ln(R_u/R_i)}.\frac{R_u-R_i}{R_u^2-R_i^2} \qquad \text{eq.(3.8)}$$

eq.(3.9): $$\Delta t = 46.7*10^6.\frac{\ln(R_u/R_i)}{V}.(R_u^2-R_i^2)$$

Substitution of $R_u/R_i = 3$ and $R_u = \frac{1}{2}d$ gives:

$$\Delta t = 1.28*10^6.\frac{d^2}{V} \qquad \text{eq.(3.10)}$$

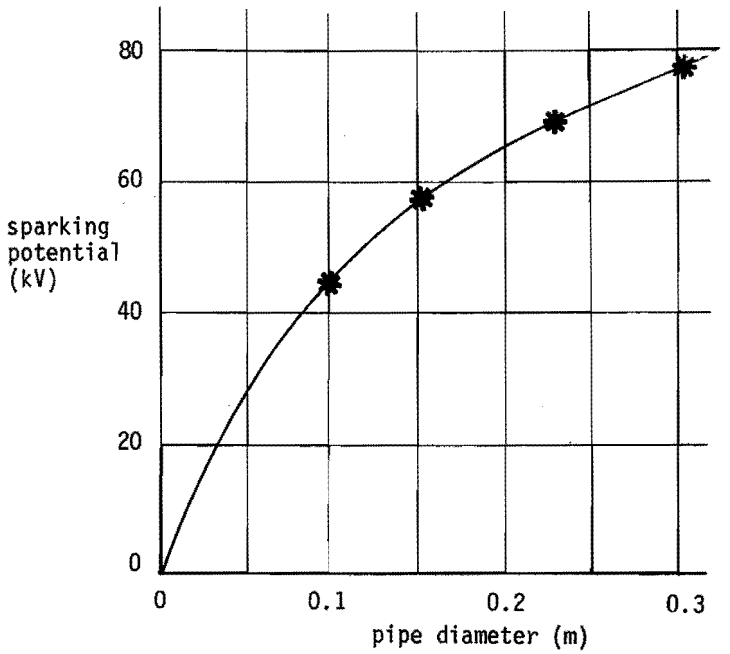

Fig.1 Sparking potential for wire in cylinder. Negative corona. Air, water vapor, CO_2 mist. Temperature: 38°C.

eq. (3.11): $$v_{sup,max} = \frac{G_n}{n.\frac{1}{4}.\pi d^2} = \frac{(G_n.\rho)}{n.\frac{1}{4}.\pi d^2.\rho} = \frac{2.28*10^{-2}}{n.d^2}$$

eq. (3.12): $$L = \Delta t * v_{sup,max} = \frac{2.92\ 10^4}{n.V}$$

Results of calculations:

d(m)	n n.d >0.315	V(V) 0.5*V (fig.1)	L(m) ($2.92*10^4$/n.V)
0.2	2	35,000	0.42
0.1	4	25,000	0.29
0.05	7	15,000	0.28
0.03	11	10,000	0.27
0.02	16	6,000	0.31

The minimum that occurs in L as a function of d is remarkable. Decreasing the pipe diameter (d) leads to a decreased sparking potential (V) and to an increase of the number of pipes required (n). How L varies with d depends on V = f(d) as $L = \frac{\text{constant}}{n.V}$ and $n \backsim 1/d$.
The following set for n and L was selected on the basis of practical considerations:
d = 50 mm, n = 7 pipes.

2. Influence of turbulences

It was assumed that the particle concentration is homogeneous over the cross area of the pipes as a result of the turbulences. By definition, the particles that reach the wall in period of time Δt were at the beginning of that period at a distance dz from the wall (fig. 3.17). Then:

t=0, x=x : particle concentration: $\bar{c}_x = \frac{n}{(R_u^2-R_i^2)}$

t=Δt, x=x+dx: particle concentration: $\bar{c}_{x+dx} = \frac{n-n.(\frac{dz.2\pi.R_u}{\pi(R_u^2-R_i^2)})}{\pi.(R_u^2-R_i^2)}$

The decrease of particle concentration is given by:

$$-d\bar{c} = \bar{c}_x - \bar{c}_{x+dx} = \frac{n}{\pi(R_u^2-R_i^2)} - \frac{n}{\pi(R_u^2-R_i^2)} + n.\left(\frac{dz.2\pi.R_u}{\pi^2.(R_u^2-R_i^2)^2}\right)$$

$$= 0$$

The relative decrease in particle concentration is given by:

$$-\frac{d\bar{c}}{\bar{c}} = \frac{\bar{c}_x-\bar{c}_{x+dx}}{\bar{c}_x} = \frac{2\pi.R_u.dz}{\pi(R_u^2-R_i^2)} . \qquad \text{(eq.(3.15))}$$

As $u = \frac{dz}{dt}$ (eq. (3.13)) and $dx=v_{sup}.dt$ (eq.(3.14)) the above equation may be written as:

$$-\frac{d\bar{c}}{\bar{c}} = \frac{2.R_u}{R_u^2-R_i^2} . \frac{u}{v_{sup}} . dx$$

It is assumed that the migration velocity u is given by:

$$u = 1.07*10^{-7} \frac{V}{R_u . \ln(R_u/R_i)}$$

(eq. (3.6)), $r=R_u$). Hence:

$$-\frac{d\bar{c}}{\bar{c}} = \frac{2.R_u}{R_u^2\ R_i^2} \cdot \frac{1.07*10^{-7} \cdot V}{v_{sup} . R_u . \ln(R_u/R_i)} \cdot dx$$

Integration from x=L ($\bar{c}=\bar{c}_i$) to x=L ($\bar{c}=\bar{c}_u$) yields:

$$\frac{\bar{c}_u}{\bar{c}_i} = \exp\left\{ - \frac{2.R_u.L}{(R_u^2-R_i^2).v_{sup}} \cdot 1.07*10^{-7} \cdot \frac{V}{R_u . \ln(R_u/R_i)} \right\} \quad \text{(eq.(3.17))}$$

With:

$$v_{sup} = \frac{2.28*10^{-2}}{n.d^2}$$

(see calculations for laminar flow) and substituting the variables that have been found for the case of laminar flow except L (n=7, $d=2R_u$=50 mm; R_i=7.5 mm and V=15 kV) eq.(3.17) may be reduced to:

$$\frac{\bar{c}_u}{\bar{c}_i} = \exp\{-3.58*L\}$$

The collection efficiency is defined by:

$$\eta = 1 - \frac{\bar{c}_u}{\bar{c}_i}$$

Therefore η= 1-exp(-3.58*L). To obtain a collection efficiency of 99% in this worst possible case a pipe length L=1.30 m must be chosen.

Appendix 3.8 The design of a spray tower

Water flow rate through the spray nozzle: V m^3/sec
Assumed average diameter of water droplets: d_p = 0.5 mm
Fall velocity of a droplet of that diameter: v_p = 2.3 m/sec.

The value given here is the stationary free fall velocity of a water droplet (d_p = 0.5 mm) in air of 21°C [3.9]. The actual fall velocity of the droplets in the tower will be somewhat higher as a result of their initial velocity and because the density and viscosity of the pyrolysis gas are lower than those of air of 21°C.
The Ranz-Marschall equation could be solved after calculating λ, μ, ρ and Cp of the pyrolysis gas (appendix 3.1) at the average temperature of the gas in the tower ($\frac{150+25}{2}$ °C). The Nusselt number found was Nu_p = 5.2. The Nusselt number used in the calculations was Nu_p = 5 because of the reasons summed up in § 3.3.4.3.
From: maximum water production = $3.5*10^{-5}$ kg/sec
maximum gas flow = $11.5*10^{-3}$ m^3/sec (°C, 1 atm)
temperature of incoming gas stream = 150°C
temperature of outgoing gas stream = 25°C
and spray water flow (V) = 10 ℓ/min (estimated)
the total area of water droplets A required was found to be: 0.53 m^2.
The water hold-up in the spray tower is given by:

$$\bar{r} = \frac{V.L}{v_p}$$

in which: r = water hold up (m^3)
V = spray water flow rate (m^3/sec)
L = distance covered by the free falling water droplets (m)
v_p = fall velocity of water droplets (m/sec)

As $A = \frac{6r}{d_p}$ and A > 0.53 m this led to: $V.L > 1.02*10^{-4}$ m^4/sec.

The dimensions of the spray tower that was designed on the basis of the above calculations are:

Cross area : 0.16 m^2 (0.4*0.4 m)
Effective height : 0.9 m (fig. 3.23)

The spray water flow rate must therefore be > 6.8 ℓ/min.

The heat exchanger that has been installed in the closed water circuit to keep the temperature of the spray water constant must be able to remove the maximum heat released in the tower. A heat exchanger was available that contained 5 parallel pipes with an inner diameter of 23 mm and a length of 4 m. It was assumed that the average temperature of the cooling water is 16^{o}C. The logarithmic average temperature difference between spray and cooling water could then be calculated. The overall heat transfer coefficient (U) was found to be 770 J/m.sec.^{o}C. The heat transfer coefficient α_i on the inside of the pipes is given by:

$$\frac{1}{\alpha_i} = \frac{1}{U} - \frac{d_w}{\lambda_w}$$

in which: d_w = thickness of pipe wall ($1.5*10^{-3}$ m)
λ_w = thermal conductivity of pipe material (stainless steel, 16 J/m.sec.^{o}C)

So: α_i = 830 J/m^2.sec.^{o}C.
Further calculations showed that this value of α_i can be obtained when the total flow of spray water through the heat exchanger is about 24 ℓ/min.

Appendix 3.9 The design of a fluidisation gas heater

It was mentioned in § 3.4.3.1 that heating experiments were carried out using heaters of different diameter and with different types of Kanthal strip. The power supplied to the Kanthal strip was varied in these experiments for different air flow rates. The following quantities were measured in the experiments for each of the heaters:
- the flow rate of the air through the heater
- the pressure drop over the heater
- voltage and current (Kanthal strip)
- temperature of quartz pipe in the middle and at the end of the heater
- temperature of the air leaving the heater.

The results of the experiments were used in a physical model of the gas heater from which the heat transfer coefficient α_i for heat transport from the coil to the gas was calculated. It was assumed in setting up this model that the aera of heat transfer may be held to be equal to the

internal area of the quartz pipe and that the heat transfer coefficient α_u for heat transfer to the environment (through the insulation) is constant for the entire length of the heater. The model divides the heater into different sections with length Δx. The α_i, the gas temperature T_x (at the beginning of Δx), $T_{x+\Delta x}$ and the wall temperature T_w were calculated for each section. α_u is adjusted by a process of trial and error so that the calculated temperature of the gas leaving the heater is about the same as the temperature measured in the experiments. The relationship applied in the model to calculate α_i is the following one proposed by Gambill [3.13] for the case when large heat fluxes are introduced into a gas that flows turbulently through a pipe:

$$(Nu_b)_y = 0.021.(Re_b)^{0.8}.(Pr_b)^{0.4}.\left(\frac{T_w}{T_b}\right) - (0.29+0.0019.\frac{y}{D})$$

for $10 < L/D < 240$

$110 < T_b < 1550^oK$

$1.1 < \frac{T_w}{T_b} < 8$

where Nu = Nusselt number
Re = Reynolds number
Pr = Prandtl number
T_w = gas temperature at the wall (^oK)
T_b = gas temperature in the bulk (^oK)
y = length co-ordinate along the pipe (m)
D = internal diameter of pipe (m)
L = total length of the pipe (m)
subscript b = bulk
y = at place y

The diameter of the quartz pipe (18*15 mm) and the type of Kanthal strip (5*0.5 mm) were selected on the basis of the results for the different heaters. The model was tested for air, nitrogen and pyrolysis gas of the theoretical composition above. The model was found to be satisfactory for air and nitrogen but less satisfactory for pyrolysis gas because of its high heat transfer coefficient α_i. The heat transfer from Kanthal strip to pyrolysis gas was found to be larger than had been calculated as a result of this higher α_i.

Taking this into account the length of the gas heater was chosen to be 1.50 m.

Appendix 3.10 Measurement points in the pyrolysis plant

Temperatures and pressure differences are measured at many points in the installation. Temperature is measured by means of Chromel-Alumel thermocouples. In the thermocouples used the thermocouple wires were inbedded in ceramic insulations. The minimum diameter of the thermocouple wires is 0.52 mm. The hot joint of both thermocouple wires is insulated from the thermocouple jacket by MgO. The jacket is made of Inconel-600 and has a diameter of 3.2 mm. The insert length of the thermocouples is 250 mm and their response time is 1.6 sec. The places in the installation where the temperature is measured are indicated in fig. 1. All tempera-

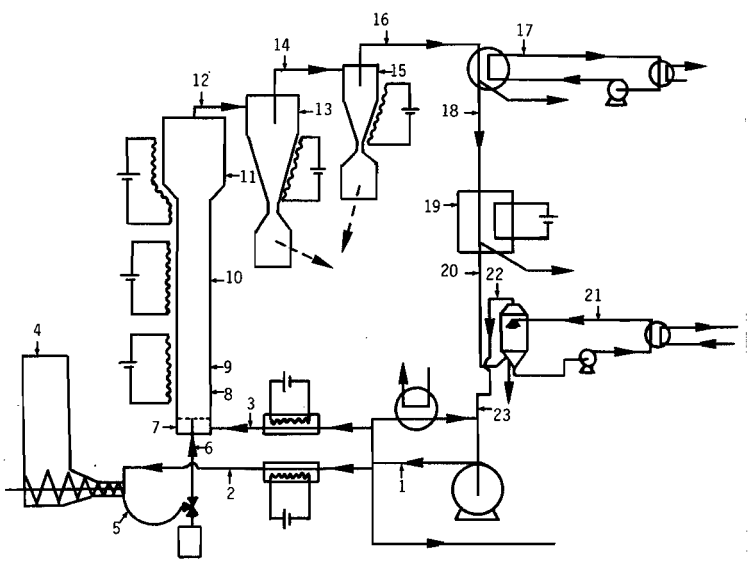

points 1,2,3,12,14,16,20,22,23 : temperature of gas, pressure
points 4,5,6,7 : pressure
point 8: on different places the pressure and temperature in the bed are measured. The thermocouples are inserted at different depths in the bed.
8a,c,e,g,k : temperature of bed
8b,d,f,h,ℓ : pressure of bed
points 9,10,11,13,15,19 : wall temperature
point 17 : temperature of coolant
point 18: 18a after condensor (1): temperature of gas
18b after condensor (2): temperature of gas
18c combined streams before electrostatic precipitator : temperature of gas, pressure
point 21 : temperature and pressure of spray water

Fig.1 Temperature and pressure measurement points

tures are recorded and can be read at any time on the control panel. Pressure differences are measured by means of Hottinger-Baldwin probes. The different pressure measurement points (fig. 1) are scanned two at a time with a programmed connection system. One pressure difference at a time is supplied to one of the probes (see table 1). A second probe is used for a continuous registration of the pressure drop over the spout gas line (p_5-p_6) to check the pneumatic transport of the solid feed by the spout gas. A third probe is used to register the pressure in the installation just downstream from the Roots blower (p_1). All pressure differences are recorded.

Table 1 Pressure differences that are successively measured using one probe.

Measurement points	pressure drop over
p_1-p_2	spout gas heater
p_1-p_3	fluidisation gas heater
p_6-p_{8b}	spout pipe in reactor
p_7-p_{8b}	sieve plate
p_{8b}-p_{8d}	first part of the bed
p_{8d}-p_{8f}	second part of the bed
p_{8f}-p_{8h}	third part of the bed
p_{8h}-p_{8l}	fourth part of the bed
p_{12}-p_{14}	cyclone 1
p_{14}-p_{16}	cyclone 2
p_{16}-p_{18c}	tube cooler
p_{18c}-p_{20}	electrostatic precipitator
p_{20}-p_{22}	spray tower
p_{22}-p_{23}	suction line Roots blower
p_{23}-p_{23}	zero check

Appendix 3.11 Safety measures

The points were temperature and pressure are measured are indicated in fig. 1 in appendix 3.10.

1. Protection of the apparatus

- Temperature of gas entering the electrostatic precipitator.
  When T_{18} exceeds the set point nitrogen is injected into the gas stream just upstream from the precipitator (+ signal light). When the temperature remains too high for a longer period an alarm is sounded to warn the operator. The reason is that Teflon parts are used in the electrostatic precipitator so the temperature in the precipitator must be limited to below the softening point of this material.
- Temperature of gas entering the Roots blower.
  When T_{23} exceeds the set point an alarm is sounded to warn the operator. When the temperature remains too high for a longer period the emergency shut down sequence is activated (see below). The reason is that the temperature in the blower must remain below a certain value (see § 3.4.1).

  The following actions are carried out automatically and simultaneously in case of an emergency shut down:

  a. The valves to the stack are opened
  b. The valves upstream from the electrostatic precipitator and Roots blower are shut.
  c. Nitrogen is injected into the unit in several places (see fig. 1).
  d. All electrical heatings except the heating of electrostatic precipitator are switched off.
  e. The high voltage power supply to electrostatic precipitator is switched off.
  f. The current supply to the Roots blower is switched off.
  g. The current supply to the solid feed conveyor is switched off.
  h. The three-way valve in the spout gas line under the reactor is set in such a position that the bed material drops out of the reactor into the vessel below the reactor.
  k. An alarm is sounded.

  The above actions put an abrupt end to several potentially dangerous situations: the installation is divided into two compartments (b,f)

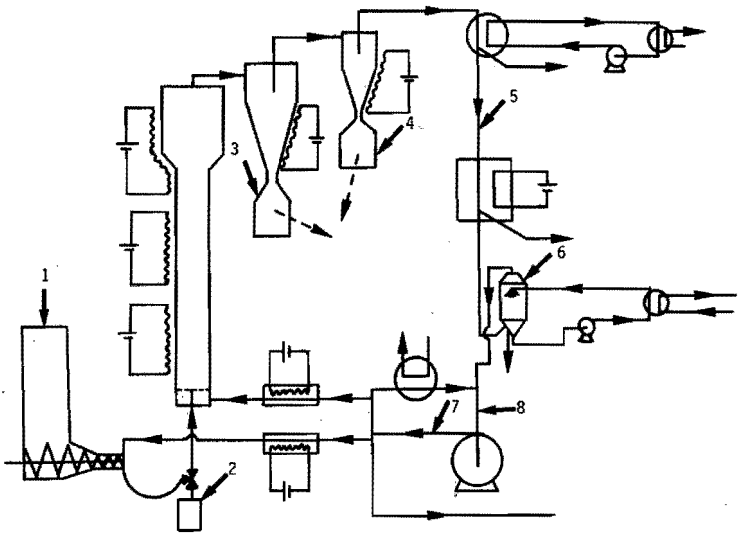

Fig.1 Nitrogen injection points

that are flushed with nitrogen (c) so that the gases present in the installation are driven out through the stack (a). The solid feed supply is stopped (g), all electrical heatings but one are switched off (d) and the hot bed contents drop out of the reactor (h). As the electrostatic precipitator is not functional under these conditions and as an electrical spark may cause an explosion if an explosive mixture is present, the high voltage power supply is switched off (e). The electrical heating of the electrostatic precipitator is continued to keep the tar fluid so it may be drawn off.

- Temperature of quartz pipe inside fluidisation gas heater.
  When the temperature of the quartz pipe (measured by means of a Pt/PtRh thermocouple) becomes too high the current supply to the gas heater is switched off (+ signal light). This is done to prevent the Kanthal strip from melting.
- Excess pressure in the reactor.
  When p_{12} exceeds a set point the emergency shut down sequence is activated.
- Temperature of spray water.
  When T_{21} exceeds a set point an alarm is sounded. This is done to protect the recirculation pump.

- Temperature coolant tube cooler.
  When T_{17} exceeds a set point more cooling water is fed to the cooling coil (fig. 3.15). An alarm is sounded.
- Temperature of gas leaving the reactor.
  When T_{12} exceeds a set point the current supply to the electrical heatings of the fluidisation gas and reactor wall is switched off (+ signal light). The reason is that only the reactor itself is made of heat resistant steel, the rest of the installation is made of stainless steel that is resistant to temperatures up to 900°C only.

2. Protection of the process operation

- Flow through spout gas line.
  When flow exceeds set point 1 an alarm is sounded.
  When flow drops below set point 2 an alarm is sounded.
  When flow drops below set point 3 the emergency shut down sequence is activated.
  Set point 1 > set point 2 > set point 3.
  The reason is that when the spout gas flow rate becomes too high sand and waste particles will be blown out of the reactor. When the flow rate is too small bed materials will drop into the spout pipe and the feedstock will no longer be transported. This causes obstruction of the spout gas line.
- Flow through fluidisation gas line.
  When flow exceeds set point 1 an alarm is sounded.
  When flow drops below set point 2 the fluidisation gas heating is switched off (+ signal light) to prevent the Kanthal strip from melting.
- Pressure control.
  When p_1 falls below set point 1 nitrogen is injected at injection point 5 and an alarm is sounded. When p_1 remains too low for a long period of time the emergency shut down sequence is activated.
  When p_1 exceeds set point 2 an alarm is sounded and after some time the emergency shut down sequence is activated. The reason is that p_1 being low for a longer period indicates a considerable gas leakage. p_1 getting too large indicates an obstruction downstream in the installation.

- Pressure of spray water circuit.
  When p_{21} exceeds a set point an alarm is sounded. The reason is that high pressure indicates that the nozzle might be obstructed. This causes malfunctioning of the cooler.
- Temperature of the electrostatic precipitator.
  When T_{19} falls below set point an alarm is sounded. The reason is that the tar might become too viscous so that the precipitator might be obstructed by it.

3. Safety measures in connection with risks of explosion and drop out of current or pressure

- Protection against partial vacuum in the installation.
  When p_{23} falls below a set point nitrogen is injected upstream from the electrostatic precipitator and into the spray tower. An alarm is sounded. When p_{23} remains below the set point too long the emergency shut down sequence is activated. The reason is that in case of low pressure air might be sucked into the installation which might cause the formation of an explosive gas mixture in the installation (hydrogen).
- Protection against too high oxygen concentration in the installation.
  The oxygen concentration just downstream from the Roots blower is being monitored continuously. When the oxygen concentration exceeds a set point the emergency shut down sequence is activated.
- Low pressure in the bunker.
  When p_4 falls below a set point nitrogen is injected into the bunker (+ signal light). In case of lasting low pressure the emergency shut down sequence is activated.
- Drop out of cooling water pressure, compressed air pressure or nitrogen supply leads to a delayed activation of the emergency shut down sequence but a signal is given to the operator first.
- Drop out of electricity supply or Roots blower: the emergency shut down sequence activated.
- Drop out of pumps in coolant circuit of tube cooler and spray water circuit: an alarm is sounded.

Appendix 4.1 Standard analyses

The analyses discussed here are standard analyses that have been carried out for each experiment. Most of the analyses were carried out in duplicate.

a. Moisture content of feed

The moisture content of the feedstock was determined by measuring the decrease of weight of a sample from the feedstock after it had been dried at a temperature of 105-110°C. Moisture content of feed =

$$\left(1 - \frac{\text{weight of dried sample}}{\text{weight of sample before drying}}\right) * 100\%$$

The sample size was about 300-400 gram.

b. Ash content

The determination of the ash content depended on the nature of the material

- Ash content of the tar.
  A weighed amount of tar (about 50 gram) was heated for 18 hours at about 420°C while air was passed over the sample.

  $$\text{Ash content} = \frac{\text{weight of ash}}{\text{weight of original sample}} * 100\%$$

  The above procedure is recommended by Jolly [4.10].
- Ash content of the char: the analysis is identical to that of the ash content of the tar.
- Ash content of cardboard: the analysis is identical to that of the ash content of the tar.
- Ash content of fractions from shredded domestic waste.
  The ash content of fractions from shredded domestic waste was determined by heating a sample (about 300-400 gram) of the shredded waste for at least 5 hours at a temperature of about 775°C in an oven-type furnace. The temperature of 775°C is recommended in literature [4.11]. It corresponds to the glowing temperature in the determination of the ash content of solid fuels according to DIN 51719. Air was introduced in the furnace during heating.

  $$\text{Ash content} = \frac{\text{weight of ash}}{\text{weight of dry sample}} * 100\%$$

c. Elemental composition

The elemental compositions of feedstock, tar and char were determined either by TNO - Utrecht or by the Laboratory for Organic Chemistry of the Eindhoven University of Technology. The Laboratory for Organic Chemistry is able to determine the weight percentages of C, H and N of solids. The determination of the oxygen content was done by difference. TNO - Utrecht is able to determine almost every element in solids as well as liquids. The determinations of the percentages C, H, N and O were carried out routinely on the feedstock and on the tar and char obtained from pyrolysing the feedstock in all experiments. The elemental analysis methods for determining C, H and N contents that were applied by the Laboratory for Organic Chemistry is briefly discussed below. TNO uses a similar method for the analysis of C, H, O, N and S.
A Perkin-Elmer 240 Elemental Analyser is used:
A weighed sample (3-5 mg) is combusted in a pure oxygen atmosphere. The products of the combustion (carbon dioxide, water vapor and nitrogen oxides) pass through a reduction tube where the oxides of nitrogen are converted to molecular nitrogen. The residual oxygen and other interfering combustion products are removed. The carbon dioxide, water vapor and nitrogen are completely mixed. The mixture is then analysed by passing it through a series of 3 high-precision thermal conductivity detectors using helium as the carrier gas. Each detector consists of two sensing cells. Water vapor is detected in the first detector. All water vapor is removed between the pair of cells in an absorbing trap. The differential signal obtained before and after the trap is a measure of the water concentration and thus of the amount of hydrogen in the original sample. Carbon dioxide is detected in a similar way in the second detector. A CO_2 absorbing trap is used here. The third detector measures the nitrogen concentration by comparing the output of the cell to that of a reference cell through which pure helium flows.
The sample sizes applied in the elemental analyses were:

- Domestic waste fractions.
  A sample of about 300-500 gram was taken from the waste fraction (by means of quartering) and shredded extensively using a domestic shredder provided with rotating knives that actually cuts the material. About 500 mg was taken from this finely shredded waste for sending to either the Laboratory for Organic Chemistry or TNO - Utrecht. They used 3-5 mg

of it for each analysis.

- Char.

  A few grams of the char (which is a powder) was pulverised furthermore in a mortar by means of a pestle. A sample of about 500 mg was separated from it for elemental analysis. 3-5 mg of it was used for each analysis.

- Tar.

  No pretreatment was carried out in this case. Sample size: 500 mg.

d. Gas composition

The composition of the gas in the pyrolysis unit (or rather: that leaves the unit) was determined by use of the gas chromatographic system described below.

Gas-chromatograhic system

The gas is analysed by means of a gas chromatograph with two columns. One column which serves to separate polar from non-polar components has a stationary phase of porous polymers (porapak). The other column is filled with molecular sieve particles. This column separates the non-polar components from each other. However, this molecular sieve is inactivated by CO_2 and water. It is therefore necessary to make arrangements so that these two components of the gas will not pass through it. This problem was solved by using the two columns alternatively in series and in parallel (fig. 1). At the start of an analysis the columns are placed in series. The non-polar gases (N_2, O_2, H_2, CO, CH_4, C_2H_6) have short and almost identical retention times in the porapak column so that they leave the column virtually unseparated.

Before CO_2 leaves the porapak column the columns are switched into parallel position. CO_2 and the components that have longer retention times (including water) are passed through the porapak column only. The non-polar gases are passed through the molecular sieve also. However, the retention time of water in the porapak column is about the same as the retention times of CH_4 and CO in both columns together so that these compounds are detected by the detector at the same time. This makes quantitative analysis of these components impossible.

The water content of the gas that leaves the spray tower can, however, be determined in a different manner: This gas stream is saturated with water so that the water content can be found my measuring the temperature

in series position:

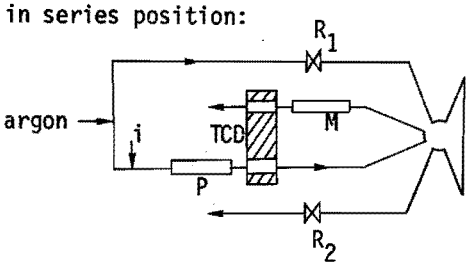

in parallel position:

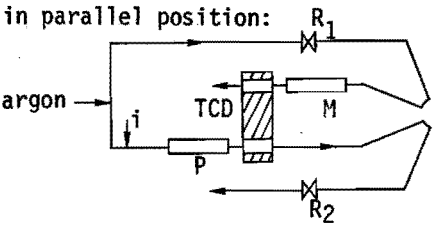

R_1,R_2: needle valves
M : molsieve 5A column
P : porapak Q column
i : injection point

resistance to flow of R_1 = resistance to flow of porapak Q column
resistance to flow of R_2 = resistance to flow of molsieve 5A column

Fig.1 System of two columns for the gaschromatographic analysis

of the stream. The water may therefore be removed from the gas stream prior to gas chromatographic analysis. This is done by adsorbing the water in a column packed with silicagel.

Gas chromatography data:

Carrier gas : argon (3.5 ato)
Detector : TCD (thermal conductivity detector)
Column 1 : porapak Q; 2 m: Ø 2 mm
Column 2 : molsieve 5 A (45-60 mesh); 4 m: Ø 2 mm
Temperature columns : 65°C
Temperature detector : 101°C

The concentrations of the following gases were detected: N_2, O_2, H_2, CO, CO_2, CH_4 and C_2H_6. These gases account for 99-100% of the sampled gas. The pilot plant unit is flushed with nitrogen at the beginning of each pyrolysis experiment. The composition of the gas that leaves the unit changes from 100% nitrogen to the steady state composition during the first 20-60 minutes of operation. The composition of the pyrolysis gas that is produced can be determined by calculating the gas composition on a nitrogen free basis for each measurement. When the composition of the gas on nitrogen free basis is about constant in time during an experiment this steady state composition is assumed to be the composition of the pyrolysis gas produced at the conditions of that experiment.

e. Total organic carbon (TOC) content of spray water.

The total amount of organic carbon in the spray water was determined by means of a TOC-analyser. 30 µℓ of spray water are acidified and heated in a platinum container to 90°C to evaporate the water and to decompose the carbonates.The organic components that have been evaporated are temporarily adsorbed in a column. These components are then flushed and combusted. The contents of the container are combusted at 850°C using MnO_2 as a catalyst. The CO_2 formed in both combustions is converted to CH_4 by hydrogenation using a nickel catalyst. The methane is detected in a flame-ionisation detector.

f. Heat of combustion

The heat of combustion of the pyrolysis gas was calculated. When the concentrations of the various components in the pyrolysis gas are known the heat of combustion of the gas can be calculated from $\Delta H = \sum_j x_j \Delta H_j$ in which x_j = concentration of component j

H_j = heat of combustion of component j

The heats of combustion used in the calculations are [4.12]:

component	$\Delta H^{*)}$ (kcal/mole)
H_2	57.7979
CO	67.6361
CH_4	191.759
C_2H_6	341.261

*) Combustion products: H_2O (gas) and CO_2 (gas).

The heat of combustion of feedstock, tar from the electrostatic precipitator and char from cyclone 1 were either determined by TNO - Apeldoorn (Social Technology Section) or were calculated from the ultimate analysis. The heat of combustion determined by TNO is the gross heat of combustion. The preparation of the samples and the sample sizes were identical to those for the elemental analysis. TNO used about 100 mg for each determination. The determination is carried out according to N.E.N. 935 II in an adiabatic bomb-calorimeter. The heat of combustion can also be calculated from the ultimate analysis. Several formulas for calculating the heat of combustion are given in f.i. literature no. [4.13]. For the cardboard experiments nos. 1 through 5 (see Chapter 5) the heats of combustion for feedstock, tar and char were both determined by TNO and calculated using the formula:

Heat of combustion = 329*C + 1510*H - 139*O (kJ/kg)

where: C = percentage of carbon present in the material (wt.%)
H = percentage of hydrogen present in the material (wt.%)
O = percentage of oxygen present in the material (wt.%)

(No nitrogen was found in cardboard or its pyrolysis products).
The agreement of experimental and calculated values was very good. The difference was less than 3% in most cases. The heat of combustion was therefore calculated from the above formula in other cardboard experiments also.

The heats of combustion of the organic fractions from shredded domestic waste and their pyrolysis products were sometimes determined by TNO. In most cases, however, the heat of combustion was calculated from the equation:

Heat of combustion = 329*C + 1510*H - 139*O + 93*S + 24*N (kJ/kg)

where: C = percentage of carbon present in the material (wt.%)
H = percentage of hydrogen present in the material (wt.%)
O = percentage of oxygen present in the material (wt.%)
S = percentage of sulphur present in the material (wt.%)
N = percentage of nitrogen present in the material (wt.%)

Some chlorine was present in the feedstock as well as in the pyrolysis products. It was assumed that this element does not contribute to the heat of combustion [4.13]. The experimental and calculated values were in good agreement bearing in mind that it is difficult to obtain a representative and homogeneous sample from the waste fractions for either ultimate analysis or the determination of the heat of combustion.

Appendix 7.1 Parameter values used in the introductory sensitivity analysis([7.1], except (*))

thermal conductivity solid	$\lambda = 0{,}11313$	J/m.sec.^{o}C
heat capacity cellulose	$C_{p1} = 2304.5$	J/kg.^{o}C
dehydrocellulose	$C_{p2} = 2304.5$	J/kg.^{o}C
char	$C_{p3} = 2304.5$	J/kg.^{o}C
frequency factor reaction a	$k_{ao} = 8.2*10^{4}$	sec^{-1}
reaction b	$k_{bo} = 8.2*10^{6}$	sec^{-1}
reaction c	$k_{co} = 8.2*10^{8}$	sec^{-1}
activation energy reaction a	$E_a = 1*10^{5}$	J/mole
reaction b	$E_b = 1.3*10^{5}$	J/mole
reaction c	$E_c = 1.5*10^{5}$	J/mole
gas yield factor reaction a	$y_a = 0.1$	-
reaction b	$y_b = 1$	-
reaction c	$y_c = 0.167$	-
heat capacity gas a (*)	$C_{pga} = 2000$	J/kg.^{o}C
gas b (*)	$C_{pgb} = 2000$	J/kg.^{o}C
gas c (*)	$C_{pgc} = 2000$	J/kg.^{o}C
heat of reaction reaction a	$\Delta\hat{H}_a = 69135$	J/kg
reaction b	$\Delta\hat{H}_b = 691350$	J/kg
reaction c	$\Delta\hat{H}_c = -394700$	J/kg
heat flux	constant=3393.9	J/m^{2}.sec.
initial temperature	$T_o = 300$	^{o}K
initial density solid	$\rho_o = 600$	kg/m^{3}
half slab thickness (*)	$L = 0.01$	m
Nusselt number	$Nu = 2$	-
temperature continuous phase (*)	$T_{cont.phase}=873$	^{o}K
thermal conductivity gases (*)	$\lambda_g = 0.0419$	J/m.sec.^{o}C

Appendix 7.2 Experimental determination of the thermal conductivity of the solids

The determination of the thermal conductivity is based on the measurement of a heat flux through a material in which a stationary temperature gradient exists. The thermal conductivity of the material can then be calculated from:

$$\lambda = \phi . \left| \frac{dx}{dt} \right| \qquad (1)$$

where: λ = thermal conductivity (J/m.sec.^{o}C)

ϕ = heat flux (J/m^2.sec)

$\frac{dT}{dx}$ = temperature gradient (^{o}C/m)

Experimental set up

The apparatus that was used for measuring the thermal conductivity of paper and char was constructed for samples that have the shape of a circular slice (diameter 80 mm, thickness 12 mm). The sample is fixed in between two copper plates (ϕ = 80 mm). The junction of a copper-constantane thermocouple has been fixed in each plate just below the surfaces, that contact the sample. The temperature difference over the sample can thus be measured. The temperature gradient $\frac{dT}{dx}$ is calculated from this temperature difference and the sample thickness. The high thermal conductivity of copper (λ = 400 J/m.sec.^{o}C) provides a homogeneous temperature distribution parallel to the contact planes of sample and copper plates. The temperature gradient is maintained by heating the upper plate with the aid of a heating element and by cooling the lower plate with the aid of a thermostated element. The temperature of the heated plate at the sample surface is kept constant by means of a P.I.D.-controller which supplies more or less power to the heating element depending on the variations in this temperature. A heat flux mat has been placed in between the lower copper plate and the thermostated element. The mat consists of a large number of thermocouples in series inbedded in plastic. One junction of each thermocouple is situated at the upper and the other junction is situated at the bottom part of the mat (fig. 1).

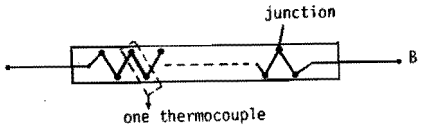

Fig.1 Side view of heat flux mat

A temperature difference ΔT must inevitably be present between upper and lower part of the mat because of heat transport. This temperature difference causes a voltage difference ΔV between the two junctions of each thermocouple. ΔV is a function of ΔT:

$$\Delta V = f(\Delta T) \qquad (2)$$

When n thermocouples in series are present in the heat flux mat the voltage difference between points A and B (fig. 1) is given by:

$$\Delta V_{tot} = n.f(\Delta T) \qquad (3)$$

The series of thermocouples is located in the mat as indicated in fig. 2.
The voltage difference measured between A en B is a measure of ΔT. It is also a measure of the heat flux when the thickness of the mat and the thermal conductivity of the plastic are taken into account. The heat flux mat must be calibrated in order to find the relation between ΔV_{tot} and the heat flux.
Sample, heating element, copper plates and heat flux mat are placed in an isolating container to avoid heat loss through the cylinder mantel of the sample. The thermostated element acts as pedestal for the whole. A schematic representation of the apparatus is given in fig. 3.

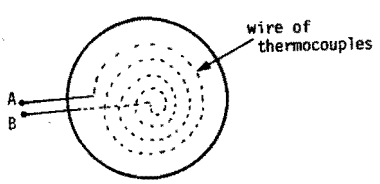

Fig.2 Top view of heat flux mat

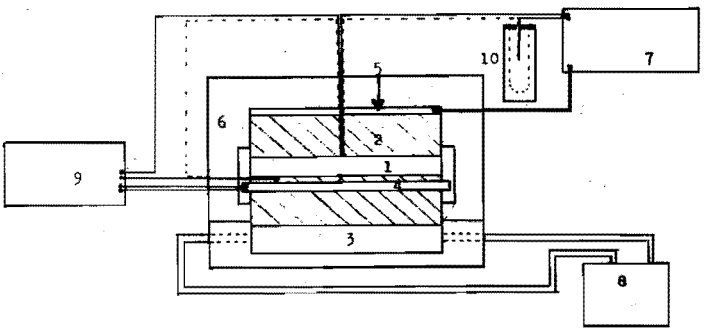

Fig.3 Schematic representation of apparatus for thermal conductivity measurement

1. sample
2. copper plate (with the junctions of the thermocouples)
3. thermostated element
4. heat flux mat
5. heating element (500 W at 220 V)
6. isolating container
7. P.I.D.-controler
8. thermostat
9. recorder (recording the voltage difference over the mat and the thermocouples).
10. Dewar vessel (filled with melting ice for the cold junctions of the thermocouple connected to the P.I.D.-controler).

——— copper
------- constantane } wires of thermocouples

Calibration of heat flux mat

The heat flux mat was calibrated using samples of materials with well-known thermal conductivity. The heat flux can be calculated from:

$$\emptyset = - \lambda \frac{\Delta T}{d} \qquad (4)$$

The voltage difference delivered by the heat flux mat corresponds to the heat flux $\emptyset$. The relation between $\emptyset$ and ΔV_{tot} can be found by applying different temperature gradients over the sample. PTFE (Teflon)

and pyrex glass were used for calibration of the heat flux mat (λ = 0.244 resp. 1.14 J/m.sec.^{o}C). The following relation was found:

$$\phi = \beta * V_{tot} \qquad (5)$$

where β = 5.57 J/m .sec.mV.

Determination of the thermal conductivity of paper

125 dried, circular paper sheets (pressed on top of each other) were used to prepare a suitable paper sample. Measurements were carried out at different temperatures of the upper copper plate (30-60^{o}C). No sensitivity of the thermal conductivity to this temperature was observed. The average value of the thermal conductivity that was measured was: λ = 0.116 $\pm$ 0.003 J/m.sec.^{o}C.

Determination of the thermal conductivity of char

The thermal conductivity of powdered char obtained in pyrolysis of shredded thin cardboard was determined. The following emperical relationship was used to calculate the thermal conductivity of the char itself from the thermal conductivity of the powder [7.3]:

$$\frac{\lambda_g}{\lambda_\ell} = 2. \left| \frac{v.p^{2/3} + 1 - p^{2/3}}{v.(p^{2/3} - p) + 1 - p^{2/3} + p} \right| \qquad (6)$$

where: λ = thermal conductivity (J/m.sec.^{o}C)

$v = \lambda_c/\lambda_\ell$

$p = \frac{\rho_c - \rho_g}{\rho_c - \rho_\ell}$

ρ = density (kg/m^3)

subscripts c = char

g = powder

ℓ = gas (air)

The determinations of λ_g were carried out at different temperatures of the upper copper plate (45-85^{o}C). The value of the thermal conductivity found was: λ_g = 0.1343 J/m.sec.^{o}C. The following data were used in calculating λ_c:

V = volume of sample : $6.03*10^{-5}$ m^3 ($\emptyset \cong 80$ mm, d = 12 mm)

G = mass of sample : 15.25 gram

ρ_c = density of char : 825 kg/m^3

λ_ℓ = thermal conductivity of air : 0.026 J/m.sec.^oC.

The bulk density of the char sample is given by: $\rho_g = \frac{G}{V} = 253$ kg/m^3.

The porosity p is then given by: $p = 1 - \frac{\rho_g}{\rho_c} = 0.693$

It follows from eq. (6) that v = 4.20, so that $\lambda_c = v * \lambda_\ell = 0.109$ J/m.sec.^oC.

STELLINGEN

1. Het door Maa voorgestelde shrinking core model voor de hoge temperatuur pyrolyse van cellulose-achtige materialen is strijdig met het wezen van de pyrolyse van vaste, cellulose-achtige stoffen.

   P.S.Maa, Ph.D.Thesis, West Virginia University (1971)
   Dit proefschrift, hoofdstuk 2

2. Lage temperatuur pyrolyse van huishoudelijk afval biedt voordelen boven directe verbranding ervan.

   Dit proefschrift, hoofdstuk 1

3. De toepassing van een electrostatisch filter als enig apparaat voor het afvangen van de druppels van olie en teer, die ontstaan bij de lage temperatuur pyrolyse van organische afvallen, moet worden ontraden.

   M.D.Bowen, E.D.Smyly, ACS Symp.Series, no.76, p.94 (1978)
   Dit proefschrift, hoofdstukken 3 en 8

4. Het is uit milieuhygiënische overwegingen gewenst, dat de toepassing van polyvinylchloride (PVC) in kleinere gebruiksgoederen wordt verboden.

5. De slibbelasting is in het algemeen geen voldoende maat voor het zuiveringseffect van een actief slib afvalwaterzuiveringsinstallatie.

   A.C.J.Koot, Behandeling van afvalwater, Uitg. Waltman-Delft (1964)

6. Ten onrechte stelt O.Lauer dat het ziftproces in een centrifugaal zig zag zifter met geforceerde vortexstroming vergeleken kan worden met dat in een zig zag zifter die in het zwaartekrachtveld werkt.

O.Lauer, Chemie-Ingenieur-Technik, 41, p.491 (1969)

7. De aanname van Alter c.s., als zouden deeltjes, die zich in een roterende trommelzeef bevinden, het zeefoppervlak verlaten op het punt waar de component van de zwaartekracht loodrecht op het zeefoppervlak gelijk is geworden aan de centrifugaalkracht, is in het algemeen onjuist.

H.Alter, J.Gavis, M.L.Renard, Resources and Conservation, 6, p.223 (1981)

8. De wijze van beoordeling van aanvragen voor voorwaardelijk gefinancierd onderzoek, die de minister van onderwijs en wetenschappen heeft voorgesteld, maakt de voorwaardelijke financiering ongeschikt om te dienen als middel om aan het academisch onderzoek in Nederland richting te geven.

Beleidsnota Voorwaardelijke Financiering, Ministerie van Onderwijs en Wetenschappen (18 mei 1982)

9. Er bestaat geen andere reden tot het voeren van de Brede Maatschappelijke Discussie over de toekomstige energievoorziening in Nederland dan de angst van de Nederlandse volksvertegenwoordigers voor het nemen van een beslissing.

10. Propagandisten voor het gebruik van macrobiotisch voedsel propageren een meedogenloos egoïsme.

10 september 1982 C.P.M. van Ginneken